University of Albertа

The Design and Folding of Coiled-coils

by

Jennifer Rae Litowski ©

A thesis submitted to the Faculty of Graduate Studies and Research in partial fulfillment of the requirements for the degree of Doctor of Philosophy

Department of Biochemistry

Edmonton, Alberta

Spring 2003

National Library
of Canada

Acquisitions and
Bibliographic Services

395 Wellington Street
Ottawa ON K1A 0N4
Canada

Bibliothèque nationale
du Canada

Acquisisitons et
services bibliographiques

395, rue Wellington
Ottawa ON K1A 0N4
Canada

Your file Votre référence
ISBN: 0-612-82133-1
Our file Notre référence
ISBN: 0-612-82133-1

The author has granted a non-exclusive licence allowing the National Library of Canada to reproduce, loan, distribute or sell copies of this thesis in microform, paper or electronic formats.

L'auteur a accordé une licence non exclusive permettant à la Bibliothèque nationale du Canada de reproduire, prêter, distribuer ou vendre des copies de cette thèse sous la forme de microfiche/film, de reproduction sur papier ou sur format électronique.

The author retains ownership of the copyright in this thesis. Neither the thesis nor substantial extracts from it may be printed or otherwise reproduced without the author's permission.

L'auteur conserve la propriété du droit d'auteur qui protège cette thèse. Ni la thèse ni des extraits substantiels de celle-ci ne doivent être imprimés ou aturement reproduits sans son autorisation.

Canada

University of Alberta

Library Release Form

Name of Author: Jennifer Rae Litowski

Title of Thesis: The Design and Folding of Coiled-coils

Degree: Doctor of Philosophy

Year this Degree Granted: 2003

Permission is hereby granted to the University of Alberta Library to reproduce single copies of this thesis and to lend or sell such copies for private, scholarly or scientific research purposes only.

The author reserves all other publication and other rights in association with the copyright in the thesis, and except as herein before provided, neither the thesis nor any substantial portion thereof may be printed or otherwise reproduced in any material form whatever without the author's prior written permission.

Jennifer R. Litowski

Permanent address:

P. O. Box 465
Cabri, Saskatchewan
Canada S0N 0J0

Date: Feb. 24/03

University of Alberta

Faculty of Graduate Studies and Research

The undersigned certify that they have read, and recommend to the Faculty of Graduate Studies and Research for acceptance, a thesis entitled The Design and Folding of Coiled-coils submitted by Jennifer Rae Litowski in partial fulfillment of the requirements for the degree of Doctor of Philosophy.

Dr. Robert S. Hodges
(supervisor)

Dr. J. N. Mark Glover

Paul G Scott
Dr. Paul G. Scott

David Bundle
Dr. David R. Bundle

P. Burkhard
Dr. Peter Burkhard
(external examiner)

Date: Feb 24/03

Abstract

Coiled-coils are formed when two or more α-helices wind around each other in a left-handed supercoil. They are found in a wide variety of proteins, including transcription factors, cytoskeletal and motor proteins, and chaperones. Their sequences are characterized by a heptad repeat (**abcdefg**) where positions **a** and **d** are occupied by nonpolar residues. Our lab has designed the E/K-coil, a heterodimeric coiled-coil, for use in biomedical applications. A major goal of this thesis has been to expand this design, creating a series of heterodimeric coiled-coils with a wide range of stabilities and affinities.

The E/K-coil sequence was modified by changing its length (3, 4, and 5 heptads, or 21, 28 and 35 residues), hydrophobicity, and α-helical propensity. Extension by one heptad caused stability increases from 2.0–4.3 kcal/mol, depending on length and the presence of a disulfide bridge. Increasing hydrophobicity (valine to isoleucine) caused stability increases of 0.47 kcal/mol per substitution. Increasing α-helical propensity (serine to alanine) caused stability increases of 0.41–0.45 kcal/mol per substitution. The resulting series of heterodimeric coiled-coils had stabilities ranging from 6.8–11.2 kcal/mol. The folding mechanism of these coiled-coils was investigated by BIAcore analysis. The five-heptad coiled-coil folded through a simple, two-state mechanism. In contrast, coiled-coils of other lengths folded through complex mechanisms, comprised of a bimolecular association followed by a unimolecular rearrangement. The free energy contribution of central heptads was found to be three-fold greater than that of heptads at coiled-coil ends (3.89 vs. 1.26 kcal/mol).

A complementary approach to understanding coiled-coil folding and structure is to examine coiled-coils from native proteins. Dynamin, which is involved in endocytosis, has two regions found to form tetrameric coiled-coils, D2 (residues 323-352) and D4 (residues 712-740). They are proposed to be involved in the tetrameric assembly of dynamin, which is important to its function. Dynein, a motor protein, binds microtubules through an extended stalk domain. A biophysical analysis of the stalk domain revealed it to be an antiparallel, intramolecular coiled-coil. Both the coiled-coil and the microtubule-binding region were required to form an autonomous folding unit; the structure and stability of each region was disrupted when expressed individually.

Acknowledgements

I wish to thank my supervisor, Robert S. Hodges, for being a mentor, both scientifically and professionally. He has provided a rich environment to learn and practice science, and his passion for science has been an inspiration.

I wish to thank members of the Hodges lab who I have worked with over the years. In particular, Heman Chao for introducing me to the E/K coiled-coil, Lorne Burke for teaching me about techniques and instrumentation, and Paul Cachia, Colin Mant, Janine Mills and Elsi Vacano for many stimulating discussions. Thank you to Morris Aarbo, Mundeep Chana, Jason Chen, Rob Hodgins, Mike Houston, Devon Husband, Wayne Kohn, Les Kondejewski, Stanley Kwok, Masoud Jelokhani-Niaraki, Pierre Lavigne, Darin Lee, Anthony Mehok, Traian Popa, Brian Tripet, and Kurt Wagschal - you have all contributed to making our lab an interesting place to work.

I would like to thank members of the PENCE chemistry lab, particularly Marc Genest, Jennifer Labrecque, and Paul Semchuk for years of assistance and advice in peptide chemistry. Thank you to the members of the Alberta Peptide Institute for performing amino acid analysis and sequencing on countless samples. Thank you as well to Bob Luty for teaching me about CD spectroscopy and Les Hicks for performing so many analytical ultracentrifugation runs. I would also like to thank Maureen O'Connor-McCourt and Greg De Crescenzo for many fruitful discussions about coiled-coil folding and kinetics.

For financial support, I would like to thank PENCE and the Canadian Institutes for Health Research for supporting the research, and the Alberta Heritage Foundation for

Medical Research, the Izaak Walton Killam Memorial Fund, and the Natural Sciences and Engineering Research Foundation for graduate scholarships over the years.

Finally, I would like to thank my husband, Andrew Quick, for his continued support, encouragement, and love. This journey would have been extraordinarily difficult without you.

Table of Contents

Page

Chapter I. Introduction

A. General Introduction to Coiled-coils........ 1

B. Coiled-coil Sequence and Structure........ 5
    Stability........ 7
        a. Hydrophobicity........ 7
        b. Packing in the Core........ 10
        c. Electrostatic Interactions........ 11
        d. Hydrogen Bonding........ 15
        e. α-Helical Propensity........ 16
    Oligomerization State........ 17
    Orientation........ 19
    Specificity of Association........ 20

C. Coiled-coil Folding........ 21
    Protein Folding........ 21
    Short Coiled-coils........ 24
    Long Coiled-coils........ 25

D. Design of the E/K Heterodimeric Coiled-coil........ 27

E. Native Coiled-coils........ 34
    Dynamin........ 36
    Dynein........ 36

Chapter II. Methods and Materials........ 45

A. Materials........ 45

B. Solid-Phase Peptide Synthesis........ 46

C. High-Performance Liquid Chromatography........ 55
    Reversed-Phase Chromatography........ 57
    Cation-Exchange Chromatography........ 60
    Hydrophilic Interaction/Cation-Exchange Chromatography........ 61

D. Amino Acid Analysis........ 62

E. Mass Spectrometry........ 63

F. Peptide Oxidation..64

G. Circular Dichroism Spectroscopy..66

H. Guanidine Hydrochloride Denaturation Analysis........................70

I. Analytical Ultracentrifugation..74
    Sedimentation Equilibrium..75
    Sedimentation Velocity..78

J. Redox Equilibrium Experiments..79

H. Tryptic Digests...80

Chapter III. Designing heterodimeric two-stranded α-helical coiled-coils: The effect of chain length on protein folding, stability and specificity........ 82

A. Summary...82

B. Introduction..83

C. Results..83
    Peptide Design...83
    Structural Characterization...87
    Oligomerization State..91
    Conformational Stability...93
    Redox Equilibrium Experiments..97

D. Discussion...104

Chapter IV. Designing heterodimeric two-stranded α-helical coiled-coils: The effects of hydrophobicity and α-helical propensity on protein folding, stability, and specificity.. 109

A. Summary...109

B. Introduction..110

C. Results..110
    Peptide Design...110
    CD Spectroscopy...114
    Sedimentation Equilibrium..119
    Conformational Stability...121

D. Discussion...125

Chapter V. Real-time monitoring of the interactions of *de novo* designed coiled-coils using surface plasmon resonance: Effect of chain length on the kinetic and thermodynamic constants of interaction 131

A. Summary 131

B. Introduction 132

C. Materials and Methods 133
  Equipment and Reagents 133
  Immobilization of K coils in the sensor chips 133
  Kinetic Assays in the BIAcore 134
  Data preparation and analysis 134
  Mathematical modeling and parameter estimation 135

D. Results 136
  Peptide Design 136
  Optimization of the BIAcore experiments 139
  Characterization of the E/K interactions 142

E. Discussion 150

F. Conclusion 160

Chapter VI. Hydrophilic interaction/cation-exchange chromatography for the purification of synthetic peptides from closely related impurities: serine side-chain acetylated peptides 161

A. Summary 161

B. Introduction 162

C. Results and Discussion 165
  Purification and analysis of a 21-residue peptide 165
  Characterization of the acetylated peptides 177
  HILIC/CEC of acetylated serine peptides 179

D. Conclusions 185

Chapter VII. Multiple distinct coiled coils are involved in dynamin self-assembly 186

A. Summary 186

B. Introduction 187

C. Materials and Methods..190
    cDNA Constructs..190
    Co-Immunoprecipitation Assay for Dynamin Self-Association.......190
    Yeast Interaction Trap...191
    Sucrose Density Gradient Centrifugation...............................192
    Endocytosis Assays..192

D. Results 193
    Assays for dynamin self-association 193
    Peptide Analysis 203

E. Discussion 211
    Nature of self-assembly species 211
    Role of coiled-coils 215
    Structural and physiological role of assembly domains 217

Chapter VII. Biophysical Characterization of the Dynein Heavy Chain Stalk Domain..219

A. Summary...219

B. Introduction...219

C. Methods and Materials...220
    Cloning, expression, and purification......................................220

D. Results...221
    Sequence Analysis...221
    Construct Design..229
    CD spectroscopy..231
    Conformational Stability..234
    Analytical Ultracentrifugation..236

E. Discussion and Future Directions..242

References 244

Appendix I. Use of a heterodimeric coiled-coil system for biosensor application and affinity purification 277

List of Figures

Figure **Page**

1-1 A selection of coiled-coil structures........ 2

1-2 The heptad repeat and hydrophobic face of coiled-coils........ 3

1-3 Models of leucine side chain packing at positions **a** and **d**........ 12

1-4 Protein folding........ 23

1-5 The E/K heterodimeric coiled-coil........ 29

1-6 Use of the E/K-coil as an immobilization domain for biosensor experiments........ 31

1-7 The use of the E/K coiled-coil in an expression and purification system for recombinant proteins........ 33

1-8 Dynein is a multi-protein complex composed of heavy chains, intermediate chains, light intermediate chains, and light chains........ 38

1-9 Domain organization of the dynein heavy chain........ 40

2-1 A general outline of the solid-phase peptide synthesis reaction cycle........ 47

2-2 Chemical structures of SPPS reagents........48

2-3 Formation of a new peptide bond during SPPS........ 50

2-4 Formation of the OBt active esters with in situ coupling reagents........ 52

2-5 RP-HPLC analysis of the peptide VAAL K3........53

2-6 Mass spectrometry analysis of the purified peptide VAAL K3........65

2-7 Typical CD spectra of α-helical, β-sheet, and random coil structure........ 68

2-8 Concentration dependence of GdnHCl denaturation........73

2-9 Sedimentation equilibrium analysis of coiled-coil peptides N19**a**(ox) and L19**a**(ox)........ 77

3-1 Helical wheel representation of the E4/K4 heterodimer.......................... 85

3-2 CD spectra of the non-crosslinked and oxidized coiled-coils of 3, 4, and 5 heptads length.. 88

3-3 Titration of peptides E4 and K4, as monitored by CD spectroscopy............ 92

3-4 Guanidine hydrochloride denaturation curves....................................... 94

3-5 Sample chromatograms from the redox equilibrium experiments................ 95

3-6 The mole fraction of the oxidized and reduced species with time................ 100

3-7 GdnHCl denaturation of the hetero-stranded E5/K5ox and an equimolar mixture of the homo-stranded E5ox and K5ox....................................... 102

3-8 Air oxidation of the E5 and K5 peptides.. 103

3-9 The effect of GdnHCl on the redox equilibrium curves........................... 105

4-1 Helical wheel representation of the E4/K4 heterodimer.......................... 112

4-2 CD spectra of the E-coils, K-coils and 1:1 mixtures of the E- and K-coil peptides.. 115

4-3 Guanidine hydrochloride denaturation curves....................................... 122

5-1 Helical wheel representation of the E/K coiled-coil heterodimer................. 137

5-2 Schematic representation of the different kinetic models used to globally fit the E/K interactions.. 143

5-3 Global analysis of the E5 interaction with K5....................................... 144

5-4 Global analysis of the E4 interaction with K4....................................... 147

5-5 The effect of chain length on the kinetic and thermodynamic constants for the E/K interactions derived when using the conformational change model.. 148

5-6 Variation of the free energy of binding with the length of the shortest coil within the dimers... 157

5-7 Experimental free energies versus free energies calculated using the multiple-linear regression approach... 159

6-1 RP-HPLC of crude peptide N..167

6-2 RP-HPLC of semipurified peptide N.. 168

6-3 CEC of semipurified peptide N... 170

6-4 HILIC/CEC of semipurified peptide N... 173

6-5 Sequence of peptide N presented as an α-helical net..............................175

6-6 Two-step purification of peptide N... 176

6-7 Tryptic digest of compounds 1, 2, and 3 from Figure 6-4..........................178

6-8 Separation of acetylated serine peptides by RP-HPLC and HILIC/CEC.. 182

6-9 The effect of acetonitrile on the separation of the acetylated serine peptides...184

7-1 Co-immunoprecipitation of HA- and Myc-tagged dynamin-1 constructs....... 194

7-2 Assay for dynamin-dynamin interaction using the yeast interaction trap........ 196

7-3 Reversal of endocytic inhibition by deletion of assembly sequences............ 197

7-4 Heterotypic interaction between the dynamin-1 and dynamin-2 isoforms...... 199

7-5 Sucrose density gradient centrifugation of various dynamin-1 C-terminal deletion mutants.. 200

7-6 Buffer-dependent dissociation of C733...201

7-7 Summary of the mapping results..202

7-8 Secondary structure analysis.. 204

7-9 CD spectra of peptides D1-D5.. 207

7-10 Denaturation of dynamin-1 peptides D2, D3, and D4..............................208

7-11 Equilibrium ultracentrifugation of helical peptides.................................210

7-12 Models for the structural organization of dynamin tetramers..................... 212

8-1 The analysis of the dynein stalk sequence by the coiled-coil prediction programs STABLECOIL, COILS, and PAIRCOIL.................. 223

8-2 The sequence of the dynein stalk and knob domains from Leu3202 to Thr3409.. 224

8-3 Computer modeling of the parallel and antiparallel coiled-coil structures to show the orientations of leucine side chains at positions **a** and **d**...226

8-4 The "Pro/Pro" antiparallel alignment of the dynein stalk coiled-coil............ 230

8-5 CD spectra of the dynein constructs were measured in benign buffer............232

8-6 Temperature denaturation profiles of Stalk81 and Linker......................... 235

8-7 Sedimentation equilibrium analysis of Stalk81 and Linker....................... 237

8-8 Stalk81 sedimentation velocity data was modeled as a prolate ellipsoid, using the program SEDNTERP..241

List of Tables

Table **Page**

1-1 Effect of **a** and **d** position residues on coiled-coil stability and oligomerization state........ 9

2-1 List of Materials........ 45

3-1 Peptide Sequences........ 86

3-2 CD Spectroscopy........ 90

3-3 GdnHCl denaturation parameters........ 95

4-1 Peptide Sequences........ 113

4-2 CD Spectroscopic data of synthetic peptides used in this study........ 116

4-3 Biophysical analysis of the heterodimeric coiled-coils........ 120

4-4 Contributions of hydrophobicity, α-helical propensity and chain length to stability........ 124

5-1 Peptide sequences and nomenclature........ 138

5-2 Standard deviation of the residuals and Z1 and Z2 statistics........ 145

5-3 Kinetic and thermodynamic constants related to the global fit of interactions of the different E/K coiled-coil pairs to a conformational change (rearrangement) model........ 149

6-1 Peptide sequences........ 166

6-2 MS/MS fragments of ions 531 and 573........ 180

7-1 Amino acid sequences of the synthetic peptides used in this study........ 205

7-2 Ellipticities and stabilities of the synthetic peptides........ 209

8-1 Sequence analysis of the dynein stalk coiled-coil........ 228

8-2 CD analysis of the dynein constructs........ 233

8-3 Stalk81 hydrodynamic parameters........ 239

List of Abbreviations

Amino Acids:

Ala, A	Alanine
Arg, R	Arginine
Asn, N	Asparagine
Asp, D	Aspartic acid
Cys, C	Cysteine
Gln, Q	Glutamine
Glu, E	Glutamic acid
Gly, G	Glycine
His, H	Histidine
Ile, I	Isoleucine
Leu, L	Leucine
Lys, K	Lysine
Met, M	Methionine
Phe, F	Phenylalanine
Pro, P	Proline
Ser, S	Serine
Ser(Ac)	O-acetylserine
Thr, T	Threonine
Trp, W	Tryptophan
Tyr, Y	Tyrosine
Val, V	Valine

Ac-	Acetylated N-terminus
t-BOC	*tert*-Butyloxycarbonyl
CD	Circular dichroism
CEC	Cation-exchange chromatography
DCM	Dichloromethane
DMF	Dimethylformamide
DTNP	2,2′-dithiobis(5-nitropyridine)
DTT	Dithiothreitol
EDC	N-ethyl-N’-(3-dimethylaminopropyl) carbodiimide hydrochloride
EDTA	Disodium ethylenediaminetetraacetate
EM	electron microscopy
FMOC	9-Fluorenylmethyloxycarbonyl
GdnHCl	Guanidine hydrochloride
GST	Glutathione-S transferase
HA	Hemagglutinin
HBS	Hepes buffered saline
HBTU	2-(1H-benzotriazole-1-yl)-1,1,3,3-tetramethyluronium hexafluorophosphate
HC	dynein heavy chain
HEPES	N-(2-hydroxyethyl)piperazine-N’-2-ethane-sulfonic acid
HILIC/CEC	Hydrophilic interaction/cation exchange chromatography
HPLC	High performance liquid chromatography
IC	dynein intermediate chain

LC	dynein light chain
LC-MS	Liquid chromatography-mass spectrometry
LCPL	left circularly polarized light
LEM	Linear extrapolation method
LIC	dynein light intermediate chain
MS	Mass spectrometry
NHS	N-hydroxysuccinimide
PBS	Phosphate buffered saline
PCR	Polymerase chain reaction
PDEA	2-(2-pyridinyldithio)ethaneamine hydrochloride
PH	Pleckstrin homology
RCPL	right circularly polarized light
RP-HPLC	Reversed-phase high performance liquid chromatography
RU	Resonance unit
SEC	Size-exclusion chromatography
SPR	Surface plasmon resonance
TEAP	Triethylammonium phosphate
TFA	Trifluoroacetic acid
TFE	Trifluoroethanol

CHAPTER I

Introduction

A. General Introduction to Coiled-coils

The coiled-coil is an oligomerization domain that is formed when two or more α-helices wrap around each other in a left-handed supercoil. Coiled-coils are found throughout nature and occur in a wide variety of proteins (Figure 1-1). In the 1950s, Crick proposed that if two α-helices lie against each other at an angle of approximately 20°, they would wind around each other, resembling a two-stranded rope. The side chains at the interface have a characteristic "knobs-into-holes" packing (Crick 1953). The sequence of tropomyosin, the first coiled-coil to be sequenced, revealed a pattern where hydrophobic residues are found with an alternating spacing of every third then every fourth residue (Hodges *et al.* 1972, Sodek *et al.* 1972). This was dubbed a heptad repeat (**abcdefg**), where positions **a** and **d** were occupied by hydrophobic residues (Figure 1-2A). This pattern has proved to be a hallmark of coiled-coil sequences. Coiled-coils were first known to exist in fibrous proteins, such as keratin, myosin and tropomyosin (Cohen 1998, Cohen & Parry 1990). Interest in coiled-coils grew in the 1990s, after they were identified in a family of DNA-binding proteins (Landschulz *et al.* 1988, O'Shea *et al.* 1989a). A word of explanation regarding the term "leucine zipper" is in order. Landschultz *et al.* (1988) observed the occurrence of leucine every seventh residue in a number of transcription factors, and proposed that these proteins interacted by the leucine side chains interdigitating like the teeth of a zipper. This model is in fact incorrect, and they were identified as coiled-coils soon after (O'Shea *et al.* 1989a). The

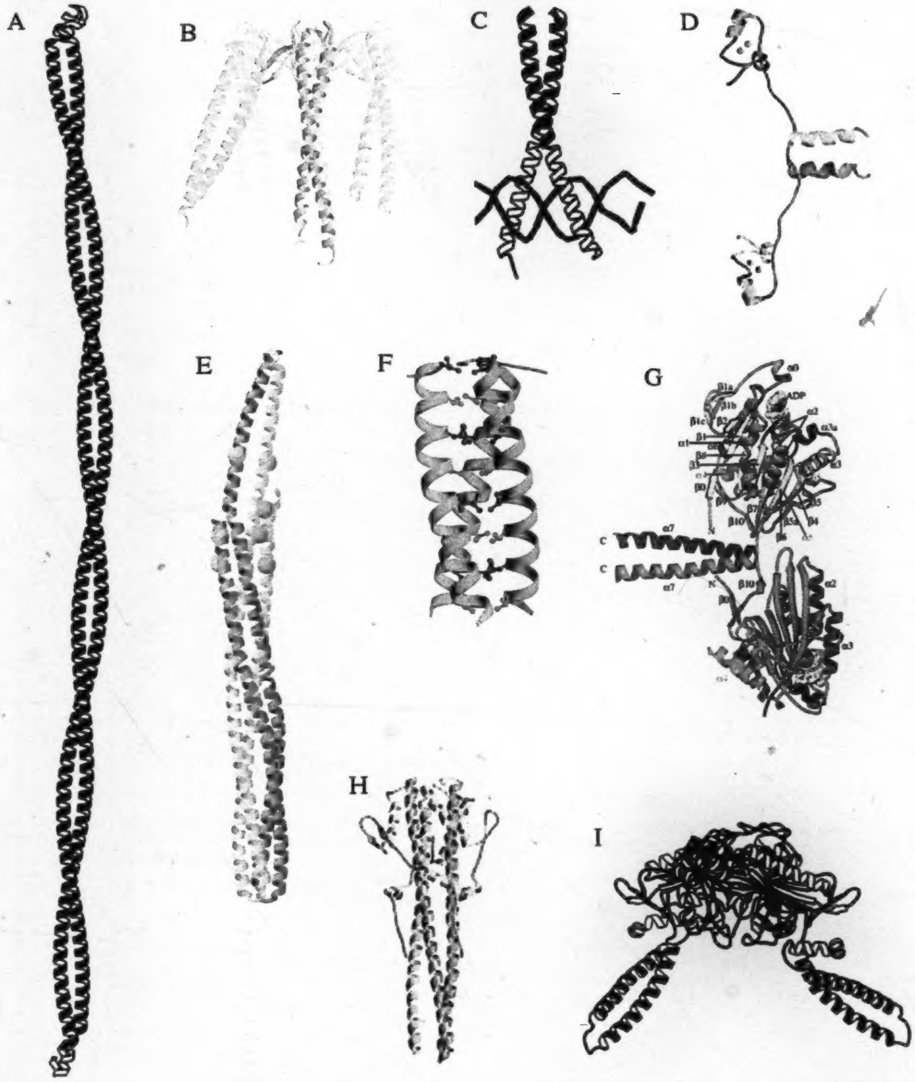

Figure 1-1. A selection of coiled-coil structures. **A)** Tropomyosin **B)** Prefoldin **C)** GCN4 **D)** GAL4 **E)** Serine chemotaxis receptor **F)** Coil-V_aL_d **G)** Kinesin **H)** Hemagglutinin **I)** Seryl tRNA-synthase. Figures were adapted from Kim *et al.* (1999), Kohn *et al.* (1997), Kozielski *et al.* (1997), Lupas (1996), Ogihara *et al.* (1997), and Siegert *et al.* (2000).

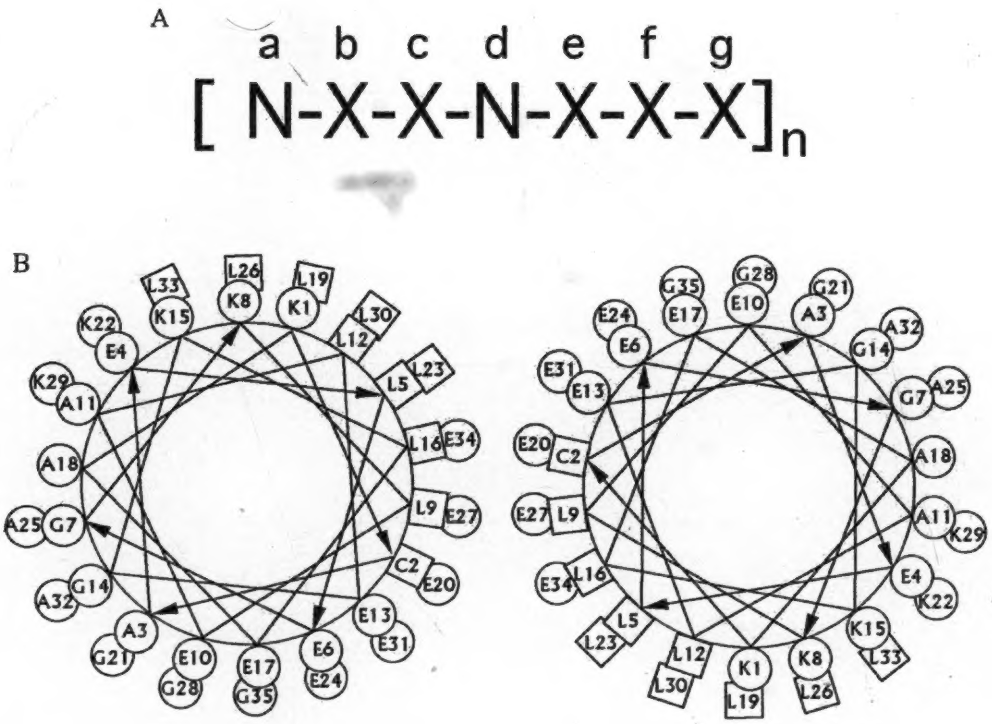
A
a b c d e f g
[N-X-X-N-X-X-X]n
B
L33 L26 L19 K15 K8 K1 L30 L12 K22 E4 L23 L5 K29 A11 L16 E34 A18 L9 E27 A25 G7 C2 E20 A32 G14 E13 A3 E31 G21 E10 E17 E6 G28 G35 E24
G35 G28 G21 E24 E17 E10 A3 A32 E6 G14 E31 E13 G7 A25 E20 C2 A18 E27 L9 A11 K29 E34 L16 E4 K22 L5 K15 L23 L12 K1 K8 L33 L30 L19 L26

Figure 1-2. **A)** The heptad repeat is a characteristic feature of coiled-coils. It is labeled **a** through **f**, where positions **a** and **d** are occupied by nonpolar residues (N). **B)** If the α-helices had a perfectly straight alignment, the hydrophobic faces (denoted by squares) would curve away from each other around the α-helices. Figures were adapted from Hodges *et al*. (1988).

term "leucine zipper" has often been used to refer to these short coiled-coils found in DNA-binding proteins, such as GCN4 and the Fos/Jun heterodimer, but it is not a general synonym for "coiled-coil".

Coiled-coils are an interesting topic of study for many reasons. They are an extremely common structural motif and are found in every kingdom of life. Recent surveys of genomic databases suggest that up to 10% of eukaryotic proteins contain regions predicted to form coiled-coils (Liu & Rost 2001). They occur in a wide variety of proteins that play important biological roles including transcription factors, chaperones, motor proteins, viral fusion proteins, cytoskeletal proteins, the 26S proteasome, and in the type III secretion system of pathogenic bacteria (Burkhard *et al.* 2001, Delahay & Frankel 2002, Fu *et al.* 2001, Kohn *et al.* 1997, Lupas 1996, Siegert *et al.* 2000). A sample of coiled-coil structures is shown in Figure 1-1. Dynamic conformational changes have been observed in a number of coiled-coils. A drop in pH triggers large conformational changes in the coiled-coil domains of the macrophage scavenger receptor and in viral fusion proteins, such as hemagglutinin and gp41 (Burkhard *et al.* 2001, Oas & Endow 1994, Skehel & Wiley 1998). The coiled-coil domain of Xrcc4, a protein involved in DNA repair, undergoes a conformational change to form a binding interface for DNA ligase IV (Sibanda *et al.* 2001).

Coiled-coils are an excellent model system for studying protein folding and de novo design (Hodges 1996, Kohn & Hodges 1998). They have a simple structure, composed of a single type of secondary structure, making their folding easy to monitor by circular dichroism spectroscopy. They form stable quaternary structures in aqueous solution, under physiological conditions. However, they are small enough to make by solid-phase peptide synthesis, allowing large quantities of material to be generated. The physical forces which govern their structures and folding, such as hydrophobicity and electrostatic interactions, are the same as those present in all other proteins. More recently, our laboratory has used a de novo designed coiled-coil template for generating conformation-specific antibodies that recognize α-helices in proteins (Lu & Hodges 2002).

Coiled-coils have great potential for use in protein engineering and biomedical applications (reviewed in Muller *et al.* 2000). Coiled-coil domains have been used to direct the assembly of extra-cellular receptor domains (Hoyne *et al.* 2000, Liparoto & Ciardelli 1999, Wu *et al.* 1995, 1999) and of miniature antibodies (Arndt *et al.* 2001, Cocca *et al.* 1999). They have been used as tags in affinity purification (Catimel *et al.* 2001, Tripet *et al.* 1996) and for immobilization on biosensor surfaces (Chao *et al.* 1996, 1998). They have even been harnessed as a potential therapeutic, for the inhibition of HIV entry into cells (Root *et al.* 2001).

More than ten years of study has yielded many of the rules governing coiled-coil structure and folding. It is now possible to examine these interactions in more detail, in the hope of understanding and applying them in a more subtle fashion. This knowledge will be important for the de novo design of proteins and will improve their design for biomedical applications.

B. Coiled-coil sequence and structure

The basic structural features of coiled-coils have been extensively reviewed (Kohn & Hodges 1998, Lupas 1996, Muller *et al.* 2000) and are described below. The sequence is described by a heptad repeat, denoted abcdefg, where positions **a** and **d** are occupied by hydrophobic residues (Figure 1-2A). This places hydrophobic side chains every 3.5 residues, on average. However, α-helices typically have 3.6 residues per helical turn. This means that one heptad repeat is less than two full turns of the helix, resulting in an amphipathic structure in which the hydrophobic face curves around the α-helix (Figure 1-2B). Because of this curvature, the helices must lie against each other at an angle of approximately 20° and supercoil around one another for the two hydrophobic faces to remain in contact. The pitch is the distance required for the α-helices to complete a full turn around each other and varies from 90 Å to several hundred Å (Phillips Jr. 1992, Seo & Cohen 1993). The hydrophobic core is well-packed in a "knobs-into-holes" fashion, where a side chain from helix 1 (the "knob") packs into a space created by four side chains of the facing helix 2 (the "hole") (Crick 1953). Residues at positions **e** and **g** are typically occupied by charged residues, which participate in interchain i to i′+5 electrostatic interactions. These residues lie across the hydrophobic core, so the aliphatic portion of the side chains, which have some hydrophobic character (e.g. Arg, Glu, and Lys), contribute to the hydrophobic core as well.

The apparent simplicity of the coiled-coil structure is deceptive; a surprising diversity in coiled-coil structures exists (Figure 1-1). Oligomerization state, or the number of helices in the coiled-coil, varies from dimeric to pentameric (two to five α-helices). The strands of a coiled-coil may interact in a parallel or antiparallel orientation. Coiled-coil length varies from 20 - 40 residues in transcription factors to several hundred to over 1000 residues in cytoskeletal proteins. Numerous coiled-coil sequences contain discontinuities in their heptad repeats, termed skips (an insertion of one residue), stutters (a deletion of three residues), and stammers (a deletion of four residues) (Brown *et al.* 1996, Hicks *et al.* 1997). Coiled-coils accommodate these discontinuities by a local unwinding of the left-handed supercoil, an unwinding of the individual α-helices, or both (Strelkov & Burkhard 2002). Coiled-coils are also known to assemble into larger structures, such as the α-sheets and α-cylinders described by Walshaw and Woolfson (2001a).

Stability

Coiled-coils are stabilized by the same noncovalent interactions present in other types of protein structure: hydrophobicity, close-packing interactions, electrostatic interactions, and hydrogen bonds (Dill 1990, Honig & Yang 1995, Pace *et al.* 1996). Folding is generally opposed by the loss in conformational entropy of the polypeptide chain. The stabilizing effects of enthalpy and the destabilizing effects of entropy are of similar magnitudes, resulting in marginal stability (5-10 kcal/mol) for most protein structures (Dill 1990, Honig & Yang 1995, Pace *et al.* 1996).

a. Hydrophobicity

Hydrophobicity refers to the tendency of nonpolar molecules to associate with one another rather than with water. The transfer of nonpolar compounds from a nonpolar solvent to water is thermodynamically unfavourable (Cornette *et al.* 1987, Honig & Yang 1995, Karplus 1997, Pace *et al.* 1996). The burial of hydrophobic surface area is a major driving force in protein folding (Bilsel & Matthews 2000, Dill 1990, Honig & Yang 1995). Several approaches have been used to measure and rank the hydrophobicity of the amino acids, including measuring their partitioning between an organic solvent and water

(Fauchere & Pliska 1983), calculating solvent accessible surface area (Eisenberg & McLachlan 1986), and measuring RP-HPLC retention time (Monera *et al.* 1995, Sereda *et al.* 1994). The most hydrophobic amino acids are those with aliphatic (Ile, Met, Leu, and Val) and aromatic (Phe) nonpolar side chains. A number of others have side chains with mixed hydrophobic, polar and charged character (Arg, Lys, Tyr, and Trp). Calorimetric analysis of large numbers of protein analogs have shown that a single methylene (CH_2) group can contribute 0.1 - 1.5 kcal/mol to stability (Fersht & Serrano 1993, Jelesarov & Bosshard 1996, Pace *et al.* 1996).

Hydrophobicity is equally important to the stability of coiled-coils and the most stable hydrophobic cores are formed by the large hydrophobic residues, Ile, Met, Leu, Val, and Phe (Harbury *et al.* 1993, Hodges *et al.* 1990, Hu *et al.* 1990). Good correlations have been found between stability and the hydrophobicity of **a** and **d** position residues for native proteins, such as tropomyosin (Greenfield & Hitchcock-DeGregori 1995) and M proteins from group A bacteria (Cedervall *et al.* 1997). Numerous studies with model coiled-coil peptides have shown that the replacement of a large hydrophobic residue in the core with alanine is very destabilizing (Jelesarov & Bosshard 1996, Moitra *et al.* 1997, Tripet *et al.* 2000, Wagschal *et al.* 1999b, Zhou *et al.* 1992a, 1992b). This means that modifying the composition of a coiled-coil hydrophobic core can yield molecules with a wide range of stabilities. All naturally occurring amino acid residues except cysteine were substituted in a single **a** or **d** position of a de novo designed coiled-coil, yielding coiled-coils with stabilities over a range of 6 kcal/mol (**a** position) and 7.4 kcal/mol (**d** position) (Table 1-1, adapted from Tripet *et al.* 2000, Wagschal *et al.* 1999a, 1999b). The authors observed a good, but not exact correlation between coiled-coil

Table 1-1. Effect of **a** and **d** position residues on coiled-coil stability and oligomerization state.

	Position **a**		Position **d**	
Amino Acid[a]	$\Delta\Delta G_u$(Ala)[b]	Oligomerization[c]	$\Delta\Delta G_u$(Ala)[b]	Oligomerization[c]
Leu	3.5	3	3.8	m
Met	3.4	m	3.2	m
Ile	3.9	m	3.0	3
Tyr	2.2	3	1.4	2
Phe	3.0	m	1.2	m
Val	4.1	m	1.1	3
Gln	-0.1	3	0.5	m
Ala	0.0	m	0.0	m
Trp	0.8	2	-0.1	m
Asn	0.9	2	-0.6	m
His	-1.2	3	-0.8	m
Thr	0.2	m	-1.2	m
Lys	-0.4	2	-1.8	2
Asp	–	2	-1.8	2
Ser	-1.3	m	-1.8	m
Glu	-2.0	m	-2.7	2
Arg	-0.8	2	-2.9	2
Orn	-1.9	2	-3.1	2
Gly	-2.5	m	-3.6	m
Pro	–	–	–	–

[a] Amino acid residues substituted at position 22**d** or 19**a** of a model coiled-coil protein.

[b] $\Delta\Delta G_u$(Ala) is the difference in free energy of unfolding (ΔG_u) relative to the Ala-substituted analog.

[c] Oligomerization states were observed by high-performance size exclusion chromatography (HPSEC). "2" refers to a two-stranded coiled-coil, "3" refers to a three-stranded coiled-coil, and "m" refers to a mixture of the two- and three-stranded states. Table is adapted from Tripet *et al.* (2000) and Wagschal *et al.* (1999a, 1999b).

stability and side chain hydrophobicity, indicating that other factors such as packing must also be considered. Recent papers have shown that fluorinated analogs of valine and leucine are more stabilizing than the natural amino acids (Bilgicer *et al.* 2001, Tang *et al.* 2001). The increase in stability is purely due to hydrophobicity, for the side chain steric and packing interactions were identical.

b. Packing in the core

Amino acid side chains in the interior of proteins are tightly packed, with a density similar to that seen in crystals of small organic molecules (Richards 1977). Close-packing allows increased van der Waals interactions and is one of the major stabilizing interactions of protein structure (Honig & Yang 1995, Lazar & Handel 1998, Pace *et al.* 1996, Richards & Lim 1994). The net gain to stability of an individual methylene group has been estimated to be only 0.15 kcal/mol (Honig & Yang 1995). Over the length of an entire protein, however, this adds up to a significant contribution to stability. The importance of packing was demonstrated by mutational studies in which residues with large side chains, such as Ile and Leu were substituted with smaller residues, such as Ala and Val. The resulting destabilization was much greater than could be explained by differences in hydrophobicity (Kellis Jr. *et al.* 1988, 1989, Matthews 1995, Xu *et al.* 1998). Conversely, mutations which introduce larger side chains are also destabilizing because the larger side chain disrupts the packing and creates strain in the protein backbone (Liu *et al.* 2000).

In coiled-coils, the packing of residues in the hydrophobic core (positions **a** and **d**) has a large effect on stability. This is why a single Val-to-Ile substitution in the middle of a Val(**a**)/Leu(**d**) core is destabilizing (Wagschal *et al.* 1999b), but a coiled-coil with Ile at all **a** positions is more stable than one with Val at all **a** positions (Harbury *et al.* 1993, Zhu *et al.* 1993). Packing is also the cause of the increased stability of the β-branched residues Ile and Val at position **a** (Tripet *et al.* 2000, Wagschal *et al.* 1999b, Zhu *et al.* 1993) and of Leu at position **d** (Moitra *et al.* 1997, Tripet *et al.* 2000, Wagschal *et al.* 1999b). These findings could not be explained by differences in hydrophobicity, but examination of a crystal structure of a two-stranded coiled-coil revealed a critical difference in the packing of residue side chains at positions **a** and **d** (Harbury *et al.* 1993). In position **a**, the side chain Cα-Cβ bond vector points away from the interface, parallel to the Cα-Cα bond vector of the "hole" formed by the opposing helix (Figure 1-3). This is called parallel packing. The side chain is directed away from the core, leaving a small cavity which can be filled by the side chains of β-branched residues. In contrast, the Cα-Cβ bond vector of **d** position residues points into the interface, making a 90° angle with the Cα-Cα bond vector of the neighbouring helix "hole" (Figure 1-3). This is described as perpendicular packing. β-Branched side chains experience a steric clash in this packing geometry, making them less stabilizing than leucine.

c. *Electrostatic interactions*

Electrostatic interactions in proteins can occur between the charges on side chains (Arg, Asp, Glu, His, and Lys), the free amine and carboxy termini, groups added through post-translation modifications (i.e. phosphates), and bound molecules (metal ions, nucleotides, etc.). The actual contribution of charged groups to protein stability has proven to be controversial and difficult to measure (Dill 1990, Honig & Yang 1995, Kumar & Nussinov 2002). The burial of charged groups in the nonpolar protein interior carries a substantial desolvation penalty, which may or may not be fully compensated for

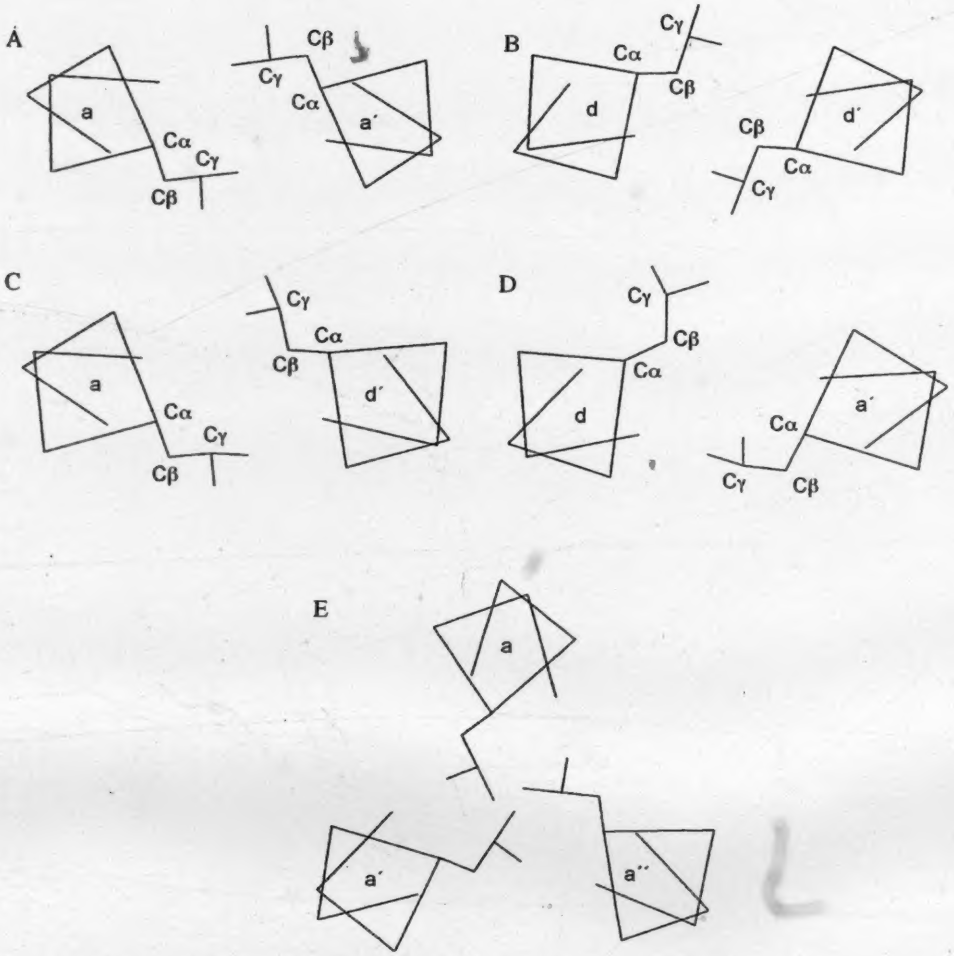
A
Cβ
Cγ
Cα
a
a′
Cα
Cγ
Cβ
B
Cγ
Cα
Cβ
d
Cβ
d′
Cα
Cγ
C
Cγ
Cα
Cβ
a
d′
Cα
Cγ
Cβ
D
Cγ
Cβ
Cα
d
a′
Cα
Cγ
Cβ
E
a
a′
a″

Figure 1-3. Models of leucine side chain packing at positions **a** and **d**. Parallel two-stranded coiled-coils have parallel packing at position **a** (**A**) and perpendicular packing at position **d** (**B**). Antiparallel two-stranded coiled-coils have **a-d′** (**C**) and **d-a′** (**D**) layers with mixed packing. Three-stranded coiled-coils have acute packing (**E**). Only the side chain carbons of leucine and seven surrounding main chain α-carbons are displayed. The figure is adapted from Monera *et al.* (1993).

by the formation of a salt bridge. This is further complicated by the strong dependence of electrostatic interactions upon the distance between charged groups and their geometry (Kumar & Nussinov 2002). It is clear, however, the electrostatic interactions play important roles in the structural organization of proteins (Dill 1990, Honig & Yang 1995, Kumar & Nussinov 2002). Interestingly, the high stability of proteins from thermophilic bacteria has been attributed to increased numbers of complex salt bridge networks (Kumar & Nussinov 2002).

Several types of electrostatic interactions are found in coiled-coils. Intrahelical interactions occur between i to i+3 and i to i+4 residues. Interhelical electrostatic interactions are observed between residues at positions **e** and **g** (i to i′+5) and in tetramers, may occur between residues at positions **b** and **c**. Hydrophobic core residues have been observed to form **d-e′**, **g-a′** and **d-a′** electrostatic interactions in cortexillin (Burkhard *et al.* 2000a) and in the c-Myc/Max heterodimer (Lavigne *et al.* 1995, 1998). There has even been a successfully designed **a-a′** electrostatic interaction in a de novo designed coiled-coil (Schneider *et al.* 1997).

The contribution of electrostatic interactions to the stability of coiled-coils has been no less controversial. There are two arguments that their net contribution is destabilizing. First, many native and synthetic coiled-coils have increased stability at low pH where salt bridges have been disrupted by the protonation of Asp and Glu (Hodges *et al.* 1988, Lowey 1965, Noelkin & Holtzer 1964, O'Shea *et al.* 1992, Zhou *et al.* 1992c, Zhu *et al.* 1993). Secondly, NMR experiments have consistently shown that glutamic acid residues thought to be involved in salt bridges do not show the expected lowered pKa values (Lumb & Kim 1995b, Marti *et al.* 2000, Phelan *et al.* 2002). However, Lavigne *et al.* (1996) have argued that salt bridges can be stabilizing without having lowered pKa values.

There is also substantial evidence that electrostatic interactions are stabilizing to coiled-coil structure. The double mutant cycle experiment was devised to measure the free energy of interaction between two residues while controlling for their differences in parameters such as α-helical propensity and hydrophobicity (Serrano *et al.* 1990). Careful use of double mutant cycles has shown that Glu to Lys i to i′+5 electrostatic attractions are stabilizing by 0.3 - 1.0 kcal/mol (Kohn & Hodges 1998, Krylov *et al.* 1994, 1998, Spek *et al.* 1998, Zhou *et al.* 1994a). Intrahelical i to i+4 salt bridges have been found to stabilize coiled-coils by 0.2 - 0.88 kcal/mol (Spek *et al.* 1998, Zhou *et al.* 1993). Yu *et al.* (1996) found that the stability of a coiled-coil at pH 2 was highly salt dependent. At low salt concentrations, the coiled-coil was more stable at pH 7 than at pH 2. However, at salt concentrations above 100 mM, the coiled-coil was stabilized at pH 2, by the preferential binding of anions to the folded form. There is also considerable circumstantial evidence for the stabilizing effect of electrostatic interactions in coiled-coils. The trigger sequence identified in cortexillin is stabilized by a network of intra- and interhelical ion pairs, and disruption of any of these is clearly destabilizing (Burkhard *et al.* 2000a, Kammerer *et al.* 2001). The geometric optimization of a series of intra- and interhelical ion pairs was key to the design of a two-heptad coiled-coil (Burkhard *et al.* 2000b, 2002). Removal of a single i to i′+5 salt bridge completely disrupted the coiled-coil, yielding an octameric assembly of α-helices (Meier *et al.* 2002).

The destabilizing effect of electrostatic repulsions has been well established. A single **e-g′** repulsion between glutamic acid residues was shown to be destabilizing by 0.4

- 0.8 kcal/mol (Kohn *et al.* 1995a, Krylov *et al.* 1998). These charge repulsions can often be screened by salt, permitting coiled-coil folding (Hoshino *et al.* 1997, Jelesarov *et al.* 1998, Kohn *et al.* 1995b, 1998b). It is well documented that electrostatic interactions also play critical roles in specifying other aspects of coiled-coil structure, such as chain orientation and association specificity. These effects will be discussed in sections to follow.

d. Hydrogen bonding

A hydrogen bond is the sharing of a single hydrogen atom between two electronegative atoms (recently reviewed in Dill 1990, Honig & Yang 1995, Pace *et al.* 1996). They play key roles in organizing secondary structure; α-helices, β-sheets and β-turns are all stabilized by regular patterns of hydrogen bonds (Brandon & Tooze 1991). Each main chain hydrogen bond has been estimated to contribute 0.6 – 0.9 kcal/mol to the stability of an α-helix (Pace *et al.* 1996, Scholtz *et al.* 1991a, Serrano 2000). Others have argued that their contribution to stability is much less because of the desolvation cost of burying a polar group in the interior of a protein (Honig & Yang 1995). At the least, hydrogen bonds play an important role in alleviating the destabilization that would be caused by the burial of a polar group which could not form a hydrogen bond.

The α-helices which comprise coiled-coils are stabilized by the same patterns of main chain hydrogen bonds as other α-helices. Hydrogen bond forming polar groups are occasionally found in the hydrophobic core of coiled-coils, such as the **a** position Asn found in the GCN4 coiled-coil. The net effect of such buried polar groups is destabilizing compared to a hydrophobic residues (Lumb & Kim 1995a).

e. α-Helical Propensity

α-Helical propensity is a measure of the effect of a particular amino acid residue upon the stability of an α-helix. The first propensity scale was actually a measure of the statistical frequency with which the different amino acids were found to occur in α-helices (Chou & Fasman 1978). More recently, α-helical propensity has been measured as the effect of different residues upon the free energy of folding of a host peptide or protein (Lyu *et al.* 1990, O'Neil & DeGrado 1990, Yang *et al.* 1997, Zhou *et al.* 1994c). Although there are differences between different scales, there are common trends. For example, Ala is always among the highest, Glu, Met, Leu and Lys score reasonably high, Gly, Ser, and Thr are low, and Pro is very disruptive to helical structure (Krittanai & Johnson Jr. 2000). Encouragingly, Myers *et al.* (1996, 1997) found propensity values to be the same in a protein and in a helical peptide derived from that protein.

The physical causes of differences in α-helical propensity appear to be side chain entropy and solvation of the polypeptide backbone. The α-helical structure restricts the number of rotamers that can be adopted by side chains, reducing side chain entropy (Creamer & Rose 1992, Luo & Baldwin 1999). Because of its small size, alanine is the only residue that does not have a reduced number of accessible rotamers in an α-helix. The β-branched side chains were particularly restricted by steric interference between the Cγ and the carbonyl oxygens of the i-2 and i-3 residues. Solvation of the peptide backbone affects the strength of hydrogen bonds between water and the main chain amide and carbonyl groups. Model building has shown that nonpolar side chains block the access of water to backbone carbonyl groups, particularly in the i and i-4 positions (Luo & Baldwin 1999). Examination of a series of basic side chains containing 1 - 4 methylene groups found that helical propensity increased with increasing side chain length (Padmanabhan *et al.* 1996). This suggests that polar and charged side chains are destabilizing due to competition with the peptide backbone for hydrogen bonds.

α-Helical propensity has been shown to have an effect on coiled-coil stability. Gly to Ala substitutions in **b** and **f** positions of GCN4-p1 caused stability increases of 0.7 - 1.0 kcal/mol per substitution (Sosnick *et al.* 1996, Zitzewitz *et al.* 2000). Kwok *et al.* (1998) found an excellent correlation between coiled-coil stability and the α-helical propensity of substituted residues, but only when the substitutions were made in solvent-exposed positions. Substitutions in the hydrophobic core were dominated by hydrophobicity and packing interactions.

Oligomerization state

The oligomerization state of coiled-coils is dominated by packing interactions in the hydrophobic core (Harbury *et al.* 1993, Tripet *et al.* 2000, Wagschal *et al.* 1999b). This is in contrast to globular proteins, where the overall fold is insensitive to packing interactions, though mutations in the hydrophobic core can cause rearrangements in side chain packing over long distances (Lazar & Handel 1998). A series of GCN4 analogs were made in which the entire hydrophobic core was replaced with a single type of hydrophobic residues (I, L or V) at positions **a** and **d**, resulting in a set of coiled-coils that were 2, 3, and 4-stranded (Harbury *et al.* 1993). This was explained in terms of packing interaction of core residues. Dimeric coiled-coils have parallel **a-a′** and perpendicular **d-d′** layers (Figure 1-3), while tetramers have the reversed situation (perpendicular **a-a′** and parallel **d-d′** layers). Both the **a** and **d** layers of trimers have acute packing. In general, Ile is preferred for parallel packing, Leu is preferred for perpendicular packing, and Val shows little preference (Harbury *et al.* 1993). These results were used to develop a computer program, SCORER, which predicts coiled-coil oligomerization state based on these amino acid frequencies (Woolfson & Alber 1995). It has since been found that it is not necessary to change the entire hydrophobic core – substitution at even single **a** or **d** position can change coiled-coil oligomerization state (Tripet *et al.* 2000, Wagschal *et al.* 1999b). The placement of large (Leu) versus small (Ala) residues has also been shown to affect oligomerization state (Monera *et al.* 1996a). The placement of alanine residues in the same layer promoted the formation of two-stranded coiled-coils because a four-stranded coiled-coil would be destabilized by a large cavity in the hydrophobic core. In contrast, the placement of alanine residues in different layers promoted the formation of four-stranded coiled-coils, which have a greater amount of buried surface area.

Hydrophilic residues also play important roles in determining the oligomerization state of coiled-coils. This was first observed in GCN4, which has an **a** position Asn that forms a hydrogen bond buried in the hydrophobic core (O'Shea *et al.* 1991). This **a** position Asn was found to specify a parallel, two-stranded structure, though at a thermodynamic cost. It is extremely destabilizing to have such a hydrophilic residue in the core if it cannot form a hydrogen bond, which is only possible in a two-stranded structure. Analogs with all-leucine cores were more stable, but formed a mixture of parallel and antiparallel tetramers (Lumb & Kim 1995a). Other experiments have shown that Arg and Lys specify for dimers at both **a** and **d,** Gln specifies for trimers when at **a**, Thr specifies for trimers when at **d**, and Tyr specifies for trimers when at **a** and dimers when at **d** (Akey *et al.* 2001, Campbell & Lumb 2002, McClain *et al.* 2002, Tripet *et al.* 2000, Wagschal *et al.* 1999b). Removal of a single **g-e′** ion pair via an Arg-to-Gln substitution caused a change in oligomerization state from trimer to tetramer (Beck *et al.* 1997). Solvent condition have also been shown to play a role. A two-heptad de novo designed coiled-coil was observed to be dimeric in low salt buffer (150 mM NaCl) but trimeric in high salt (2 M NaCl) (Burkhard *et al.* 2000b). Ligand binding can also direct oligomerization state. The binding of benzene to a hydrophobic core cavity induced a switch from a dimer to a trimer (Gonzalez Jr. *et al.* 1996). An HSF/GCN4 chimeric protein was dimeric in solution, but bound to its target DNA sequence as a trimer (Drees *et al.* 1997).

Orientation

Both parallel and antiparallel coiled-coils are found in nature, although more parallel structures have been solved to date. The core of an antiparallel coiled-coil is made up of mixed **a-d′** and **d-a′** layers (Figure 1-3) and packing angles that are somewhat in between those of parallel and perpendicular (Walshaw & Woolfson 2001b). Perhaps because of this, a greater diversity of residues are found at all heptad positions in antiparallel coiled-coils (Walshaw & Woolfson 2001b). When all other interactions are equal, an antiparallel orientation appears to be slightly more stabilizing, due to interactions between the helix dipoles (Monera *et al.* 1993, 1994a). Coiled-coil orientation can be specified through the placement of large and small residues in the hydrophobic core to form complementary surfaces (Betz *et al.* 1997, Monera *et al.* 1996b). Electrostatic interactions at positions **e** and **g** can direct coiled-coil orientation, based on maximizing attractions and minimizing repulsions (Monera *et al.* 1993, 1994a). Hydrophilic residues, such as Asn, can specify orientation when hydrogen bonds are possible in one orientation, but not in the other (Lumb & Kim 1995a, Oakley & Kim

1998). Interestingly, an **a** position Asn and charge repulsion at positions **e** and **g** appear to have similar effects on stability. When a coiled-coil was designed in which the presence of Asn in the core specified one orientation and charge repulsions at positions e and g specified the opposite orientation, the resulting sequence had no specificity and formed a mixture of parallel and antiparallel coiled-coils (McClain *et al.* 2001).

Specificity of Association

Coiled-coils can form between identical (homo-association) or different (hetero-association) proteins. The specificity of association is critical to biological function. For example, there are large numbers of B-ZIP transcription factors present in the nucleus at any given time, and their association must be regulated. It is well documented that i to i′+5 electrostatic interactions can control association in both natural (Baxevanis & Vinson 1993, Lavigne *et al.* 1995, Moll *et al.* 2000) and designed (Chao *et al.* 1996, 1998, Graddis *et al.* 1993, Vinson *et al.* 1993, Zhou *et al.* 1994b) coiled-coils. Similar electrostatic interactions have been used to design coiled-coils that are heterotrimeric (Nautiyal *et al.* 1995) and heterotetrameric (Fairman *et al.* 1996, Vu *et al.* 2001). The recent completion of the human and *Drosophila* genomes has allowed a comparison of all B-ZIP protein sequences. Their patterns of charged residues at positions **e** and **g** and the presence or absence of Asn at position **a** was used to predict all potential homo- and heterodimerization partners in this family of proteins (Fassler *et al.* 2002, Vinson *et al.* 2002).

Hetero-association can also be specified through the design of complementary surfaces in the hydrophobic core. A de novo designed coiled-coil containing Ala and Leu in the hydrophobic core preferentially hetero-associated with an all Leu peptide (Zhu *et* *al.* 1992b). When Ala is in the **a** position, two Leu-Ala interaction are preferred to one Ala-Ala interaction. Heterotrimer association has also been specified through the design of Ala-Ala-Trp (Kiyokawa *et al.* 2001) and Ala-Ala-cyclohexanylalanine (Schnarr & Kennan 2001, 2002) layers. An interesting recent paper examined a series of heterodimeric coiled-coils and found that interactions between identical hydrophobic residues (I, V, and L) were more stabilizing than between different residues (Acharya *et al.* 2002). In contrast, when Lys was found in an **a** position, it was more stabilizing for it to interact with any of the other residues (A, I, L, N or V) in the neighbouring coiled-coil. Avoidance of **a** position Lys residues could be another mechanism for preventing homo-association.

C. Coiled-coil folding

Protein folding

Proteins fold into specific three-dimensional shapes that are critical to their function. The question of how an amino acid sequence specifies a particular fold has been an area of active research (recently reviewed by Baker 2000, Baldwin & Rose 1999a, 1999b, Bilsel & Matthews 2000, Dinner *et al.* 2000, Honig 1999, Radford 2000). Folding must be a directed process, for a random search for the native fold through all potential conformations would take a near eternity (Levinthal 1968). Protein folding is driven by the enthalpy provided by the hydrophobic force and close packing in the core and is opposed by a loss of conformational entropy of the polypeptide chain upon folding. As enthalpy and entropy are of a similar magnitude, most proteins are only marginally stable, with free energies of 5 – 10 kcal/mol (Honig & Yang 1995, Pace *et al.* 1996).

The process of folding is generally thought to be hierarchic. Early stages involve the transient formation of low stability secondary structural elements. If these small folded segments collide, they can be stabilized through tertiary interactions. Larger folded structures are formed through this process of collision and stabilization until the native fold has been reached. In this model, the early stages of structure formation are thought to be dominated by local contacts. An alternate view holds that the early stages of folding are dominated by hydrophobic collapse, which is influenced more by contacts between residues distant in sequence. It seems most likely that both processes are occurring, if not simultaneously, then at least in the early stages of folding. The process of folding is often pictured as a funnel (Figure 1-4A). Conformational changes that result in a more native-like structure are energetically favourable, and, so, are more likely to occur. This is often visualized as the protein moving down the well.

The equilibrium denaturation experiment has been a mainstay in the study of protein folding. In this technique, the protein is monitored, typically by spectroscopy, while exposed to increasing temperature or increasing concentrations of denaturant. In many proteins, the resulting denaturation curve has a sigmoidal shape, as seen in Figure 1-4B. This is because protein folding is highly cooperative and the vast majority of protein molecules are in the folded or unfolded state, with a negligible population of partially folded molecules. This is referred to as a two-state unfolding mechanism. At any stage in the denaturation process, the ratio of folded and unfolded molecules is described by an equilibrium constant.

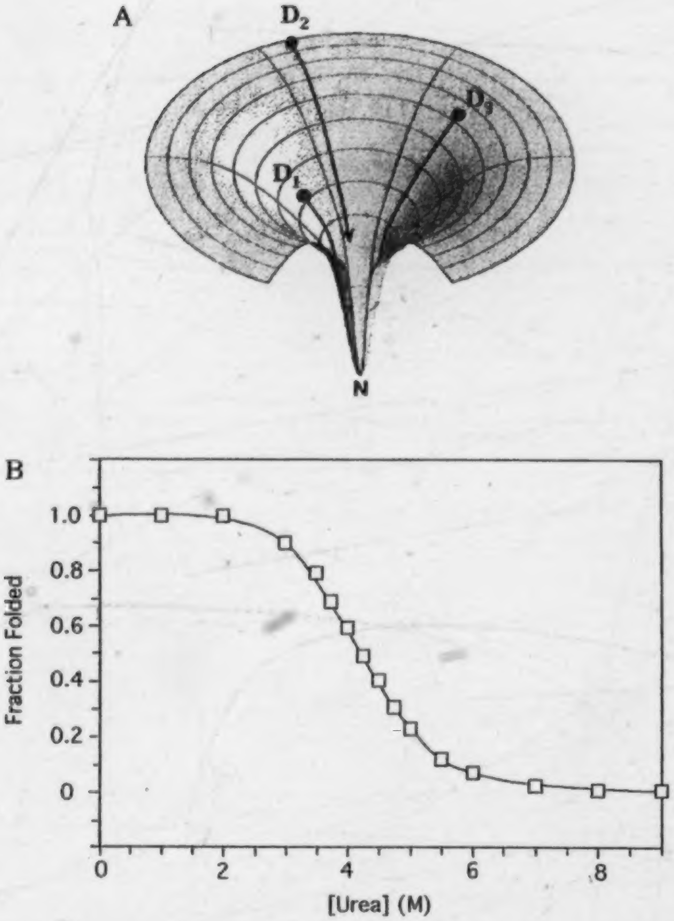

Figure 1-4. Protein folding. **A)** Funnel-shaped protein energy landscapes, which can be smooth or rough (Dill & Chan 1997). **B)** An example of a two-state denaturation curve, adapted from Kohn *et al.* (1998a).

Short Coiled-coils

Coiled-coil folding falls into two distinct categories: short coiled-coils (20-40 residues), such as GCN4, and long coiled-coils (>100 residues), such as tropomyosin. Short coiled-coils fold extremely quickly and follow either two-state (1) or multi-state (2) mechanisms:

(1) $M + M \longleftrightarrow D$ (2) $M + M \longleftrightarrow D^* \longleftrightarrow D$

Generally, single α-helices are extremely unstable in aqueous solution. In the two-state mechanism, the unfolded monomers associate to form the fully-folded coiled-coil in a single step. This type of folding has been observed for both GCN4 and de novo designed coiled-coils (Durr *et al.* 1999, Sosnick *et al.* 1996, Wendt *et al.* 1995, 1997, Zitzewitz *et al.* 1995). In the multi-state mechanism, the unfolded monomers interact to form a partially folded intermediate which then undergoes a conformational rearrangement to form a fully-folded coiled-coil. Multi-state kinetics have also been observed for both native and de novo designed coiled-coils (Dragan & Privalov 2002, Durr & Bosshard 2000, Jelesarov *et al.* 1998, Knappenberger *et al.* 2002, Wendt *et al.* 1994, 1995). Interestingly, the folding mechanism appears to be very sensitive to sequence, for a single substitution has been observed to change the folding mechanism from two-state to multi-state. Wendt *et al.* (1995) designed a series of de novo coiled-coils with a position alanine and asparagine substitutions in an otherwise all leucine hydrophobic core. Approximate half of the analogs folded via two-state kinetics, while the others folded via multi-state kinetics. Holzter and co-workers investigated folding mechanisms by monitoring the chemical shifts of $^{13}C^{\alpha}$-labeled sites of GCN4-p1 analogs. They found that the native sequence unfolded via a two-state mechanism, but analogs with quite conservative substitutions (Lys was substituted for Arg and His) unfolded via multi-state mechanisms (d'Avignon *et al.* 1998, 1999, Holtzer *et al.* 1997, 2001b, Lovett *et al.* 1996). Others found that the placement of an **a** position asparagine residue in the second vs. the third heptad changed folding from two-state to multi-state mechanisms (Zhu *et al.* 2001). It is not yet understood what causes coiled-coils to fold by one mechanism versus another, or why this is so sensitive to sequence changes.

Even though numerous coiled-coils have been observed to fold via multi-state kinetics, the two-state mechanism is still a useful approximation for the analysis of equilibrium denaturation studies. Coiled-coil folding is so fast that intermediates are extremely short-lived and do not accumulate, so an overwhelming majority of molecules are either in the folded or unfolded states. Computational modeling of coiled-coil folding has provided useful insights (Mohanty *et al.* 1999, Qian 1994, Vieth *et al.* 1994). Typically, the simulations start with two random coils in which short helical stretches transiently form. However, if the helical regions collide, the helical structure is stabilized and propagates the entire length of the molecule. Small rearrangements then yield the final dimeric coiled-coil. This sequence of events can be considered to be two-state as long as the two-states are recognized to be ensembles of similar, but not identical, conformations. The unfolded state is largely random coil, but does include transient α-helical structure. The folded state is primarily two-stranded α-helical coiled-coil, but does include small amounts of unfolded polypeptide, especially at the ends of the helices.

Long coiled-coils

The folding of long coiled-coils, frequently of 100 residues length or more, is considerably more complex than that experienced by short coiled-coils. Tropomyosin has been long known to fold with multi-state kinetics, comprised of, at minimum, a rapid association phase and a slower rearrangement step (Holtzer & Holtzer 1990, Mo *et al.* 1991, O'Brien *et al.* 1996). It is not uncommon for long coiled-coils to have distinct regions of higher and lower stability, as is seen in kinesin (Tripet *et al.* 1997) and tropomyosin (Holtzer *et al.* 1994). Many coiled-coils are autonomous folding units, subdomains that cooperatively fold independently of the rest of the polypeptide chain (Peng & Wu 2000). Others, however, require interactions with nearby regions of the protein in order to stably fold (Tripet & Hodges 2002). A long standing puzzle has been to explain why long fragments (often 80 to 100 residues) of these proteins do not fold as stable coiled-coils, despite the presence of clear heptad repeats (Holtzer *et al.* 1994, Holtzer & Holtzer 1991, Paulucci *et al.* 2002, Steinmetz *et al.* 1998, Trybus *et al.* 1997). This led to the discovery of a discrete region, named a "trigger sequence", that was required for the folding of cortexillin, an actin cross-linking protein (Kammerer *et al.* 1998, Steinmetz *et al.* 1998). Subsequently, trigger sequences have also been identified in GCN4 (Kammerer *et al.* 1998) and in the human macrophage scavenger receptor (Frank *et al.* 2000). These trigger sequences were suggested to act as nucleation sites in the folding of coiled-coils. Recent experiments, however, have demonstrated that they function by increasing the stability of the coiled-coil sequence to the threshold required for folding (Lee *et al.* 2001). It is not necessary for these stabilizing interactions to be clustered into a trigger sequence - the same effect can be obtained by scattering them throughout the coiled-coil sequence, evidence that the stability of the entire coiled-coil is the critical factor. However, trigger sequences have been identified in a number of different proteins, suggesting that there is a functional advantage to this arrangement.

They could delay folding of the emerging protein during ribosomal synthesis, or facilitate regulation through disruption of labile regions via protein interactions. However, care must be taken when identifying regions as trigger sequences. The C-terminal half of tropomyosin contains a match with the consensus trigger sequence, but this region does not fold independently. Instead, folding depends on the presence of residues 260-284, which have no resemblance to the consensus sequence (Paulucci *et al.* 2002).

D. Design of the E/K Heterodimeric Coiled-coil

Heterodimeric coiled-coils have great potential for use in a wide variety of protein engineering and biotechnological applications that require specific heterodimerization. Examples include affinity purification, oligomerization of antibody Fab fragments, and the targeting and delivery of drugs to particular organs or tissues (Hodges 1996, Muller *et al.* 2000). For many of these applications, there are significant advantages to the use of de novo designed rather than native coiled-coils. De novo coiled-coils can be designed to have binding affinities in a desired range, and may be considerably greater than that of most native sequences (transcription factors typically have affinities in the range of 10^5 – 10^8 M). They do not have naturally occurring binding partners, which greatly reduces the number of undesirable interactions. It is possible to design a set of related applications using a single coiled-coil system, simplifying experimental design. Our laboratory has designed a heterodimeric coiled-coil, named the E/K coil, to have these and additional advantages (Chao *et al.* 1996, 1998).

The E/K heterodimeric coiled-coil was designed according to principles identified by over a decade of research in the design and folding of coiled-coils. Specificity was obtained through the placement of glutamic acid in all **e** and **g** positions in the E-coil and lysine in all **e** and **g** positions in the K-coil (Figure 1-5). The potential E-coil and K-coil homodimers are both destabilized by ten i to i′+5 electrostatic repulsions, while the E/K heterodimer is stabilized by ten i to i′+5 electrostatic attractions. Valine and leucine were chosen for the **a** and **d** positions, because they are abundant in native sequences and have been shown to form stable hydrophobic cores (Hu *et al.* 1990, Tripet *et al.* 2000, Wagschal *et al.* 1999b). Alanine was chosen for position **c** because its has the highest α-helical propensity, stabilizing helical structures (Lyu *et al.* 1990, O'Neil & DeGrado 1990, Yang *et al.* 1997, Zhou *et al.* 1994c). Serine, with its small polar side chain was chosen for position **b** to increase peptide solubility. Position **f** was filled with Lys in the E-coil and with Glu in the K-coil in order to reduce the net charge of the molecule and improve solubility.

Characterization of the E/K-coil showed it to have the characteristics of a stable, specific heterodimeric coiled-coil (Chao *et al.* 1996, 1998). Circular dichroism spectroscopy, which is sensitive to secondary structure, showed that the E and K-coils were random coils individually, but, when mixed in a 1:1 molar ratio, formed an α-helical coiled-coil. This complex is very stable, with a denaturation midpoint of 3.9 M GdnHCl. Sedimentation equilibrium experiments showed the E/K-coil to fit a monomer-dimer-tetramer association, with the dimeric species being preferred at concentrations below 0.46 mM. Chemical denaturation, analytical ultracentrifugation, and BIAcore analysis all yielded dissociation constants in the range of 10^{-9} M. BIAcore experiments showed that this was due to fast association ($4.5 \times 10^{5}\ M^{-1}s^{-1}$) and slow dissociation (2.1

A Ac-EVSALEKEVSALEKEVSALEKEVSALEKEVSALEK-NH_2
Ac-KVSALKEKVSALKEKVSALKEKVSALKEKVSALKE-NH_2

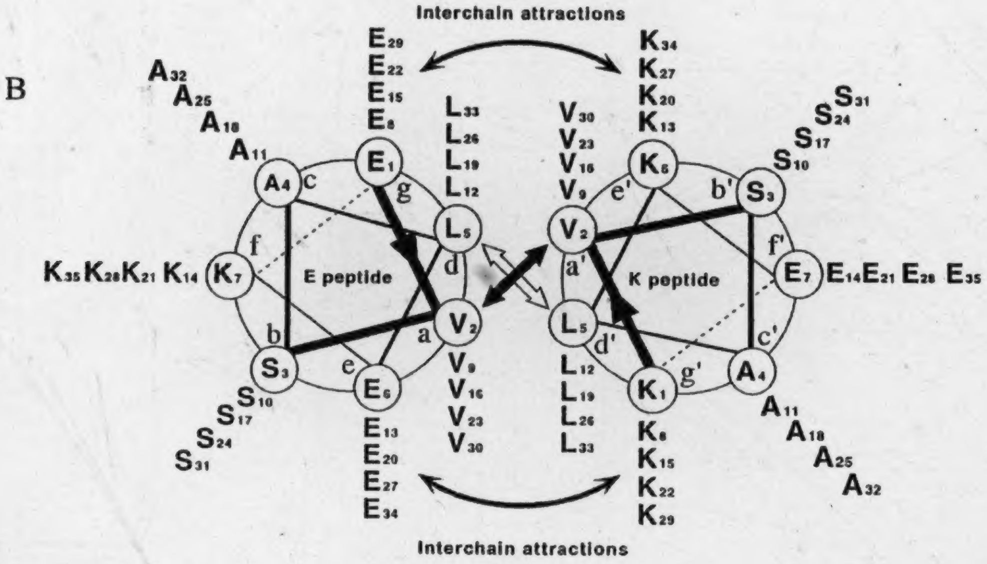
B
Interchain attractions
E29 E22 E15 E8
K34 K27 K20 K13
A32 A25 A18 A11
S31 S24 S17 S10
L33 L26 L19 L12
V30 V23 V16 V9
E1
g
L5
A4
c
f
K35 K28 K21 K14
K7
E peptide
d
V2
a
b
S3
e
E6
S10 S17 S24 S31
E13 E20 E27 E34
V9 V16 V23 V30
K8
e'
b'
S3
V2
a'
f'
K peptide
E7
E14 E21 E28 E35
L5
d'
c'
A4
K1
g'
L12 L19 L26 L33
K8 K15 K22 K29
A11 A18 A25 A32
Interchain attractions

Figure 1-5. The E/K heterodimeric coiled-coil. **A)** Amino acid sequences of the E-coil (upper) and K-coil (lower) peptides. **B)** Helical wheel representation, with the polypeptide chain propagating into the page from the N- to the C-terminus. The hydrophobic residues at positions **a**, **a′**, **d** and **d′** interact and are mainly responsible for the formation and stability of the coiled-coil. Potential electrostatic attractions at positions **g**-**e′** or **g′**-**e** provide additional stability and specify heterodimerization rather than homodimerization.

x 10^{-4} s^{-1}), making the E/K-coil suitable for use as an immobilization domain. The E and K-coils were also shown to be resistant to degradation when incubated in human serum for a 24 hour period. When expressed as fusions with target proteins, the small size and random structure of the E and K-coils will be an advantage, as they are unlikely to cause steric problems associated with folding. Detection is simple with the use of a biotinylated K-coil and streptavidin-alkaline phosphatase, as no expensive antibodies are required. The use of a single system for immobilization greatly reduces the time required for optimization of experimental conditions for each protein.

The E/K heterodimeric coiled-coil has been successfully adapted for use as a capture/display system for biosensors, such as the BIAcore. In this technique, the ligand molecule is immobilized to the surface of a chip and a solution containing the analyte flows across it (Karlsson *et al.* 1991). Binding of the analyte to the ligand generates a signal through the phenomenon of surface plasmon resonance (SPR). Much better results are obtained when the ligand is immobilized by a tag in a specific orientation, rather than randomly through surface amines. The E/K-coil has significant advantages over existing immobilization processes, which have problems such as heterogeneity or poor stability. The E/K-coil was successfully used for the immobilization of peptides derived from troponin I in order to measure troponin C binding, as illustrated in Figure 1-6 (Tripet *et al.* 2002). E-coil was chemically conjugated to the troponin I peptides and immobilized to a K-coil derivatized surface. The E/K-coil provided a stable surface suitable for the measurement of complex binding kinetics. Because the interaction of E and K-coils are highly reproducible, the amount of ligand immobilized could be finely controlled. The

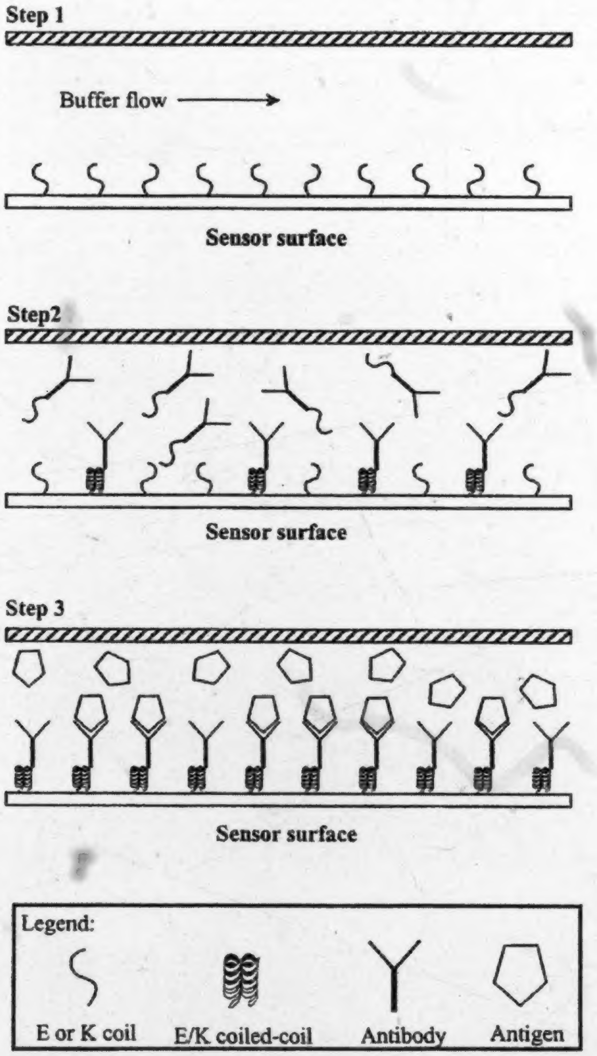
Step 1
Buffer flow
Sensor surface
Step2
Sensor surface
Step 3
Sensor surface
Legend:
E or K coil
E/K coiled-coil
Antibody
Antigen

Figure 1-6. Use of the E/K-coil as an immobilization domain for biosensor experiments. In this application, one of the two peptides (step 1) is first immobilized on the sensor surface. The second peptide is conjugated to an antibody, for instance, and injected over the sensor surface (step 2). Formation of the heterodimeric coiled-coil generates an antibody surface for biosensing (step 3). In theory, the sensor surface can be used repeatedly as long as it is charged with a sufficient amount of coiled-coil peptide conjugate. The figure is adapted from Chao *et al.* (1998).

same K-coil surface was used to measure the binding of a number of different E-coil conjugated peptides.

The other application that successfully employed the E/K-coil was an expression and affinity purification system (Figure 1-7). A fusion of the *Pseudomonas aeruginosa* PAK-pilin peptide (residues 128-144 of the pilin protein) and E-coil was constructed and expressed in *E. coli* (Tripet *et al.* 1996). It was purified by affinity chromatography on a K-coil column to very high purity. Because the E/K coil is stabilized by both hydrophobic and electrostatic interactions, it was stable enough to withstand washing with high salt (0.5 M KCl) and then with organic solvent (80% acetonitrile). Elution was carried out with low pH (0.1% aqueous trifluoroacetic acid) and high levels of organic solvent (50% acetonitrile).

Similar design principles have been used by other groups for the design of heterodimeric (Graddis *et al.* 1993, Jelesarov & Bosshard 1996, Moll *et al.* 2001, O'Shea *et al.* 1993, Wendt *et al.* 1997), heterotrimeric (Nautiyal & Alber 1999, Nautiyal *et al.* 1995), and heterotetrameric coiled-coils (Fairman *et al.* 1996, Vu *et al.* 2001). Interestingly, a “library vs. library” genetic screen yielded heterodimeric coiled-coils which contained a mixture of electrostatic attractions and repulsions (Arndt *et al.* 2000, Pelletier *et al.* 1999). Attempts to improve the design by eliminating the repulsions and introducing the maximum number of attractions increased the stability but decreased in vivo expression, indicating that as yet unknown factors determine expression efficiency (Arndt *et al.* 2002). De novo designed coiled-coils have been used in a number of protein engineering applications, including the directed assembly of complexes of Fab fragments (Arndt *et al.* 2001), interleukin-2 receptors (Wu *et al.* 1995, 1999), and MHC

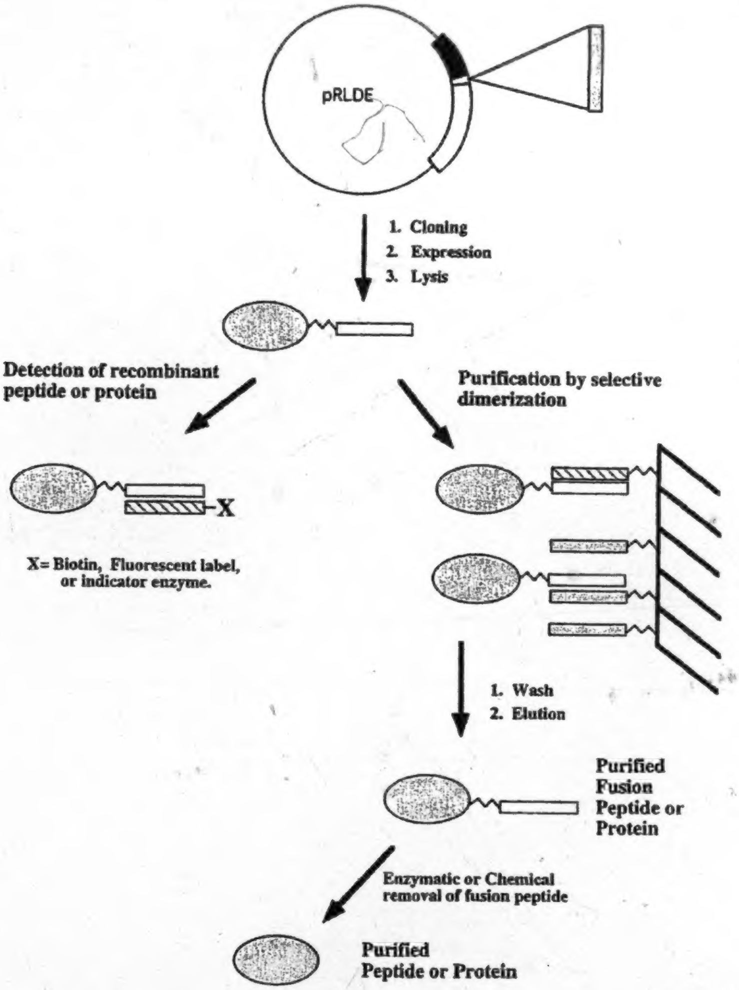
pRLDE
1. Cloning
2. Expression
3. Lysis
Detection of recombinant peptide or protein
Purification by selective dimerization
X
X= Biotin, Fluorescent label, or indicator enzyme.
1. Wash
2. Elution
Purified Fusion Peptide or Protein
Enzymatic or Chemical removal of fusion peptide
Purified Peptide or Protein

Figure 1-7. The use of the E/K coiled-coil in an expression and purification system for recombinant proteins. The system consists of an expression vector pRLDE and a K-coil affinity column. The expression vector pRLDE codes for one copy of the E-coil with a signal peptide that directs the fusion product to the periplasmic space of the bacteria. The fusion protein can be released from the bacteria by osmotic shock and the lysate can be loaded onto the K-coil affinity column directly after clarification by centrifugation or filtration. The loaded column is then washed with appropriate buffer and the desired product can be eluted. If necessary, chemical or enzymatic cleavage can be carried out to remove the tag. The figure is adapted from Tripet *et al.* (1996).

receptors (Scott *et al.* 1996). In addition, native coiled-coil sequences have been used to direct the assembly of Fab fragments (Kostelny *et al.* 1992) and the extracellular domains of growth hormone receptors (Behncken *et al.* 2000). The use of coiled-coils for these types of applications has been recently reviewed (Muller *et al.* 2000, Rieker & Hu 2000).

The next step in the design of this heterodimeric coiled-coil is to modify its stability while retaining high specificity. The elution step in our affinity chromatography procedure worked extremely well, but could be too harsh for some applications. It would be a great advantage to have a set of heterodimeric coiled-coils with a wide range of stabilities, allowing us to tailor the E/K system for the needs of a particular application. In order to achieve this, the sequences of the E and K coils will be modified. Sequence features amenable to change are the nature of the hydrophobic core, α-helical propensity and the chain length.

E. Native Coiled-coils

An important complementary approach to understanding the structure and folding of coiled-coils is to attempt to explain the behaviour of native coiled-coils on the basis of the principles learned from model peptide studies. We have examined regions predicted to form coiled-coils in two proteins: dynamin, which is involved in the process of endocytosis, and dynein, a eukaryotic motor protein.

The prediction of coiled-coil formation is based on the presence of a heptad repeat, and is usually performed by computer prediction programs. The earliest of these is COILS, which is based on the frequency of occurrence of each amino acid in a database of coiled-coil sequences (Lupas *et al.* 1991). This statistical approach was refined in the program PAIRCOIL, which is based on pairwise correlations between residues occurring at i, i+1, i+2, and i+4 heptad repeat positions (Berger *et al.* 1995). A different approach was taken for the design of the program STABLECOIL, which is based upon experimentally determined values for the contribution of each amino acid to stability in the hydrophobic core and through α-helical propensity (Tripet & Hodges 2001). Despite many successful predictions, all of these programs suffer from significant shortcomings. None are able to predict hetero-association or parallel versus antiparallel orientation. Furthermore, we are not yet able to predict whether a coiled-coil sequence contains a nucleation site for folding. For example, remarkably long fragments (80 - 100 residues) from a number of coiled-coil proteins do not fold in isolation (Holtzer *et al.* 1994, Holtzer & Holtzer 1991, Paulucci *et al.* 2002, Steinmetz *et al.* 1998, Trybus *et al.* 1997).

Many more sequences and structures are known for parallel coiled-coils, and, consequently, far more is known about the interactions governing their structure and folding. Antiparallel coiled-coils differ in at least two important respects: their hydrophobic cores are composed of mixed **a-d′** and **d-a′** layers and a much broader distribution of amino acids are found at each heptad position (Walshaw & Woolfson 2001b). The role of the many destabilizing residues in the hydrophobic core is not yet known. In addition, we still do not understand the interactions that control stability, oligomerization state and specificity of association. Clearly, an experimental approach will be necessary for the study of native coiled-coils for some time.

Dynamin

Dynamin, discovered in 1989 (Shpetner & Vallee 1989), is a large GTPase that is required for receptor-mediated endocytosis (recently reveiwed in Danino & Hinshaw 2001, Sever 2002). It has a multi-domain structure, composed of an N-terminal GTPase domain, a middle domain, a pleckstrin-homology domain (PH), and GTPase effector domain (GED), and a C-terminal proline/arginine rich domain (PRD). The GED contains two regions predicted to form coiled-coils. Dynamin undergoes two distinct phases of self-assembly: first to tetramers (Muhlberg *et al.* 1997) and then to large helical arrays (Hinshaw & Schmid 1995, Shpetner & Vallee 1989, Takei *et al.* 1995). Dynamin's mechanism of action is still not known, although the two prominent theories are that it is a mechanochemical enzyme that "pinches off" vesicles, or that it is a more traditional signaling molecule (Danino & Hinshaw 2001, Sever 2002). A more detailed description of the structure and function of dynamin can be found in the introduction to Chapter VII.

Dynein

Transportation within a cell is a complex task; the cytoplasm is far too viscous and crowded to allow simple diffusion of large organelles and macromolecular complexes. Instead, a family of proteins has evolved which is capable of transforming chemical energy into mechanical energy that is harnessed to provide motion. These proteins transport membrane organelles, protein complexes, nucleic acid/protein complexes and other types of cargo along the cell cytoskeleton (Karcher *et al.* 2002). Eukaryotes have three types of motor proteins - myosins, kinesins, and dyneins. Myosins are responsible for movement along the actin cytoskeleton, including that which produces muscle contraction. Kinesins produce both anterograde and retrograde transport along microtubules (plus and minus end directed). Dyneins are responsible for retrograde movement along the microtubules (minus end directed). High resolution structures have been determined for both myosins and kinesins and considerable progress has been made in understanding their mechanisms of action (Hirose & Amos 1999, Vale & Milligan 2000). In contrast, progress in understanding dynein has been much slower, due to the challenge posed by its great size and structural complexity.

Axonemal dynein was discovered by Gibbons and Rowe (1965) and is responsible for the movements of flagella and cilia. The cytoplasmic form of dynein was discovered by Vallee and coworkers (Mikami *et al.* 1993, Paschal *et al.* 1987b). Cytoplasmic dynein is involved in a broad array of biological processes, including the retrograde transport of membranous organelles, the organization and orientation of the mitotic spindle, maintaining the centrosomal localization of the Golgi complex, the transport of endocytic vesicles, and the transport of viral particles to the nucleus during infection (Hirokawa 1998, Kamal & Goldstein 2000, Karki & Holzbaur 1999, Ploubidou & Way 2001, Vallee & Gee 1998). Surprisingly, a single dynein motor protein is responsible for this diverse set of functions. The mechanisms which target dynein to a particular function are thought to involve accessory proteins and are a subject of active research.

The structure and complex organization of dynein has been extensively reviewed (Asai & Koonce 2001, Gee & Vallee 1998, Hirokawa 1998, Vallee & Gee 1998). Dynein is an extremely large protein complex (1.2 - 2 x 10^6 Da), composed of a large number of subunits, including heavy chains (HCs, 530 kDa), intermediate chains (ICs, 74 kDa), light intermediate chains (LICs, 55-60 kDa), and light chains (~ 8 kDa) (Figure 1-

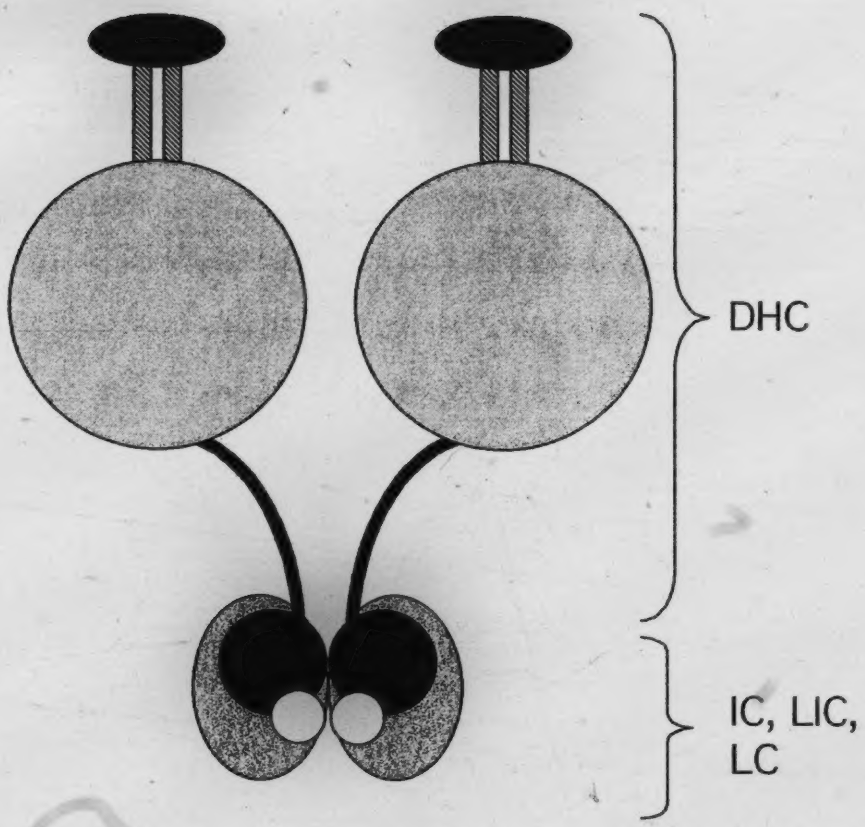

Figure 1-8. Dynein is a multi-protein complex composed of heavy chains (DHC), intermediate chains (IC), light intermediate chains (LIC), and light chains (LC).

8). The heavy chain contains the ATPase, microtubule-binding, and force production activities. The ICs, LICs, and LCs are thought to be involved in regulation and targeting of dynein to specific cargo molecules. Many, if not all, dynein functions also require association with dynactin, a complex of at least ten different polypeptides (actin, actin capping protein α and β-subunits, Arp1, dynamitin, p150, p135, p62, p27 and p24) which mediates interactions with cargo molecules (Hirokawa 1998, Karki & Holzbaur 1995). Electron microscopy has shown dynein to contain large globular particles with extended tails, often resembling a two-headed bouquet. These particles have been observed to attach to microtubules through a slender stalk, called a B-link, that is 10-12 nm in length (Amos 1989, Goodenough & Heuser 1982, 1984). Image averaging of electron micrographs has resolved the globular HC head domain into 7 smaller globular subdomains, surrounding a central cavity (Samso *et al.* 1998).

The dynein heavy chain is a remarkably large polypeptide that is more than 4600 residues in length and contains a number of functional domains (Figure 1-9). The N-terminal third corresponds to the "tail" seen in electron micrographs and is the site of numerous protein interactions, including HC dimerization (residues 629-780), IC binding (residues 446-701), and LIC binding (residues 646-800) (Habura *et al.* 1999, Tynan *et al.* 2000). These different interactions do not appear to be competitive, suggesting that the individual binding sites may be topologically distinct. The C-terminal two-thirds of the HC contains the ATPase activity and corresponds to the globular head domain observed by EM (Gee *et al.* 1997, Koonce 1997). The dynein HC has been identified as a member of the AAA family of ATPases (Neuwald *et al.* 1999). Six AAA modules are found in this C-terminal region and are predicted to form a ring structure similar to the hexameric

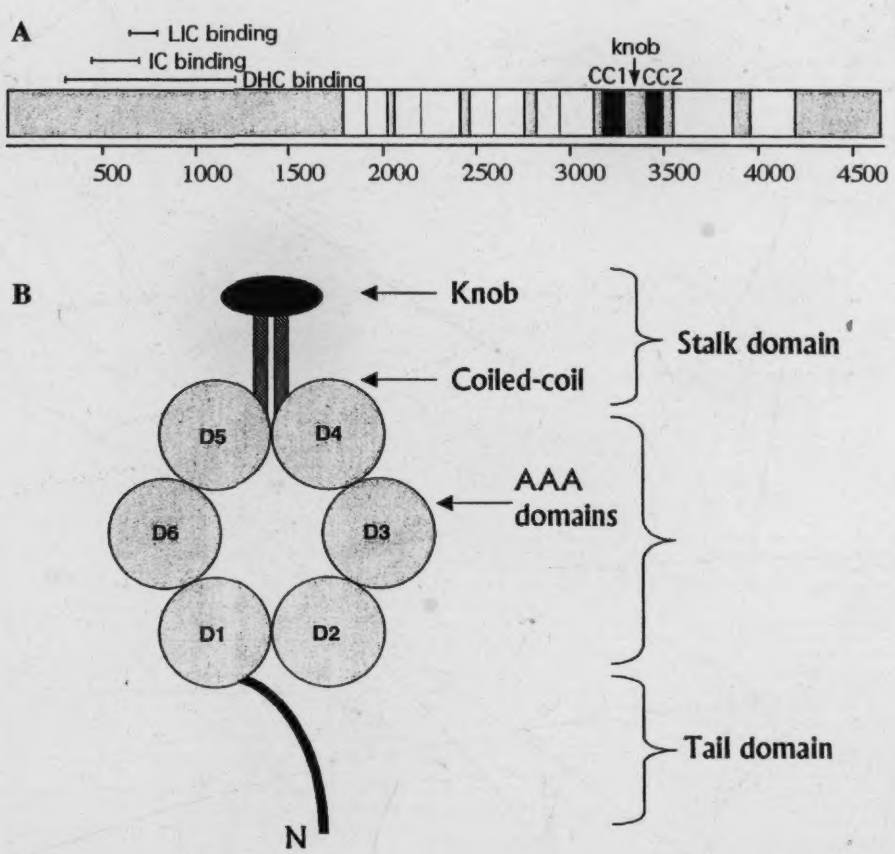
A
LIC binding
IC binding
DHC binding
knob
CC1
CC2
500
1000
1500
2000
2500
3000
3500
4000
4500
B
Knob
Coiled-coil
Stalk domain
D5
D4
D6
D3
D1
D2
AAA domains
Tail domain
N

Figure 1-9. Domain organization of the dynein heavy chain. **A)** The DHC sequence is represented as a bar. The six AAA domains are marked by white boxes, the P-loop motifs are marked by gray lines, the stalk coiled-coil regions are represented by black boxes, and the regions important for protein interactions are marked by horizontal lines. **B)** The domains of the DHC are represented as a cartoon. The figure is adapted from King (2000a).

rings formed by other AAA proteins (Vale 2000). The first four AAA modules have recognizable P-loops, a nucleotide-binding motif (Asai & Koonce 2001, Gee & Vallee 1998, Milisav 1998). All four P-loops bind ATP molecules in a cooperative manner, with dissociation constants ranging from 30 - 80 μM, although only the first, P1, has ATPase activity (Mocz & Gibbons 1996). The fifth and sixth AAA modules are highly degenerate and do not have recognizable P-loops. A homology model of this region of the sea urchin outer arm axonemal β DHC has been created (Mocz & Gibbons 2001). Finally, the function of the C-terminal region is not known.

Microtubule binding occurs in a 125-residue globular domain, identified in 1997 (Gee *et al.* 1997, Koonce 1997). Flanking this domain were two long regions (approximately 100 residues) predicted to form coiled-coils. Gee *et al.* (1997) proposed that this region formed an intramolecular, antiparallel coiled-coil that projects from the globular ATPase domain. This places the microtubule-binding domain at the tip of an extended stalk, at a considerable distance from the site of ATP hydrolysis. Sequence comparison has found similar predicted coiled-coil regions in axonemal and cytoplasmic HCs from diverse organisms including alga (*Chlamydomonas*), protozoa (*Tetrahymena*), sea urchin, rat, and humans. Although the sequence conservation is relatively low (~ 33%), the length of the predicted coiled-coils does appear to be conserved, suggesting an important role in function or structural organization (Asai & Koonce 2001, Vallee & Gee 1998). Other supporting evidence comes from electron microscopy, where the length of the B-link, 10-12 nm (Goodenough & Heuser 1982, 1984), is similar to that predicted for a coiled-coil of 100 residues length (120 Å, or 12 nm). The model of the stalk as an antiparallel coiled-coil has been well received and is supported by sequence and EM data.

However, there is no structural or biophysical data to date that conclusively proves the existence of a coiled-coil in this region.

The kinetics of the dynein ATPase cycle have been investigated for both axonemal (Johnson 1983, Omoto & Johnson 1986) and cytoplasmic dynein (Shpetner *et al.* 1988). The HC binds to ATP, causing a rapid release of the HC from the microtubule. One molecule of ATP is then hydrolyzed, yielding ADP, which remains bound, and phosphate, which is released. The dynein-ADP complex then binds to the microtubule, which stimulates ADP release. ADP release is thought to be both the rate limiting step and the point at which the power stroke occurs. Axonemal dynein has a relatively high basal ATPase rate, 0.15-0.38 μmol ATP/mg per min, which is further increased by the presence of microtubules (Johnson 1983, Omoto & Johnson 1986). In contrast, the basal ATPase activity of cytoplasmic dynein is much lower, 32 nmol ATP/mg per min, and it increases 5.7-fold in the presence of microtubules (Shpetner *et al.* 1988).

Microtubule gliding assays have been an effective technique for demonstrating the ability of dynein to produce force. These results have shown cytoplasmic dynein to have a motor velocity of about 1.2 μm/s (Paschal *et al.* 1987b, Paschal & Vallee 1987). Faster velocities, in the range of 4-10 μm/s, have been observed for axonemal dyneins (Paschal *et al.* 1987a, Sale & Fox 1988, Vale & Toyoshima 1988). Cytoplasmic dynein is quite processive, meaning that it is capable of traveling a considerable distance along a microtubule without dissociating, a necessary characteristic for intracellular transport (Wang *et al.* 1995). In contrast, axonemal dynein has a much lower processivity and microtubule gliding is only observed when axonemal dynein is present at high densities, such as 50 μg/ml, equivalent to approximately 1000 dyneins/μm^2 (Vale *et al.* 1989). This is not surprising, for the axonemal form functions in the large, stable structures of cilia and flagella, where many dynein molecules work in tandem. Intriguingly, an inner arm dynein from *Chlamydomonas* has been found to act processively when only a single DHC is present (Sakakibara *et al.* 1999). This dynein cannot be using a "hand-over-hand" mechanism, as thought to be used by kinesin (Hirose & Amos 1999, Vale & Milligan 2000). An interesting clue to its processivity may lie in recent work showing that the dynactin complex plays an important role in increasing the processivity of dynein, possibly by acting as an additional tether to the microtubule (King & Schroer 2000).

The regulation of dynein, given its numerous and diverse tasks in the cell, is likely to be complex. The diverse and varying ICs, LICs, and LCs present in the dynein complex have been long suspected of playing an important role in the biological targeting of dynein. Before dynein can produce retrograde motion, it must be transported in the anterograde direction to the cell periphery, as cargo. This anterograde motion can be divided into fast and slow components, thought it is not yet clear which motors are responsible. The rate at which the dynein complex is transported has been found to be determined by the presence of particular IC isoforms obtained by alternate splicing and phosphorylation. Dynein containing IC74-2c experienced fast anterograde transport, while dynein containing all other IC74 isoforms experienced slow anterograde transport (Susalka *et al.* 2000). IC74 has also been found to decrease HC ATPase activity; and was found to account for the different levels of ATPase activity in brain and testis dynein (Kini & Collins 2001). Other regulatory mechanisms are believed to include phosphorylation, either directly to the HC or to associated ICs and LCs (King 2000b).

One striking aspect of HC structure is the location of the microtubule-interaction site at the tip of the stalk at a considerable distance from the ATPase active site. This raises two important question: how are changes in the ATPase cycle communicated to the distant microtubule binding site and what is the mechanism of force production? The hexameric ring of AAA domains suggests that a conformational change in the first AAA module (the site of ATP hydrolysis) could be propagated throughout the ring in a concerted conformational change, as seen in other AAA proteins (Bochtler *et al.* 2000). Electron micrographs have shown changes in the shape of dynein particles which are thought to be associated with changes in the ATPase cycle (Goodenough & Heuser 1982, 1984). It is not clear, however, how such a conformational change could be communicated through the stalk to the microtubule-binding domain. The stalk may act as a rigid lever arm or a conformational change could be transmitted through the coiled-coil in order to change the orientation of the binding site with respect to microtubules (Asai & Koonce 2001, Vallee & Gee 1998).

CHAPTER II

Materials and Methods

A. Materials

All solutions were prepared in water from a Milli-Q purification system.

Table 2-1. List of Materials

Reagent	Supplier
acetic acid, glacial	Fisher Scientific (Fairlawn, NJ)
acetic anhydride	Fisher Scientific (Fairlawn, NJ)
acetonitrile	EM Science (Gibbstown, NJ), HPLC grade
ammonium bicarbonate	BDH (Poole, UK)
anisole	Aldrich Chemical Co. (Milwaukee, WI)
*t*Boc protected amino acids	Advanced ChemTech (Louisville, KY)
calcium chloride	JT Baker (Phillipsburg, NJ)
dichloromethane (DCM)	Fisher Scientific (Fairlawn, NJ)
diisopropylethylamine (DIEA)	Aldrich Chemical Co. (Milwaukee, WI)
diethyl ether	Fisher Scientific (Fairlawn, NJ)
dimethylformamide (DMF)	Fisher Scientific (Fairlawn, NJ)
2,2'-dithiobis(5-nitropyridine) (DTNP)	Aldrich Chemical Co. (Milwaukee,WI)
dithiothreitol (DTT)	Aldrich Chemical Co. (Milwaukee, WI)
1,2-ethanedithiol	Aldrich Chemical Co. (Milwaukee, WI)
Disodium ethylenediaminetetraacetate (EDTA)	Fisher Scientific (Fairlawn, NJ)
glutathione, oxidized	Aldrich Chemical Co. (Milwaukee, WI)
glutathione, reduced	Aldrich Chemical Co. (Milwaukee, WI)
guanidine hydrochloride (GdnHCl)	Fisher Scientific (Fairlawn, NJ)
2-(1H-benzotriazole-1-yl)-1,1,3,3-tetramethyluronium hexafluorophosphate (HBTU)	Novabiochem (La Jolla, CA)
N-(2-hydroxyethyl)piperazine-N'-2-ethane-sulfonic acid (HEPES)	Fisher Scientific (Fairlawn, NJ)
hydrogen fluoride (HF)	Matheson Tri-Gas (Newark, CA)
N-hydroxybenzotriazole (HOBt)	Novabiochem (La Jolla, CA)
methylbenzhydrylamine (MBHA) resin	Novabiochem (La Jolla, CA)
o-phosphoric acid	Anachemia (Toronto, ON)
potassium chloride	Sigma Chemical Co. (St. Louis, MO)
potassium phosphate, dibasic	Fisher Scientific (Fairlawn, NJ)
potassium phosphate, monobasic	Fisher Scientific (Fairlawn, NJ)
sodium perchlorate (HPLC grade)	Fisher Scientific (Fairlawn, NJ)
tris(2-carboxyethyl)phosphine HCl (TCEP)	Sigma Chemical Co. (St. Louis, MO)
triethylamine, redistilled	Anachemia (Toronto, ON)
trifluoroacetic acid (TFA)	Halocarbon Products Corp. (River Edge, NJ)

trifluroethanol (TFE)	Aldrich Chemical Co. (Milwaukee, WI)
trypsin (sequencing grade)	Promega (Madison, WI)

B. Solid-phase peptide synthesis (SPPS)

Solid-phase peptide synthesis (SPPS) was developed by R. B. Merrifield (1963), an accomplishment for which he was awarded the Nobel Prize in Chemistry in 1984. SPPS techniques have been widely used and extensively reviewed (Bodanszky 1993, Fields 1997, Grant 1992, Gutte 1995, Merrifield 1995). In this technique, a growing peptide chain is covalently linked to an insoluble polymeric support and amino acids are added sequentially to the N-terminus (Figure 2-1). In order for this to work, it is necessary to be able to selectively block and expose functional groups at the α-amino and side chain groups. The *tert*-butyloxycarbonyl (*t*Boc) and 9-fluorenylmethoxycarbonyl (Fmoc) groups have been developed as labile protecting groups for the α-amide, which can be removed without disturbing the more stable side chain protecting groups (Figure 2-2). After the first (C-terminal) residue is covalently attached to the resin, synthesis proceeds as a cycle of deprotection of the α-amine group and formation of a new peptide bond with the next protected amino acid (Figure 2-1). At the end of the synthesis, the completed peptide is cleaved from the resin and the side chain protecting groups are removed in a single step. This results in a crude product which must be purified, usually by HPLC. Because purification does not occur until the very end, each reaction must be extremely efficient (> 99%). For example, if the coupling efficiency is 99% for the synthesis of a 100 residue peptide, the desired product will only be 37% of the final mixture.

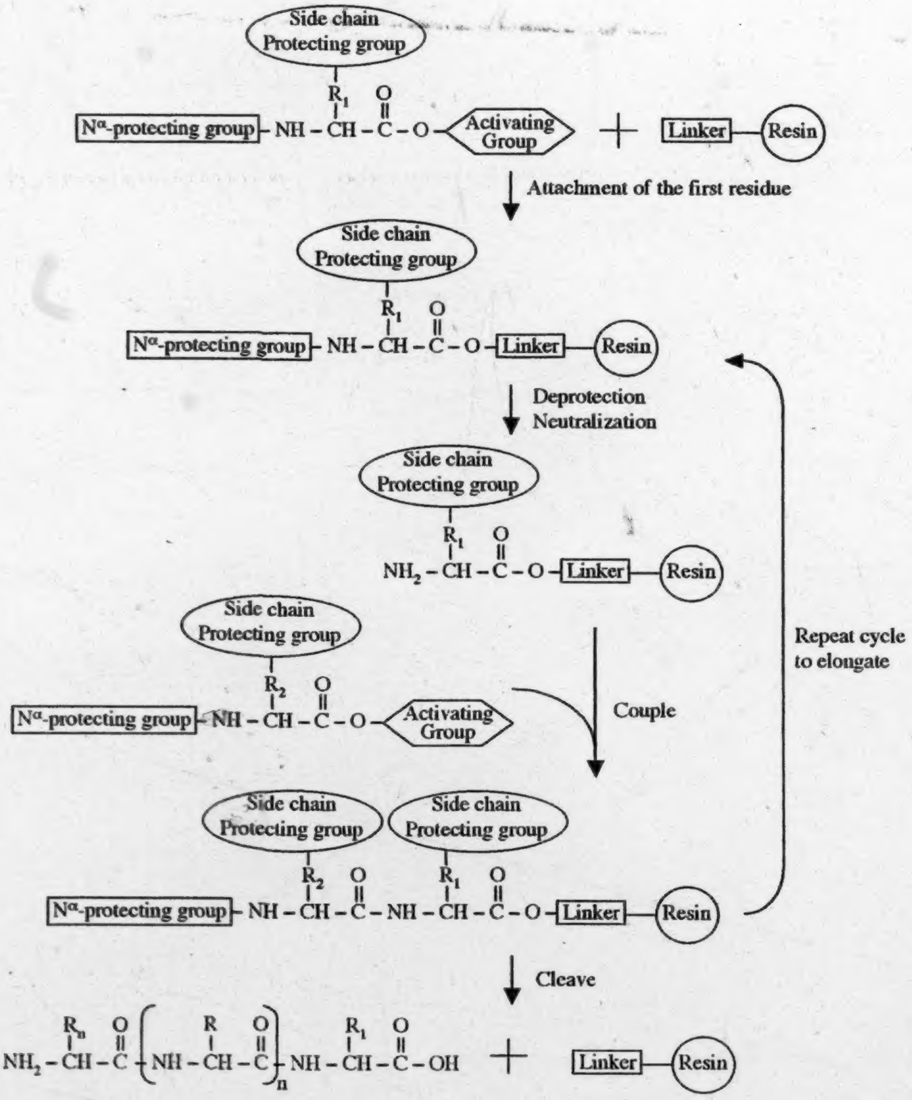
Side chain Protecting group
R_1
O
Nα-protecting group
NH - CH - C - O
Activating Group
Linker
Resin
Attachment of the first residue
Deprotection
Neutralization
NH_2 - CH - C - O
Couple
R_2
Repeat cycle to elongate
Nα-protecting group - NH - CH - C - NH - CH - C - O
Cleave
R_n
R
n
NH_2 - CH - C - NH - CH - C - NH - CH - C - OH

Figure 2-1. A general outline of the solid-phase peptide synthesis reaction cycle.

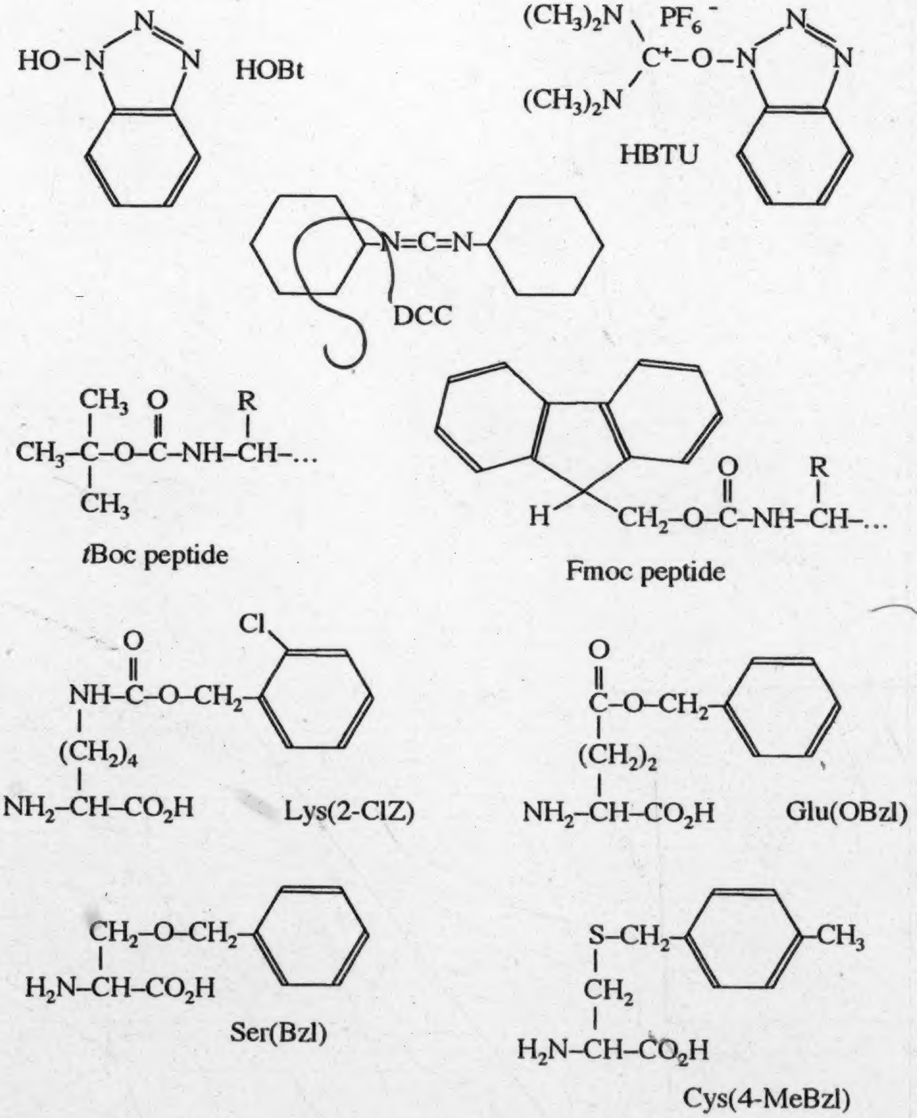
HO–N
N
N
HOBt
(CH3)2N
PF6 -
C+–O–N
(CH3)2N
HBTU
N=C=N
DCC
CH3 O R
CH3–C–O–C–NH–CH–...
CH3
tBoc peptide
H
CH2–O–C–NH–CH–...
O
R
Fmoc peptide
Cl
O
NH–C–O–CH2
(CH2)4
NH2–CH–CO2H
Lys(2-ClZ)
O
C–O–CH2
(CH2)2
NH2–CH–CO2H
Glu(OBzl)
CH2–O–CH2
H2N–CH–CO2H
Ser(Bzl)
S–CH2
CH3
CH2
H2N–CH–CO2H
Cys(4-MeBzl)

Figure 2-2. Chemical structures of SPPS reagents.

The most common polymeric support is a cross-linked 1% divinylbenzene-polystyrene resin. This material is physically stable, swells reversibly in solvents such as dichloromethane (DCM) and dimethylformamide (DMF), and can be derivatized with a wide variety of functional groups, providing great flexibility in the chemistry. For *t*Boc chemistry, methylbenzhydrylamine (MBHA) resin has numerous advantages. The peptides are attached via an acid-labile amide bond which can be cleaved with HF, yielding a peptide amide product.

After the C-terminal amino acid has been covalently attached to the resin, the N-terminal α-amine must be deprotected. The *t*Boc group is acid-labile and can be removed by trifluoroacetic acid (TFA) in DCM. This yields a charged α-amine, which must be neutralized with a base such as triethylamine or diisopropylethylamine (DIEA) in DCM. It is critical that the linkage to the resin and the side chain protecting groups are not susceptible to hydrolysis under these conditions. Therefore, the side chain functional groups are best protected by groups such as 2-chlorobenzyloxycarbonyl for amine groups, O-benzyl for carboxylic acids, and benzyl for alcohols (Figure 2-2). These protecting groups require considerably stronger acid, such as hydrogen fluoride (HF), to be cleaved.

The coupling step occurs by a nucleophilic attack of a free amine (the N-terminal residue of the growing peptide chain) upon a carboxyl group (the next amino acid to be added) (Figure 2-3). Carboxylic acids have very low reactivity, so this bond must be activated by replacing the hydroxyl group with an electron-withdrawing substituent. This makes the carbon atom more electrophilic and facilitates nucleophilic attack by the amine. This is typically carried out by coupling agents which can be added to a mix of

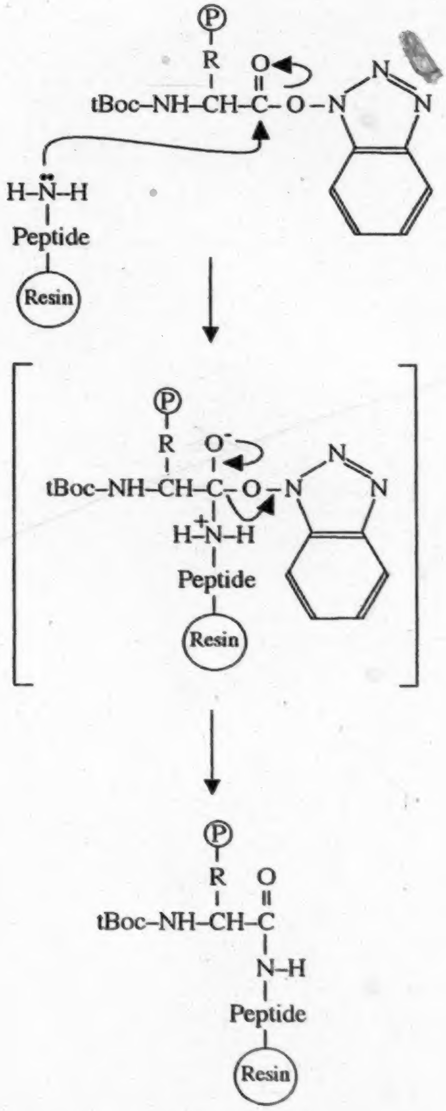
P
R
O
tBoc–NH–CH–C–O–N
N
N
H–N̈–H
Peptide
Resin
P
R
O⁻
tBoc–NH–CH–C–O–N
N
N
H–N⁺–H
Peptide
Resin
P
R
O
tBoc–NH–CH–C
N–H
Peptide
Resin

Figure 2-3. Formation of a new peptide bond during SPPS. The N^{α}-amino protected amino acid with an activated carboxyl group is coupled to the free amine on the growing polypeptide chain attached to the solid support, or resin.

concurrently. Two commonly used examples are dicyclohexylcarbodiimide (DCC) and 2-(1H-benzotriazole-1-yl)-1,1,3,3-tetramethyluronium hexafluorophosphate (HBTU) (Figure 2-2). DCC reacts with carboxylic acids to form an O-acyl-isourea, a highly active intermediate. This intermediate has several possible fates: direct nucleophilic attack by the free amine to yield the peptide bond, attack by a second carboxyl group to form a symmetric anhydride (which can also react with the amine to yield a peptide bond), or rearrangement to form an N-acylurea, an inactive side product. The preference for any one of these reactions is determined by the reaction conditions. Another popular coupling agent is HBTU, which reacts with the α-carboxyl group to form the activated O-benzotriazolyl ester (Figure 2-4). The peptide bond is formed by nucleophilic attack by the free amine upon this ester intermediate. Both DCC and HBTU coupling can be improved in terms of reaction rates and reduced side product formation by the addition of N-hydroxybenzotriazole (HOBt) as an auxiliary nucleophile.

Once the peptide chain is complete, the product must be cleaved from the resin and the side chain protecting groups removed. Liquid HF can perform both tasks in a single step, though such a dangerous reagent must be carefully handled in a special Teflon apparatus. Scavenging agents, such as anisole and thioanisole, scavenge cations produced during the cleavage of protecting groups, preventing certain side reactions, such as alkylation of the indole ring of tryptophan or the phenolic side chain of tyrosine. After cleavage, the resin-peptide mixture is washed with ethyl acetate to remove organic contaminants. The crude peptide is then extracted from the resin with acetic acid and lyophilized (Figure 2-5A).

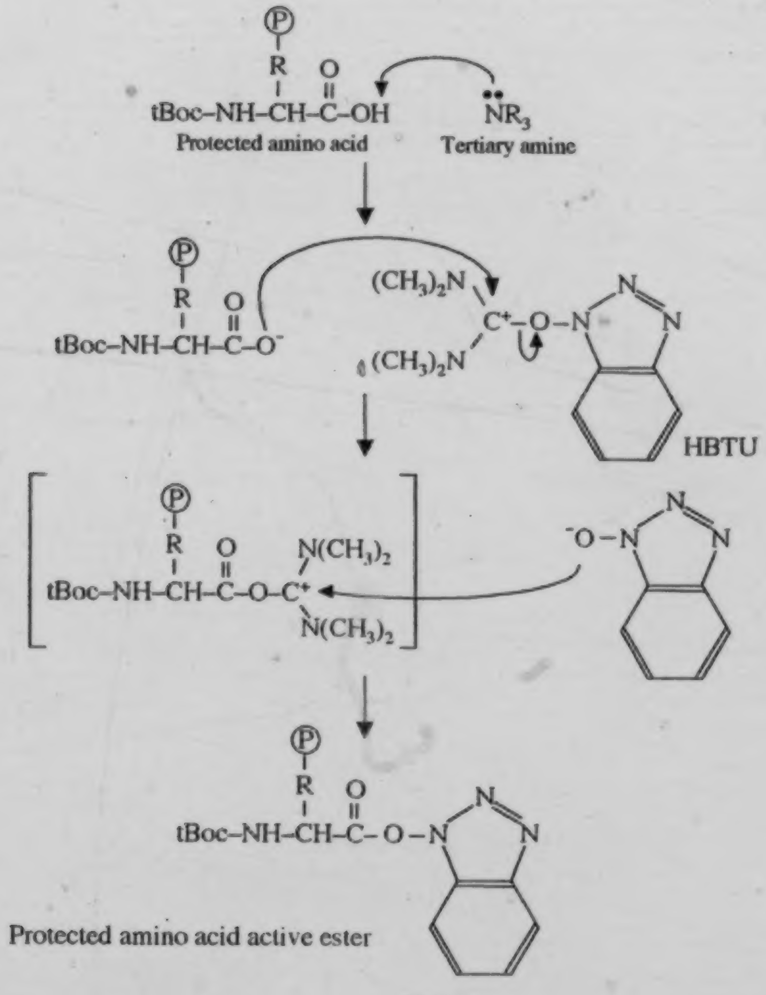
Ⓟ
R
O
tBoc–NH–CH–C–OH
Protected amino acid
NR3
Tertiary amine
tBoc–NH–CH–C–O⁻
(CH3)2N
C⁺–O–N
N
N
(CH3)2N
HBTU
tBoc–NH–CH–C–O–C⁺
N(CH3)2
N(CH3)2
⁻O–N
tBoc–NH–CH–C–O–N
Protected amino acid active ester

Figure 2-4. Formation of the OBt active esters with in situ coupling reagents. The circled P denotes the protecting group on the side-chain, R.

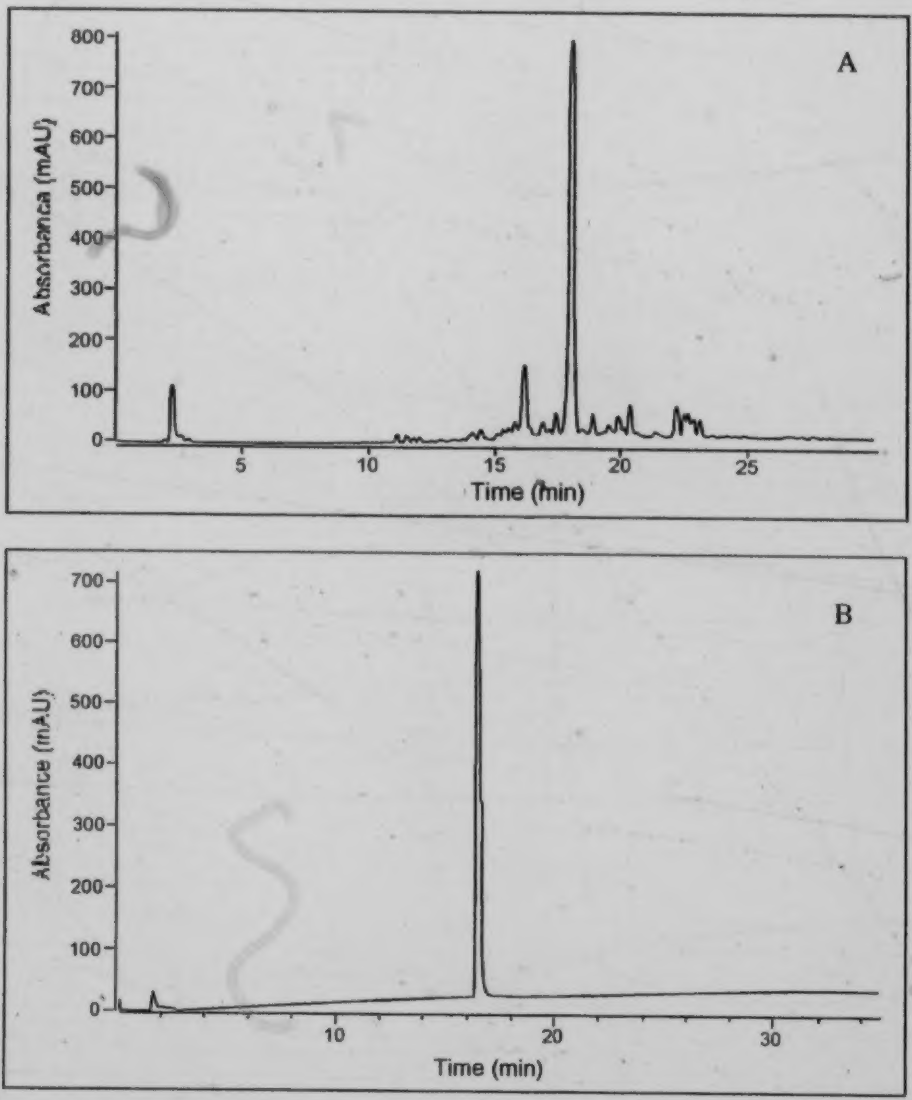

Figure 2-5. RP-HPLC analysis of peptide VAAL K3 (Ac-KVAALKEKVAALKEKV AALKE-NH_2) **A)** Analysis of the crude peptide. **B)** Analysis of VAAL K3, following shallow gradient RP-HPLC purification.

In this study, peptides were synthesized on an Applied Biosystems peptide synthesizer model 430A (Foster City, CA, USA), using 4-methylbenzhydrylamine (MBHA) resin (0.74 mmol of NH_2/g of resin) (Bachem, Torrance, CA, USA) on a 0.5 mmol scale. All amino acids were protected at the α-amino position with the *t*Boc group. The side-chain protecting groups were 2-chlorobenzyloxycarbonyl (ClZ) for lysine, O-benzyl for glutamic acid, benzyl for serine, and 4-methylbenzyl for cysteine. The *t*Boc groups were removed at each cycle with 30% TFA/DCM. Neutralizations were carried out with 10% DIEA/DMF. Activation and coupling were performed *in situ* by dissolving a 4-fold molar excess of amino acid (2 mmol) in DMF and activating with slightly less than equimolar amounts of HBTU and HOBt and a 5-fold molar excess of DIEA. N-terminal residues were acetylated using acetic anhydride/DCM.

The acetylated serine peptides were synthesized by the following protocol: residues up to, but not including, Ser(Ac) were added to MBHA resin as described above. After the addition of these residues, the resin was removed and N^{α}-Fmoc-O-*t*-butyl-serine was added manually by coupling with a five-fold excess and activation with 1:1.2 HBTU:N-methylmorpholine (NMM). The Fmoc group was then removed with 20% piperidine in DMF for 30 min. The next amino acid was coupled as the *t*Boc protected amino acid. After coupling, the resin was treated with 95% aq. TFA for 1 h to remove the t-butyl group from the serine. The hydroxyl group of serine was then acetylated by treatment with 2:2:0.1 equivalents of acetic anhydride:triethylamine: dimethylaminopyridine in DCM overnight. The resin was then replaced on the synthesizer and the remaining residues were added by standard *t*Boc chemistry.

The peptides were cleaved from the resin by reaction with hydrogen fluoride (20 ml/g resin) containing 10% anisole and 2% 1,2-ethanedithiol for 1.5 h at -5°C. The resin was washed with diethyl ether to remove the organic scavengers. The peptides were extracted from the resin with glacial acetic acid and the extract was lyophilized.

C. High-performance liquid chromatography (HPLC)

HPLC, or high-performance liquid chromatography, has been exceptionally useful in the analysis and purification of peptides and proteins and the practical and theoretical aspects have been extensively reviewed (Aguilar & Hearn 1996, Cunico *et al.* 1998, Gooding & Regnier 2002, Hearn 1991, Mant & Hodges 1991a, 1997). In this technique, a liquid sample is introduced to a column which is packed with stationary phase, and through which, the mobile phase solvent is pumped. Sample compounds interact with the stationary phase to varying degrees, affecting the length of time that these compounds are retained within the column (Cunico *et al.* 1998). After leaving the column, compounds present in the mobile phase are typically detected through UV/visible spectrometry. The major types of HPLC separation are based on differences in size (size exclusion chromatography, SEC), net charge (ion exchange chromatography, IEC), hydrophobicity (reversed-phase chromatography, RP-HPLC) and specific molecular recognition (affinity chromatography). Peptides and proteins have multiple sites of interaction with the stationary phase, and their behaviour is best described as an "on-off" mechanism, in contrast with small molecules which partition between the stationary and mobile phases along the length of the column. This means that isocratic elution is possible for peptides and proteins over only a very narrow range of mobile phase composition. Therefore, gradient elution is almost always preferred, as it yields shorter run times and better peak shapes.

High quality packing materials are critical for efficient separations of biological macromolecules. Silica, an inorganic polymer of silicon dioxide, is the most common HPLC packing material because of its rigidity, good mechanical stability to high pressure, and finely controlled particle size and shape (Cunico *et al.* 1998, Mant & Hodges 2002, Unger 2002). Ideally, the packing material should consist of small, spherical particles (i.e. 5 µm in diameter) for uniform packing and have pores of 300 Å diameter, which are large enough for most proteins to freely diffuse in and out, and greatly increase the stationary phase surface area and loading capacity. In addition, the surface of silica particles can be derivatized by a wide variety of organosilane compounds, allowing the creation of packing material with specificities for different types of molecular interactions. The chief disadvantages of silica-based packings is that they dissolve at pH levels greater than 7, restricting their use to pH 2-6. In addition, free silanol groups at the surface ionize at pH 4-7 ($SiOH \rightarrow SiO^-$), causing nonspecific interactions with positively charged molecules.

Detection of peptides and proteins is typically done by UV spectroscopy (Cohen & Gilby 2002, Cunico *et al.* 1998, Mant & Hodges 2002). The peptide bond absorbs strongly in the far UV (200-230 nm). Detection at 210 nm is a good compromise between sensitivity (which is higher at lower wavelengths) and reducing interference from solvent absorbance. Alternately, the column eluent can be monitored at 250-290 nm, where the aromatic side chains absorb. Of course, only peptides and proteins which contain these residues will be detected.

Reversed-Phase HPLC (RP-HPLC)

Reversed-phase HPLC is one of the most widely used modes of HPLC for peptide separations, due to its high efficiencies, fast separations, and wide scope for optimizing separations by varying mobile phase conditions (Mant & Hodges 2002). Separations in RP-HPLC are based on hydrophobic interactions between the stationary phase (typically C8 or C18 alkyl chains) and the sample molecules. Mobile phases are mixtures of water and organic solvent, with a gradient of increasing organic solvent effecting elution in order of increasing hydrophobicity. Acetonitrile has proven to be highly effective for the elution of peptides, yielding good peak shape and having low UV absorbance. Methanol and isopropanol may be more useful for the separation of very hydrophilic and very hydrophobic peptides, respectively. The stability of reversed-phase packings has been greatly improved by the use of diisopropyl and diisobutyl protecting groups for the organosilane stationary phases. These sterically bulky groups increase resistance to elevated temperature and extremes of pH (both acidic and basic), greatly improving column performance and lifetimes (Boyes & Walker 1995, Kirkland *et al.* 1993). Operation at pH 2 suppresses the ionization of silanol groups, which otherwise interact with basic residues, causing long retention times and peak broadening. Chromatographic behaviour is also improved by the presence of ion-pairing agents in the mobile phase (Guo *et al.* 1987). These are small, charged molecules which improve the interaction between polypeptides and the stationary phase. Their mechanism of action is not fully known; one model is that the ion-pairing agent binds to the sample molecules in solution, forming a neutral "ion-pair" with an increased affinity for the stationary phase, while the second model proposes that the ion-pairing agent binds to the stationary phase, forming a point for ion-exchange with the charged sample. Trifluoroacetic acid (TFA) is a highly successful ion-pairing agent, due to its volatility and low UV absorbance.

Analytical RP-HPLC runs were performed on HP1090 and Agilent 1100 liquid chromatographs from Agilent Technologies (Englewood, CO, USA). Routine analysis was performed on Zorbax 300SB-C8 analytical (150 x 4.6 mm i.d., 5 μm particle size, 300 Å pore size) and narrow-bore (150 x 2.1 mm i.d., 5 μm particle size, 300 Å pore size) columns. The following conditions were used: a linear AB gradient of 1-2% CH_3CN/min, where eluent A was 0.05% aqueous TFA (pH 2.0) and eluent B was 0.05% TFA in CH_3CN. The flow rate was 1 ml/min for the analytical columns and 0.25 ml/min for the narrow-bore columns. RP-HPLC analysis of a typical crude peptide is shown in Figure 2-5A. Runs containing peptides IAAL E4, IAAL E3, ISAL E4, VAAL E4, and VSAL E4 were performed at 70°C to prevent aggregation and improve resolution and peak shape; all other runs were performed at room temperature. Detection was based on monitoring the UV absorbance of the peptide bond at 210 nm.

In the case of difficult separations (Chapter VI), additional RP-HPLC conditions were used to attempt to optimize the separation. In this case, the analysis was performed on a Zorbax Eclipse XDB-C8 column (150 x 4.6 mm i.d., 5 μm particle size, 300 Å pore size) which has a greater stability at pH 7. For the pH 2.0 run, the following conditions were used: a linear AB gradient of 1% CH_3CN/min, where eluent A was 0.1% aqueous H_3PO_4 and eluent B was 0.1% H_3PO_4 in CH_3CN. The runs were performed at room temperature with a flow rate of 1 ml/min. For the pH 6.5 run, the following conditions were used: a linear AB gradient of 1% CH_3CN/min, where eluent A was 10 mM aqueous

TEAP, 100 mM $NaClO_4$, and eluent B was 10 mM TEAP, 100 mM $NaClO_4$, 50% CH_3CN (v/v). The runs were performed at room temperature with a flow rate of 1 ml/min.

The purification of synthetic peptides can be challenging, for solid-phase peptide synthesis typically results in a mixture of the desired product and closely related impurities, such as deletion peptides and peptides with side-chain modifications. In this study, the crude peptides were purified by a shallow gradient RP-HPLC approach (Burke *et al.* 1991), using a semi-preparative Zorbax 300SB-C8 column (250 x 9.4 mm i.d., 5 μm particle size, 300 Å pore size) from Agilent Technologies (Englewood, CO, USA) and a Varian Vista Series 5000 Liquid Chromatograph (Varian, Walnut Creek, CA, USA). The following conditions were used: a linear gradient of 1% CH_3CN/min from 0% to 10% CH_3CN, followed by a gradient of 0.2% CH_3CN/min, where eluent A was 0.05% aqueous TFA and eluent B was 0.05% TFA in CH_3CN (v/v). The flow rate was 2 ml/min. The RP-HPLC analysis of VAAL K3, a typical peptide used in these studies, is shown in Figure 2-5 as the crude product and after RP-HPLC purification. Peptides IAAL E4, IAAL E3, ISAL E4, VAAL E4, and VSAL E4 were purified at 70°C to prevent aggregation and improve resolution and peak shape. The remaining peptides were purified at room temperature. One minute fractions were collected and analyzed by analytical RP-HPLC, amino acid analysis, and mass spectroscopy.

Cation-exchange Chromatography (CEC)

During ion-exchange chromatography, sample molecules bind to a charged stationary phase through reversible electrostatic interactions and are then displaced by an increasing salt gradient in order of increasing net charge (Cunico *et al.* 1998). This HPLC mode has a completely different selectivity than that of RP-HPLC, making it a useful complementary approach (Mant & Hodges 2002). During cation-exchange chromatography (CEC), positively charged sample molecules bind to an anionic stationary phase. CEC can be further categorized into strong and weak CEC, depending on the pKa of the stationary phase functional groups (sulfonic acid, pKa < 3, for strong and carboxylic acids, pKa of 4.0-4.5, for weak). Under acidic conditions (pH < 4), acidic residues will be protonated and uncharged, giving the vast majority of peptides and proteins a net positive charge. This makes strong CEC useful for a wide selection of peptides. Elution is typically effected by a rising salt gradient, such as 2-20 mM NaCl/min (Mant & Hodges 2002), although pH gradients have also been used. A small amount of organic solvent is commonly added to the mobile phase to suppress nonspecific hydrophobic interactions between the sample and the stationary phase.

CEC runs were performed with a PolySulfoethyl A strong-cation exchange column (200 x 4.6 mm i.d., 5 μm particle size, 300 Å pore size) from PolyLC (Columbia, MD, USA) on an HP1090 Liquid Chromatograph from Agilent Technologies (Englewood, CO, USA). The following conditions were used: a 5 minute isocratic elution with eluent A, followed by a linear AB gradient of 5 mM $NaClO_4$/min, where eluent A is 10 mM TEAP, 10% CH_3CN (pH 3.0) and where eluent B is 10 mM TEAP, 500 mM $NaClO_4$, 10% CH_3CN (pH 3.0). The run was performed at room temperature with a flow rate of 1 ml/min. Additional CEC runs were performed with the same conditions as described, but where the buffers were titrated to pH 6.5.

Hydrophilic interaction/cation-exchange chromatography (HILIC/CEC)

Hydrophilic interaction chromatography, or HILIC, is a term coined by Alpert *et al.* (1990) to describe the HPLC separation of peptides by hydrophilic interactions with a polar stationary phase. It was then found that, in the presence of high amounts of organic solvent, strong-cation exchange columns would show separation of peptides based on increasing hydrophilicity superimposed upon the expected separation by net charge (Zhu *et al.* 1991). Mixed-mode separations have been dismissed as "nonideal", but HILIC/CEC was found to be sensitive to subtle variations in hydrophilicity and to be complementary to RP-HPLC. In fact, the ability of HILIC/CEC to separate peptides rivals that of RP-HPLC (Zhu *et al.* 1992a). Typical conditions are a salt gradient of 2-20 mM $NaClO_4$/min in buffers containing 15-80% CH_3CN. In some cases, a decreasing gradient from 90-80% CH_3CN improves separation.

HILIC/CEC was performed with a PolySulfoethyl A strong-cation exchange column (200 x 4.6 mm i.d., 5 μm particle size, 300 Å pore size) from PolyLC (Columbia, MD, USA) on an HP1090 Liquid Chromatograph from Agilent Technologies (Englewood, CO, USA). The following conditions were used: a 10 minute isocratic elution of 10% eluent B, followed by a linear AB gradient of 2.5 mM $NaClO_4$/min, where eluent A is 10 mM TEAP, 65% CH_3CN (pH 6.5) and eluent B is 10 mM TEAP, 350 mM

$NaClO_4$, 65% CH_3CN (pH 6.5). The run was performed at room temperature with a flow rate of 1 ml/min. Additional runs were performed in which the buffer pH was changed to 3.0 and the CH_3CN content varied from 25-65% (v/v).

D. Amino Acid Analysis

The concentrations of all peptide solutions were determined by amino acid analysis (as reviewed in Arrizon-Lopez *et al.* 1991, Ozols 1990, Smillie & Nattriss 1991). An aliquot of the peptide solution (typically 5-10 µl), 10 µl of a norleucine external standard, and 200 µl of 6 N HCl (0.1% phenol) were added to test tubes. Acid hydrolysis was then carried out by one of two procedures: 1) heating to 160°C for 1 hour, under vacuum, or 2) heating to 110°C for 22 hours. The hydrolyzed samples were dried under vacuum, with a separate container of KOH present in the desiccator to neutralize the acid. The hydrolyzed material was then dissolved in an appropriate volume (200-300 µl) of buffer (0.2 M sodium citrate, pH 3.25).

Analysis was carried out on a Beckman System 6300 Amino Acid Analyzer (Beckman, San Ramon, CA, USA), which is based on cation exchange chromatography and post column ninhydrin derivatization. The cation exchange column resin, a sulfonated divinyl benzene polystyrene, has significant nonpolar character, so separation is based on hydrophobicity as well as net charge. Elution is based on both increasing pH and salt concentration, and is carried out with a series of three buffers: 1) 0.2 M sodium citrate, pH 3.25, 2) 0.2 M sodium citrate, pH 4.25, and 3) 0.35 M sodium citrate, 0.75 M NaCl, pH 7.9. After elution from the column, the eluent is mixed with the ninhydrin reagent on stream and then passed through a heating coil (≥ 100°C). The ninhydrin product is quantitatively detected by spectrophotometry (primary amines at 570 nm and proline, a secondary amine, at 440 nm) and the amino acids are identified by retention time.

E. Mass Spectrometry

Masses of all peptides and proteins in these studies were determined by a VG Quattro electrospray/triple quadrupole mass spectrometer from VG BioTech (Altrincham, UK). Electrospray was developed as a gentle method for transferring biological molecules to the gaseous phase without imparting excess energy to the sample. In this procedure, the sample solution flows through a fine needle at a high voltage, creating a fine spray of μm sized droplets. Solvent evaporates from the surface of the drops, yielding ionized gaseous molecules (reviewed in Mann *et al.* 2001). Separation of the charged species occurs in the quadrupole. An oscillating electric field is applied to a set of four rods, which allows only molecules of a specific mass to pass through to the detector. Scanning the amplitude of the electric field allows a mass spectrum to be determined.

In our system, 10 μl aliquots of the sample were injected. The running buffer was 0.1% formic acid in 50% aqueous CH_3CN and the flow rate was 50 μl/min. The detector was operated in positive ion mode. Spectra were scanned 7-10 times from 500 to 1500 Da, and the resulting data was baseline subtracted, smoothed and centered. Liquid-chromatography mass spectrometry (LC-MS) was performed with a Zorbax 300SB-C8 narrow bore column (150 x 2.1 mm i.d., 5 μm particle size, 300 Å pore size). After equilibration at 10% CH_3CN, a linear AB gradient (2% CH_3CN/min) was carried out, where eluent A is 0.05% aqueous TFA and eluent B is 0.05% TFA in CH_3CN. The flow-rate through the column was 250 μl/min and stream splitting was used to reduce the eluent to 50 μl/min. The resulting spectra were scanned from 500 to 1500 Da. Mass spec analysis of a typical purified peptide is shown in Figure 2-7.

MS/MS fragmentation was performed on the tryptic fragments of peptide N. The solvent used was 0.05% TFA in 50% aqueous CH_3CN; flow-rate 20 μl/min. The daughter ions of the tryptic fragments ISALK (531 Da) and IS(Ac)ALK (573 Da) were produced by collision-induced dissociation using argon gas at a pressure of 3×10^{-3} mBar and a collision energy of 25.0 eV. The daughter ion spectra were scanned from 40 to 600 Da.

F. Peptide Oxidation

Homostranded disulfide-bridged peptides (e.g. VSAL E5ox) were prepared by air oxidation. Milligram quantities of the pure, reduced peptide were dissolved in 100 mM NH_4HCO_3 (to 2-5 mg/ml) and stirred, exposed to the atmosphere. Progress of the reaction was monitored by RP-HPLC. The oxidized peptide was then desalted and purified by RP-HPLC, and the product mass was confirmed by mass spectrometry.

The disulfide-bridged heterostranded peptides were prepared by the method of Rabanal *et al.* (1996). The K-coil peptides (2-8 mg) were dissolved in a 3:1 acetic acid/water solution (~ 5 mg/ml) and reacted with 2,2'-dithiobis(5-nitropyridine) (DTNP) at a 3-5 molar excess to form the 5-nitro-2-pyridinesulfenyl derivative. The derivatized peptides were then lyophilized, dissolved in 0.05% aqueous TFA, and washed with a 7:3 mixture of diethyl ether and DCM to remove the excess DTNP. Lyophilization of the

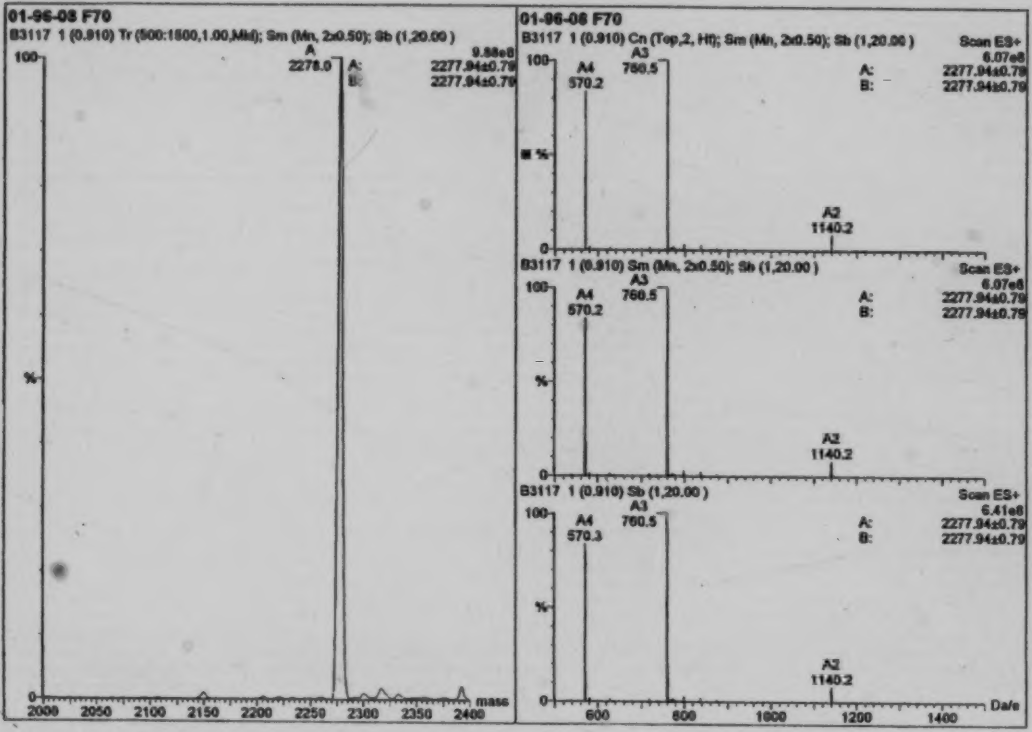

Figure 2-6. Mass spectrometry analysis of purified peptide VAAL K3 (Ac-KVAALKEKVAALKEKVAALKE-NH$_2$), using an electrospray - triple quadrupole mass spectrometer. The panels on the right show (from top to bottom) three stages of data processing, namely, baseline subtraction, smoothing, and centering. The three peaks (A4, A3, and A2) were identified by their mass/charge ratios as the +4, +3, and +2 ions. The transformed mass spectrum, on the left, is based on the +4, +3, and +2 ions and shows the mass of the parent molecule.

aqueous phase yielded the pure product. The derivatized K-coils were then dissolved in 50 mM acetic acid (~ 5 mg/ml) and reacted with the corresponding E-coil to form the disulfide-bridged heterostranded molecules. The products were purified by RP-HPLC and their mass confirmed by mass spectrometry.

The specificity of the interaction between VSAL E5 and VSAL K5 was demonstrated by an air oxidation assay. The conditions consisted of a mixture of 100 μM reduced VSAL E5 and 100 μM reduced VSAL K5 in a buffer of 100 mM NH_4HCO_3, pH 8.0. Aliquots (10 μl) were withdrawn at different time points, quenched with 5 μl neat TFA, and analyzed by RP-HPLC. The amounts of the different species were quantified by their relative peak areas.

G. Circular Dichroism Spectroscopy

Circular dichroism (CD) spectroscopy has played a key role in the study of protein structure and folding, and its theory and practice have been extensively reviewed (Fasman 1996, Greenfield 1996, Johnson Jr. 1990, Kelly & Price 1997, Woody 1995). Central to this technique is the phenomenon of circularly polarized light, in which the electric vector rotates about the direction of a light beam. The more familiar plane polarized light is composed of equal amounts of left and right circularly polarized light (lcpl and rcpl). Chiral molecules absorb different amounts of lcpl and rcpl. As lcpl and rcpl absorbance obeys Beer's law ($A = \varepsilon Cl$), this behaviour of chiral molecules can be expressed as a difference in extinction coefficients (ε_l-ε_r = $\Delta\varepsilon$), although the common convention in biochemistry is to convert it to molar ellipticity ($[\theta] = 3298\Delta\varepsilon$). This results in a spectrum composed of a series of bands, each corresponding to an electronic transition of an electron from the ground state to an excited state. In contrast to UV/VIS spectroscopy, however, the bands in a CD spectrum may be either positive or negative.

The far UV spectrum (170-250 nm) of peptides and proteins is dominated by the amide bond. This region is highly sensitive to protein secondary structure, with different structures displaying distinctive spectra (Figure 2-7). The α-helix has an intense spectrum with a characteristic positive band at 190 nm and double minima at 208 and 222 nm. The bands at 190 and 208 nm are attributed to a $\pi\pi^*$ transition of the peptide bond π orbital and the 222 nm band is attributed to an $n\pi^*$ transition of the carbonyl oxygen lone pair. The β-sheet spectrum is characterized by a negative band at 215 nm that is attributed to the $\pi\pi^*$ transition and a positive band at 198 nm that is attributed to the $n\pi^*$ transition. β-turns have no single characteristic spectrum, and so are more difficult to identify. Unstructured regions display a large negative band below 200 nm and a small band near 220 nm that may be either positive or negative. The aromatic side chains of Trp, Tyr, and Phe have characteristic $\pi\pi^*$ bands in the near UV region (250-300 nm). The more rigid the side chain, the greater the intensity of this band. This can be a useful indication of the presence or absence of stably folded tertiary structure.

CD spectra were recorded on Jasco J-500C, J-720 and J-810 spectropolarimeters (Jasco, Easton, Maryland, USA). The light source was a xenon lamp, which required nitrogen to be flushed through the system to prevent ozone formation. The spectropolarimeters were routinely calibrated with an aqueous solution of recrystallized D-10-(+)-camphorsulfonic acid at 290.5 nm. Cylindrical quartz cells were used, with path lengths of 0.02 cm for the CD spectra scans and 0.05 cm for the denaturation

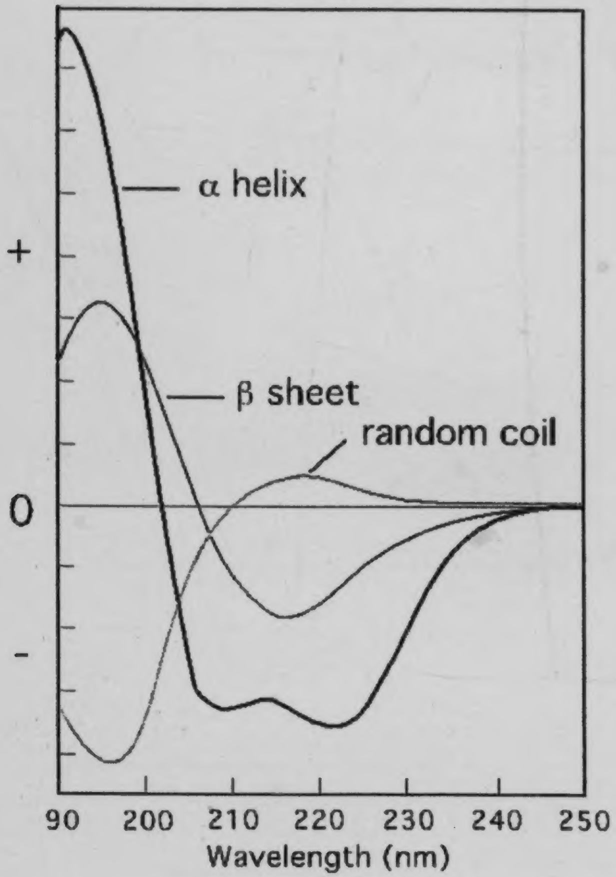

Figure 2-7. Typical CD spectra of α-helical (myoglobin), β-sheet (poly(KLKL) in 0.5 M NaF), and random coil (poly(PKLKL) in the absence of salt) structure. The figure is adapted from Brahms& Brahms (1980).

studies. CD spectra are the average of four scans obtained by collecting data at 0.1 nm intervals from 250 nm to 190 nm, or as low as possible. The results are expressed as mean residue molar ellipticity [θ] with units of deg·cm^2·dmol^{-1} and calculated from the following equation:

$$[\theta] = (\theta_{obs} \text{ x } \mathrm{MRW})/(10lc)$$

where θ_{obs} is the ellipticity measured in millidegrees, MRW is the mean residue molecular weight (molecular weight of the peptide divided by the number of residues), *c* is the peptide concentration in mg/ml, and *l* is the optical path length of the cell in cm. Samples were prepared by diluting an aqueous peptide stock solution of known concentration (~10 mg/ml) into buffer (50 mM PO_4, 100 mM KCl, pH 7.0). For the scans in the presence of trifluoroethanol (TFE), the above buffer was diluted to 50% with TFE.

Guanidine hydrochloride (GdnHCl) denaturation studies were carried out by monitoring the molar ellipticity at 222 nm as a function of GdnHCl concentration. Samples were prepared from the aqueous peptide stock solutions, buffer (50 mM PO_4, 100 mM KCl, pH 7.0) and the GdnHCl buffer (50 mM PO_4, 100 mM KCl, 8 M GdnHCl pH 7.0), and allowed to equilibrate at room temperature overnight. Five 10 second scans were recorded and averaged to yield the ellipticity value at a given concentration of GdnHCl. Analysis of the titration data was performed as described in section H.

Temperature denaturations of the dynein constructs was performed in a rectangular quartz cell with a path length of 1 mm; the temperature was controlled with a Peltier device. The ellipticity at 222 nm was measured every 0.5°C over a range of 5-

95°C, with a gradient of 1°C/min. The sample was then cooled to 25°C to test for reversibility.

When the structure of a peptide or protein is primarily α-helical and random coil, the molar ellipticity at 222 nm has been found to be linearly related to the α-helical content. The equation of Chen *et al.* (1974) describes the length dependence of the CD spectrum of an α-helix:

$$[\theta]^{n} = [\theta]^{\infty}(1 - k/n)$$

where $[\theta]^{\infty}$ is the molar ellipticity of an α-helix of infinite length, k is a chain dependence factor, and n is the number of residues in the α-helix. We used the values of $[\theta]_{222}^{\infty} = -40{,}000$ and k = 4.58, which were obtained by Gans *et al.* (1991) after a reanalysis of this equation to fit new data. For example, a fully α-helical peptide that is 35 residues in length is predicted to have a $[\theta]_{222}$ of -34,766.

H. Guanidine hydrochloride denaturation analysis

Chemical denaturants, such as GdnHCl and urea, have been used for the study of protein stability for many decades. They act by increasing the solubility of the constitutive parts of proteins, but their precise mechanism is not well understood (Bolen & Yang 2000, Pace 1986, 2000, Zou *et al.* 1998). It is clear that these substances increase the solubility of the different chemical groups with comprise proteins. Two types of mechanism have been proposed: short range interactions, such as direct binding of denaturant molecules to the protein, or long range interactions, such as changes in the properties of the solvent. Calorimetric analysis has provided evidence that the interaction between peptide amide groups and urea is characterized by favourable (negative) enthalpy and unfavourable (negative) entropy, suggesting a specific interaction such as hydrogen bonding (Zou *et al.* 1998). In contrast, the interaction between hydrophobic groups and urea is characterized by unfavourable (positive) enthalpy and favourable (positive) entropy, suggesting that urea acts to diminish the hydrophobic effect (Zou *et al.* 1998). GdnHCl effects denaturation through both electrostatic interactions and a nonionic denaturant activity similar to that of urea. This combination makes GdnHCl nearly twice as effective as urea for protein denaturation (Myers *et al.* 1995). Interestingly, increasing the ionic strength of urea solutions increases the denaturation ability to a level similar to that of GdnHCl (Monera *et al.* 1994b).

Three different approaches have been developed for the analysis of chemical denaturation curves (described in Pace 1986). First, Tanford and coworkers studied the effect of denaturants on the aqueous solubility of the constitutive parts of a protein. Protein conformational stability is calculated as the sum of the free energies of transfer between water and denaturant for the constitutive amino acids and of the change in solvent accessibility upon unfolding. In the second approach, the interaction between denaturant and protein molecules is treated as a specific binding interaction. The folding equilibrium is shifted because unfolded proteins have more binding sites. The third and most common approach is the linear extrapolation method (LEM), which was developed by Pace and coworkers (1986, 2000). The linear relationship between ΔG and denaturant concentration which is observed in the transition region is assumed to continue to zero denaturant, obeying the following equation: $\Delta G = \Delta G^{H_2O} - m[\mathrm{GdnHCl}]$. This long extrapolation yields the value of ΔG^{H_2O}, the free energy difference between the native and denatured ensembles of a particular protein. Analysis of denaturation curves is much simpler with the approach, and appears to be equal in accuracy as the more complex approaches to analysis (Pace & Shaw 2000). A calorimetric study found that both ΔH and ΔS were linear functions of [urea], supporting the use of the LEM (Zou *et al.* 1998). The slope term of the LEM equation (m) has been attributed to the change in accessible surface area (ΔASA) upon protein denaturation (Alonso & Dill 1991, Myers *et al.* 1995) and to changes in the denatured ensemble (Shortle 1989, Shortle *et al.* 1990). However, m values have also been shown to be affected by the solution conditions and the presence of intermediates, making interpretation difficult (Baskakov & Bolen 1999).

The GdnHCl denaturation curves were analyzed using a two-state unfolding model to determine the fraction folded, using the equation $F_f = ([\theta] - [\theta]_D)/([\theta]_F - [\theta]_D)$, where $[\theta]$ is the observed molar ellipticity and $[\theta]_F$ and $[\theta]_D$ are the ellipticities of the folded and denatured states, respectively (Pace 1986). For reduced coiled-coils, the free energy of unfolding is dependent on peptide concentration, due to the monomer-dimer equilibrium (Figure 2-8). As a consequence, the free energy of denaturation must be calculated by the following equation, $\Delta G_D = -RT \ln(2P_tF_u^2/F_f)$, where P_t is the total peptide concentration and F_u is the fraction unfolded ($F_u = 1 - F_f$) (De Francesco *et al.* 1991). In the oxidized state (disulfide-bridged), the free energy of denaturation is independent of concentration (Figure 2-8) and is calculated by the following equation, $\Delta G_D = -RT \ln((1 - F_f)/F_f)$. We then used the linear extrapolation method to calculate the free energy of unfolding in the absence of denaturant (ΔG^{H_2O}), $\Delta G_D = \Delta G^{H_2O} - m[\text{GdnHCl}]$ (Pace 1986). This assumes that the linear relationship between ΔG_D and

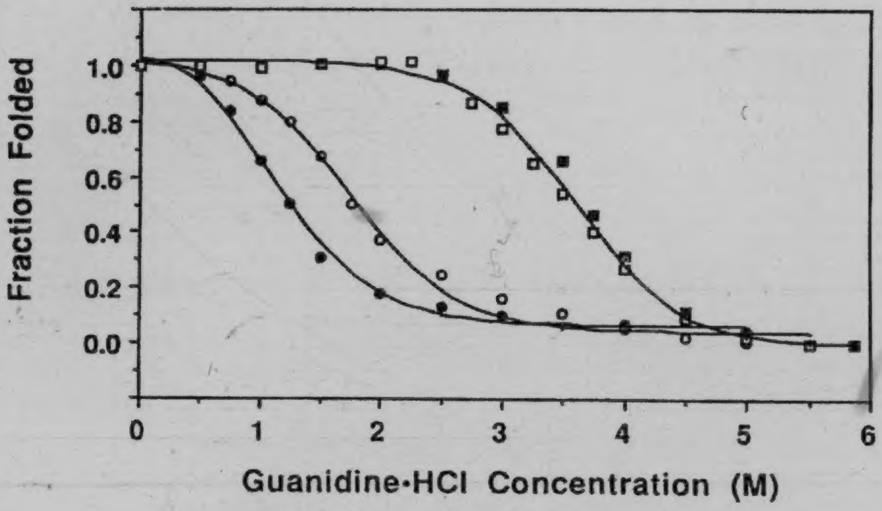

Figure 2-8. Concentration dependence of the GdnHCl denaturation of the coiled-coil peptide (Ac-KCAEAEGKLEALEGKLEALEGKLEALEGKLEALEG-NH_2), when oxidized (squares) or reduced (circles). The denaturation midpoint of the reduced peptide is dependent on concentration, whereas that of the oxidized peptide is not. The spectra were measured in 50 mM PO_4, 100 mM KCl buffer, pH 7 at 20°C. The concentrations of the reduced peptide samples were 48 μM (●) and 213 μM (○) and of the oxidized peptide samples were 23 μM (■) and 113 μM (□). The figure is taken from Zhou *et al.* (1992c).

[GdnHCl], which is observed in the transition region, continues to zero [GdnHCl]. We calculated the difference in free energy of unfolding between two peptides ($\Delta\Delta G$) using the equation of Serrano *et al.* (1990):

$$\Delta\Delta G_D = ([\text{denaturant}]_{1/2,A} - [\text{denaturant}]_{1/2,B})([m_A + m_B]/2)$$

This equation gives the value of $\Delta\Delta G_D$ at the denaturant concentration half way between the denaturation midpoints of peptides A and B. The ΔG^{H2O} values were not used to calculate $\Delta\Delta G$, because they were obtained through a long extrapolation that is very sensitive to error.

I. Analytical ultracentrifugation

Analytical ultracentrifugation is the method of choice for the determination of a wide variety of hydrodynamic and thermodynamic properties, including size, purity, gross conformation, association equilibrium constants, and mechanisms of self-assembly (Cole & Hansen 1999, Schuster & Toedt 1996). Solutions of biological macromolecules are placed in special cells with sloping walls and transparent windows. These cells are placed in a rotor that spins with radial velocities reaching 50,000 rpm. The resulting movement of sample molecules within the cell is monitored by either absorbance or interference spectroscopy, and reveals important information about the sample. There are two types of experiment that can be done in the analytical ultracentrifuge – sedimentation velocity and sedimentation equilibrium. In sedimentation velocity experiments, the sample is exposed to a high centrifugal field that sediments the sample molecules to the bottom of the cell. The velocity of this movement is determined by the size and shape of the sample molecule. In sedimentation equilibrium experiments, a lower speed is used which allows an equilibrium to be reached between centrifugal force, diffusion, and buoyancy, resulting in a stable distribution of sample molecules. This distribution is affected by the mass, but not the shape, of the molecule (Cole & Hansen 1999).

Sedimentation equilibrium

Sedimentation equilibrium is one of the best methods available for molecular weight determination and for the characterization of association reactions (Schuster & Toedt 1996). Once equilibrium has been reached, the sample molecule distribution can be described by this equation:

$$c_r = c_0 \exp [M(1 - \text{v-bar}*\rho)\omega^2(r^2 - r^2_0)/2RT]$$

where c_r is the sample concentration at radial position r, c_0 is the sample concentration at the meniscus, M is the molecular weight, v-bar is partial specific volume, ρ is the solvent density, ω is the angular velocity, R is the gas constant, and T is the absolute temperature. Deviations from this simple behaviour occur when there are multiple species present or when there is thermodynamic nonideality. Different association reaction mechanisms (i.e. monomer to dimer, or dimer to tetramer) have characteristic effects on the shape of the distribution, and can be described by the following equation (McRorie & Voelker 1993):

$$\text{N monomers} \longleftrightarrow \text{N-mer}$$

$$c_r = c_{monomer,r0}\exp[M(1 - \text{v-bar}*\rho)\omega^2(r^2 - r^2_0)/2RT] + (c_{monomer,r0})^n K_a \exp[M(1 - \text{v-bar}*\rho)n\omega^2(r^2 - r^2_0)/2RT]$$

where n is the number of subunits in the oligomer and K_a is its association constant. Extra terms can be included for equilibria with more than two species. The other complicating factor is thermodynamic nonideality, which is commonly experienced by highly asymmetric molecules or by highly charged molecules in low ionic strength buffer. These effects can be accounted for by adding the second viral coefficient, B, to the equation.

Traditionally, sedimentation equilibrium data was analyzed by taking the natural log of the equation, which converts it to the linear form:

$$\ln c_r = \ln c_0 + \frac{M(1 - \text{v-bar}^*\rho)\omega^2}{2RT}(r^2 - r^2_0)$$

A plot of ln c_r vs. $(r^2 - r^2_0)$ yields a line with a slope directly proportional to M (Figure 2-9). However, this approach is notoriously insensitive to heterogeneity. In 1975, van Holde and coworkers (1975) produced a data that fit a straight line exceptionally well, yet the sample was a deliberate mixture of ovalbumin (0.7 mg/ml) and bovine serum albumin (0.5 mg/ml). Because of these problems, the standard approach now is to use nonlinear least squares methods to fit the data directly to the exponential form of the equation (Figure 2-9), using programs such as Nonlin (Johnson *et al.* 1981). Global fitting of multiple data sets obtained at different loading concentrations and speeds allows greatly improved determination of molecular weight and association constants.

In these studies, sedimentation equilibrium experiments were performed on Beckman Model Optima XL-I and XL-A centrifuges. Detection was with Rayleigh interference optics on the XL-I and with absorbance optics on the XL-A, using a xenon flash lamp and a scanning monochromator. Six-sector cells with charcoal-filled Epon centerpieces and quartz windows were used. Samples were dissolved in buffer and dialyzed overnight at 4°C against the same buffer. Experiments with the de novo designed coiled-coils were performed in 50 mM phosphate, 100 mM KCl, pH 7.0.

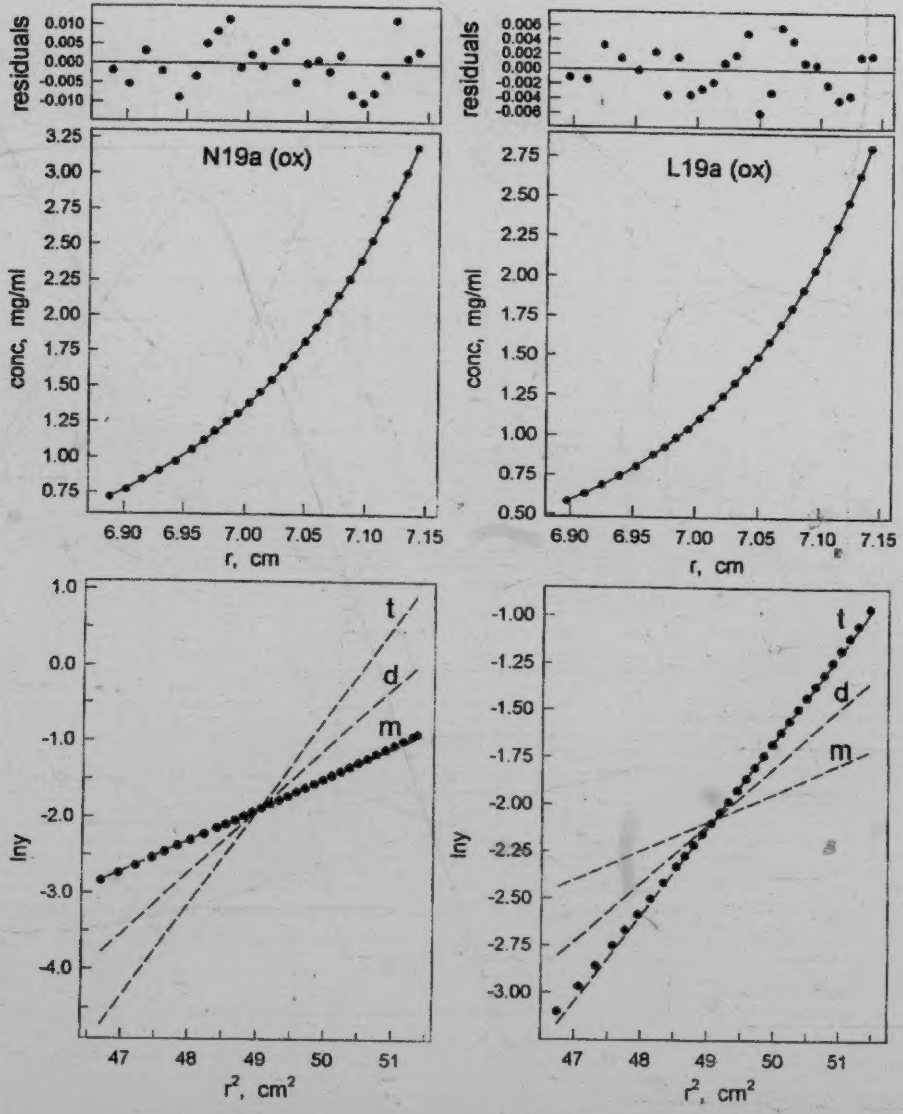

Figure 2-9. Sedimentation equilibrium analysis of coiled-coil peptides N19**a**(ox) (Ac-CGGEVGALKAQVGALQAQNGALQKEVGALKKEVGALKK-NH_2) and L19**a**(ox) (Ac-CGGEVGALKAQVGALQAQLGALQKEVGALKKEVGALKK-NH_2). The middle panels (concentration *versus* radius) show the best fits for a single species monomeric curve fit for N19**a**(ox) and a single species trimeric curve fit for L19**a**(ox). The upper panels show the residuals from the curve fits, and the lower panels show lnY *versus* r^2 for the data (filled circles) compared to theoretical monomer (m), dimer (d), and trimer (t) single species plots (broken lines), where y is the fringe displacement, which is proportional to the concentration. The figure is taken from Wagschal *et al.* (1999a).

Experiments with peptides based on dynamin sequences were performed in 50 mM phosphate, 100 mM KCl, 2 mM DTT, pH 7.0. Experiments with the dynein constructs were performed in 50 mM phosphate, 150 mM KCl, pH 7.0. The samples were analyzed at three loading concentrations and three speeds at 20°C. We determined that equilibrium had been reached by subtracting scans taken 2h apart. The data were evaluated by nonlinear least squares analysis, using the program Nonlin (Johnson *et al.* 1981). The program Sednterp (Sedimentation Interpretation Program, version 1.01) was employed to calculate the partial specific volumes of the sample peptides and proteins from their amino acid compositions as well as the solvent densities and viscosities using known values from physical tables, as described in Laue *et al.* (1992).

Sedimentation Velocity

The rate at which a macromolecule sediments in a centrifugal field is directly related to its size, shape and purity (Cantor & Schimmel 1980, Cole & Hansen 1999, Schuster & Toedt 1996). As the sample molecules move to the outside of the cell, a boundary is formed between the region of the cell which contains sample and that which does not. The Svedberg equation describes this movement in terms of a centrifugal force which causes the molecule to move away from the center of rotation and is opposed by buoyancy and frictional forces:

$$s = \frac{v}{\omega^2 r} = \frac{M(1 - \nu\text{-bar}*\rho)}{Nf}$$

where s is the sedimentation coefficient, v is the velocity of sedimentation, $\omega^2 r$ is the centrifugal force, M is the sample molecular mass, v-bar is the sample partial specific volume, ρ is the solvent density, N is Avogadro's number, and f is the frictional coefficient. The sedimentation coefficient, s, describes the movement of the sample molecule. The simplest method for determining s is to plot ln $[r_b(t)/r_m(t_0)]$ vs. $(t-t_0)$, where r_b and r_m are the radial positions of the boundary midpoint and the meniscus, respectively. The slope of this plot will be equal to $\omega^2 s$. This approach will work for simple systems, but samples which are undergoing significant amounts of aggregation or diffusion must be analyzed through more sophisticated approaches (Cole & Hansen 1999, Schuster & Toedt 1996). The frictional coefficient, *f*, is very sensitive to the sample molecule shape. Although we cannot derive detailed structural information from these experiments, the deviation of the observed *f* from that calculated for a spherical particle gives a crude estimate of molecular asymmetry.

Sedimentation velocity experiments were performed on Beckman Model Optima XL-I, using Rayleigh interference optics for detection. A two-sector cell with charcoal-filled Epon centerpieces and quartz windows was used. The Stalk81 sample was dialyzed overnight at 4°C against buffer (20 mM HEPES, 150 mM KCl, 2 mM DTT, pH 7.0). The experiments were carried out at 5°C and 60,000 rpm, for a run time of 4.5 h. The data was analyzed using the Second Moment contained in the Beckman software to determine the sedimentation coefficient, and the program Sednterp was then used to calculate $s^\circ_{20,w}$, f/f_o and the axial ratio *a/b*.

J. Redox equilibrium experiments

Redox equilibrium experiments have been used to demonstrate the preference for hetero-association of coiled-coils (Monera *et al.* 1993, O'Shea *et al.* 1989b). The presence of an equimolar mixture of oxidized and reduced glutathione, in excess over the protein species, allows a free exchange of disulfide bonds. At equilibrium, the species present should be thermodynamically most stable. In these experiments, the initial solution contains two homostranded species (e.g. EEox and KKox), which will be converted to the heterostranded species (EKox), if it is more stable. If there is no specificity, a random association will be observed, yielding a product ratio of 1:2:1.

The redox conditions consisted of a mixture of 50 μM oxidized E-coil and 50 μM oxidized K-coil in a buffer of 50 mM KPO_4, 100 mM KCl, 1 mM EDTA, pH 7.0 with equal amounts of oxidized and reduced glutathione (100 μM each) which allowed the disulfide bonds to exchange freely. The reaction was carried out under N_2., to prevent the self-oxidation of the reduced glutathione. Aliquots (10 μl) were withdrawn at different time points, quenched with 5 μl neat TFA, and analyzed by RP-HPLC. The amounts of the different species were quantified by their relative peak areas. We examined the effect of peptide concentration on the rate of formation of the hetero-stranded molecules. As expected, reducing the initial peptide concentration caused a reduction in the reaction rate. In subsequent reactions, the KCl was substituted with varying amounts of GdnHCl, to attempt to screen the electrostatic interactions. For the redox experiments in the presence of GdnHCl, the concentrations of oxidized and reduced glutathione were increased to 1 mM each to overcome self-oxidation of reduced glutathione, which is catalyzed by metal ion impurities in the GdnHCl.

H. Tryptic digests

Complete digests of peptide samples were performed by incubating 100-500 μg peptide and 2 μg trypsin in 100 μl buffer (50 mM NH_4HCO_3, 1 mM $CaCl_2$, pH 7.6) at

37°C overnight. The peptide digests were analyzed by analytical RP-HPLC and mass spectrometry.

Limited proteolysis was performed on the pseudostalk dynein construct, based on the protocol described by Morrice and Carrey (1997). A 100 µl sample of a 1 mg/ml protein solution (50 mM phosphate, 150 mM KCL, pH 7.0) was equilibrated to 37°C in a water bath. Trypsin was then added, to a ratio of 1/5000 (w/w) and the sample was incubated at 37°C. Aliquots were withdrawn at timed intervals, and proteolysis was quenched by dilution with 2X sample buffer (80 mM Tris-HCl, 15% glycerol, 100 mM DTT, 2% SDS, 0.006% bromphenol blue, pH 6.8) and heating to 95°C for 10 min. The times samples were then analyzed by SDS-PAGE (15% Tris-HCl gels), RP-HPLC, and mass spectroscopy.

CHAPTER III

Designing heterodimeric two-stranded α-helical coiled-coils: The effect of chain length on protein folding, stability and specificity

A version of this chapter has been published: Litowski, J.R., and Hodges, R.S. (2001) *J. Peptide Research* 58:477-492. The introduction has been rewritten and condensed, because these topics have been discussed in depth in the general introduction (Chapter I). A detailed description of the methods has been presented in Chapter II.

A. Summary

We have designed the E/K coil, a heterodimeric coiled-coil, as a universal peptide capture and delivery system for use in applications such as biosensors and affinity chromatography. In this design, heterodimer formation is specified through the placement of charged residues at the **e** and **g** positions of the heptad repeat. We have modified the affinity and stability of the E/K coil in order to allow a greater range of conditions for association and dissociation by varying the chain length to obtain three, four, and five heptad coiled-coils (21, 28, and 35 residues per polypeptide chain). The effect of chain length on stability and folding was examined by CD spectroscopy, guanidine hydrochloride denaturations, and redox equilibrium experiments. We found that increases in chain length produced increases in the stability of heterodimeric coiled-coils, but in a nonlinear fashion. The resulting disulfide-bridged hetero-stranded molecules and reduced heterodimers span a wide range of stabilities ($\Delta G = 3.3 - 11.9$ kcal/mol), greatly expanding their scope for use in protein engineering and biomedical applications.

B. Introduction

Modifying the stability and affinity of the E/K coil heterodimer will increase the flexibility of this design and its potential for use in applications. Previous studies have found that the stability of a de novo designed coiled-coil was related to its chain length, though in a nonlinear fashion (Su *et al.* 1994). That is, the same increase in chain length (i.e. one heptad) conferred different increases in stability to peptides of different length. A similar effect was found to occur in four-stranded coiled-coils (Fairman *et al.* 1995). These results suggest that reducing the length of the E and K coil peptides will be a useful approach to modulate the stability of the E/K coil. We will also be able to quantify the effect of chain length changes upon the stability of heterodimeric coiled-coils. In this study, we have modified our heterodimeric coiled-coil design by reducing its length from the original five heptads (35 residues) to three and four heptads (21 and 28 residues). The structure, stability, and specificity were then examined by a variety of biophysical approaches.

C. Results

Peptide Design

Greater than fifteen years of investigation have revealed the basic forces underlying coiled-coil stability, knowledge which has proven vital in the de novo design of heterodimeric coiled-coils (Chao *et al.* 1996, Graddis *et al.* 1993, O'Shea *et al.* 1993, Zhou *et al.* 1994b). The major stabilizing interactions are the hydrophobic interactions in the core (Harbury *et al.* 1993, Tripet *et al.* 2000, Wagschal *et al.* 1999b, Zhou *et al.* 1992a, 1992b), electrostatic attractions across the interface (Kohn & Hodges 1998, Krylov *et al.* 1994, Vinson *et al.* 1993, Zhou *et al.* 1994b), and helical propensity effects (Chakrabartty *et al.* 1994, Lyu *et al.* 1990, Monera *et al.* 1995, O'Neil & DeGrado 1990, Zhou *et al.* 1994c).

In our design (Figure 3-1 and Table 3-1), valine and leucine were chosen for the **a** and **d** positions, because of their high hydrophobicity and proven ability to form a highly stable hydrophobic core. Due to packing effects, β-branched hydrophobic residues (Val and Ile) are most stabilizing at position **a** (Zhu *et al.* 1993) and leucine is most stabilizing at position **d** (Moitra *et al.* 1997). These trends were confirmed and elaborated by recent papers in which the stabilities of all twenty naturally occurring residues were determined at the **a** and **d** positions of a coiled-coil model system (Tripet *et al.* 2000, Wagschal *et al.* 1999b). Building on experience (Chao *et al.* 1996, Graddis *et al.* 1993, O'Shea *et al.* 1993, Zhou *et al.* 1994b), we chose to specify heterodimer formation by the placement of charged residues at positions **e** and **g**. One strand of the coiled-coil, the E-coil, has glutamic acid (preferable to aspartic acid because of its higher helical propensity) at all **e** and **g** positions, while the complementary K-coil has lysine at all **e** and **g** positions (Figure 3-1). In this way, the two homodimers are destabilized by electrostatic repulsions and the E/K heterodimer is stabilized by electrostatic attractions. Serine was placed at position **b** to increase solubility. Although it has a low helical propensity, it is the smallest polar, uncharged residue that can increase solubility while minimally interacting with the other side-chains. To compensate, position **c** was filled with alanine, the residue with the highest helical propensity (Chakrabartty *et al.* 1994, Lyu *et al.* 1990, Monera *et al.* 1995, O'Neil & DeGrado 1990, Zhou *et al.* 1994c). Although nominally a hydrophobe, alanine has the smallest side-chain, which should discourage aggregation.

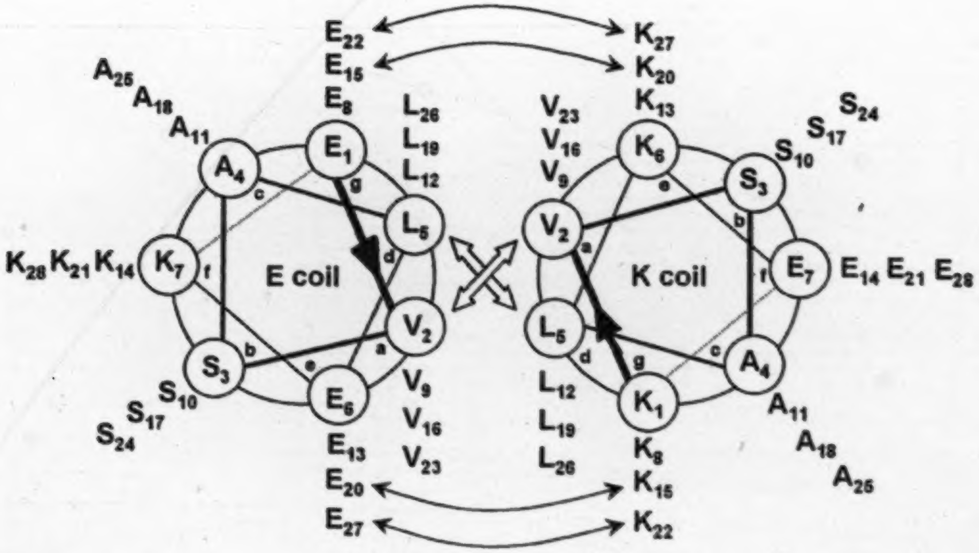
E_{22}
E_{15}
E_{8}
K_{27}
K_{20}
K_{13}
A_{25}
A_{18}
A_{11}
L_{26}
L_{19}
L_{12}
V_{23}
V_{16}
V_{9}
S_{24}
S_{17}
S_{10}
E_1
g
A_4
c
L_5
d
$K_{28}K_{21}K_{14}$
K_7
f
E coil
V_2
a
S_3
b
e
E_6
S_{10}
S_{17}
S_{24}
V_9
V_{16}
V_{23}
E_{13}
E_{20}
E_{27}
K_6
e
S_3
b
V_2
a
K coil
f
E_7
E_{14} E_{21} E_{28}
L_5
d
g
K_1
c
A_4
L_{12}
L_{19}
L_{26}
K_8
K_{15}
K_{22}
A_{11}
A_{18}
A_{25}

Figure 3-1. Helical wheel representation of the E4/K4 heterodimer, in which the coiled-coil is viewed in cross-section and the peptide chain propagates into the page from the N- to the C-terminus. The interhelical hydrophobic interactions are marked with wide arrows. The thin arrows denote the four pairs of interchain electrostatic interactions on each side of the hydrophobic core (e.g. E_{15}-K_{20}, E_{22}-K_{27}, etc.). Peptide nomenclature is described in Table 3-1 and under Peptide Design in the Results section.

Table 3-1. Peptide Sequences

Name[a]	Sequence[b]
	gabcdefgabcdefgabcdef
VSAL E3	Ac-EVSALEKEVSALEKEVSALEK-NH_2 Ac-CGGEVSALEKEVSALEKEVSALEK-NH_2
VSAL E4	Ac-EVSALEKEVSALEKEVSALEKEVSALEK-NH_2 Ac-CGGEVSALEKEVSALEKEVSALEKEVSALEK-NH_2
VSAL E5	Ac-EVSALEKEVSALEKEVSALEKEVSALEKEVSALEK-NH_2 Ac-CGGEVSALEKEVSALEKEVSALEKEVSALEKEVSALEK-NH_2
VSAL K3	Ac-KVSALKEKVSALKEKVSALKE-NH_2 Ac-CGGKVSALKEKVSALKEKVSALKE-NH_2
VSAL K4	Ac-KVSALKEKVSALKEKVSALKEKVSALKE-NH_2 Ac-CGGKVSALKEKVSALKEKVSALKEKVSALKE-NH_2
VSAL K5	Ac-KVSALKEKVSALKEKVSALKEKVSALKEKVSALKE-NH_2 Ac-CGGKVSALKEKVSALKEKVSALKEKVSALKEKVSALKE-NH_2

[a] VSAL denotes the peptide sequence in positions **a**, **b**, **c**, and **d** of the coiled-coil heptad repeat (**abcdefg**). E and K denote peptides in which the **e** and **g** positions are occupied by glutamic acid or lysine, respectively. The number describes the peptide length in number of heptads. The peptide sequences containing CGG were used to prepare the disulfide-bridged two-stranded α-helical coiled-coils and are denoted with the suffix "ox". For example, E3ox refers to the disulfide-bridged homo-stranded molecule, and E3/K3ox refers to the disulfide-bridged hetero-stranded molecule composed of the E3 and K3 peptides. See Peptide Design in the Results section for more details.

[b] The sequences are written in the one letter amino acid code. Ac represents an N^{α}-acetyl group, and NH_2 represents a C^{α}-amide group. Positions **a** and **d** of the heptad repeat are underlined and form the hydrophobic core of the coiled-coil.

Lysine was chosen for position **f** in the E-coil and glutamic acid in the K-coil in order to balance the net charge of each peptide and to increase solubility. The N-terminus of each peptide was acetylated and the C-terminus amidated, to prevent repulsions between the charged termini. Each peptide was also made with a Cys-Gly-Gly extension, to allow the peptides to be covalently linked through a disulfide-bridge. This stabilizes the coiled-coil and converts folding to a unimolecular process, removing the concentration dependence of a monomer to dimer equilibrium. Finally, versions of each peptide were made which were three, four, or five heptads long (equivalent to 21, 28, or 35 residues).

The nomenclature of our peptides is based on their sequences (Table 3-1). This entire series of peptides is named VSAL, after the residues at positions **a** through **d**. E and K refer to the identity of the residues at positions **e** and **g**; the number refers to the chain length in heptads. For example, E3 is the three heptad peptide with glutamic acid at all **e** and **g** positions. E4/K4 denotes the heterodimeric coiled-coil formed by the interaction of the E4 and K4 peptides. Peptides which have been covalently linked via a disulfide bond are denoted with the suffix "ox". The disulfide-bridged two-stranded molecule is a monomer and is described as homostranded or heterostranded. Thus E4ox is the two-stranded, disulfide-bridged homostranded molecule and E5/K5ox is the two-stranded, disulfide-bridged heterostranded molecule. Reduction of the disulfide-bridge yields the two-stranded dimeric coiled-coil.

Structural Characterization

The secondary structure of the peptides without a disulfide-bridge crosslink was measured by CD spectroscopy (Figure 3-2, panels A, C and E). The results show that the E and K coils of all lengths demonstrated random coil spectra when measured

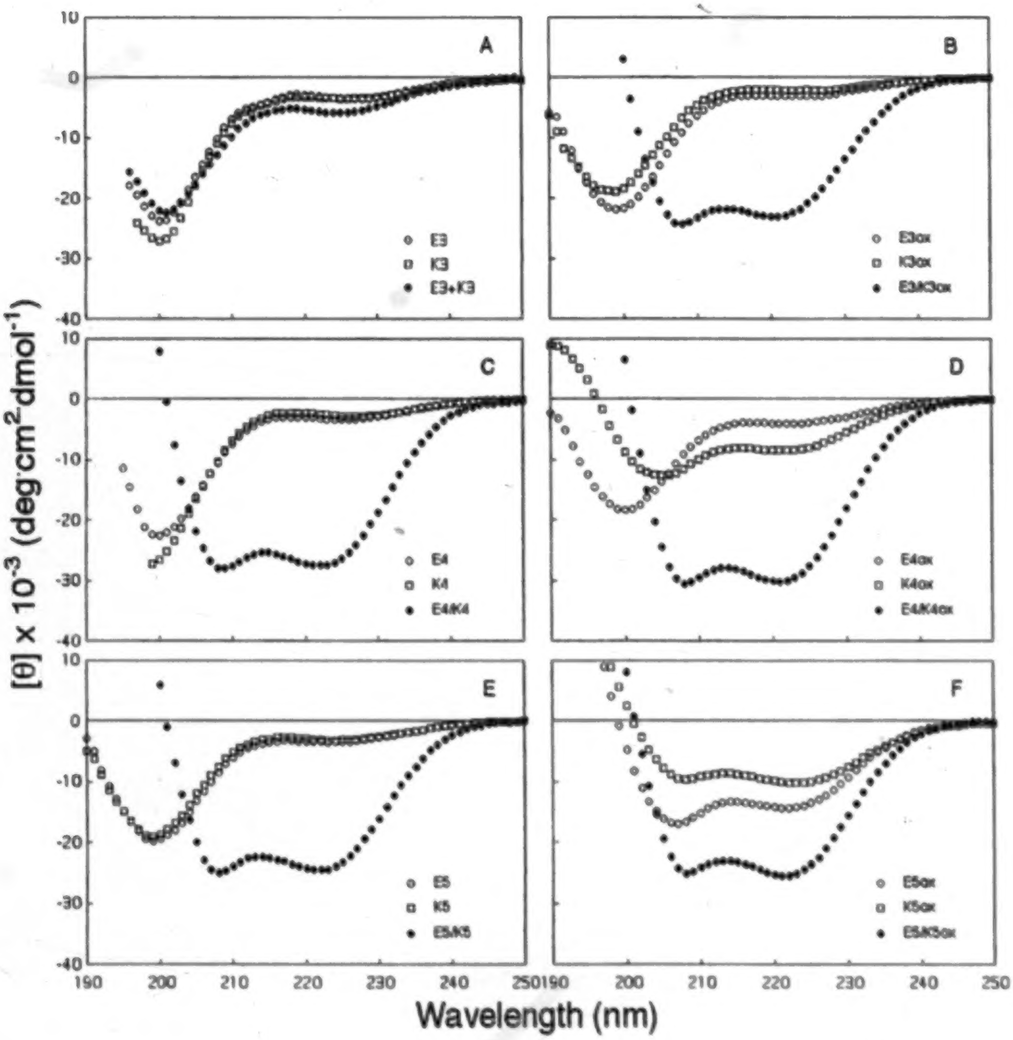

Figure 3-2. CD spectra of the non-crosslinked and oxidized (ox) coiled-coils of 3 (**A, B**), 4 (**C, D**), and 5 (**E, F**) heptads length. The spectra were recorded at 20°C in a 50 mM PO_4, 100 mM KCl, pH 7 buffer with a cell pathlength of 0.02 cm. Peptide concentrations were 1 mg/ml (120-430 μM).

individually. Equimolar mixtures of E4 and K4 or E5 and K5 showed CD spectra typical of α-helical coiled-coils, with the characteristic minima at 208 and 222 nm (Woody 1995). The molar ellipticities at 222 nm are directly proportional to the amount of helical structure present in the molecule (Chen *et al.* 1974, Gans *et al.* 1991) and are listed in Table 3-2. This clearly shows that the heterodimeric E4/K4 and E5/K5 are fully folded and highly helical coiled-coils, while the individual peptides are random coils. In contrast, E3 and K3 still exhibit a random coil spectrum when mixed, demonstrating that this sequence is not stable enough at three heptads length to fold as a coiled-coil (Figure 3-2, panel A).

The CD spectra of the oxidized homo-stranded and hetero-stranded molecules are shown in panels B, D, and F of Figure 3-2. The disulfide-bridge crosslink provided additional stability to peptide E3/K3ox, allowing it to fold as a homo-two-stranded coiled-coil. The stabilizing effect of a disulfide-bridge can also be disadvantageous; the E5ox and K5ox homostranded molecules show significant amounts of helical structure. The destabilization from the electrostatic repulsions has been partially overcome by the disulfide-bridge and the increased hydrophobic interactions from the increased chain length, allowing some folding. Trifluoroethanol (TFE) is widely used as a helix-inducing solvent to determine the potential of a given sequence to fold into an α-helix or the maximum helical content possible in the molecule (Shiraki *et al.* 1995, Sonnichsen *et al.* 1992). In our case, it was used to demonstrate that all of the peptides examined are capable of forming highly α-helical structures, as shown by the molar ellipticities at 222 nm in the presence of 50% TFE (Table 3-2).

Table 3-2. CD Spectroscopy

Peptide[a]	$[\theta]_{222}$[b]		% α-helix[c]		$[\theta]_{222}/[\theta]_{208}$	
	Benign	50% TFE	Benign	50% TFE	Benign	50% TFE
VSAL E3	-3,110	-25,160	10	81	0.31	0.83
VSAL K3	-3,330	-30,030	11	96	0.31	0.83
VSAL E3+K3	-5,670	-26,520	18	85	0.44	0.84
VSAL E3ox	-3,050	-22,220	10	71	0.34	0.78
VSAL K3ox	-2,110	-20,380	7	65	0.31	0.79
VSAL E3/K3ox	-22,830	-21,890	73	70	0.94	0.84
VSAL E4	-3,190	-28,780	10	86	0.30	0.83
VSAL K4	-2,470	-33,370	7	100	0.24	0.85
VSAL E4/K4	-27,460	-32,070	82	96	0.99	0.85
VSAL E4ox	-4,090	-21,460	12	64	0.44	0.81
VSAL K4ox	-8,500	-21,850	25	65	0.74	0.83
VSAL E4/K4ox	-29,940	-29,720	90	89	0.98	0.88
VSAL E5	-3,490	-22,000	10	63	0.41	0.82
VSAL K5	-3,060	-25,320	9	73	0.41	0.84
VSAL E5/K5	-24,490	-25,450	70	73	0.98	0.87
VSAL E5ox	-14,370	-21,040	41	61	0.87	0.82
VSAL K5ox	-10,180	-24,010	29	69	1.05	0.85
VSAL E5/K5ox	-25,519	-27,280	73	78	1.02	0.90

[a] Sequence nomenclature is described in Table 3-1 and in the Results section.

[b] The mean residue molar ellipticities at 222 nm were measured at 20°C in benign buffer (0.1M KCl, 0.05 M PO_4, pH 7). For samples containing TFE, the above buffer was diluted 1:1 (v/v) with TFE.

[c] The (%) helical content was calculated from the ratio of the observed $[\theta]_{222}$ value divided by the predicted molar ellipticity x 100. The predicted molar ellipticity was calculated from the equation $[\theta]_{222} = 40 \times 10^3 \times (1 - 4.6/n)$ for the chain length dependence of an α-helix (Chen *et al.* 1974, Gans *et al.* 1991), where *n* is the number of residues in the peptide.

The ratio of $[\theta]_{222}/[\theta]_{208}$ has been found to be 1.02-1.03 for fully folded coiled-coils in benign buffer and 0.8-0.9 in 50% TFE, which disrupts hydrophobic interactions at the coiled-coil interface and stabilizes the α-helix as a monomeric molecule (Lau *et al.* 1984, Zhou *et al.* 1992a). In our case, the coiled-coils E3/K3ox, E4/K4, E4/K4ox, and E5/K5 have $[\theta]_{222}/[\theta]_{208}$ ratios of 0.94-0.98 which decrease in the presence of TFE to 0.84-0.90, indicative of a shift to monomeric α–helices (Table 3-2). The decreased $[\theta]_{222}/[\theta]_{208}$ ratio in benign buffer (0.94-0.98 compared to 1.02-1.03) can be attributed to end fraying, which is more destabilizing to smaller peptides. End fraying in coiled-coils has been widely observed in a variety of experiments, including leucine to alanine substitutions (Zhou *et al.* 1992a) and NMR (Goodman & Kim 1991, Holtzer *et al.* 1997, Rohl *et al.* 1992).

CD spectroscopy was used to monitor titrations of E4 into K4 and vice versa (Figure 3-3). The conversion from the random coil spectrum of E4 or K4 to the α-helical coiled-coil spectrum of the mixtures is clearly visible. In both cases, the maximum helical structure was obtained at a 1:1 ratio of E4 and K4, indicative of their ratio in the coiled-coil structure. The presence of an isodichroic point in both titration series supports the two-state mechanism.

Oligomerization state

Analysis of the sedimentation equilibrium data for E3/K3 yielded an apparent molecular weight of 3574 Da, midway between the calculated mass of the monomeric and dimeric species. This is typical of a monomer-dimer equilibrium with a low association constant. E3/K3ox ran with an apparent molecular weight of 5413 Da,

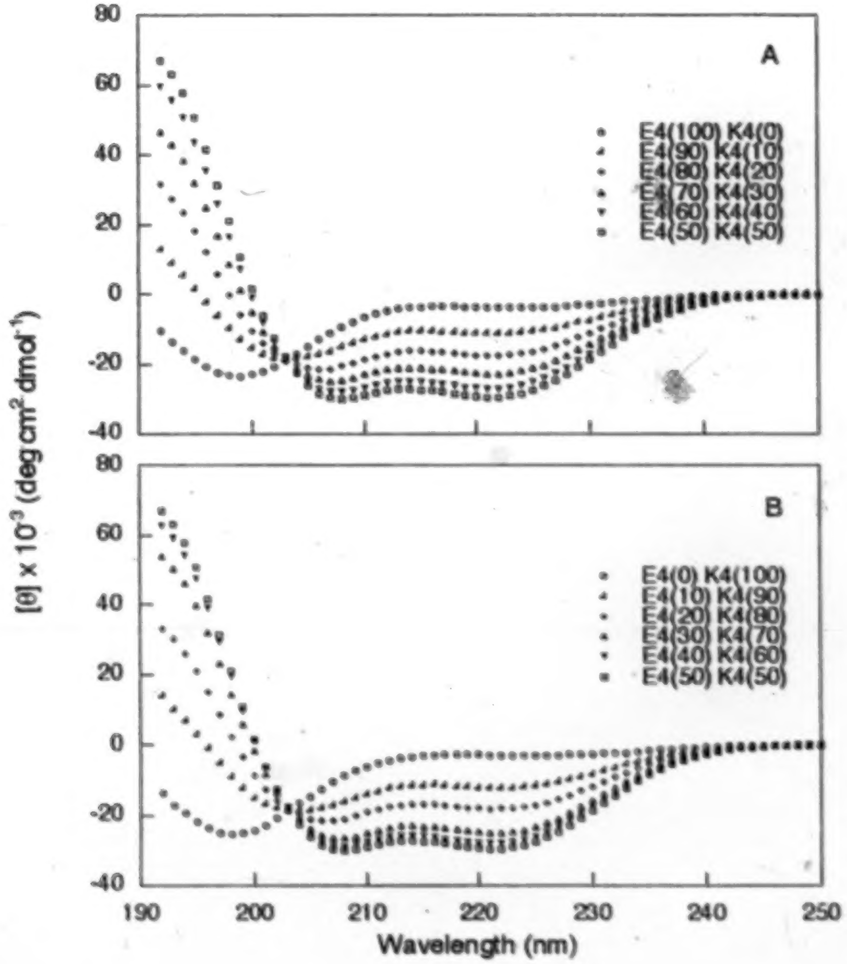

Figure 3-3. Titration of peptides E4 and K4, as monitored by CD spectroscopy. The percentage of E4 and K4 in each sample is listed on the figure (e.g. ○ E4(100) K4 (0)). The spectra were recorded at 20°C in a 50 mM PO_4, 100 mM KCl, pH 7 buffer. The total peptide concentration was 200 μM for all measurements.

slightly larger than theoretical for the two-stranded monomer (5091 Da). E4/K4 had an apparent molecular weight of 8656 Da, midway between the dimeric and tetrameric species. A trimeric species has been ruled out by the CD titration, which confirmed the one to one ratio of E4 and K4 in the folded molecule. Thus, a dimer-tetramer equilibrium can explain these results. In the case of the disulfide-bridged E4/K4ox, the disulfide bond stabilized the higher order species, yielding an apparent molecular weight of E4/K4ox of 14 kDa, slightly larger than the calculated weight for the four-stranded dimer (13 kDa).

Conformational stability

The conformational stabilities of the coiled-coils were determined by guanidine hydrochloride (GdnHCl) denaturation (Figure 3-4 and Table 3-3). A description of the equations used to analyze these curves is found in Chapter II. A clear trend of increasing conformational stability with increasing chain length was observed, in good agreement with previous results (Fairman *et al.* 1995, Su *et al.* 1994). The denaturation midpoints of E4/K4 and E5/K5 are 2.1 M and 3.9 M (Figure 3-4, panel B), an increase of 1.8 M from an increase in chain length of one heptad (seven residues). E3/K3 could not be examined by GdnHCl denaturation, due to its low stability and unfolded state under the experimental conditions. The denaturation curves of the oxidized heterostranded coiled-coils (Figure 3-4, panel A) clearly demonstrate that the relationship between stability and chain length is not linear, in good agreement with the results of Su *et al.* (1994). An increase from three to four heptads conferred an increase in $[\mathrm{GdnHCl}]_{1/2}$ of 2.1 M or a $\Delta\Delta G$ of 2.0 kcal/mol. In comparison, a further increase to five heptads resulted in a

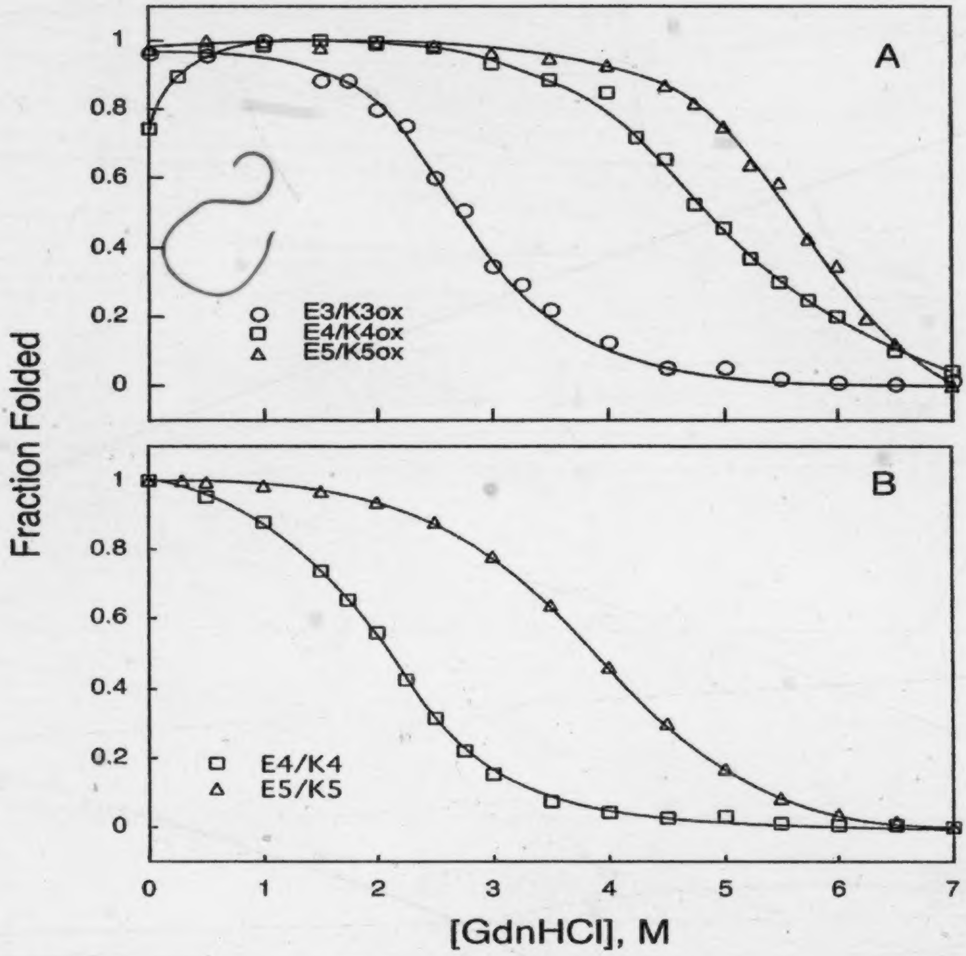

Figure 3-4. Guanidine hydrochloride denaturation curves at 20°C in a 50 mM PO_4, 100 mM KCl, pH 7 buffer. **A**) The oxidized E3/K3 (○), E4/K4 (□), and E5/K5 (Δ) hetero-stranded molecules (92 μM, 61 μM, and 30 μM). **B**) Non-crosslinked E4/K4 (□) and E5/K5 (Δ) (324 μM). The calculation of fraction of folded peptide (fn) is described in Chapter II.

Table 3-3. GdnHCl denaturation parameters

Peptide	$[\mathrm{GdnHCl}]_{1/2}$	m[a]	$\Delta\Delta G$ (kcal/mol)[b]	ΔG^{H2O}(kcal/mol)[b]
E3/K3ox	2.7 M	-1.17	0	3.3
E4/K4ox	4.8 M	-0.76	2.03 (wrt E3/K3ox)[c]	3.6
E5/K5ox	5.6 M	-1.17	3.39 (wrt E3/K3ox)	6.6
E4/K4	2.1 M	-1.73	0	8.2
E5/K5	3.9 M	-1.41	4.34 (wrt E4/K4)	11.9

[a] Obtained by the linear extrapolation method, as described in Chapter II.

[b] Obtained by the equation of Kellis *et al.* (1988), as described in Chapter II.

smaller increase in $[GdnHCl]_{1/2}$ (0.8 M) and ΔΔG (1.4 kcal/mol). This nonlinear effect can also be explained by end effects. Shorter coiled-coils are more destabilized by end effects, because a greater proportion of the total chain length is susceptible to fraying. This means that the same increase in length will contribute more to the stability of a short coiled-coil than to a long coiled-coil.

The free energies of unfolding (ΔG^{H_2O}) vary from 3.3 to 6.6 kcal/mol for the disulfide-bridged molecules and from 8.2 to 11.9 kcal/mol for the non-crosslinked molecules. Although the absolute values are subject to errors from the long extrapolation, the values are comparable to those of other heterodimeric coiled-coils. A 25-residue antiparallel coiled-coil, connected by a loop, had a ΔG of 3.2 kcal/mol (Myszka & Chaiken 1994). Longer non-crosslinked heterodimers have been designed with ΔGs in the range of 7 – 10 kcal/mol (Jelesarov & Bosshard 1996) and 11 – 16 kcal/mol (Moll *et al.* 2001).

A comparison of the crosslinked (Figure 3-4, panel A) and non-crosslinked species (Figure 3-4, panel B) shows the large stabilizing effect of a disulfide-bridge at an N-terminal flexible linker. Direct comparisons of the ΔΔG values are not valid, because one reaction is unimolecular, while the other is bimolecular. However, the introduction of the disulfide-bridge caused an increase in $[GdnHCl]_{1/2}$ of 2.7 M for E4/K4 and 1.7 M for E5/K5. The stability increase for E3/K3 could not be measured, as the non-crosslinked molecule was not folded under the experimental conditions. As the oxidized E3/K3 has a $[GdnHCl]_{1/2}$ of 2.7 M, the crosslink must increase stability by at least that much. There are two components to the stabilizing effect of disulfide-bridges in coiled-coils. The first is a reduction in the entropy of the unfolded state, which then reduces the entropic penalty of folding. In addition, a disulfide-bridge prevents end fraying at one terminus of the molecule. As the smaller coiled-coils are the most destabilized by end fraying, they experience the greatest increase in stability upon the formation of an N-terminal disulfide-bridge.

Interestingly, E4/K4ox showed an increase in molar ellipticity at low levels of GdnHCl, reaching a maximum helical structure at 1.0 M GdnHCl (Figure 3-4, panel A). This may be the result of small structural changes as GdnHCl removes aggregation. Despite its wide-spread use as a protein denaturant, low levels of GdnHCl have been observed to stabilize protein structure (Hagihara *et al.* 1993, 1994, Kohn *et al.* 1995b, Mayr & Schmid 1993). This has been attributed to its ability as a salt to screen electrostatic repulsions.

The slope of the ΔG vs. [GdnHCl] plot (the m value) has been predicted to correlate with the change in accessible surface area upon denaturation (Alonso & Dill 1991, Schellman 1978). Experimental verification was provided by Myers *et al.* (1995). The non-crosslinked peptides have larger m values, suggesting that they have a greater amount of exposed surface area upon denaturation, compared to the crosslinked coiled-coils. Similar results have previously been observed (Hodges *et al.* 1990, Regan *et al.* 1994).

Redox equilibrium experiments

In the de novo design of heterodimeric coiled-coils, we define specificity as the preference of heterodimer formation versus homodimer formation. Redox equilibrium experiments have been used effectively to demonstrate specificity (Monera *et al.* 1993, O'Shea *et al.* 1989a, 1989b). In these experiments, two oxidized homo-stranded peptides (i.e. E3ox and K3ox) are stirred in a redox equilibrium buffer. As the system reaches equilibrium, the reaction mixture will be dominated by the most thermodynamically stable species. A random association of the peptide chains yields a ratio of 1:2:1 of the three species (Eox, EKox, and Kox).

Redox equilibrium experiments were performed with the three, four, and five heptad homo-stranded Eox and Kox peptides, illustrated by selected chromatograms in Figure 3-5 and as plots of mole fraction vs. time in Figure 3-6. The disappearance of the homo-stranded peaks and the appearance of the hetero-stranded peaks can be observed over the course of the reaction. The rate of hetero-stranded molecule formation was not found to correlate with stability. The formation of E3/K3ox was rapid, and the reaction reached completion in less than 15 minutes. In contrast, the more stable E4/K4ox required 2.5 hours to reach 100%. The most stable species, E5/K5ox, was not detected over a 24 hour reaction period (data not shown).

Why does the least stable hetero-stranded molecule form the most quickly? The disulfide-bridged homo-stranded molecules become more stable with increasing chain length, as demonstrated by the CD spectra in Figure 3-2. This makes formation of the homo-stranded molecules a competing pathway to hetero-stranded molecule formation during the redox experiments. An alternate explanation is provided by an interaction between the homo-stranded molecules (i.e. E5ox and K5ox), forming a hetero-complex of the two disulfide-bridged homo-stranded molecules without undergoing disulfide-bond exchange. This second explanation is supported by CD spectroscopy, as a mixture of E5ox and K5ox yielded an increase in molar ellipticity at 222 nm (data not shown). This

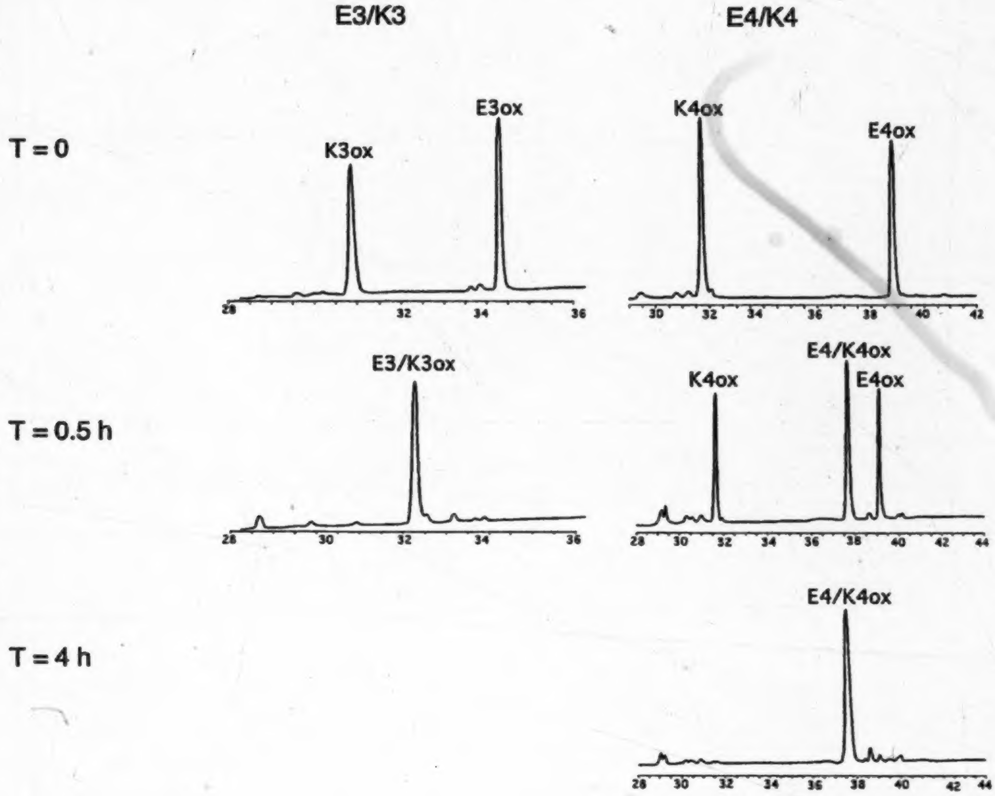

Figure 3-5. Sample chromatograms from the redox equilibrium experiments. The disappearance of the oxidized homo-stranded species and the appearance of the oxidized hetero-stranded molecule can be seen over time. The samples were analyzed by RP-HPLC with a 1% CH_3CN/min gradient.

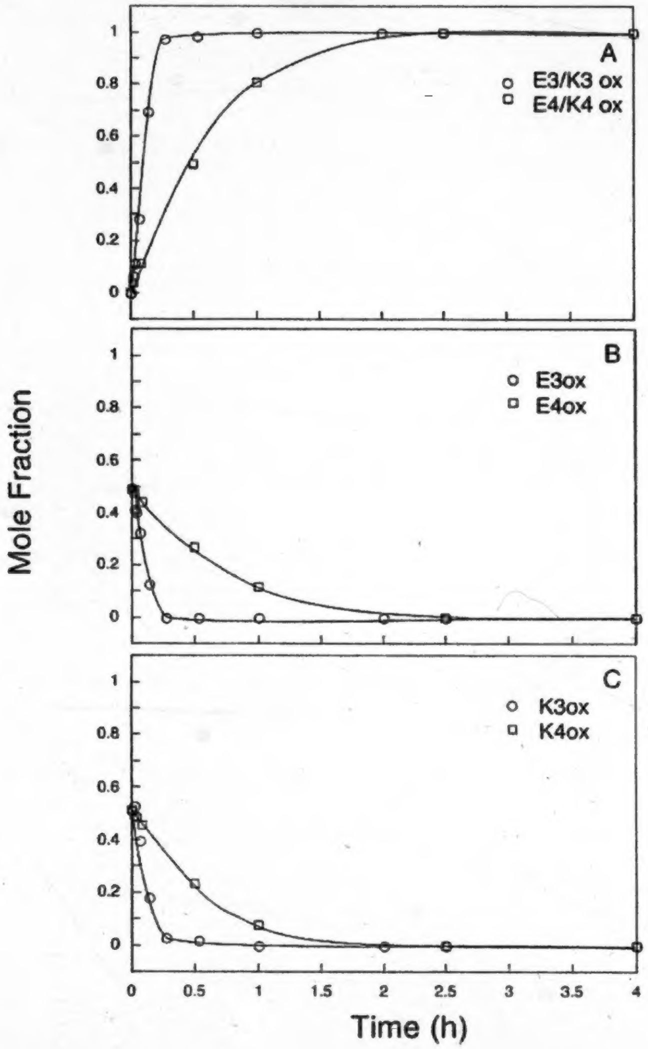

Figure 3-6. A) The rate of formation of the E/K hetero-stranded molecules, starting with the two homo-stranded molecules during the redox equilibrium experiments. **B**) The rate of disappearance of the E-coil homo-stranded molecules. **C**) The rate of disappearance of the K-coil homo-stranded molecules. The peptides of three (○) and four (□) heptads length are shown. Mole fraction is defined as the ratio of the amount of one species (i.e. E3ox) to the total of the three species (i.e. E3ox + K3ox + E3/K3ox). The amounts of each species were determined by their RP-HPLC chromatogram peak area.

complex has a reasonable stability, with a GdnHCl midpoint of 4.7 M (Figure 3-7). The disulfide-bridged E5/K5ox is more stable, and has a more cooperative denaturation curve, suggesting that packing differences exist between the two species. Still the E5ox + K5ox complex appears to be stable enough to remove the driving force for the formation of the disulfide-bridged E5/K5ox. This proves that the redox equilibrium experiment is not an appropriate method for testing specificity when there is an interaction between the disulfide-bridged homo-stranded species. This is not a concern in our peptide capture and delivery system, which consists of a monomeric strand that is immobilized as the capture peptide and the complementary monomeric delivery peptide as a peptide/target protein fusion.

Air oxidation was chosen as an alternate method of demonstrating the specificity of the interaction between E5 and K5. In this experiment, reduced E5 and K5 were mixed in an oxidizing buffer and the appearance of the oxidized homo-stranded and hetero-stranded species was monitored by RP-HPLC. As in the redox equilibrium experiments, a random association will result in a 1:2:1 ratio of species. The amounts of the different species over the course of the experiment are shown as mole fractions in Figure 3-8. The starting conditions consisted of equal amounts of the two reduced species, K5r and E5r. Over a four hour period, they declined to mole fractions of less than 0.1. This was accompanied by the increase of the hetero-stranded E5/K5ox to a mole fraction of 0.6. The oxidized homo-stranded species (K5ox and E5ox) form to a much lesser extent, reaching mole fractions of less than 0.15. It can be seen from Figure 3-8 that the ratio of E5/K5ox to the homo-stranded species is significantly greater than 2:1, a clear demonstration that E5 and K5 specifically form a hetero-stranded coiled-coil.

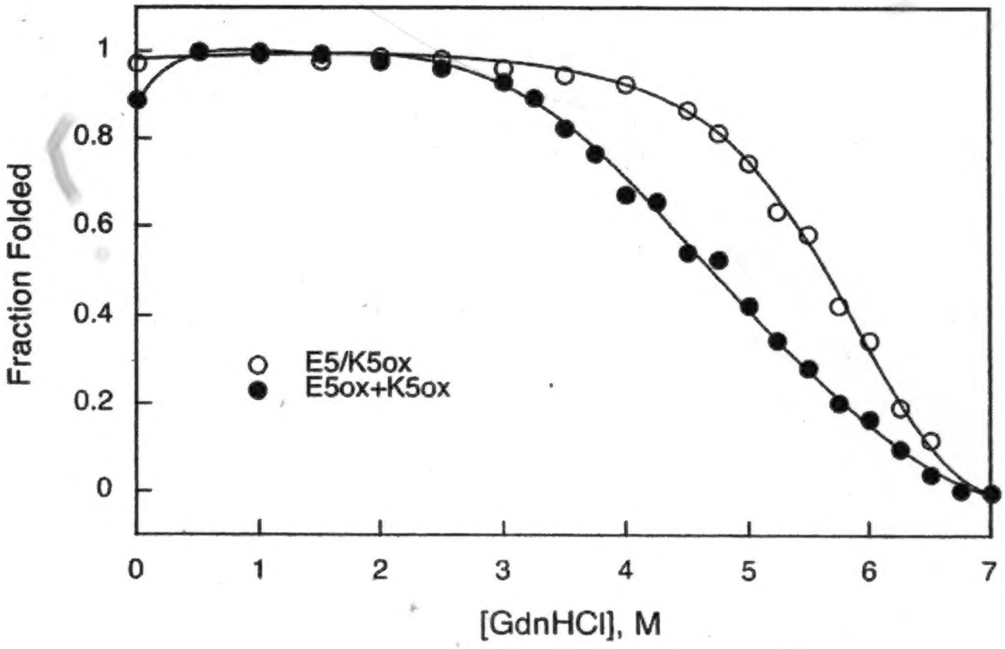

Figure 3-7. Guanidine hydrochloride denaturation of the hetero-stranded E5/K5ox (○, 30 μM) and an equimolar mixture of the homo-stranded E5ox and K5ox (●, 38 μM). The calculation of fraction of folded peptide (fn) is described in Chapter II.

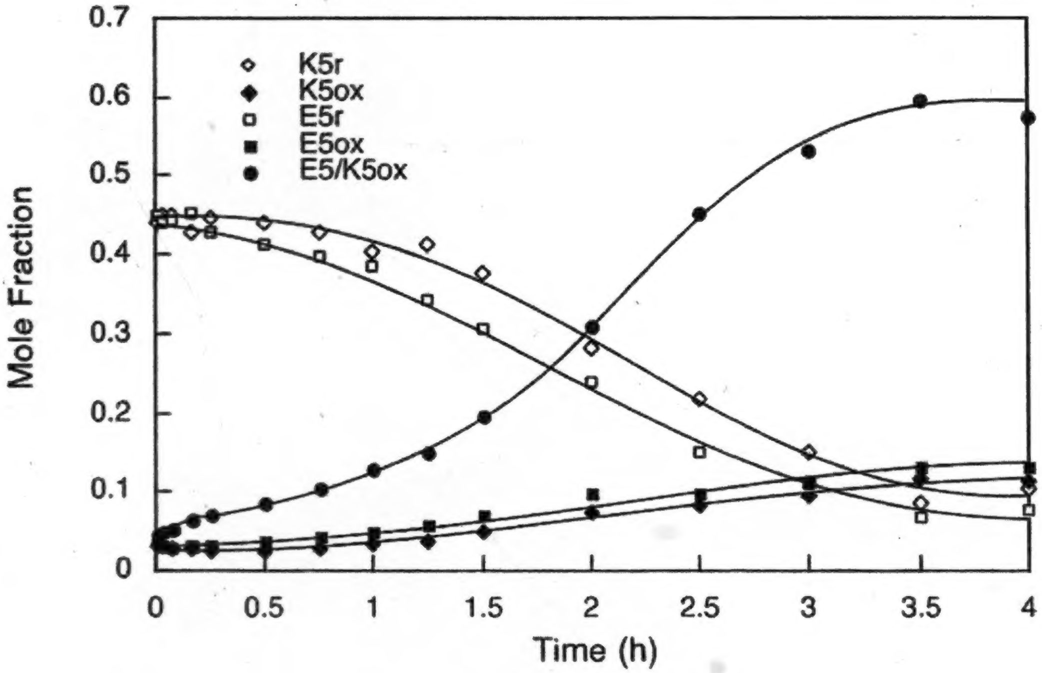

Figure 3-8. Air oxidation of the E5 and K5 peptides. E5r and K5r denote the reduced peptides, and E5ox, K5ox, and E5/K5ox denote the oxidized homo-stranded and hetero-stranded species. Mole fraction is defined as the ratio of the amount of one species (i.e. E5/K5ox) to the total of the five species (i.e. E5r + K5r + E5ox + K5ox + E5/K5ox). The amounts of each species were determined by their peak area from the HPLC chromatograms.

We were intrigued by the rapid formation of E3/K3ox, and decided to investigate further. Increasing amounts of GdnHCl were added to the redox buffer to screen electrostatic interactions and remove the driving force for specificity. These results are plotted in Figure 3-9. In benign conditions, the homo-stranded molecules, E3ox and K3ox rapidly disappeared, and were replaced by the hetero-stranded E3/K3ox. As the GdnHCl was added, the reaction rates were reduced and the amount of E3/K3ox which formed decreased. However, the 1:2:1 ratio, indicative of random formation, was not observed. This is because, as the amount of GdnHCl increased, increasing amounts of the peptide-glutathione adducts were formed. The GdnHCl removed the electrostatic interactions and disrupted the hydrophobic interactions, eliminating the driving force for coiled-coil formation or association.

C. Discussion

What is the relationship between chain length and stability in coiled-coils? In general, increases in chain length are correlated with increases in stability. This has been shown by a number of authors, studying both de novo and native coiled-coil sequences. Lau *et al.* (1984) made a series of de novo peptides, based on an idealized tropomyosin sequence. They found that increases in chain length conferred increases in stability. The degree of stability is sequence dependent – de novo peptides of 29 and 36 residues length were significantly more stable than tropomyosin, a 284 residue coiled-coil. This effect was studied in more detail by Su *et al.* (1994), who made a series of peptides based on the heptad repeat EIEALKA, of 9 to 35 residues length. Each peptide had one more hydrophobic residue in the core than the next shortest peptide. Increases in length clearly

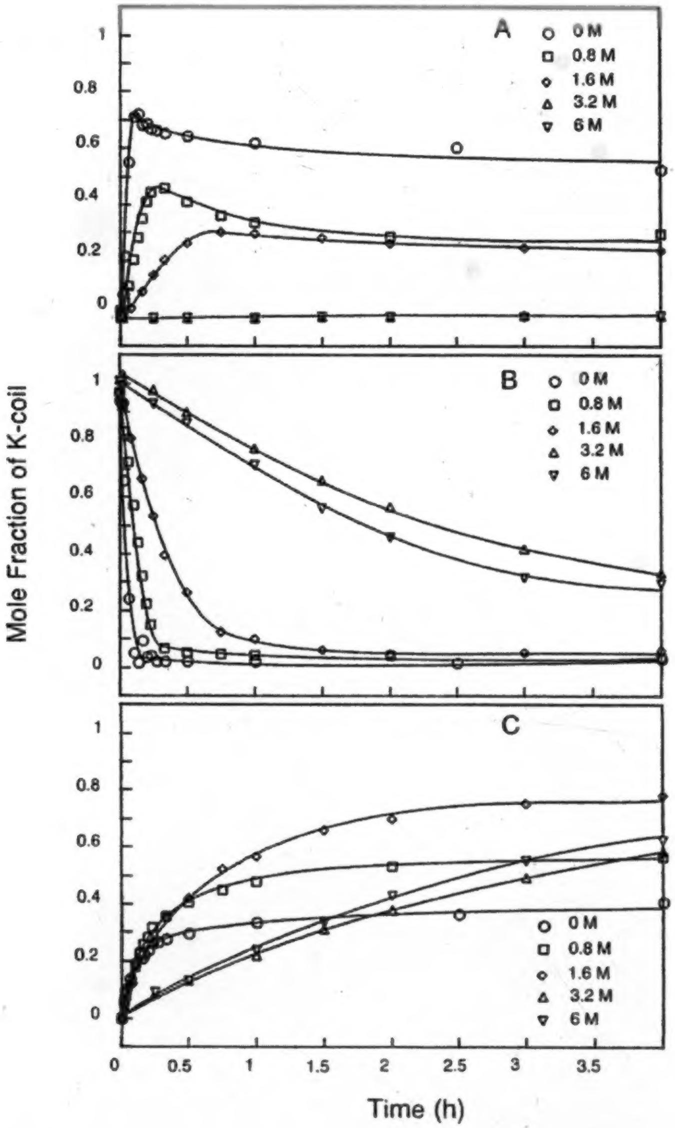

Figure 3-9. The effect of GdnHCl on the redox equilibrium curves. These show the K-coil mole fraction of E3/K3ox (**A**), K3ox (**B**), and the K3/glutathione adduct (**C**) in the presence of 0, 0.8, 1.6, 3.2, and 6 M GdnHCl. The K-coil mole fraction was defined as the ratio of the amount of each species (i.e. K3ox) over the sum of the other K-coil species (1/2 E3/K3ox, K3ox, K3, and K3/glutathione).

correlated with increases in helical structure and stability to GdnHCl denaturation. Interestingly, this relationship between stability and length was not linear. Increases in length to short peptides conferred large increases in stability, while a similar increase in length had much less effect on the stability of larger peptides. Fairman *et al.* (1995) extended these results to four-stranded coiled-coils and found that increases of one heptad conferred an increase in stability of about 4 kcal/mol per monomer. This is considerably larger than that observed in dimeric coiled-coils (Su *et al.* 1994), perhaps due to the greater amount of surface area buried upon tetramer formation.

The effect of chain length upon α-helix formation has also received attention. Scholtz (1991b) analyzed the thermal denaturation profiles of a series of poly-alanine peptides ($n = 14 - 50$ residues) in terms of the Zimm-Bragg and Lifson-Roig theories, in order to determine the helix propagation parameter, s, the helix nucleation parameter, σ, and $\Delta H°$/residue. These three parameters were found to be insensitive to chain length. More recently, however, Young *et al.* (1996) modeled hydrogen bond formation and helix propagation at the N- and C- termini of poly-alanine peptides ($n = 4 - 15$ residues). Helix propagation from the N-terminus (s_N) was found to be favourable and increased with increasing chain length. In contrast, helix propagation from the C-terminus (s_C) was slightly unfavourable and not affected by chain length. The combination of these two effects yielded an effective propagation (s_{eff}) that was favourable, with a small, but distinct, dependence upon chain length. Gutin *et al.* (1996) simulated the folding of polypeptide chains of 10 – 100 residues length, using a lattice model. They found that there was a small dependence of folding time on chain length, which was considerably weaker than that originally predicted. The effect of chain length on the predominance of α-helix vs. 3_{10} helix was investigated by Fiori *et al.* (1993). They found that the shorter of the peptides examined (16 residues) was predominantly a 3_{10} helix, but the longer peptide (21 residues) was predominantly α-helical.

The E/K heterodimers exhibited a nonlinear increase in stability with chain length, similar to that observed by Su *et al.* (1994). In general, the coiled-coils studied by Su *et al.* had higher denaturation midpoints than those in this study, due to their use of the more stable Ile/Leu hydrophobic core. The length dependent increases in $[\text{GdnHCl}]_{1/2}$ are similar for both sets of peptides. Our ΔΔG per heptad is less than that observed for tetrameric coiled-coils by Fairman *et al.* (1995), likely because larger amounts of surface area are buried in tetramers than in dimers.

How does an increase in stability result from increased chain length? One explanation is the increased number of stabilizing interactions, including hydrophobic interactions, hydrogen bonds in the helix backbone, and electrostatic attractions. The observed increases in stability are similar to those conferred by Val or Leu in the core. Recent results from our lab have shown that Val at a central "**a**" position contributes 1.66 kcal/mol more than Ala, and Leu at a central "**d**" position contributes 3.8 kcal/mol more than Ala (Tripet *et al.* 2000, Wagschal *et al.* 1999b). The other key factor is end fraying, a partial and temporary unfolding of the helix termini. This phenomenon is predicted by both Zimm-Bragg and Lifson-Roig theories of helix formation (Rohl *et al.* 1992). Experimental evidence includes the tolerance of coiled-coils to leucine to alanine substitutions at the helix termini (Zhou *et al.* 1992a). More direct observations of end fraying are the dependence of hydrogen-deuterium exchange rates and $^{13}C^{\alpha}$ chemical shifts upon helical position (Goodman & Kim 1991, Holtzer *et al.* 1997). As peptides increase in length, a smaller proportion of the residues are subject to fraying, making end fraying less destabilizing.

Modification of chain length has allowed us to design a series of heterodimeric coiled-coils with a wide range of stabilities. The GdnHCl midpoints vary from 2.7 to 5.6 M, and the $\Delta G_u^{H_2O}$ values vary from 3.3 to 6.6 kcal/mol for the disulfide-bridged hetero-stranded coiled-coils (3, 4, and 5 heptads). The non-crosslinked heterodimeric coiled-coils (4 and 5 heptads) had GdnHCl midpoints of 2.1 to 3.9 M and $\Delta G_u^{H_2O}$ values of 8.2 to 11.9 kcal/mol. This range of specificities and stabilities allows considerable scope for tailoring heterodimeric coiled-coils for specific applications. For example, affinity chromatography dissociation conditions of the heterodimers can be less harsh with the shorter chain lengths. The E3 and K3 peptides did not fold into a heterodimeric coiled-coil in the absence of a disulfide-bridge, rendering them unsuitable for applications requiring the dimerization of two separate polypeptide chains. However, coiled-coils of this chain length have the potential for use, provided their sequences have additional stabilizing factors such as increased hydrophobicity or α-helical propensity. These results are an important step towards increasing the flexibility of our heterodimeric coiled-coil design.

CHAPTER IV

Designing heterodimeric two-stranded α-helical coiled-coils: The effects of hydrophobicity and α-helical propensity on protein folding, stability and specificity

A version of this chapter has been published: Litowski, J.R., and Hodges, R.S. (2002) *J. Biol. Chem.* **277**(40):37272-37279. The introduction has been rewritten and condensed, because these topics have been discussed in depth in the general introduction (Chapter I). A detailed description of the methods has been presented in Chapter II.

A. Summary

The E/K coil, a heterodimeric coiled-coil, has been designed as a universal peptide capture and delivery system for use in applications such as biosensors and as an expression and affinity purification tag. In this design, heterodimer formation is specified through the placement of charged residues at the **e** and **g** position of the heptad repeat such that E-coil contains all glutamic acid residues at these positions and K-coil contains all lysine residues at these position. The affinity and stability of the E/K coil has been modified in order to allow a greater range of conditions for association and dissociation. Increasing the hydrophobicity of the coiled-coil core, by substituting isoleucine for valine, gave increases in stability of 2.81 and 3.73 kcal/mol (0.47 kcal/mol per substitution). Increasing the α-helical propensity of residues outside the core, by substituting alanine for serine, yielded increases in stability of 2.68 and 3.28 kcal/mol (0.41 and 0.45 kcal/mol per substitution). These sequence changes yielded a series of heterodimeric coiled-coils whose stabilities varied from 6.8 – 11.2 kcal/mol, greatly expanding their scope for use in protein engineering and biomedical applications.

B. Introduction

Our success in modifying the stability of the E/K coil design through chain length encouraged us to try additional approaches. The shortest E/K analog (VSAL E3/K3) was quite labile and was only able to fold when stabilized by an interhelical disulfide bond (Litowski & Hodges 2001). It would be a great advantage to stabilize this peptide, while maintaining its short size. We chose two sequence modifications that were predicted to be stabilizing. The first approach was to increase the hydrophobicity of residues in the coiled-coil hydrophobic core, which has been shown to be closely related to coiled-coil stability (Cedervall *et al.* 1997, Tripet *et al.* 2000, Wagschal *et al.* 1999b, Zhu *et al.* 1993). The second approach was to increase the α-helical propensity of residues outside the coiled-coil interface. Helical propensity differences have been shown to affect coiled-coil stability up to 0.77 kcal/mol per substitution (O'Neil & DeGrado 1990) and up to 0.96 kcal/mol per substitution in a single stranded amphipathic α-helix (Zhou *et al.* 1994c). Different combinations of these sequence changes will yield a series of heterodimeric coiled-coils with a wide range of stabilities and affinities.

C. Results

Peptide Design

Considerable experience has been gained in understanding the interactions and features important for the design and folding of coiled-coils (Chao *et al.* 1996, Graddis *et al.* 1993, O'Shea *et al.* 1993, Zhou *et al.* 1994b). The major stabilizing features are the hydrophobic interactions in the core (Harbury *et al.* 1993, Tripet *et al.* 2000, Wagschal *et al.* 1999b, Zhou *et al.* 1992a, 1992b), electrostatic attractions across the coiled-coil interface (Kohn & Hodges 1998, Krylov *et al.* 1994, Vinson *et al.* 1993, Zhou *et al.* 1994b), and helical propensity effects (Chakrabartty *et al.* 1994, Lyu *et al.* 1990, Monera *et al.* 1995, O'Neil & DeGrado 1990, Zhou *et al.* 1994c). This knowledge and experience was used in the design of the E/K heterodimeric coiled-coils, as illustrated in Figure 4-1 and Table 4-1 (Chao *et al.* 1996, 1998). The hydrophobic core, composed of positions **a** and **d**, was occupied by valine and leucine. Due to packing effects, β-branched hydrophobic residues are the most stabilizing at position **a** (Wagschal *et al.* 1999b, Zhu *et al.* 1993) and leucine is the most stabilizing residue at position **d** (Moitra *et al.* 1997, Tripet *et al.* 2000). Serine was placed at position **b** because it is a small polar residue which will increase peptide solubility. Alanine was placed at position **c** to increase the overall helical propensity (Chakrabartty *et al.* 1994, Lyu *et al.* 1990, Monera *et al.* 1995, O'Neil & DeGrado 1990, Zhou *et al.* 1994c). Heterodimerization was specified for by the placement of charged residues at the **e** and **g** positions (Chao *et al.* 1996, Graddis *et al.* 1993, O'Shea *et al.* 1993, Zhou *et al.* 1994b). The **e** and **g** positions are occupied by glutamic acid in the E-coils and by lysine in the K-coils. Thus, potential homodimer formation will be destabilized, while the E/K heterodimer will be stabilized through electrostatic attractions (Chao *et al.* 1996, 1998). The charged residues at position **f** were opposite in charge to those at positions **e** and **g** and were incorporated to increase solubility and reduce the overall net charge. The N-terminus was acetylated and the C-terminus was amidated in order to prevent repulsions between charged termini.

There are two principal targets for increasing the stability of this sequence – the hydrophobic core of the coiled-coil (positions **a** and **d**) and the α-helical propensity of

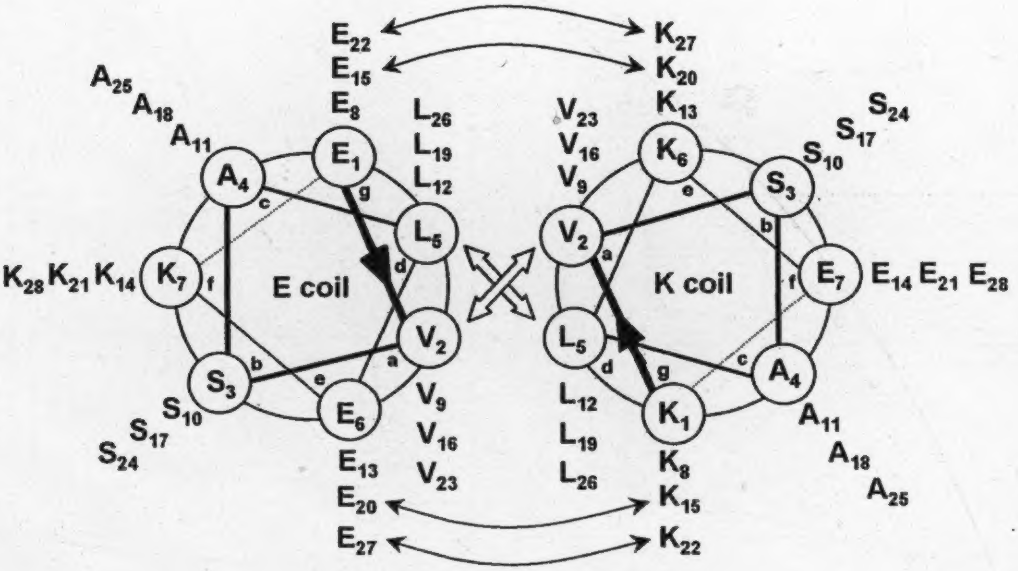
E_{22}
E_{15}
E_8
K_{27}
K_{20}
K_{13}
A_{25}
A_{18}
A_{11}
L_{26}
L_{19}
L_{12}
V_{23}
V_{16}
V_9
S_{24}
S_{17}
S_{10}
A_4
E_1
g
c
L_5
K_6
e
S_3
b
d
V_2
a
K_{28} K_{21} K_{14}
K_7
f
E coil
K coil
f
E_7
E_{14} E_{21} E_{28}
V_2
L_5
S_3
b
e
a
d
g
c
A_4
E_6
K_1
S_{10}
S_{17}
S_{24}
V_9
V_{16}
V_{23}
L_{12}
L_{19}
L_{26}
A_{11}
A_{18}
A_{25}
E_{13}
E_{20}
E_{27}
K_8
K_{15}
K_{22}

Figure 4-1. Helical wheel representation of the E4/K4 heterodimer, in which the coiled-coil is viewed in cross-section and the peptide chain propagates into the page from the N- to the C-terminus. The interhelical hydrophobic interactions are denoted with wide arrows. The thin arrows denote the four pairs of i to i' + 5 interchain electrostatic attractions on each side of the hydrophobic core (e.g. E22-K27, E15-K20, etc.). Peptide nomenclature is described in Table 4-1 and in the Results section.

Table 4-1. Peptide Sequences

Name[a]	Sequence[b]
	gabcdefgabcdefbabcdef
IAAL E3	Ac-EIAALEKEIAALEKEIAALEK-NH_2
IAAL E4	Ac-EIAALEKEIAALEKEIAALEKEIAALEK-NH_2
IAAL K3	Ac-KIAALKEKIAALKEKIAALKE-NH_2
IAAL K4	Ac-KIAALKEKIAALKEKIAALKEKIAALKE-NH_2
ISAL E3	Ac-EISALEKEISALEKEISALEK-NH_2
ISAL E4	Ac-EISALEKEISALEKEISALEKEISALEK-NH_2
ISAL K3	Ac-KISALKEKISALKEKISALKE-NH_2
ISAL K4	Ac-KISALKEKISALKEKISALKEKISALKE-NH_2
VAAL E3	Ac-EVAALEKEVAALEKEVAALEK-NH_2
VAAL E4	Ac-EVAALEKEVAALEKEVAALEKEVAALEK-NH_2
VAAL K3	Ac-KVAALKEKVAALKEKVAALKE-NH_2
VAAL K4	Ac-KVAALKEKVAALKEKVAALKEKVAALKE-NH_2
VSAL E3	Ac-EVSALEKEVSALEKEVSALEK-NH_2
VSAL E4	Ac-EVSALEKEVSALEKEVSALEKEVSALEK-NH_2
VSAL K3	Ac-KVSALKEKVSALKEKVSALKE-NH_2
VSAL K4	Ac-KVSALKEKVSALKEKVSALKEKVSALKE-NH_2

[a] The four letter name (i.e. IAAL) denotes the peptide sequence in positions **a**, **b**, **c**, and **d** of the coiled-coil heptad repeat (**abcdefg**). E and K denote peptides in which all of the **e** and **g** positions are occupied by either glutamic acid or lysine, respectively. The number refers to the peptide length in number of heptads.

[b] The sequences are written in the one letter amino acid code. Ac represents an N^{α}-acetyl group, and NH_2 represents a C^{α}-amide group. Positions **a** and **d** of the heptad repeat are underlined and form the hydrophobic core of the coiled-coil.

surface exposed positions **b**, **c**, **e**, **f** and **g**. We chose to stabilize the hydrophobic core by increasing its hydrophobicity. Isoleucine has been shown to be significantly more stable in the **a** position than valine, due to its higher hydrophobicity (Zhu *et al.* 1993). Accordingly, a series of peptides was made in which all of the **a** positions have either valine or isoleucine. The α-helical structures were stabilized by increasing the overall α-helical propensity. To do this, a series of peptides was made in which the low helical propensity residue serine was substituted with the high helical propensity residue alanine at all **b** positions. We made a series of E and K coils which contained one or both of these modifications and were 3 or 4 heptads long (21 or 28 residues). The nomenclature reflects the sequences (Table 4-1) at positions **a** through **d** (i.e. VSAL), and the number reflects the length of the peptide in heptads. E/K denotes a heterodimer formed by a 1:1 association of the E and K coils.

CD Spectroscopy

The secondary structure of the peptides was evaluated by CD spectroscopy. VSAL E4/K4 exhibits a typical α-helical spectrum (Figure 4-2B), with the characteristic minima at 208 and 222 nm (Woody 1995). Since the molar ellipticity at 222 nm is directly proportional to the amount of helical structure (Chen *et al.* 1974, Gans *et al.* 1991), VSAL E4/K4 is folded (Table 4-2). In contrast, the VSAL E4 and VSAL K4 peptides exhibited random coil spectra, with a broad minimum at 200 nm (Figure 4-2B). This clearly shows that VSAL E4 and VSAL K4 specifically interact to form a heterodimeric α-helical coiled-coil. In contrast, the smaller VSAL E3/K3 analog is still a random coil (Figure 4-2A). This shows that this sequence is not stable enough at a length of 3 heptads to form a heterodimeric coiled-coil.

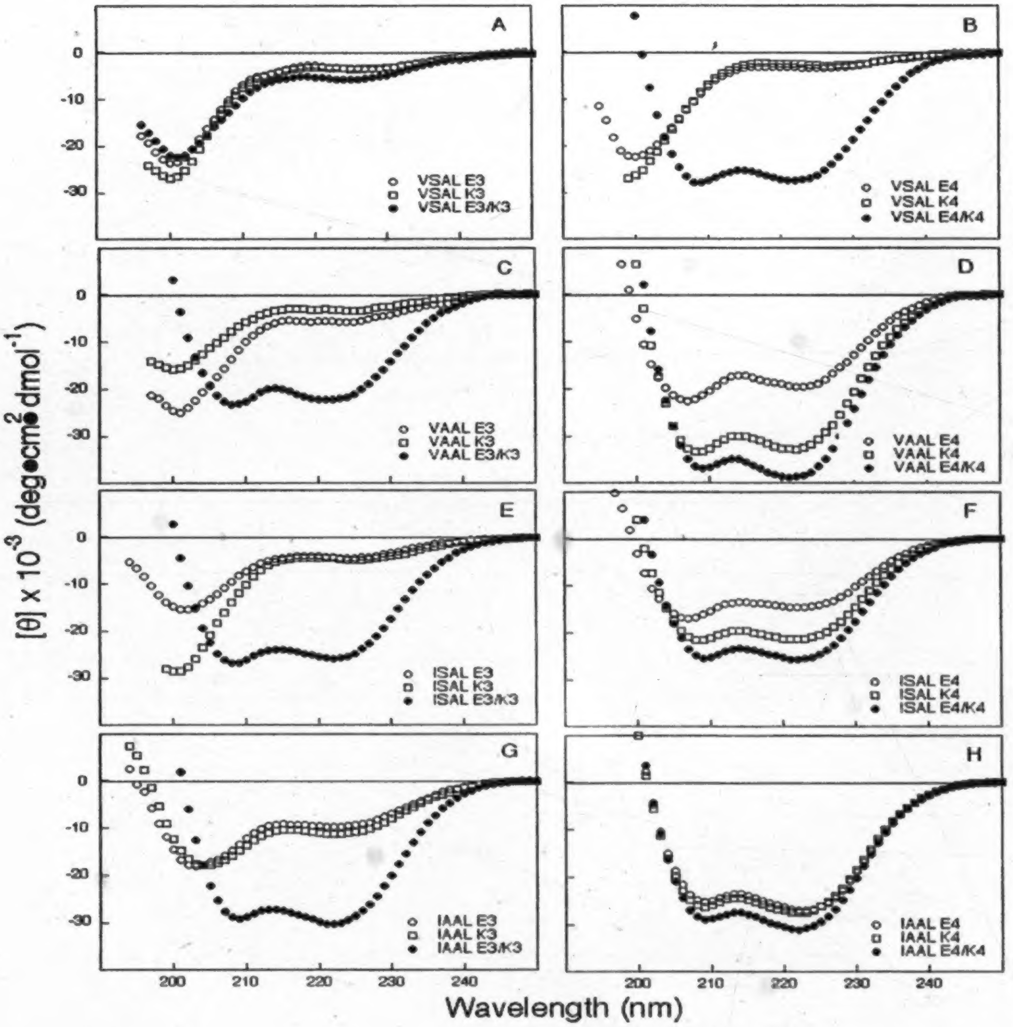

Figure 4-2. CD spectra of the E-coils (○), K-coils (□), and 1:1 mixtures of the E- and K-coil (●) peptides. The following peptides were examined: **A)** VSAL 3 heptads; **B)** VSAL 4 heptads; **C)** VAAL 3 heptads; **D)** VAAL 4 heptads; **E)** ISAL 3 heptads; **F)** ISAL 4 heptads; **G)** IAAL 3 heptads; and **H)** IAAL 4 heptads. Peptide nomenclature is described in Table 4-1 and in the Results section. The spectra were recorded at 20°C in a 50 mM PO_4, 100 mM KCl, pH 7 buffer. Peptide concentrations were 1 mg/ml (318 – 429 μM).

---

[a] Sequence nomenclature is described in Table 4-1 and in the Results section.

[b] The mean residue molar ellipticities at 222 nm were measured at 20°C in benign buffer (50 mM PO_4, 100 mM KCl, pH 7). For samples containing TFE, the above buffer was diluted 1:1 (v/v) with TFE.

[c] The (%) helical content was calculated from the ratio of the observed $[\theta]_{222}$ value divided by the predicted molar ellipticity x 100. The predicted molar ellipticity was calculated from the equation: $[\theta]_{222} = -40 \times 10^3 \times (1 - 4.6/n)$ for the chain length dependence of an α-helix , where n is the number of residues in the peptide. The predicted values for 21 and 28 residues are –31,238 and –33,429 deg·cm^2·dmol^{-1}.

[d] The + sign denotes a significant decrease in the $[\theta]_{222}/[\theta]_{208}$ ratio from benign to 50%TFE, indicative of the folded coiled-coil structure in benign medium.

On the other hand, our more stable sequences were able to form coiled-coils at three heptads in length (Figure 4-2C, E, G and Table 4-2). The result with ISAL E3/K3 (Figure 4-2E) demonstrates that increasing the hydrophobicity in the core, by substituting three isoleucines for three valines, provided sufficient stabilization for the coiled-coil to fold. VAAL E3/K3 also formed a coiled-coil, as seen in Figure 4-2C, showing that increasing α-helical propensity by substituting three alanine residues for three serines could also provide sufficient stabilization for the coiled-coil to fold. Additionally, both sequences have high specificity, demonstrated by the random coil character of the individual E and K peptides of these sequences. The peptide IAAL E3/K3 contains both substitutions and is, as expected, a fully folded α-helical coiled-coil.

All of the four-heptad sequences formed heterodimeric coiled-coils (Figure 4-2B, D, F, H and Table 4-2). Some, however, show a loss of specificity (Figure 4-2D, F, and H). These sequences were able to form homodimeric coiled-coils even in the presence of 8 Glu-Glu or 8 Lys-Lys electrostatic repulsions. This is most pronounced for the most stable sequence, IAAL, in which the E4 and K4 homodimers are nearly fully folded coiled-coils (Figure 4-2H). The negative-negative charge repulsions are more destabilizing to coiled-coil formation than positive-positive repulsions (Figure 4-2D and F). In all cases, the 1:1 mixture of E and K coils had the greatest ellipticity at 222 nm, indicating that the maximum helical structure is still observed in the heterodimeric coiled-coil. This demonstrates that achieving a balance between stability and specificity is an important principle in protein design.

Trifluoroethanol (TFE) is a helix-inducing solvent that is used to determine the ability of a sequence to adopt an α-helical structure (Shiraki *et al.* 1995, Sonnichsen *et al.*

1992). All peptides in this study are α-helical in the presence of 50% TFE (Table 4-2). TFE is also known to disrupt quaternary interactions. This is reflected in the $[\theta]_{222}/[\theta]_{208}$ ratio, typically >1.0 for interacting helices in a coiled-coil conformation and 0.85-0.95 for single α-helices (Lau *et al.* 1984, Zhou *et al.* 1992a). The coiled-coil peptides which show shifts of this type in the $[\theta]_{222}/[\theta]_{208}$ ratios are denoted by a + sign in Table 4-2. Some of the shorter coiled-coils have $[\theta]_{222}/[\theta]_{208}$ ratios less than 1.0 in benign buffer. This can be attributed to end fraying, which is more significant in short helices.

Sedimentation equilibrium

Weight-averaged molecular weights typical of a dimeric species were observed for IAAL E3/K3, ISAL E3/K3, VAAL E3/K3, IAAL E4/K4, and VAAL E4/K4 (Table 4-3). ISAL E4/K4 had a molecular weight typical of a tetrameric species, and VSAL E4/K4 showed evidence of a dimer to tetramer association. Previous studies have shown that the VSAL E4 and VSAL K4 peptides interact in a 1:1 manner, ruling out a trimeric structure (Litowski & Hodges 2001). VSAL E3/K3 showed signs of a weak monomer to dimer association in the high concentration gradient experienced in the analytical ultracentrifuge. However, it did not fold under the conditions used for our CD analysis, indicating that it is unsuitable for most applications.

The difference in the oligomerization states of ISAL E4/K4 and IAAL E4/K4 is interesting, given that they differ only in the presence of serine or alanine at position **b**. We cannot explain why this should happen, for this position is highly solvent exposed and distant from the coiled-coil interface. To our knowledge, this is the first example of a **b** position substitution causing a change in coiled-coil oligomerization state, although

Table 4-3. Biophysical analysis of the heterodimeric coiled-coils

Peptide	$[\text{GdnHCl}]_{1/2}$[a] (M)	m[b] (kcal/mol^2)	ΔG^{H_2O} [c] (kcal/mol)	Kd (app)[d] (M)	Calculated monomeric Molecular weight	Observed Molecular weight	Oligomerization State
IAAL E3/K3	4.3	-1.19	9.6	7×10^{-8}	2322	4380	dimer
ISAL E3/K3	1.7	-1.12	6.8	9×10^{-6}	2370	4450	dimer
VAAL E3/K3	1.8	-1.45	7.2	4×10^{-6}	2281	4740	dimer
VSAL E3/K3	ND[e]	—	—	—	2329	3570	monomer-dimer
IAAL E4/K4	ND[e]	—	—	—	3077	7690	dimer
ISAL E4/K4	4.6	-1.28	11.0	6×10^{-9}	3141	12 170	tetramer
VAAL E4/K4	4.4	-1.51	11.2	4×10^{-9}	3022	7230	dimer
VSAL E4/K4	2.1	-1.61	8.1	9×10^{-7}	3084	8660	dimer-tetramer[f]

[a] The concentration of GdnHCl at which the coiled-coil is 50% α-helical.

[b] The slope term in the equation $\Delta G = m[\text{GdnHCl}] + \Delta G^{H_2O}$, as described in Chapter II.

[c] Obtained by the linear extrapolation method, as described in Chapter II.

[d] Calculated from the equation $\Delta G = -RT \ln K$, using the ΔG^{H_2O} values.

[e] VSAL E3/K3 was unfolded in benign medium (Figure 4-2); the guanidine hydrochloride midpoint for IAAL E4/K4 was not determined, since the peptide was too stable and only partially unfolded at 7 M GdnHCl (Figure 4-3).

[f] Previous studies have shown that VSAL E4 and VSAL K4 interact in a 1:1 manner, thus ruling out a trimeric structure (Litowski & Hodges 2001).

interstrand electrostatic interactions between **b** and **c** position residues have been shown to affect the stability of tetrameric coiled-coils (Vu *et al.* 2001). This demonstrates that the sequence features which control coiled-coil oligomerization state are complex and still not fully understood. We are proceeding with crystallization studies of these peptides in the hope of answering this question with three-dimensional structure information. Although ISAL E4/K4 and VSAL E4/K4 form tetrameric species, this should not rule out their application as a tag system where one strand is immobilized on a solid surface, since only the dimeric species can form under these conditions.

We have previously found many examples of coiled-coils which convert from trimers or tetramers to dimers at low levels of denaturant, in a transition that is silent to the CD signal (Wagschal *et al.* 1999a). The major unfolding transition observed by CD spectroscopy was then a dimer to monomer transition. In order to determine if ISAL E4/K4 behaved in a similar fashion, we performed sedimentation equilibrium experiments in a buffer containing 2 M GdnHCl, a concentration that does not induce unfolding in ISAL E4/K4 (Figure 4-3). Molecular weights characteristic of the dimeric species were observed, confirming that these coiled-coils do undergo a silent tetramer to dimer transition before the major unfolding transition (data not shown). This allows us to compare the unfolding data (ΔG, ΔΔG) directly.

Conformational Stability

The conformational stabilities of the coiled-coils were determined by GdnHCl denaturations (Figure 4-3, Table 4-3). The denaturation curves for the three heptad coiled-coils are shown in the upper panel. VSAL E3/K3 did not have sufficient stability to fold, and so is not shown. The ISAL E3/K3 and VAAL E3/K3 peptides have similar

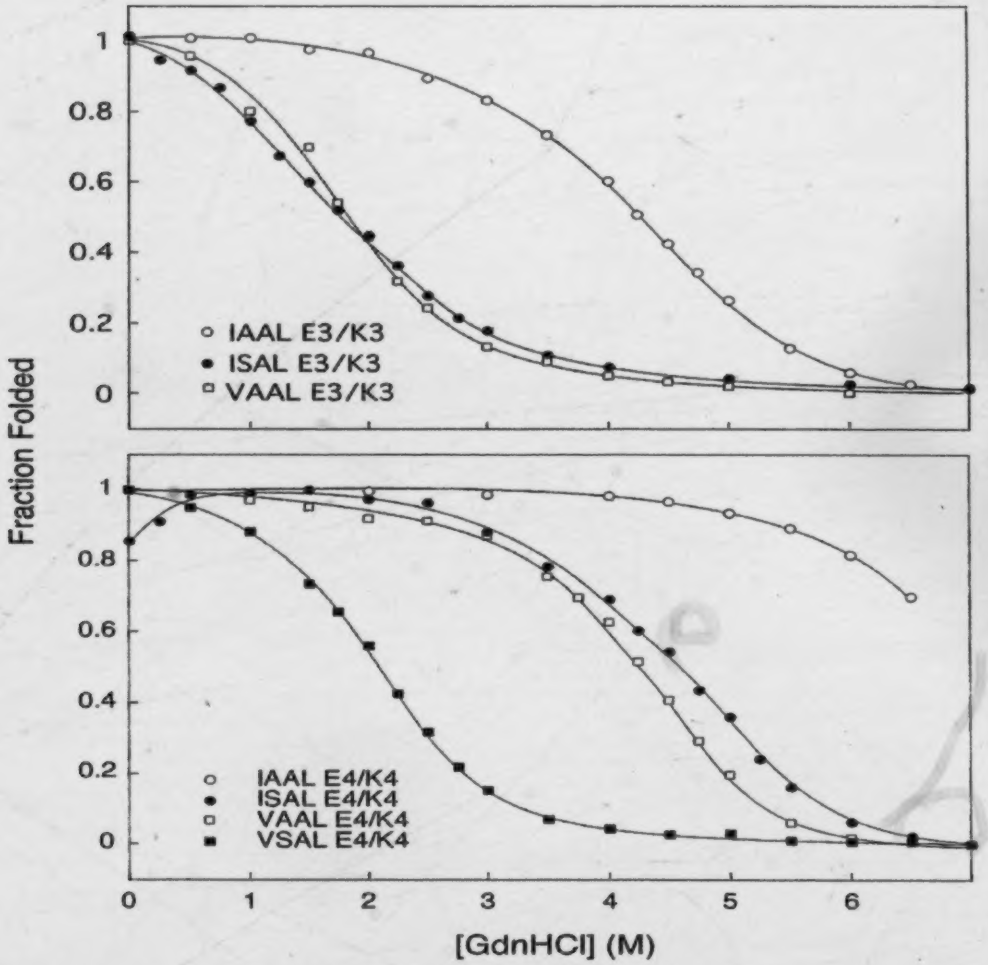

Figure 4-3. Guanidine hydrochloride denaturation curves at 20°C in a 50 mM PO_4, 100 mM KCl, pH 7 buffer. **A**) The three heptad heterodimeric coiled-coils IAAL E3/K3 (○, 431 μM), ISAL E3/K3 (●, 270 μM), and VAAL E3/K3 (□, 439 μM). **B**) The four heptad heterodimeric coiled-coils IAAL E4/K4 (○, 325 μM), ISAL E4/K4 (●, 137 μM. Repeating the denaturation at 380 μM had little effect; the denaturation midpoint increased by only 0.2 M), VAAL E4/K4 (□, 331 μM), and VSAL E4/K4 (■, 324 μM). The calculation of fraction folded is described in Chapter II.

denaturation midpoints (1.7 M and 1.8 M GdnHCl) and free energies of unfolding (ΔG^{H_2O} values of 6.8 and 7.2 kcal/mol). Our two approaches to stabilizing this sequence, increasing the hydrophobicity of the core and increasing the α-helical propensity, yielded similar gains in stability. The double mutant, IAAL E3/K3, is remarkably stable for a coiled-coil that is only 21 residues long ($[\text{GdnHCl}]_{1/2}$ = 4.3 M and ΔG^{H_2O} = 9.6 kcal/mol), making it an excellent choice for a heterodimerization domain.

The denaturation curves of the analogous four heptad coiled-coils are shown in the lower panel of Figure 4-3. The original VSAL sequence is the least stable, with a denaturation midpoint of 2.1 M and a ΔG^{H_2O} of 8.1 kcal/mol (Chao *et al.* 1996, 1998). Increasing the hydrophobicity of the core residues (ISAL E4/K4) or the α-helical propensity (VAAL E4/K4) resulted in similar increases in stability, with denaturation midpoints of 4.6 and 4.4 M and ΔG^{H_2O} values of 11.0 and 11.2 kcal/mol, respectively. The double mutant, IAAL E4/K4, is an extremely stable molecule and was still approximately 70% folded at 7 M GdnHCl.

This series of coiled-coil sequences allows us to make a number of comparisons and to evaluate the contribution of different structural features to the stability of heterodimeric coiled-coils (Table 4-4). The ΔΔG values were acquired by subtracting the ΔG values at the transition midpoints, as described in Chapter II. In addition, the ΔΔG value was divided by the number of substitutions (6 or 8) to obtain the free energy change per substitution. Each valine to isoleucine substitution increased stability by 0.47 kcal/mol when comparing the VSAL E4/K4 and ISAL E4/K4 pair and the VAAL E3/K3 and IAAL E3/K3 pair. This is in excellent agreement with the values obtained by Zhu *et*

Table 4-4. Contributions of hydrophobicity, α-helical propensity and chain length to stability

Analog Comparison More stable	 Less Stable	 Description	ΔΔG per coiled-coil[a] (kcal/mol)	Number of substitutions per coiled-coil[b]	ΔΔG per interaction[c] (kcal/mol)
IAAL E3/K3	VAAL E3/K3	Contribution of Ile vs. Val in the hydrophobic core	2.81	6	0.47
ISAL E4/K4	VSAL E4/K4	Contribution of Ile vs. Val in the hydrophobic core	3.73	8	0.47
IAAL E3/K3	ISAL E3/K3	Contribution of Ala vs. Ser in position **b**	2.68	6	0.45
VAAL E4/K4	VSAL E4/K4	Contribution of Ala vs. Ser in position **b**	3.28	8	0.41
ISAL E4/K4	ISAL E3/K3	Contribution of additional heptad	4.06	—	—
VAAL E4/K4	VAAL E3/K3	Contribution of additional heptad	3.86	—	—

[a] The relative change of the free energy of unfolding in the coiled-coil due to the substitutions. The calculation of ΔΔG is described in Chapter II.

[b] The number of interactions in a two-stranded coiled-coil.

[c] The relative change of the free energy of unfolding per substitution. This is obtained by dividing the coiled-coil ΔΔG value by the number of substitutions.

al. (1993) for a triple valine to isoleucine substitution at the **a** position, which yielded increases of 0.45 and 0.88 kcal/mol, in coiled-coils with and without disulfide-bridges, respectively.

The effect of α-helical propensity was determined by comparing different sets of coiled-coils. Each serine to alanine substitution gave an increase in stability of 0.45 kcal/mol for ISAL E3/K3 and IAAL E3/K3 and of 0.41 kcal/mol for VSAL E4/K4 and VAAL E4/K4. These numbers are well within the range of values observed before, 0.42 – 0.78 kcal/mol (Chakrabartty *et al.* 1994, Lyu *et al.* 1990, Monera *et al.* 1995, O'Neil & DeGrado 1990, Zhou *et al.* 1994c).

In addition, we could measure the effect of an increase in chain length from three to four heptads. There is a difference of 4.06 kcal/mol between ISAL E3/K3 and ISAL E4/K4, and a difference of 3.86 kcal/mol between VAAL E3/K3 and VAAL E4/K4. This agrees well with the previously observed difference of 4.34 kcal/mol between VSAL E4/K4 and VSAL E5/K5 (Litowski & Hodges 2001).

C. Discussion

We have designed a set of heterodimeric coiled-coils with a wide variety of stabilities by modifying three parameters: hydrophobicity, α-helical propensity, and chain length. Residues in the hydrophobic core of coiled-coils (positions **a** and **d**) have been shown to play key roles in determining such characteristics as stability, oligomerization state, and hetero- vs. homo-association (Gonżalez Jr. *et al.* 1996, Harbury *et al.* 1993, Jelesarov & Bosshard 1996, Kiyokawa *et al.* 2001, Schnarr & Kennan 2001, Tripet *et al.* 2000, Wagschal *et al.* 1999b, Zhu *et al.* 1992b). Single substitutions in the **a** and **d** positions of coiled-coils have yielded a series of coiled-coils whose stabilities covered a range of 7 kcal/mol (Jelesarov & Bosshard 1996, Tripet *et al.* 2000, Wagschal *et al.* 1999b). We compared the effects of valine and isoleucine in position **a**, while position **d** was constantly occupied by leucine. The side chains of these residues differ in terms of side chain length (one methylene group) and, therefore, hydrophobicity. Numerous hydrophobicity scales of the amino acid side chains have been developed, based on partitioning between water and organic solvents, reversed-phase HPLC retention behaviour, and calculations of solvent-accessible surface area (reviewed in Cornette *et al.* 1987, Karplus 1997). The relative rankings of the amino acids vary between scales, but isoleucine and valine are always classified as strongly hydrophobic, and isoleucine is always the more hydrophobic of the two. The difference between these residues has been measured to be 0.40 – 0.80 kcal/mol (Eisenberg & McLachlan 1986, Fauchere & Pliska 1983, Karplus 1997), and to cause an increase in reversed-phase HPLC retention time of 1.8 min (Monera *et al.* 1995). In our E/K coil heterodimers, each substitution of isoleucine for valine yielded an increase in stability of 0.47 kcal/mol (Table 4-4). This is well within the range given by the different hydrophobicity tables.

What effect have similar substitutions had in other coiled-coils? Zhu *et al.* (1993) compared coiled-coils in which the central three heptads (out of five) had leucine, isoleucine, or valine in the **a** positions. They found that isoleucine was more stabilizing than valine by 0.45 kcal/mol when the coiled-coil was stabilized by a disulfide bridge, and by 0.88 kcal/mol in the reduced peptides. This is a larger effect per substitution than we observed, but still within a comparable range. When a single mutation is made in the hydrophobic core of a well packed protein, the environment surrounding the substitution site can have a significant effect on the degree of stabilization or destabilization observed. These effects are often referred to as context effects, and are complicated by the ability of the side chains and the protein backbone to accommodate the substitution through conformational adjustments. Because of this, the contribution of a single methylene group to stability has been observed to vary from 0.1 – 1.5 kcal/mol (Fersht & Serrano 1993, Jelesarov & Bosshard 1996). In contrast, we have examined the contribution of an extra side chain methylene group across the entire hydrophobic core. This eliminates most context effects, so the differences in stability which we have measured are primarily due to the hydrophobicity differences between isoleucine and valine.

The second modification to our design was to substitute alanine for serine in position **b**, significantly increasing the α-helical propensity of the sequence. Serine and threonine are thought to have low α-helical propensities because their side chain hydroxyl groups compete with the peptide backbone for hydrogen bonds (Chakrabartty & Baldwin 1995). The helical propensity of a series of basic side chains increased as their side chain length increased, suggesting that the presence of polar or charged groups near the peptide backbone is destabilizing (Padmanabhan *et al.* 1996). A survey of helical propensity scales showed a surprisingly poor correlation between different scales (Krittanai & Johnson Jr. 2000), however, alanine always ranks near the top of the scales, and always has a greater helical propensity than serine does. We found that a serine to alanine substitution gave increases in stability of 0.41 – 0.45 kcal/mol (Table 4-4). This is in very good agreement with the results of O'Neil and DeGrado (1990), who found a difference of 0.42 kcal/mol between serine and alanine in a coiled-coil model system.

Studies in single stranded α-helices have given helical propensity differences of 0.5 – 0.8 kcal/mol for a serine to alanine substitution (Chakrabartty *et al.* 1994, Lyu *et al.* 1990, Yang *et al.* 1997, Zhou *et al.* 1994c). Helical propensity effects appear to be greater in single amphipathic α-helices than in coiled-coils, presumably because of the additional stabilizing interactions available to coiled-coils (Kwok *et al.* 1998).

The third aspect of our design was to reduce the chain length to three and four heptads (21 and 28 residues). Increases in chain length have been observed to cause increases in coiled-coil stability, but the relationship has been found to be nonlinear (Litowski & Hodges 2001, Su *et al.* 1994). The greatest stability gains were observed at chain lengths of three heptads; further increases in length were stabilizing, but to lesser degrees. This is primarily due to end fraying, a partial and temporary unfolding of the helix termini (Goodman & Kim 1991, Holtzer *et al.* 1997, Zhou *et al.* 1992a). We found that an increase of 3 to 4 heptads caused an increase in stability of 4.06 kcal/mol for the ISAL sequence and an increase of 3.86 kcal/mol for the VAAL sequence. This is in good agreement with our previous results, where an increase of 4 to 5 heptads length for the VSAL sequence gave an increase in stability of 4.34 kcal/mol (Litowski & Hodges 2001).

Electrostatic interactions have been widely shown to control homo- vs. heterodimerization in natural coiled-coils (Baxevanis & Vinson 1993, Lavigne *et al.* 1995, Moll *et al.* 2000). The placement of electrostatic attractions and repulsions has been used extensively in the design of heterodimeric (Chao *et al.* 1996, 1998, Graddis *et al.* 1993, Vinson *et al.* 1993, Zhou *et al.* 1994b), heterotrimeric (Nautiyal *et al.* 1995) and heterotetrameric coiled-coils (Fairman *et al.* 1996). Careful double mutant cycle analysis has shown that i to i′+5 electrostatic attractions between glutamic acid and lysine are stabilizing by ~0.50 kcal/mol (Kohn *et al.* 1998b, Krylov *et al.* 1998). The destabilizing effect of electrostatic repulsions is well established. A single i to i′+5 electrostatic repulsion between glutamic acid residues has been shown to be destabilizing by 0.4 – 0.8 kcal/mol (Kohn *et al.* 1995b, Krylov *et al.* 1998). Thus, electrostatic interactions have the potential to play a critical role in structural specificity.

These results illustrate the need to balance stability and specificity, an important principle in protein design. When we maximized the stability of our design, with IAAL E4/K4, its specificity was lost, as seen in the large amount of homodimer formed (Figure 4-2H). In this case, the E4/E4 and K4/K4 homodimers were stable enough to tolerate the destabilizing effect of eight electrostatic repulsions. In nature, many interactions which specify particular coiled-coil oligomerization states are destabilizing. Examples include the presence of asparagine in the hydrophobic core of the GCN4 coiled-coil (Harbury *et al.* 1993) and glutamic acid in the core of Max/c-Myc (Lavigne *et al.* 1995). Charged residues, though typically destabilizing in the hydrophobic core of coiled-coils, can specify a single oligomerization state (Tripet *et al.* 2000, Wagschal *et al.* 1999b).

In summary, we have created a series of heterodimeric coiled-coils whose conformational stabilities range from 6.8 – 11.2 kcal/mol (Table 4-3). This expands the potential for tailoring heterodimerization domains to particular applications. For example, we can now develop an expression tag/affinity purification system that has more gentle elution conditions, extending the usefulness of this system to more sensitive proteins. The most promising of these heterodimerization domains is IAAL E3/K3. Despite its small size (3 heptads, or 21 residues), it is a fully folded coiled-coil with a high conformational stability ($[\mathrm{GdnHCl}]_{1/2}$ = 4.3 M, ΔG^{H_2O} = 9.6 kcal/mol) and small dissociation constant (70 nM). It is highly specific, as there is no sign of homodimer formation in either the E or the K coil. We have significantly reduced the net charge (+3 on K-coil and -3 on E-coil vs. +5 on K-coil and -5 on E-coil) and hydrophobicity (6 **a** and **d** position hydrophobic residues vs. 10) compared to the original five heptad design. This reduced size is an advantage for the expression of recombinant proteins for biophysical studies, where nonnative residues can complicate results. The smaller the tag, the less likely it is to affect the conformation, function and biophysical properties of the recombinant protein. Smaller tags are therefore advantageous for the many researchers who do not remove expression tags before characterization of recombinant proteins. We have also shown that the design of our heterodimeric coiled-coil has considerable flexibility and its stability can be modulated. This is a considerable advantage compared to expression tags based on native protein sequences, which are much less amenable to redesign.

CHAPTER V

Real-time monitoring of the interactions of de novo designed coiled-coils using surface plasmon resonance: Effect of chain length on the kinetic and thermodynamic constants of interaction

A version of this chapter has been submitted to the journal *Biochemistry* for publication. The introduction has been rewritten and condensed, because these topics have been discussed in depth in the general introduction (Chapter I). Methods which are unique to this chapter are described in section C; the remaining methods are described in more detail in Chapter II.

This work was done in collaboration with Maureen O'Connor-McCourt of the Biotechnology Research Institute (BRI), National Research Council. This was a shared collaboration with equal contributions from both graduate students: myself and Gregory De Crescenzo (BRI). I was responsible for peptide design, synthesis and purification. The BIAcore experiments were performed and analyzed by Gregory De Crescenzo. We communicated extensively about coiled-coil folding, kinetic models, and data interpretation. The writing was equally shared by both laboratories.

A. Summary

We have designed a *de novo* heterodimeric coiled-coil formed by two peptides designated as K coil (KVSALKE heptad sequence) and E coil (EVSALEK heptad sequence), where positively charged or negatively charged residues occupy positions **e** and **g**, respectively. The effect of the chain length of each partner (3, 4, or 5 heptads) upon the kinetic and thermodynamic constants of interaction were determined using a surface plasmon resonance-based biosensor. Global fitting of the interactions revealed that the E5 coil interacted with the K5 coil according to a simple binding model. All the other interactions involving shorter coils were better described by a more complex kinetic model involving a rate-limiting reorganization of the coiled-coil structure. The affinities of these de novo designed coiled-coil interactions were determined to range from 60 pM (E5/K5) to 30 μM (E3/K3). From these K_ds, we were able to determine the free energy

contribution of each heptad, depending on its relative position within the coiled-coils. We found that the free energy contribution of a heptad occupying a central position was three fold higher than that of a heptad at either end of the coiled-coil. The wide range of stabilities and affinities for the E/K coil system provides considerable flexibility for protein engineering and biotechnological applications.

B. Introduction

Changes in chain length clearly caused differences in the thermodynamic stability of heterodimeric coiled-coils, as measured by GdnHCl denaturation (Chapter III and Litowski & Hodges 2001). Association and folding are intrinsically coupled in heterodimeric coiled-coils, so differences in the Gibbs free energy of unfolding must be related to changes in the rates of association and dissociation. This relationship between association and folding allows us to study heterodimeric coiled-coil folding with the BIAcore, an instrument that detects the real-time interactions of analyte and ligand (Karlsson *et al.* 1991). Earlier BIAcore studies, by Chao *et al.* (1996), showed that VSAL E5 and K5 had a relatively fast association ($k_a \approx 4 \times 10^5\ M^{-1}s^{-1}$) and a slow dissociation rate ($k_d \approx 2 \times 10^{-4}\ s^{-1}$). We have now studied the interactions of VSAL E5/K5, VSAL E4/K4 and VSAL E3/K3 to investigate the effect of chain length changes upon the mechanism of coiled-coil folding. Coiled-coils have been observed to fold by both simple two-state mechanisms (Ibarra-Molero *et al.* 2001, Sosnick *et al.* 1996, Wendt *et al.* 1997, Zitzewitz *et al.* 1995, 2000) and by more complex mechanisms involving folding intermediates (Wendt *et al.* 1994, 1995, Zhu *et al.* 2001). We wish to know which mechanism is followed by the E/K coil analogs and if this is related to chain length. In addition, the resulting kinetic data will be of practical help in adapting these coiled-coils to biotechnological applications.

C. Materials and Methods

Equipment and reagents

All the SPR experiments were performed on an upgraded BIAcore 1000. The amine coupling kit (containing NHS and EDC), PDEA, and PIONEER B1 sensor chips were purchased from BIACORE Inc.

Immobilization of K coils on the sensor chips

The different length K coil peptides, which contain N-terminal Cys-Gly-Gly extensions, were immobilized on the surfaces of PIONEER B1 sensor chips using the standard ligand thiol coupling procedure. Surface carboxylic acid groups were activated by the injection of 25 μl of a mixture containing 0.05 M NHS and 0.2 M EDC, yielding the NHS ester. The ester was reacted with the free amine of PDEA (30 μl of 80 mM PDEA in 100 mM boric acid, pH 8.5), a coupling reagent that contains a free amine and a reactive disulfide bond, to yield an active disulfide attached to the dextran via an amide linkage. The K coil was then injected (the free thiol of the N-terminal cysteine undergoes disulfide exchange with the active thiol on the dextran surface), resulting in the peptide being linked to the dextran via a disulfide bond. Specifically, 100 nM K coil freshly dissolved in 10 mM acetic acid, pH 4.0, was injected under manual control until the desired amount of peptide was coupled (50 to 120 RUs, depending on the individual K coil). Freshly prepared 0.05 M L-cysteine (35 μl, in 0.1 M sodium formate, 1 M NaCl, pH 4.3) was then injected to block any remaining activated sites on the sensor chip surface. Control surfaces were prepared similarly, except that running buffer (10 µl) was injected instead of K coil. All steps in the immobilization process were carried out at a flow rate of 5 µl/min.

Kinetic assays on the BIAcore

All the kinetic experiments were carried out at 25°C at a flow rate of 100 µl/min, with the exception of E3 and K3, for which the flow rate was 5 µl/min. The running buffer was HBS: 20 mM Hepes, 150 mM NaCl, 3.4 mM EDTA, and 0.05% Tween20 (pH 7.4). The E coils were dialysed against the running buffer (which was also used for all dilutions) in order to minimize changes in bulk refractive index upon sample injection. During the wash-on phase, different concentrations of E coil solutions were injected over a control surface and the various K coil surfaces for 120 s. This was followed by a 360 s wash-off period, during which running buffer flowed over the surface. Regeneration of the sensor chip was accomplished by two pulses of 5 M GdnHCl (15 s each), followed by an EXTRACLEAN and a RINSE procedure, as described in the BIAcore manual, in order to eliminate all traces of GdnHCl. Duplicate injections of each concentration of E coil were performed in a random order.

Data preparation and analysis

Sensorgrams (curves from the wash-on and wash-off phases) were prepared and globally fit using the SP*Revolution*© software package freely available on the Internet at the following address: http://www.bri.nrc.ca/csrg/equip.htm#biacore. The data was prepared by the method of "double referencing", as described by Rich and Myszka (2000). Briefly, each concentration of a particular E coil was injected over both the K coil-derivatized surface and the control surface; the control surface sensorgram was subtracted from the K coil sensorgram. In addition, the running buffer was injected over both the K coil-derivatized and the control surfaces. Subtraction of these sensorgrams yielded the buffer blank. Finally, the buffer blank curve was subtracted from the control surface-corrected K coil curves. The resulting data was then converted to concentration units using the molecular weight of the injected species, the equivalence of 1000 RU per 1 ng/mm^2 and a matrix thickness of 100 nm. Each data set, which consists of sensorgrams corresponding to injections of different analyte concentrations over the same surface, was then analysed using several kinetic models that are available in the SP*Revolution*© software package (Fivash *et al.* 1998) and have been described elsewhere (De Crescenzo *et al.* 2000, O'Connor-McCourt *et al.* 1998). A schematic representation of the different kinetic models is shown in Figure 5-2.

Mathematical modelling and parameter estimation

In SP*Revolution*© , the various kinetic models were transposed into differential equations that were solved numerically using an adaptive step-size Runge-Kutta method (Press *et al.* 1986) with a non-linear regression program using Marquardt's algorithm (Marquardt 1963) to estimate the values of the constants from experimental data. For each model, the kinetic parameters, as well as the quantity of active ligand immobilized on the matrix, were considered as global parameters for a given set of curves. Moreover, two local parameters were added for each curve to take into account the refractive index changes at the beginning of the wash-on and wash-off phases. An evaluation of the quality of the fit for the various kinetic models was done as described elsewhere (De Crescenzo *et al.* 2000) by calculating three statistical values: the standard deviation of the residuals (S.D.), the "+ or – signs" statistic (Z1) and the "Run up and down" statistic (Z2) (Bradley 1968).

D. Results

Peptide Design

We have designed a heterodimeric coiled-coil (Figure 5-1 and Table 5-1), based on principles revealed by more than fifteen years of investigation (Chao *et al.* 1996, Graddis *et al.* 1993, O'Shea *et al.* 1993, Zhou *et al.* 1994b). The primary stabilizing interactions are the hydrophobic interactions in the core (Harbury *et al.* 1993, Tripet *et al.* 2000, Wagschal *et al.* 1999b, Zhou *et al.* 1992a), electrostatic attractions across the interface (Kohn & Hodges 1998, Krylov *et al.* 1994, Vinson *et al.* 1993, Zhou *et al.* 1994b), and helical propensity (Chakrabartty *et al.* 1994, Lyu *et al.* 1990, Monera *et al.* 1995, O'Neil & DeGrado 1990, Zhou *et al.* 1994c). Valine and leucine were chosen for positions **a** and **d**, as they are known to form a highly stable hydrophobic core (Moitra *et al.* 1997, Tripet *et al.* 2000, Wagschal *et al.* 1999b, Zhu *et al.* 1993). We have used electrostatic interactions at positions **e** and **g** to control specificity for heterodimer versus homodimer formation, an approach successfully exploited in both natural and *de novo* sequences (Chao *et al.* 1996, Graddis *et al.* 1993, Kohn *et al.* 1995a, 1995b, 1998b, O'Shea *et al.* 1993, Zhou *et al.* 1994b). One strand of the coiled-coil, the E coil, has glutamic acid (which is preferable to aspartic acid because of its higher helical propensity) at all **e** and **g** positions, while the complementary K coil has lysine at all **e** and **g** positions (Figure 5-1). In this way, the two homodimers are destabilized by electrostatic repulsions and the E/K heterodimer is stabilized by electrostatic attractions.

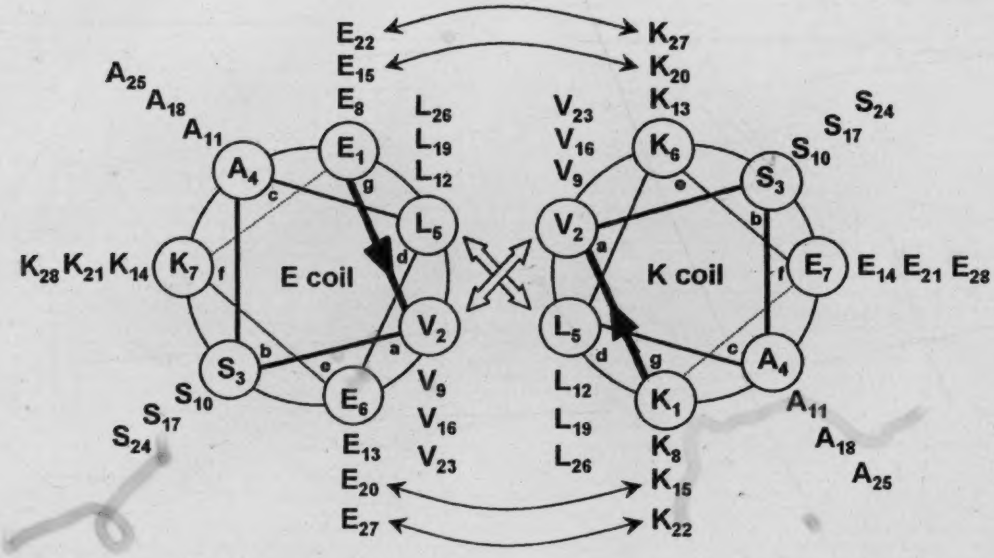
E22
E15
E8
K27
K20
K13
A25
A18
A11
L26
L19
L12
V23
V16
V9
S24
S17
S10
A4
E1
K6
S3
g
c
e
L5
V2
b
K28 K21 K14
K7
f
E coil
d
a
K coil
f
E7
E14 E21 E28
V2
L5
S3
b
e
a
d
g
c
A4
E6
K1
S10
S17
S24
V9
V16
V23
L12
L19
L26
A11
A18
A25
E13
E20
E27
K8
K15
K22

Figure 5-1. Helical wheel representation of the E/K coiled-coil heterodimer, in which one heptad is viewed in cross-section. The interhelical hydrophobic interactions are marked with the wide arrows. The narrow arrows denote the pairs of interchain electrostatic interactions on each side of the hydrophobic core. Peptide nomenclature is described in Table 5-1.

Table 5-1. Peptide Sequences and nomenclature

Name[a]	Sequence[b]
	gabcdefgabcdefgabcdef
E3	Ac-EVSALEKEVSALEKEVSALEK-NH_2
E4	Ac-EVSALEKEVSALEKEVSALEKEVSALEK-NH_2
E5	Ac-EVSALEKEVSALEKEVSALEKEVSALEKEVSALEK-NH_2
K3	Ac-CGGKVSALKEKVSALKEKVSALKE-NH_2
K4	Ac-CGGKVSALKEKVSALKEKVSALKEKVSALKE-NH_2
K5	Ac-CGGKVSALKEKVSALKEKVSALKEKVSALKEKVSALKE-NH_2

[a] E and K denote peptides in which the **e** and **g** positions are occupied by glutamic acid or lysine, respectively. The number describes the peptide length in number of heptads.

[b] The sequences are written in the one letter amino acid code. Ac represents an N^{α}-acetyl group. NH_2 represents a C^{α}-amide group. Positions **a** and **d** of the heptad repeat are underlined and form the hydrophobic core of the coiled-coil.

Serine was placed at position **b** to increase solubility. Although serine has a low helical propensity, it is the smallest polar, uncharged residue that can increase solubility while minimally interacting with the other side-chains. To compensate, position **c** was occupied with alanine, the amino acid residue with the highest helical propensity (Chakrabartty *et al.* 1994, Lyu *et al.* 1990, Monera *et al.* 1995, O'Neil & DeGrado 1990, Zhou *et al.* 1994c). Although nominally a hydrophobe, alanine has the smallest side-chain, which should discourage aggregation. The K coils have an N-terminal Cys-Gly-Gly extension, which allows them to be immobilized to the BIAcore chip surface via a disulfide-bridge.

Versions of each peptide were synthesized which were three, four, or five heptads long (equivalent to 21, 28, or 35 residues). This is reflected in the nomenclature (Table 5-1) in which E and K refer to the identity of the residues at positions **e** and **g**, and the number refers to the number of heptads in the peptide chain. For example, E3 is the three-heptad peptide with glutamic acid at all **e** and **g** positions. E4/K4 denotes the heterodimeric coiled-coil formed by the interaction of the E4 and K4 peptides.

Optimization of the BIAcore experiments

In order to monitor binding in real-time between E and K coils of different lengths, and hence to be able to determine not only the thermodynamic but also the kinetic constants depicting the interactions, we chose to use a surface plasmon resonance (SPR)-based biosensor – the BIAcore. In a classical BIAcore experiment, one of the binding partners is immobilized in the matrix of a sensor chip surface and the other interactant is injected over that sensor chip surface. As the injection proceeds, a mass accumulation of the analyte (the injected species in BIAcore terminology), as it binds to the ligand (the immobilized species), causes an increase in the refractive index of the interfacing medium at the surface and this is recorded in arbitrary resonance units (RU). This signal is proportional to the mass accumulation of the analyte. This corresponds to the wash-on phase of the experiment. The analyte solution is then replaced by buffer and dissociation of the surface complexes is recorded (the wash-off phase). If complexes still remain in the matrix at the end of the wash-off phase, their elution can be achieved by injecting a regeneration solution that promotes dissociation of the complexes without damaging the ligand. This series of steps constitutes a sensorgram. By repeating the experiment with a series of different analyte concentrations, a set of sensorgrams is recorded. Since the data are recorded in real-time, it is possible to derive kinetic parameters from the analysis of the set of curves. This experimental approach, in combination with numerical integration methods that globally fit all the sensorgrams in a set at the same time has been shown to be reliable for discriminating between different mechanisms of binding and for determining the values of the related kinetic constants (De Crescenzo *et al.* 2000, Fisher & Fivash 1994, Morton *et al.* 1995). However, artifacts that could bias the analysis must be eliminated prior to the determination of the kinetics of binding (Rich & Myszka 2000). The first step in our study was to test for and eliminate artifacts that could result from non-optimal experimental design.

Most of the BIAcore biosensor artifacts identified to date are related to surface effects since one of the interactants must be immobilized to the sensor surface. The most obvious artifact is surface ligand heterogeneity; this can occur when more than one coupling site is present in the ligand molecule (Karlsson & Falt 1997, Kortt *et al.* 1997, O'Shannessy & Winzor 1996). The *de novo* designed E and K coils are relatively small peptides whose molecular weights vary from 2300 to 4100 Da, each of them containing multiple carboxyl and amino groups. Thus, carboxyl and amine coupling strategies cannot be used. The strategy chosen for this study was to add a three residue extension (Cys-Gly-Gly) to the amino terminus of the coils. This linker enabled us to couple the K coils to the surface using thiol coupling chemistry and hence to generate homogenous, oriented surfaces. Another surface-related artifact referred to as the "parking" or "crowding" problem, corresponds to the masking of ligand molecules by previously formed complexes. This phenomenon, first described by O'Shannesy (1996), is particularly critical when the molecular weight of the analyte is large compared to the ligand. Since the two binding partners have almost the same size and are relatively small, it is unlikely that this "parking problem" would occur during our experiments. However, in order to reduce or eliminate this and other artifacts such as mass transport limitation and rebinding (Myszka *et al.* 1997), we coupled the minimal quantity of K coils required to detect the interactions with an acceptable signal-to-noise level (between 50 to 150 RUs of K coil). The flow rate was also set to the maximum possible (100 µL/min) for all experiments (except for the E3/K3 interaction) not only to minimize mass transport and rebinding artifacts, but also to promote faster changes between running and sample buffer (Rich & Myszka 2000). Non-specific interactions were minimal as assessed by performing injections over a control surface (no K coil immobilized) and were subtracted out by applying the "double referencing" procedure which Myszka has suggested to be critical in the analysis of low molecular weight analytes (Myszka *et al.* 1997, Rich & Myszka 2000).

Characterization of the E/K interaction

We applied the procedure described above to study the interactions between coils of different chain lengths. The sensorgram data set from the binding of E5 and K5 (Figure 5-3) was globally fit to a simple langmuirian model of interaction. This is a model in which the unfolded monomeric E5 and K5 peptides interact to form a fully folded dimeric coiled-coil in a single step, without discernable intermediates (Figure 5-2). The high quality of the fit can be judged visually by looking at the distribution of the residuals (the difference between calculated and experimental points, Figure 5-3B). The on-rate determined by fitting this interaction was found to be relatively fast ($k_{ass\#1} = 3.2 \times 10^6\ M^{-1}\ s^{-1}$, Table 5-2). The off-rate ($k_{diss\#1}$) was determined to be $2.0 \times 10^{-4}\ s^{-1}$, indicating that the coiled-coil complexes dissociate very slowly. Using these kinetic constants, we calculated the thermodynamic dissociation constant for the interaction ($K_d = k_{diss\#1} / k_{ass\#1} = 63$ pM). On-rates in the range of $10^6\ M^{-1}\ s^{-1}$ have been found to be the upper limit for accurate determination using the BIAcore. With faster on-rates, the diffusion of the analyte from the bulk solution to the sensor chip surface may become rate limiting (Myszka 1997). To test for the presence of this mass transport limitation effect in our data, we fit the sensorgrams using a model depicting a simple peptide-peptide interaction coupled to a mass transport limitation. The kinetic constants determined with this model were found to be the same as those obtained with the simple model, within 5% error (data not shown). This demonstrates that our experimental conditions were adequate and that the results were not biased by mass transport/rebinding artifacts. The same approach was then applied to the other coiled-coil systems.

(A) $$E + K \underset{k_{\text{diss\#1}}}{\overset{k_{\text{ass\#1}}}{\rightleftharpoons}} EK$$

(B) $$E + K \underset{k_{\text{diss\#1}}}{\overset{k_{\text{ass\#1}}}{\rightleftharpoons}} EK \underset{k_{-r}}{\overset{k_{r}}{\rightleftharpoons}} EK^{*}$$

(C) $$E + K \underset{k_{\text{diss\#1}}}{\overset{k_{\text{ass\#1}}}{\rightleftharpoons}} EK \underset{k_{-r}}{\overset{k_{r}}{\rightleftharpoons}} 1/2\ EKKE$$

Figure 5-2. Schematic representation of the different kinetic models used to globally fit the E/K interactions. For all models, E and K represent the monomeric forms of the E coil and K coil and EK depicts the coiled-coil complex. **A**) Simple Langmuirian interaction. **B**) The EK complex undergoes a conformational change (rearrangement) to give EK* (rearranged EK). **C**) The E/K complex dimerizes to form tetrameric coiled-coil (EKKE) following the initial monomer-to-dimer step. The kinetic and thermodynamic constant nomenclature is consistent with that used in the text. For the conformational change model, K_d is defined as the thermodynamic constant related to the first step; $K_d = k_{\text{diss\#1}} / k_{\text{ass\#1}}$ (M). K_r corresponds to the thermodynamic constant related to the second step; $K_r = k_{-r} / k_r$ (no unit). The apparent K_d (K_{dapp}) of the interaction corresponding to ([E] x [K]) / ([EK] + [EK*]) at equilibrium is equal to $(K_d^{-1} \times (1 + K_r^{-1}))^{-1}$.

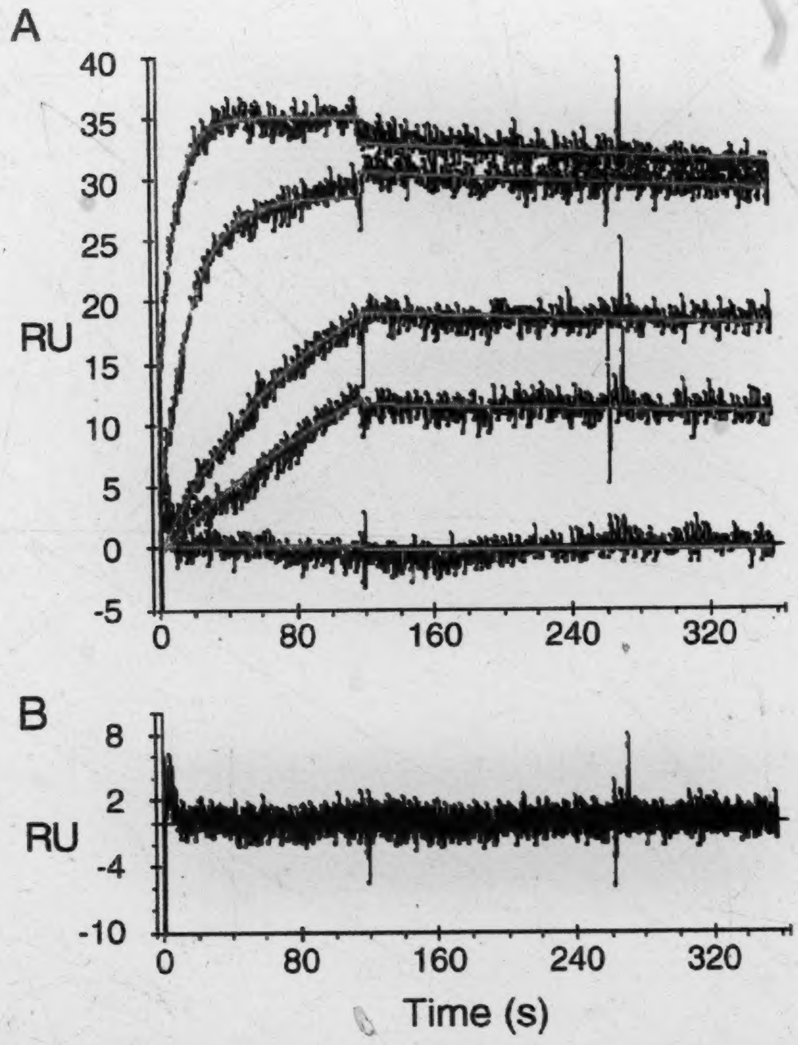

Figure 5-3. Global analysis of the E5 interaction with K5. **A)** Global fit of the E5 interaction with K5 using the simple binding model. Different concentrations of E5 ranging from 5 to 100 nM were injected over approximately 50 RUs of immobilized K5 and over a control dextran surface. The points correspond to the RUs obtained after double referencing. The solid lines represent the fit obtained by integrating the curves simultaneously to a simple Langmuirian model. **B)** residuals from **A.**

Table 5-2. Standard deviation of the residuals and Z1 and Z2 statistics[a].

	Kinetic Model	E/K coil interactions					
		E5/K5	E4/K5	E5/K4	E4/K4	E5/K3	E4/K3
S.D.	simple	**1.07**[b]	1.32	1.50	2.43	1.79	2.07
	rearrangement	1.07	**1.03**	**1.20**	**1.28**	**1.01**	**0.94**
	dimer-tetramer	1.07	1.24	1.33	1.44	1.10	1.00
Z1	simple	**7.79**	15.72	26.26	35.75	19.56	28.59
	rearrangement	7.79	**7.89**	**15.30**	**18.37**	**8.85**	**18.13**
	dimer-tetramer	7.79	14.28	19.93	19.40	13.21	18.53
Z2	simple	**0.75**	0.194	1.63	1.56	1.71	2.61
	rearrangement	0.75	**0.147**	**0.83**	**0.72**	**0.59**	**1.28**
	dimer-tetramer	0.75	0.379	0.85	0.75	0.71	1.47

[a] The statistics were calculated for global fits of each sensorgram set to simple, conformational change (rearrangement), or dimer-to-tetramer kinetic models.

[b] Low scores are indicative of good fits, and the best scores are in bold print.

Surprisingly, global fitting of the data sets obtained for every other coiled-coil interaction (namely, E5/K4, E4/K5, E4/K4, E5/K3 and E4/K3) clearly showed deviations from a simple binding mechanism. This deviation was particularly noticeable during the wash-off phase (Figure 5-4, and data not shown). Since artifacts that could lead to such a deviation were eliminated by optimizing experimental conditions, this deviation is likely due to a more complex biological mechanism of binding. Previous reports stated that some coiled-coil dimers can undergo a conformational change (Wendt *et al.* 1995). Other reports using sedimentation equilibrium experiments with the E4/K4 coiled-coil detected the presence of tetramers at high concentration (Litowski & Hodges 2001). Accordingly, we used two more complex models to fit the data: the first one depicts a change in the conformation or a rearrangement of the E/K complex (the second kinetic step is first order, Figure 5-2B) while the second model represents the interaction of two E/K dimers to form a tetramer (the second kinetic step is second order, Figure 5-2C). The quality of the data fits was judged by visual inspection (Figure 5-4C and data not shown), the standard deviation of the residuals, and the Z1 and Z2 statistics. In all the cases (except the E3/K3 interaction; discussed below), the model best depicting the experimental data was the one representing a rearrangement of the coiled-coils (Table 5-2). The kinetic constants and the related thermodynamic dissociation constants calculated using this model are shown in Figure 5-5 and Table 5-3.

In the case of the E3/K3 interaction, due to the low affinity of binding, it was necessary to couple 1200 RUs of K3 to get an acceptable signal-to-noise ratio (30 RUs maximum). The three curves corresponding to the highest concentrations of E3 (40, 20 and 10 μM) were globally fit with the rearrangement model. The quality of the fit was

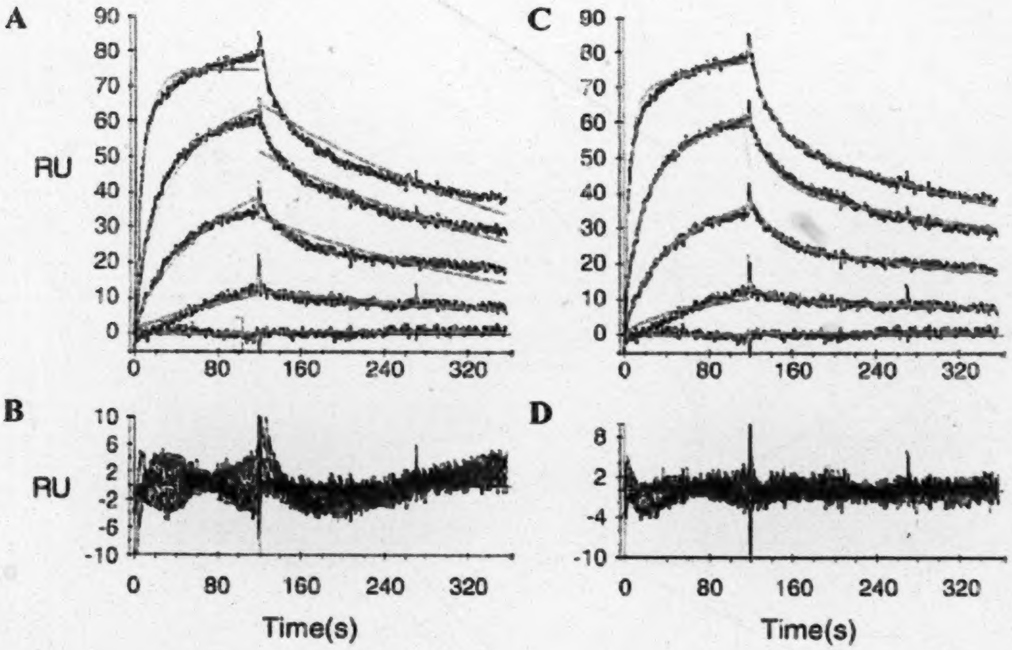

Figure 5-4. Global analysis of the E4 interaction with K4. **A)** Global fit of the E4 interaction with K4 when using the simple binding model. Different concentrations of E4 ranging from 10 to 500 nM were injected over approximately 100 RUs of immobilized K4 and over a control dextran surface. The points correspond to the RUs obtained after double referencing. The solid lines represent the fit obtained by integrating the curves simultaneously to a simple Langmuirian model. **B)** Residuals corresponding to **A**. **C)** Global fit of the E4 interaction with K4 using the conformational change (rearrangement) model. **D)** Residuals from **C**.

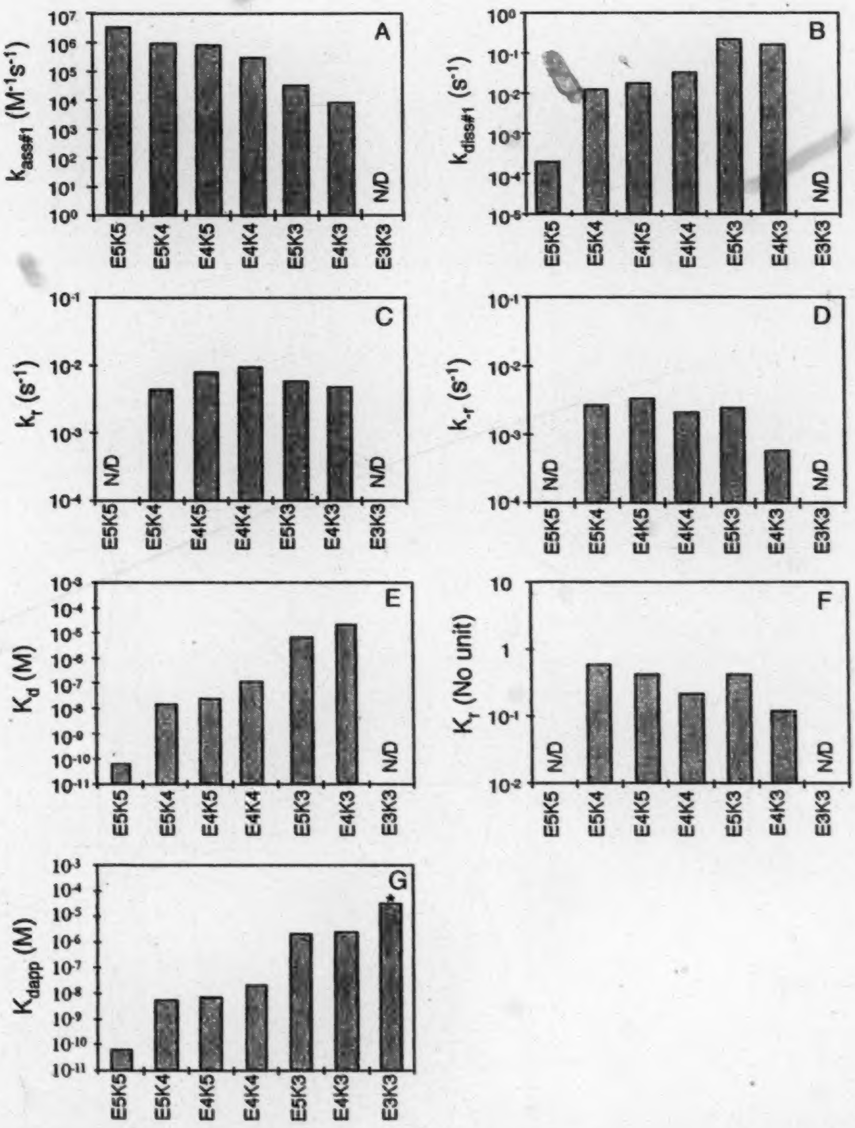

Figure 5-5. The effect of chain length on the kinetic and thermodynamic constants for the E/K interactions derived when using the conformational change model. **A-D)** $k_{ass\#1}$, $k_{diss\#1}$, k_{r} and k_{-r} kinetic constants, as determined by globally fitting the different coiled-coil interactions with the conformational change model. **E-G)** The K_{d}, K_{r} and K_{dapp} thermodynamic constants that were calculated using the kinetic constants. * K_{dapp} was determined by a Scatchard plot.

Table 5-3. Kinetic and thermodynamic constants related to the global fit of interactions of the different E/K coiled-coil pairs to a conformational change (rearrangement) model.

	E/K coiled-coils (value ± 95% confidence interval)						
Parameter	E5/K5	E5/K4	E4/K5	E4/K4	E5/K3	E4/K3	E3/K3
$k_{ass\#1}$ ($M^{-1}s^{-1}$)	3.17 ±0.05 x 10^{6}	9.2 ± 0.2 x 10^{5}	7.3 ±0.2 x 10^{5}	2.89 ±0.07 x 10^{5}	3.1 ±0.2 x 10^{4}	7.3 ±0.4 x 10^{3}	n/d[a]
$k_{diss\#1}$ (s^{-1})	2.0 ±0.1 x 10^{-4}	1.29 ±0.08 x 10^{-2}	1.8 ±0.2 x 10^{-2}	3.4 ±0.2 x 10^{-2}	2.2 ±0.1 x 10^{-1}	1.67 ±0.06 x 10^{-1}	n/d
k_r (s^{-1})	n/a[b]	4.4 ±0.6 x 10^{-3}	8.0 ±0.7 x 10^{-3}	9.6 ±0.3 x 10^{-3}	5.83 ±0.2 x 10^{-3}	4.8 ±0.2 x 10^{-3}	n/d
k_{-r} (s^{-1})	n/a	2.7 ±0.4 x 10^{-3}	3.4 ±0.2 x 10^{-3}	2.1 ±0.09 x 10^{-3}	2.5 ±0.1 x 10^{-3}	5.9 ±0.5 x 10^{-4}	n/d
K_d (M)	6.3 ±0.5 x 10^{-11}	1.4 ±0.1 x 10^{-8}	2.5 ±0.2 x 10^{-8}	1.16 ±0.08 x 10^{-7}	7.0 ±0.8 x 10^{-6}	2.3 ±0.2 x 10^{-5}	n/d
K_r (no unit)	n/a	0.6 ±0.2	0.42 ±0.6	0.22 ±0.02	0.42 ±0.04	0.12 ±0.01	n/d
K_{dapp} (M)	6.3 ±0.5 x 10^{-11}	5.4 ±1 x 10^{-9}	7.3 ±0.4 x 10^{-9}	2.08 ±0.03 x 10^{-8}	2.11 ±0.08 x 10^{-6}	2.51 ±0.04 x 10^{-6}	3.2 ±0.3[c] x 10^{-5}

[a] n/d: not determined

[b] n/a: not applicable

[c] determined by Scatchard plot analysis (3 independent experiments)

good but the error for the off-rate of the second step was larger than the off-rate parameter value itself, thus indicating that the global fitting approach was not appropriate to analyze this set of data. Nevertheless, using the plateau value of these three curves, we determined an apparent K_d value of 32 μM by Scatchard analysis for the E3/K3 interaction.

E. Discussion

To study the interactions of the different length E and K coils using the BIAcore, we coupled the K coils via a disulfide bond to the sensor chip surfaces. This immobilization approach, combined with optimization of experimental conditions, enabled us to eliminate artifacts (surface heterogeneity, parking problems, and mass transport limitations) that could have biased subsequent data analysis.

The interaction of E5 and K5, the longest peptides used in this study, was well described by a simple mechanism where the unfolded monomeric peptides are converted to the fully-folded dimer without discernable intermediates. The remarkably high affinity (K_d = 63 pM) agrees with previous results using urea and guanidine-HCl denaturations, as monitored by circular dichroism spectroscopy (Chao *et al.* 1996). This stability results from the combination of hydrophobic interactions (involving the residues at positions **a** and **d** of each heptad) and electrostatic interactions (positions **e** and **g**) between the two *de novo* designed α-helices and is reflected in a relatively fast association, or on-rate, of the two peptides ($k_{ass\#1} = 3.2 \times 10^6\ M^{-1}s^{-1}$) and a very slow dissociation, or off-rate, of the coiled-coil ($k_{diss\#1} = 2.0 \times 10^{-4}\ s^{-1}$). This off-rate is in good agreement with previous BIAcore experiments conducted by Chao *et al.* (1996), who found a $k_{diss\#1}$ value of 2.1 x

10^{-4} s^{-1} when injecting a streptavidin-bound biotinylated E5 coil over K5. The on-rate ($k_{ass\#1}$ = 4.5 x 10^5 $M^{-1}s^{-1}$) is ten fold lower than ours, which is likely due to the fact that the analyte E5 coil was linked to streptavidin. This suggests that the attachment of a protein at the C terminus of the E5 coil influenced only the on-rate of binding, without affecting the dissociation rate, hence the stability, of the dimer.

The E5/K5 heterodimer is among the most stable of the *de novo* designed coiled-coils that have been studied. Wendt *et al.* (1997) examined the interaction of the de novo designed A/B heterodimeric coiled-coil by stopped-flow fluorescence. This system displayed a rapid, ionic strength-dependent association rate (k_{ass} = 3.7 – 72 x 10^6 $M^{-1}s^{-1}$) that is in the same range as the one that we observed for E5/K5. Interestingly, the dissociation rates that they observed (k_{diss} = 3.8 – 10 x 10^2 s^{-1}), which are considerably faster than ours, were independent of ionic strength. This emphasizes the important role that electrostatic interactions can play in heterodimer association. An even faster association rate (k_{ass} = 10^7 – 10^8 $M^{-1}s^{-1}$) was measured for the acidic peptide A at pH 3.0 or at very high ionic strength (Durr *et al.* 1999, Jelesarov *et al.* 1998); however, these conditions are far from physiological. Extensive studies of the folding of GCN4-p1 have yielded association constants in the range of 10^5 – 10^6 $M^{-1}s^{-1}$, which are closer to the ones that we observed for E5/K5 (Ibarra-Molero *et al.* 2001, Sosnick *et al.* 1996, Zitzewitz *et al.* 1995). These variations can be explained by small sequence changes or differences in the techniques (e.g. presence of fluorescent labels) or the solvent conditions.

Surprisingly, we found that the interaction of the coiled-coils of every combination of chain length other than E5/K5 did not fit the simple Langmuirian model

(Figure 5-4 and data not shown). We tested two mechanistic models to see if we could account for these more complex interaction kinetics: one, a rate limiting rearrangement of the complex after the initial binding event, and, two, the formation of a tetramer after dimerization (Figure 5-2). We chose the first model because a conformational change was previously reported for a coiled-coil system (Wendt *et al.* 1995). We chose the second model since sedimentation equilibrium experiments have shown that E5/K5 can form a tetramer with a dissociation constant ($K_{d\ dimer\text{-}tetramer}$) equal to 200 μM (Chao *et al.* 1996). Additionally, although E4/K4 was shown to interact in a 1:1 manner by CD spectroscopy, the observed molecular weight in sedimentation equilibrium experiments was midway between that of the dimeric and tetrameric species, indicative of a dimer-tetramer equilibrium (Litowski & Hodges 2001). Furthermore, an interaction between two EK dimers within the matrix of the biosensor is theoretically possible since the dextran chains have been shown to be flexible enough to allow such an interaction. Indeed, Myszka and coworkers were able to reconstitute a high affinity IL-2/IL-Ra/Il-2Rb complex when both Il-2Ra and b were coupled to the matrix and IL-2 was injected over it (Myszka *et al.* 1996). Our global analysis of the experimental data showed that all coiled-coil interactions except for E5/K5 were best described by a rearrangement of the EK dimer. The quality of this fit can be judged by the random character of the residuals (Figure 5-4), the standard deviation of the residuals, and the Z1 and Z2 statistics (Table 5-2).

Inspection of the kinetic constants (Figure 5-5A-D) shows that the monomer-dimer association and dissociation steps are the most sensitive to variations in chain length. The on-rates ($k_{ass\#1}$) vary from 7.3×10^3 (E4/K3) to 3.2×10^6 $M^{-1}s^{-1}$ (E5/K5) in an exponential fashion. Interestingly, the off-rates ($k_{diss\#1}$) appear to be dependent on the length of the shortest coil of an E/K pair; $k_{diss\#1}$ is in the range of 10^{-1}, 10^{-2} and 10^{-4} s^{-1} when the shortest coil is composed of three, four or five heptads, respectively. This results in a large variation in the first equilibrium constant (K_d, Figure 5-5E), which goes from 100 pM to 10 μM, as the length of the shortest coil varies from five to three heptads. In contrast, the kinetic constants related to the second step (rearrangement) do not markedly vary with the lengths of the coils (a less than 10 fold difference is observed for k_r and k_{-r}). This results in a relatively small variation (from 0.1 to 1) in the second equilibrium constant (K_r, Figure 5-5F). From both K_d and K_r, it is possible to calculate an apparent dissociation constant K_{dapp} (Figure 5-5G) which takes into account both rearranged and unrearranged E/K dimers at equilibrium. The E4/K4 heterodimer was found to have an apparent K_d equal to 1.2×10^{-7} M. The equation $\Delta G = -RT \ln K_{dapp}$ was used to calculate the free energy of association as 9.4 kcal/mol. This is in good agreement with the free energy obtained by linear extrapolation analysis of a GdnHCl denaturation curve for the same molecule (8.2 kcal/mol, see Litowski & Hodges 2001 and Chapter III). The agreement of these numbers is very encouraging, because these two techniques are based on different principles and assumptions.

Both monophasic and biphasic folding mechanisms have been observed for coiled-coils. Monophasic folding has been observed for GCN4-p1 and related peptides by a number of researchers, using techniques such as DSC, stopped-flow CD and fluorescence spectroscopy (Ibarra-Molero *et al.* 2001, Sosnick *et al.* 1996, Wendt *et al.* 1997, Zitzewitz *et al.* 1995). However, biphasic folding has been observed by others using stopped-flow fluorescence experiments with GCN4-p1 (Wendt *et al.* 1994, Zhu *et* *al.* 2001) and analogs of the *de novo* designed LZ peptides (Wendt *et al.* 1995). Additionally, Holtzer and co-workers have conducted extensive $^{13}C^{\alpha}$ NMR experiments in which the transition of a coiled-coil from the unfolded to the folded state is monitored at specific residues (d'Avignon *et al.* 1998, 1999, Holtzer *et al.* 1997, 2001a, Lovett *et al.* 1996). Briefly, they have found that the kinetics of exchange between the two states differs between sites on the same molecule. This is a persuasive argument that folding is not two-state in these coiled-coils. They have also observed exchange between what appears to be two different folded states, adding more complexity to the picture.

A few researchers have observed a switch from monophasic to biphasic folding mechanisms upon relatively minor sequence changes. Holtzer and coworkers (2001a) found that the peptides GCN4-lz and GCN4-lzK, which differ by four conservative mutations (Arg to Lys and His to Lys), folded by monophasic and biphasic mechanisms, respectively. Mutational f analysis by Moran *et al.* (1999) found that oxidation of the peptide GCN4-p2 (which has an N-terminal CGG extension) appeared to restrict folding to a single transition state as compared to the multiple transition states available to the reduced peptide.

Wendt and coworkers (1995) showed by stopped-flow fluorescence that the *de novo* designed LZ, LZ(12A), or LZ(16A) coiled-coils obeyed complex kinetics of dissociation that could be depicted, as in our case, by the presence of a change in the conformation of the dimer. These LZ coiled-coil systems were also shown to form trimers at micromolar concentrations by sedimentation equilibrium and electrospray mass spectrometry. However the change in the conformation they reported was still observed at concentrations at which the trimeric form of the coiled-coil was negligible. Recently, Zhu *et al.* (2001) showed that the thermal unfolding of a GCN4 variant in which the Asn residue was moved from position 16 to 9 followed a two-state transition mechanism. The authors were able to show the presence of a transient, partially folded dimer, that could then rearrange itself to form a trimeric coiled-coil structure.

These studies, in addition to our present results, strongly suggest that the observed first order kinetic rearrangement of the coiled-coil may be a common phenomenon, and may be a kinetically limiting prerequisite for coils to be able to form higher order complexes (trimers or tetramers). Since the on-rates for the rearrangement for the E/K dimers were in the range of 10^{-3} s^{-1} (Figure 5-5C), and were relatively independent of the length of the coils, such a change in the conformation could also occur for the E5/K5 pair without being kinetically limiting and hence be undetectable. Our data do not exclude the formation of tetramers at the surface of the BIAcore; this additional step will not be detectable by the SPR biosensor technology if its related rate constants are not limiting.

Increases in chain length have been clearly shown to cause increases in stability (Lau *et al.* 1984, Litowski & Hodges 2001, Su *et al.* 1994). One obvious stabilizing effect of increased chain length is the increase in the number of stabilizing contacts, such as hydrophobic interactions at the coiled-coil interface and **e** to **g'** electrostatic attractions. Recent studies have shown that valine at a central **a** position contributes 1.66 kcal/mol more than alanine, and leucine at a central **d** position contributes 3.8 kcal/mol more than alanine (Tripet *et al.* 2000, Wagschal *et al.* 1999b). The other key factor is end fraying, a partial and temporary unfolding of the helix termini. In the case of the study carried out by Zhu *et al.* (2001), the observed rearrangement of the dimeric coil was attributed to an increase in the fraying of the N-terminal ends of the coils which was induced by an Asn mutation. Such a fraying phenomenon was also reported in dimeric *de novo* designed coiled-coils. Indeed, Zhou *et al.* (1992a) observed only a small decrease in stability at either end of a de novo designed parallel coiled-coil, when systematically performing Leu-Ala substitution at every **a** and **d** positions of a 35 residue polypeptide chain. This demonstrated that the contribution of Leu-Leu hydrophobic interactions to the stability of the coiled-coil structure were less important at the ends of the coiled-coil, and that the ends of the coiled-coil were more flexible. More recently, Holtzer *et al.* (1997) clearly demonstrated by $^{13}C^{\alpha}$ chemical shifts that such an end-fraying also occurred in a GCN4-like leucine zipper. All these studies suggest that the different heptads which make up a dimeric coiled-coil structure contribute differently to its stability; the heptads located at the ends of the coiled-coil are able to fray whereas the ones composing the core of the coiled-coil are more stable due to the tighter packing of the hydrophobic residues.

From the apparent K_d shown in Figure 5-5G, it appears that the main factor governing the overall stability of the dimer is the length of the shortest coil present in the complex. This conclusion is even more obvious when plotting the free energy (ΔG), deduced from the K_{dapp} as a function of the length of the shortest coil involved in the dimers (Figure 5-6). The contribution of the heptads which are not in direct contact with the other strand is minimal as compared to the ΔG contribution of the paired ones, since there is only a 15% change in the slope of the regression lines depending on whether the ΔG corresponding to the mismatching length coiled-coil interactions are taken into account during the regression or not.

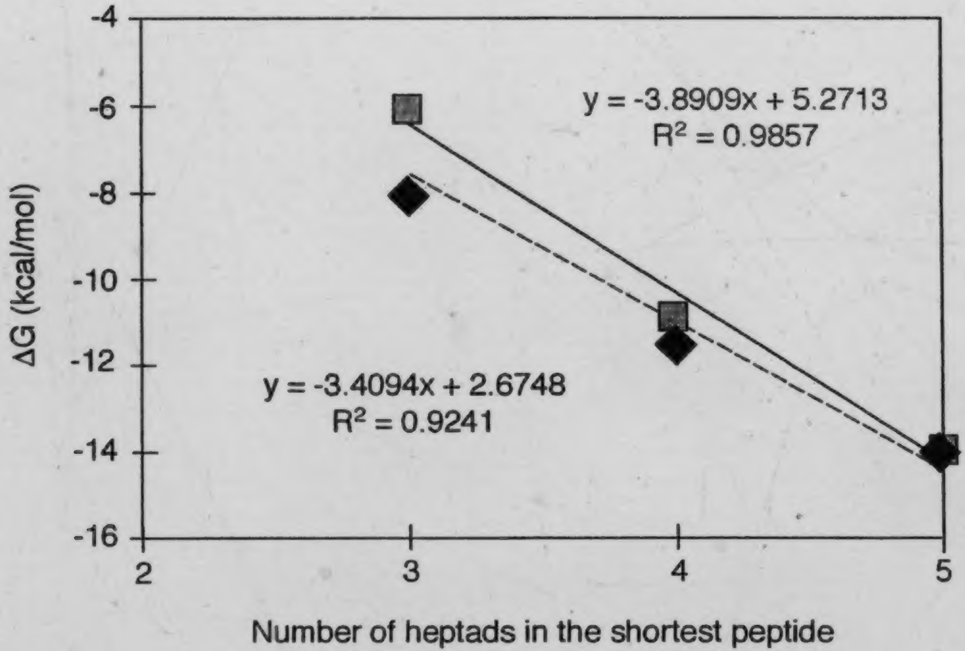

Figure 5-6. Variation of the free energy of binding with the length of the shortest coil within the dimers. The solid line and top equation correspond to the linear regression when taking into account the matching coil pairs only (■, E3/K3, E4/K4 and E5/K5) and the dashed line and bottom equation to linear regression when taking into account all the coiled-coil interactions (■ and ◆).

From the linear equation corresponding to the matching pairs of E/K (Figure 5-6), it is possible to deduce the ΔG contribution of the heptads composing the core of the coiled-coil (ΔG_{core}) versus the ΔG contribution of the heptads at the ends of the dimers ($\Delta G_{paired\text{-}end}$). That is, the slope of the curve corresponds to the contribution of a heptad composing the core and is equal to -3.89 kcal/mol of dimerized core heptad; $\Delta G_{paired\text{-}end}$ can be obtained by term substitution, giving a value of –1.26 kcal/mol per heptad involved in the paired-end.

In an effort to refine the calculations and take the mismatching length coiled-coil interactions into consideration, we assigned to the heptads composing the dimers one of the three following ΔG values, depending if the heptad is part of the core (ΔG_{core}), part of one of the two paired-ends ($\Delta G_{paired\text{-}end}$), or is not in direct contact with the other strand ($\Delta G_{unpaired\text{-}end}$). This corresponds to defining a system of seven equations (one for each coiled-coil interaction studied) that can be solved by multiple-linear regression. Figure 5-7 shows the results of such an approach and gives a ΔG_{core} value of –3.84, a $\Delta G_{paired\text{-}end}$ value of –1.38 and a $\Delta G_{unpaired\text{-}end}$ value of –0.93 kcal/mol of heptads with a R^2 coefficient of 0.9776. The two approaches to calculating the ΔG contribution of a heptad give remarkably close estimations for the ΔG contribution of the heptads composing the core versus the ends of the coiled-coil and clearly indicate that the ΔG contribution of the core heptads is three fold higher than the ΔG contribution of the heptads located at the ends of the dimer. These differences in the contribution of the core versus the end heptads to the stability of the dimer are consistent with our E3/K3 data which were shown to be low affinity; i.e. such a low affinity can be attributed to the presence of only one core heptad in the coiled-coil dimer. Similarly, Su *et al.* (1994) showed, by varying the length of a

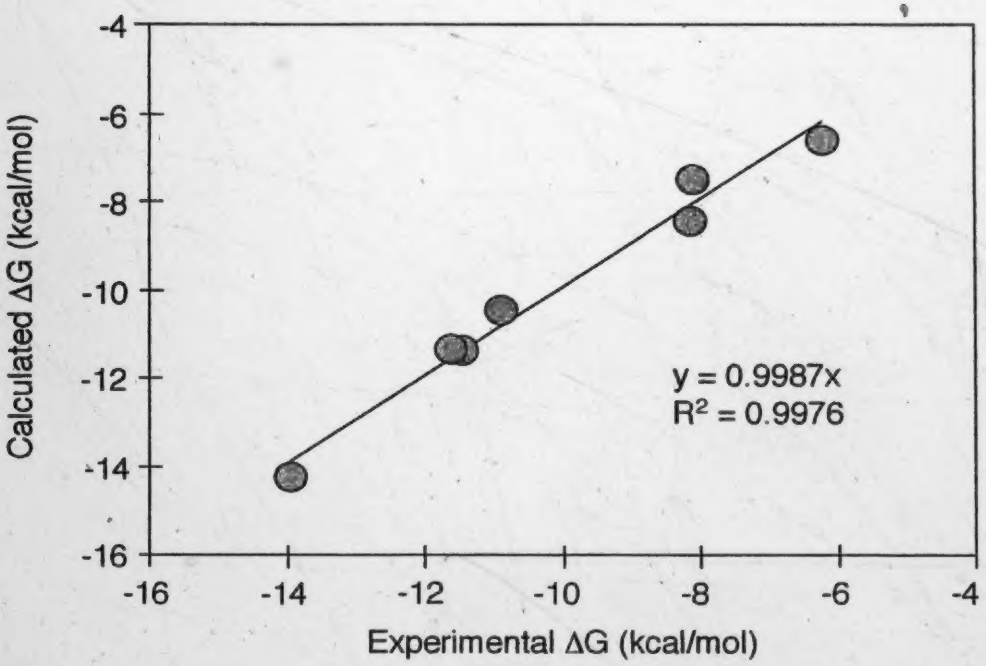

Figure 5-7. Experimental free energies versus free energies calculated using the multiple-linear regression approach.

coil whose heptad motif was IEALKAE, that a minimum of three heptads was required to form a stable two-stranded a-helical coiled-coil.

F. Conclusion

We have shown that the association of heterodimeric coiled-coils can be studied with the BIAcore. The E5/K5 interaction was found to be rapid and of high affinity, and could be described by a simple mechanism. The shorter E/K coiled-coil interactions were better depicted by a more complex mechanism, i.e. dimer formation followed by a conformational rearrangement. Analysis of the relationship between affinity and chain length suggested that heptads at different positions within the coiled-coil provide different amounts of free energy. Specifically, the core heptads contributed more than twice as much to the free energy of interaction as compared to heptads at the ends of the coiled-coil. As expected, heptads at the ends that were paired (i.e. the two strands were of the same length) contributed more than unpaired heptads. However, unpaired heptads did contribute slightly to the free energy of binding, giving mismatched coiled-coils an intermediate stability, with respect to the two matched pairs.

Our generation of a series of E/K heterodimeric coiled-coils with varying length and, consequently, a wide range of stabilities and affinities provides for considerable flexibility in designing applications based on these coiled-coils. For instance, a single protein (e.g. an E5-fusion) could be used in several applications that require different degrees of coiled-coil stability, e.g. purification versus immobilization, by simply varying the length of the partner K coil.

CHAPTER VI

Hydrophilic interaction/cation-exchange chromatography for the purification of synthetic peptides from closely related impurities: serine side-chain acetylated peptides

This project was performed when problems arose in the purification of peptides needed for the work described in Chapter IV. A version of this chapter has been published: Litowski, J. R., Semchuk, P. D., Mant, C. T., and Hodges, R. S. (2001) *J. Chromatogr.* **54**, 1-11.

A. Summary

Mixed-mode hydrophilic interaction/cation-exchange chromatography (HILIC/CEC) is a novel HPLC technique which has excellent potential for peptide separations. Separations by HILIC/CEC are carried out by subjecting peptides to linear increasing salt gradients in the presence of high levels of acetonitrile, which promotes hydrophilic interactions overlaid on ionic interactions with the cation-exchange matrix. Complex peptide mixtures produced by solid-phase synthesis are a frequently encountered and challenging purification problem. In the present study, a two-step protocol, consisting of HILIC/CEC followed by RPC, was required for the successful purification of a 21-residue synthetic amphipathic α-helical peptide from serine side-chain acetylated impurities, with HILIC/CEC proving to be highly sensitive to subtle differences in hydrophilicities between the acetylated peptides and the desired product. Investigation of the three potential sites of serine acetylation through solid-phase synthesis of acetylated analogs of the desired peptide (peptides of the same sequence and secondary structure, but acetylated at different positions on the hydrophilic face of the α-helix) demonstrated that acetylation was occurring at different sites on the peptide.

HILIC/CEC was able to take advantage of very subtle changes in environment around the acetylation sites and thus effect a separation of these analogs not achievable by RPC or CEC alone.

B. Introduction

A common purification problem is the separation of a complex mixture of peptides produced by solid-phase peptide synthesis (SPPS), with deletion and termination peptides frequently being encountered. Side-chain modifications also may occur, such as oxidation of methionine, alkylation of the indole ring of tryptophan, ring closure of aspartyl residues with subsequent production of a mixture of α- and β-aspartyl residues upon ring opening, and cyclization of N-terminal glutamines to form pyrrolidones (Bodanszky 1988, Erickson & Merrifield 1976). Purification frequently presents a challenge because these impurities may differ from the desired product by a single residue or less, resulting in very similar peptide properties (Mant *et al.* 1997).

Reversed-phase chromatography (RPC) has become the standard method of analysis and purification of synthetic peptides due to its excellent efficiency and resolving power (Gooding & Regnier 1990, Hearn 1991, Mant & Hodges 1991a). Its advantages include reasonable elution times and the availability of volatile mobile phases, such as aqueous trifluoroacetic acid (TFA) and acetonitrile (CH_3CN), which eliminate the need for a desalting step. RPC has been used previously for the detection and purification of side-chain modified products from SPPS (Szokan *et al.* 1987). However, no single technique is likely to be universally successful, and there are many examples of peptides which are extremely difficult, if not impossible, to purify to homogeneity from their impurities by RPC alone (Mant *et al.* 1997).

In 1990, Alpert (1990) introduced a novel mode of high-performance liquid chromatography (HPLC) based on hydrophilic interactions between the solute and a hydrophilic stationary phase (polyhydroxyethyl aspartamide), such interactions being promoted by high levels of organic modifier (acetonitrile) in an aqueous mobile phase. Thus, this approach is essentially an interesting variant of normal-phase chromatography, denoted hydrophilic interaction chromatography, or HILIC (Zhu *et al.* 1991). Elution during HILIC is in the order of increasing solute hydrophilicity, or decreasing hydrophobicity, i.e. the opposite of characteristic RPC elution behaviour. Taking this concept one step further, Zhu *et al.* (1991) demonstrated how to take advantage of the inherent hydrophilic character of ion-exchange packings, specifically cation-exchange, by subjecting peptide mixtures to linear salt gradients in the presence of high levels of organic modifier. The separations based on hydrophilicity are thus superimposed on top of those based on charge, resulting in mixed-mode hydrophilic interaction/cation-exchange chromatography (HILIC/CEC). Such a mixed-mode approach takes simultaneous advantage both of the charged character of peptides as well as any hydrophilic/hydrophobic properties they possess. Indeed, such an approach has already been demonstrated to be an effective complementary technique to RPC for complex peptide mixtures. For the separation of two synthetic peptides and their deletion impurities (serine and cysteine), HILIC/CEC was clearly superior to RPC (Mant *et al.* 1997). HILIC/CEC has been shown to be particularly effective for the separation of amphipathic α-helical and cyclic β-sheet peptides (Mant *et al.* 1998a, 1998b). The hydrophobic and hydrophilic faces of an amphipathic peptide act as preferred binding domains during RPC (Zhou *et al.* 1990) and HILIC/CEC (Mant *et al.* 1998a, 1998b), respectively. As expected, HILIC/CEC was most effective for the separation of peptides which differed in their hydrophilic faces and RPC was most effective for the separation of peptides which differed in their hydrophobic faces.

Mixed-mode HILIC/CEC has also been used for the separation of H1 histones (Lindner *et al.* 1996, 1997). The subtypes of these proteins have been notoriously difficult to separate by traditional HPLC techniques. In addition, histones have multiple acetylation and phosphorylation sites. These post-translational modifications are thought to influence chromatin structure and transcription. The ability to separate histone proteins that have been acetylated or phosphorylated to different degrees is essential to carrying out functional studies of these proteins. These H1 histones variants were successfully separated by a multi-step procedure involving both HILIC/CEC and RPC (Lindner *et al.* 1996, 1997).

This paper describes the purification of a 21-residue peptide following its synthesis by SPPS. Standard RPC purification was unable to remove acetylated impurities and HILIC/CEC was required for the successful purification of this peptide. The impurities were identified through a combination of different analytical techniques, including tryptic digests and mass spectrometry. Further experiments with model peptides were then performed to investigate the ability of HILIC/CEC to separate peptides with side-chain modifications. That is, in this case, to separate serine O-acetylated peptides which have identical sequences but differ in the position of sidechain modification.

C. Results and Discussion

Purification and Analysis of a 21-residue Peptide

The amphipathic α-helical 21-residue peptide, denoted N (Table 6-1), was synthesized by solid-phase peptide synthesis techniques with an acetylated N-terminus and an amidated C-terminus. RPC analysis of the crude peptide revealed the presence of many impurities which were eluted close to the desired product (Figure 6-1), and electrospray mass spectrometry showed that the main peak (denoted N) was the desired product (mass of 2368 Da). This main peptide component was purified by RPC , and the resulting fractions were analyzed by mass spectrometry and analytical RPC. To obtain a reasonable yield of the desired peptide, several fractions were pooled, resulting in a "semipure" peptide which still displayed a group of closely related impurities. Mass spectrometry showed that an impurity with a mass of 2410 Da was present in significant amounts. The impurity was 42 mass units higher than the desired peptide, suggesting that side-chain acetylation had taken place. Since the peptide contained three serines and three lysines, several potential acetylation sites existed.

In an attempt to resolve more efficiently the impurities from the desired product, the semipure peptide obtained from preparative RPC was analyzed under different RPC conditions (Figure 6-2). Different anionic ion-pairing agents were used to take advantage of the dramatic effects these agents can have on peptide separations (Guo *et al.* 1987). The upper and middle panels of Figure 6-2 show RPC in the presence of TFA and phosphoric acid, respectively. In both cases there is good separation between peptide N and compound 4, a lysine-deletion peptide; however, the acetylated analogs (compounds 2 and 3) were poorly resolved. The product and peptide impurities were all eluted earlier when phosphoric acid was used because the negatively charged phosphate ion is a more hydrophilic ion than trifluoroacetate. Since such anionic ion-pairing agents interact with positively charged groups on the peptide, the lysine deletion peptide (compound 4) was

Table 6-1. Peptide Sequences

Name	Sequence[a]
N	Ac-KIS----ALKEKIS----ALKEKIS----ALKE-NH_2
Ac3	Ac-KIS(Ac)ALKEKIS----ALKEKIS----ALKE-NH_2
Ac10	Ac-KIS----ALKEKIS(Ac)ALKEKIS----ALKE-NH_2
Ac17	Ac-KIS----ALKEKIS----ALKEKIS(Ac)ALKE-NH_2
S2	Ac-RGGGGLGLGK-NH_2

[a] The sequences are written with the one letter amino acid codes. Ac represents an N^{α}-acetyl group. NH_2 represents a C^{α}-amide group. S(Ac) represents a serine residue that has an acetylated β-hydroxyl group.

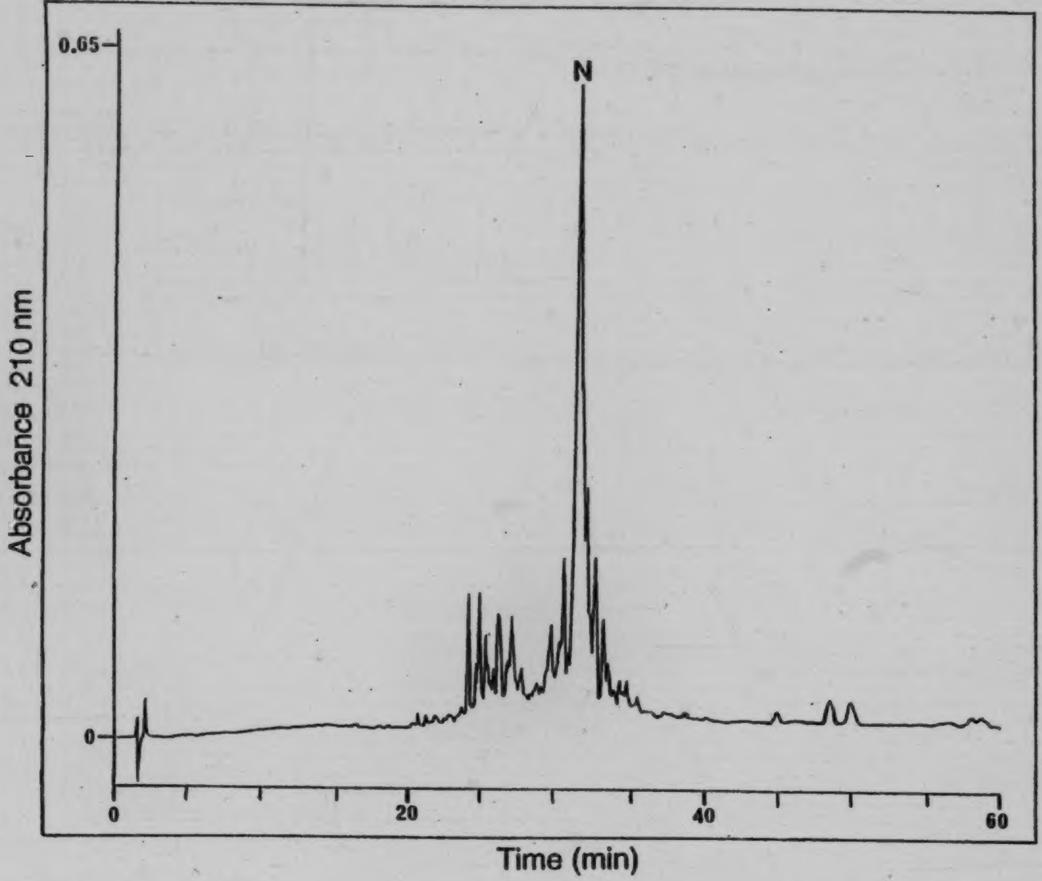

Figure 6-1. RPC of crude peptide N. Column: Zorbax 300SB-C8. Conditions: linear AB gradient (1% acetonitrile/min) where eluent A is 0.05% aqueous TFA and eluent B is 0.05% TFA in acetonitrile; flow-rate, 1 ml/min.

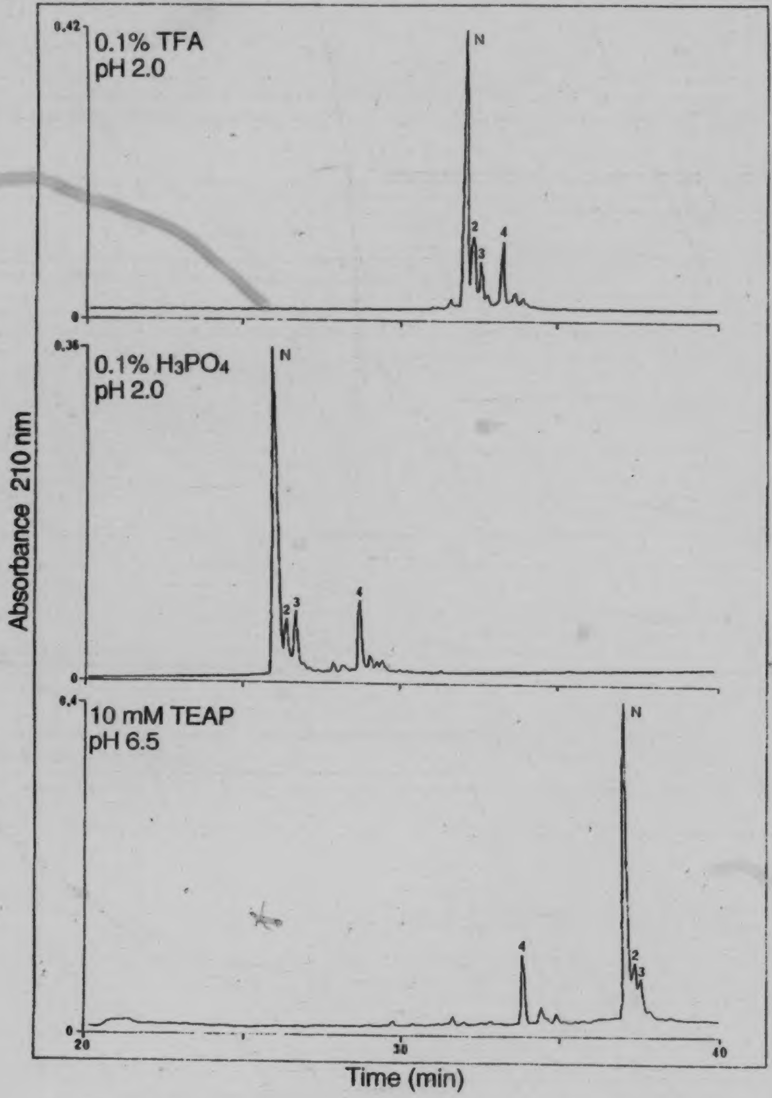

Figure 6-2. RPC of semipurified peptide N. Column: Zorbax Eclipse XDB-C8. Conditions: linear AB gradient (1% acetonitrile/min); flow-rate, 1 ml/min. Upper panel: eluent A is 0.1% aqueous TFA and eluent B is 0.1% TFA in acetonitrile, pH 2.0. Middle panel: eluent A is 0.1% aqueous phosphoric acid and eluent B is 0.1% phosphoric acid in acetonitrile, pH 2.0. Lower panel: eluent A is 10 mM aqueous TEAP, pH 6.5, and eluent B is 10 mM TEAP in 50% aqueous acetonitrile (v/v), pH 6.5, both eluents containing 100 mM $NaClO_4$.

less affected by the switch from TFA to phosphoric acid. The lower panel shows a run at pH 6.5 using a TEAP/$NaClO_4$ buffer. Both the higher pH, which deprotonates the glutamic acid residues and, hence, changes the charged character of the peptide, and the aq. TEAP/$NaClO_4$ mobile phase may affect the separation relative to the low pH mobile phases. The hydrophobic character of the peptide is increased by the interaction of the positively charged triethylammonium ion with the negatively charged residues and the interaction of the negatively charged perchlorate ion with the positively charged residues. The later elution of all peptides in the pH 6.5 run compared to the TFA and phosphoric acid systems is likely due to the high concentration (100 mM) of perchlorate compared to TFA and H_3PO_4 (10 - 20 mM) overcoming any increase in peptide hydrophilicity due to the deprotonation of the acidic residues (Sereda *et al.* 1997). Note the switch in the elution of compound 4 relative to the other components at pH 6.5 compared to pH 2, since, with a lysine deletion, the high perchlorate concentration has a lesser effect on elution behaviour of the peptide compared to the native peptide N and its acetylated analogs. Again, good separation was achieved between peptide N and compound 4, but compounds 2 and 3 were not resolved from the product.

Since a straightforward isolation of the desired peptide product by RPC appeared difficult to achieve, we then attempted to resolve the semipure material (Figure 6-2) by cation-exchange chromatography (Figure 6-3). The peaks were collected and analyzed by LC-MS to identify the components. The largest peak was composed of two species: the parent peptide, N (2368 Da); and compounds 2 and 3, acetylated peptides (each of 2410 Da). The middle peak contained compound 4, a lysine-deletion peptide (2239 Da); and compound 5, a lysine-deletion peptide with an acetyl modification (2282 Da). The earlier elution of compounds 4 and 5 compared to compounds 1-3 indicated the loss of a positive charge, confirming the lysine deletion indicated by mass spectrometry. The smallest peak contained compound 6, a double lysine-deletion peptide (2111 Da); and

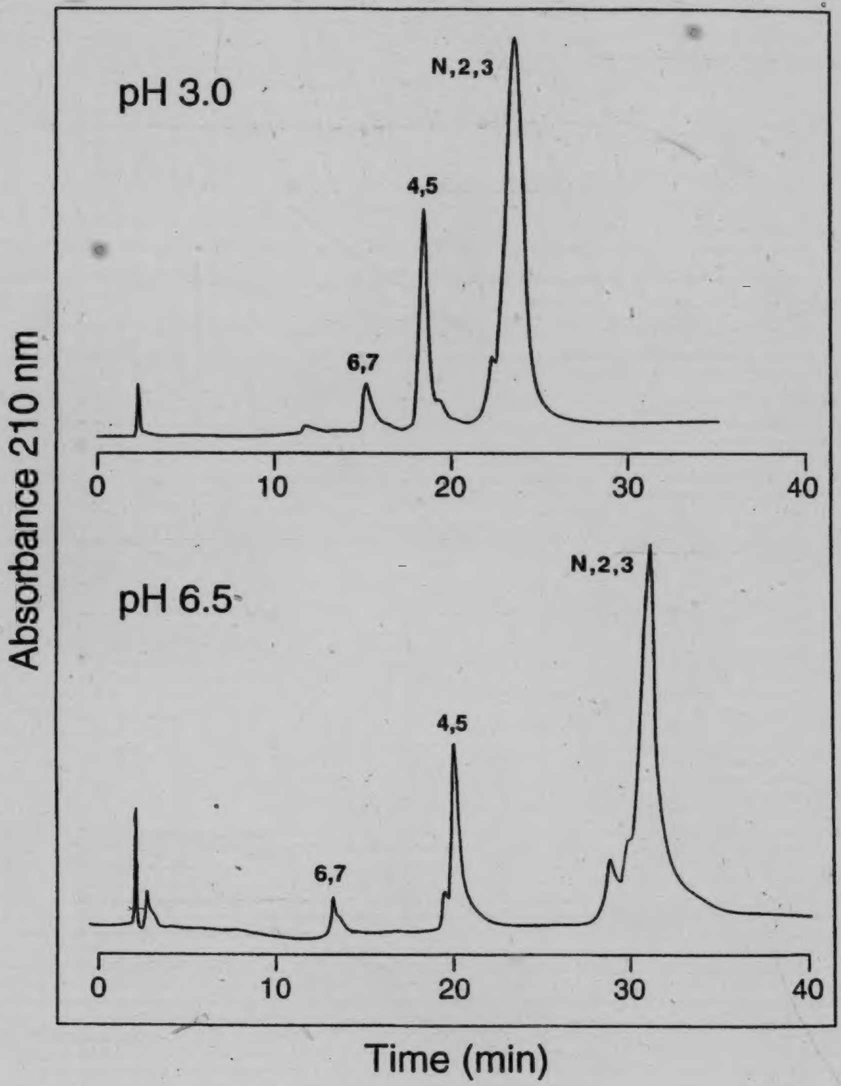

Figure 6-3. CEC of semipurified peptide N. Column: PolySulfoethyl A. Conditions: linear AB gradient (5 mM $NaClO_4$/min, following 5-min isocratic elution with eluent A), where eluent A is 10 mM aqueous TEAP, pH 3.0 or pH 6.5, containing 10% acetonitrile (v/v) and eluent B is eluent A containing 500 mM $NaClO_4$; flow-rate, 1 ml/min.

compound 7, a double lysine-deletion peptide with an acetyl modification (2153 Da). Changing the pH from pH 3.0 to pH 6.5 did not improve the separation, although the peptides were eluted earlier at pH 3.0, when their net positive charge was greater, than at pH 6.5. This perhaps unexpected observation has been previously reported for strong cation-exchange columns, where this apparent anomaly appeared to arise from the induction of some non-specific positively charged character of the packing matrix as the pH was lowered, leading to reduced column retention (Mant & Hodges 1985, 1991b).

From Figure 6-3, CEC was unable to separate the acetylated peptides from their non-acetylated analogs, i.e., no particular advantage of CEC over RPC (Figure 6-2) was apparent. If the peptides had been acetylated at lysine, they would have lost a positive charge and hence would be eluted earlier during CEC. Since this was not the case, serine was the more probable site of acetylation. This was supported by the RPC behaviour of compounds 2 and 3 in response to different ion pairing agents, which interact with positively charged groups on the peptide. Acetylation at a lysine position would remove a positive charge and change the response to ion pairing agents, as illustrated by the RPC behaviour of the lysine-deletion impurity (compound 4) in Figure 6-2. An acetylated serine, on the other hand, should have no effect. This is consistent with the closely related elution times of peptide N and compounds 2 and 3 in RPC compared to the behavior of compound 4 (Figures 6-2 and 6-3).

With both RPC and standard CEC unable to achieve the desired peptide purity, clearly another approach was required. From Figure 6-2, although the O-acetylated serine impurities were eluted very close to peptide N, some resolution was possible, indicating that hydrophobicity/hydrophilicity differences, however subtle, did exist between the desired product and its side-chain modified analogs. Thus, acetylation of serine residues had made peptide N slightly more hydrophobic, as illustrated by the later elution of these impurities. The question remained as to whether advantage could be taken of such subtle peptide hydrophobicity variations. It has been shown previously (Mant *et al.* 1997) that the conditions characteristic of HILIC/CEC (i.e., a high acetonitrile concentration in the mobile phase) appear to enhance the hydrophilic contribution to HILIC/CEC peptide retention behaviour of a residue such as serine which is only classed as mildly hydrophilic in RPC terms. Hence, the next step taken to attempt further purification of the semipurified peptide N (Figure 6-2) was analysis by HILIC/CEC in the hope of enhancing the slight hydrophobicity/hydrophilicity differences between peptide N and its impurities and, hence, effect a separation superior to that of RPC or standard CEC.

Figure 6-4 shows the result of analyzing semipure peptide N by mixed-mode HILIC/CEC, the four main peaks being collected and subsequently analyzed by LC-MS. The separation obtained by HILIC/CEC was clearly superior to that obtained by RPC (Figure 6-2) or CEC (Figure 6-3), with subsequent analysis by mass spectrometry confirming only a single peptide mass in each of the four peaks. As expected, the lysine-deletion peptide (peak 4) was well separated from the desired product, N (peak 1). Acetylated impurities (peaks 2 and 3) were also well resolved from peak 1, their earlier elution reflecting their greater hydrophobicity (lower hydrophilicity), however subtle the difference, relative to peptide N (Figure 6-2). An interesting observation was that impurities 2 and 3 have the same mass (both 42 mass units greater than peptide N), indicating that both peaks contain component(s) acetylated on only a single serine

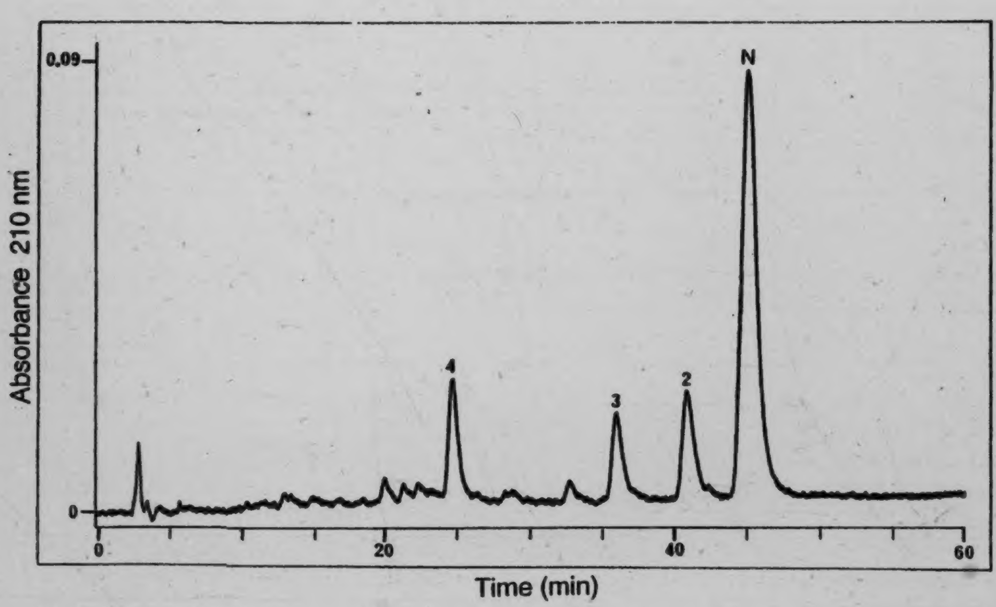

Figure 6-4. HILIC/CEC of semipurified peptide N. Column: PolySulfoethyl A. Conditions: linear AB gradient (2.5 mM $NaClO_4$/min, following 10-min isocratic elution with 10% eluent B), where eluent A is 10 mM aqueous TEAP, pH 6.5, containing 65% acetonitrile (v/v) and eluent B is eluent A containing 350 mM $NaClO_4$; flow-rate, 1 ml/min.

residue. This suggests that HILIC/CEC is able to separate efficiently acetylated analogs where the only difference is in the position of side-chain acetylation. From Figure 6-5, which represents peptide N as a helical net, it can be seen that there are three potential serine-acetylation sites in the hydrophilic face of the helix. However, only two peaks containing acetylated impurities were observed (Figure 6-4). Thus, either only two of the serine sidechains were acetylated or, where three acetylated derivatives were formed, two were co-eluted by HILIC/CEC. Although the question of which of these possibilities is the case is interesting, it has no immediate bearing on the approach now clearly required for an efficient purification of peptide N from its crude mixture, i.e. a two-step approach with HILIC/CEC being followed by RPC.

This new purification procedure is illustrated in Figure 6-6. The crude peptide N was first separated by HILIC/CEC (upper panel) and the peak containing the desired product (marked with a bar) was collected. Following lyophilization, this peak was then applied to RPC for a final desalting and purification step. Note that this two-step approach demonstrates well the complementary nature of these HPLC modes, for those impurities that were not removed by the first step were removed by the second. Note also that the superiority of HILIC/CEC in resolving the acetylated impurities (Figures 6-4 and 6-6) compared to RPC (Figure 6-2) supports previous work on amphipathic peptides, where substitutions made in the hydrophilic face (Figure 6-5) are best separated by HILIC/CEC because this face binds preferentially to the cation-exchange matrix. Thus, in the present case, the acetylation sites will generally be oriented away from the narrow hydrophobic face of the helix (Figure 6-5), which is the preferred binding domain for

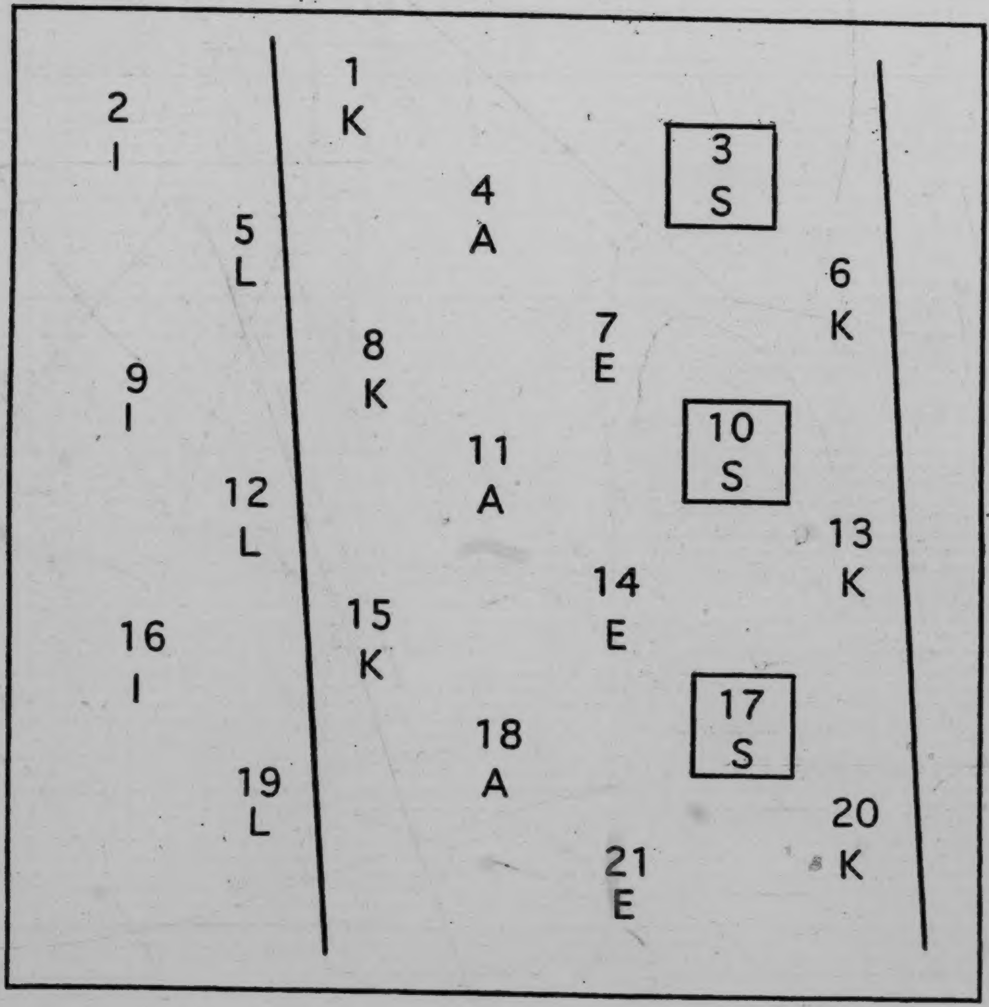
1
K
2
I
3
S
4
A
5
L
6
K
7
E
8
K
9
I
10
S
11
A
12
L
13
K
14
E
15
K
16
I
17
S
18
A
19
L
20
K
21
E

Figure 6-5. Sequence of peptide N presented as an α-helical net. The radius of the α-helix is taken as 2.5 Å with 3.6 residues per turn, a residue translation of 1.5 Å and thus a pitch of 5.4 Å. The area between the solid lines represents the more hydrophilic face of the peptide, with the Leu and Ile residues representing the narrow hydrophobic face. The boxed serine residues represent potential sites of side-chain acetylation.

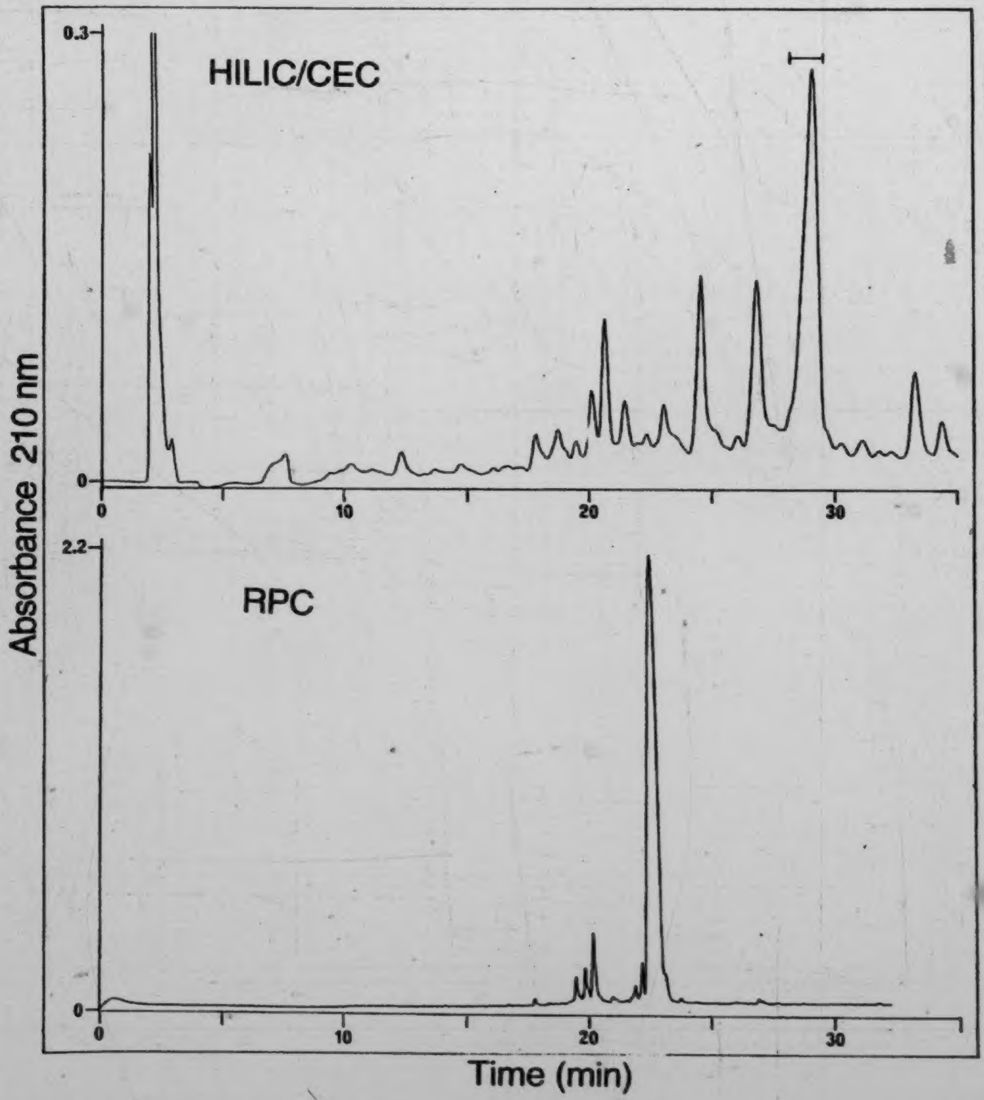

Figure 5-6. Two-step purification of peptide N. Crude peptide was purified by HILIC/CEC (upper panel); column and conditions as in Figure 6-4, with a gradient of 5 mM $NaClO_4$/min. Peptide N (marked with a bar) was collected. After several runs, the collected fractions were pooled and purified by RPC (lower panel); column and conditions as in Figure 6-1.

RPC, and hence will contribute little to the reversed-phase retention behaviour of the peptides.

Characterization of the Acetylated Peptides

Further characterization of compounds 2 and 3 (Figure 6-4) was carried out to identify the site of acetylation. To confirm the CEC results which suggested that serine was the acetylation site, a tryptic digest was performed on peptide N and compounds 2 and 3 (from Figure 6-4). The sequence of N is a repeating heptad (Table 6-1), so three identical five-residue fragments (ISALK) are produced by the digest. The presence of an acetylated lysine residue would block cleavage by trypsin, producing longer peptide fragments; in comparison, the presence of an acetylated serine would not interfere with cleavage, resulting in a mixture of fragments with the same number of residues, but with different masses (531 Da for the non-acetylated fragment vs. 573 Da for the acetylated fragment). After tryptic cleavage, the samples were analyzed by RPC and mass spectrometry (Figure 6-7). The upper panel shows that peptide N yielded a single fragment, while compounds 2 and 3 both yielded two fragments. Fragments Na, 2a, and 3a were all shown to have the sequence ISALK and a mass of 530 Da; in comparison, fragments 2b and 3b were shown to have a mass of 573 Da and are thus the acetylated analogs of ISALK. Clearly, since the action of trypsin was uninhibited, lysine is ruled out as the site of acetylation.

Final confirmation of the nature of the side-chain modification was obtained by analyzing fragments produced by MS/MS. One of the advantages of MS/MS experiments is the ability to differentiate between sample components on the basis of size, reducing the need for chromatographic separations (D'Agostino *et al.* 1998). The

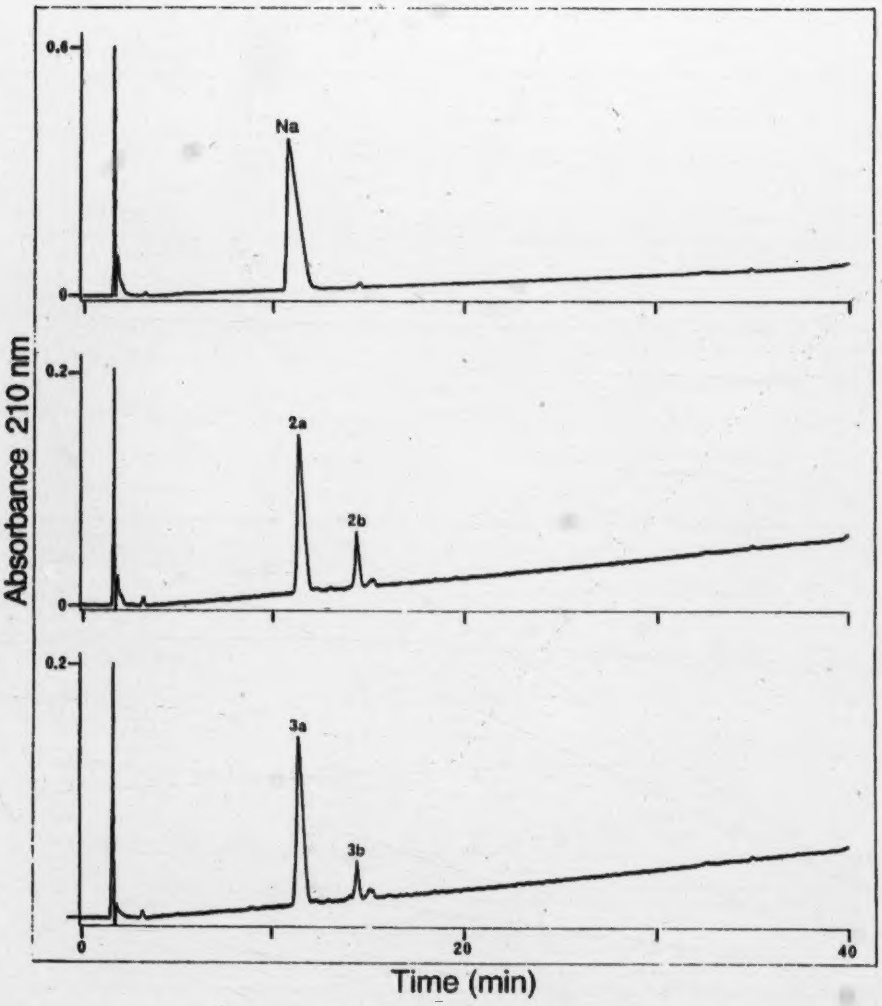

Figure 6-7. Tryptic digest of compounds 1, 2, and 3 from Figure 6-4. Each peptide (100 - 500 μg) was dissolved in 100 μl of buffer (50 mM aqueous NH_4HCO_3, pH 7.6, containing 1 mM $CaCl_2$) and incubated with 2 μg trypsin at 37°C overnight. The peptide digests were then analyzed by RPC (column and conditions as in Figure 6-1). The peaks were collected and analyzed by mass spectrometry.

crude peptide mixture was digested with trypsin overnight. Mass spectrometry showed that two of the major products were ISALK (531 Da) and IS(Ac)ALK (573 Da), as expected. These two peptides were selected and fragmented in turn (Table 6-2). A variety of fragments were produced from the a_n, b_n, c_n, and y_n series. Because ISALK and its acetylated analog differ at only a single residue, many of their daughter fragments are identical. Differences in mass are found only in those fragments which contain serine (b_2, b_3, and y_4). As predicted, these three fragments are 42 Da greater in mass when derived from the acetylated fragment ISALK (573 Da). This is conclusive evidence that serine residues have been O-acetylated at some point during the peptide synthesis or subsequent extraction procedure.

HILIC/CEC of Acetylated Serine Peptides

From Figure 6-4, the analysis of the semipure N by HILIC/CEC identified at least two acetylated impurities, peaks 2 and 3. Both peaks showed a mass of 2410 Da, thus indicating the presence of one extra acetyl group. As noted above, these two peaks can be reliably separated by HILIC/CEC, but on what basis? The most likely explanation is that the peptide components have been acetylated at different serine residues. The ability of HILIC/CEC to separate these peptides is remarkable, for they have the same charge and extremely similar, if not identical, hydrophilicities. In order to explore further the sensitivity of this HPLC mode, a series of peptide N analogs was made with acetylated serines introduced at one of the three serine positions (Ac3, Ac10, and Ac17, Table 6-1). These three synthetic peptides were used to identify and assign the structures of the impurities observed in the synthetic crude by co-elution during HPLC and their identical mass and sequence. As can be seen on the helical net diagram (Figure 6-5), all three serines are in the middle of the hydrophilic face of the amphipathic helix. Ser10 and

Table 6-2. MS/MS Fragments of ions 531 and 57

Fragment	Ion Series	Theoretical Mass	Observed Fragments Ion 531	Observed Fragments Ion 573
H_2N-Ile	a_1	86.10	86.28	86.28
H_2N-Ile-CO-NH	c_1	129.10	129.22	129.36
NH-Lys-CO_2	y_1	147.11	147.21	147.41
H_2N-IleSer-CO	b_2	201.12(243.12[a])	201.07	242.66
NH-LeuLys-CO_2	y_2	260.20	260.26	259.96
H_2N-IleSerAla-CO	b_3	272.16(314.16[a])	272.05	313.75
NH-AlaLeuLys-CO_2	y_3	331.23	330.87	331.18
NH-SerAlaLeuLys-CO_2	y_4	418.27(460.27[a])	417.98	459.67

[a] Theoretical mass of the O-acetylated fragment.

Ser17 are surrounded by four potentially charged residues (two lysines and two glutamic acids). Ser3, in contrast, is near the N-terminus of the peptide and has only two potentially charged residues (one lysine and one glutamic acid) as neighbors. It is possible that this difference in environment may cause subtle differences in the relative hydrophilicities of acetylated serine residues at position 3 compared to positions 10 and 17.

The three acetylated peptides were then analyzed by RPC and by HILIC/CEC (Figure 6-8). The nonacetylated parent peptide, N, was also present as an impurity in one or more of the acetylated peptides. The nonhelical peptide S2 (Table 6-1) was included as an internal standard. From Figure 6-8 (top left) RPC was not able to resolve the four helical peptides and they were coeluted as a single peak. Other RPC solvent systems were used (phosphoric acid, TEAP), but they showed no advantages (data not shown). As expected from previous runs (Figures 6-4 and 6-6), HILIC/CEC was much more successful at resolving the peptides. From Figure 6-8 (top right) the first conditions tried were those used earlier in the purification of peptide N. Under these conditions, peptides Ac10 and Ac17 were coeluted, but Ac3 was separated from the coeluted Ac10 and Ac17 by 2.6 min, and N was separated by 1.8 min. This result supports the view that an acetylated serine at position 3 experiences a different environment and so has a different relative hydrophilicity compared to the same residue at positions 10 or 17 (Figure 6-5). Note also that this result allows for the identification of peaks 2 and 3 in Figure 6-4, where peak 3 can now be denoted as peptide N modified at Ser3; in addition, peak 2 contains either peptide N modified at Ser10 or Ser17 or a mixture of the two. In an attempt to resolve the coeluted Ac10 and Ac17, the salt gradient was then reduced to 2.5

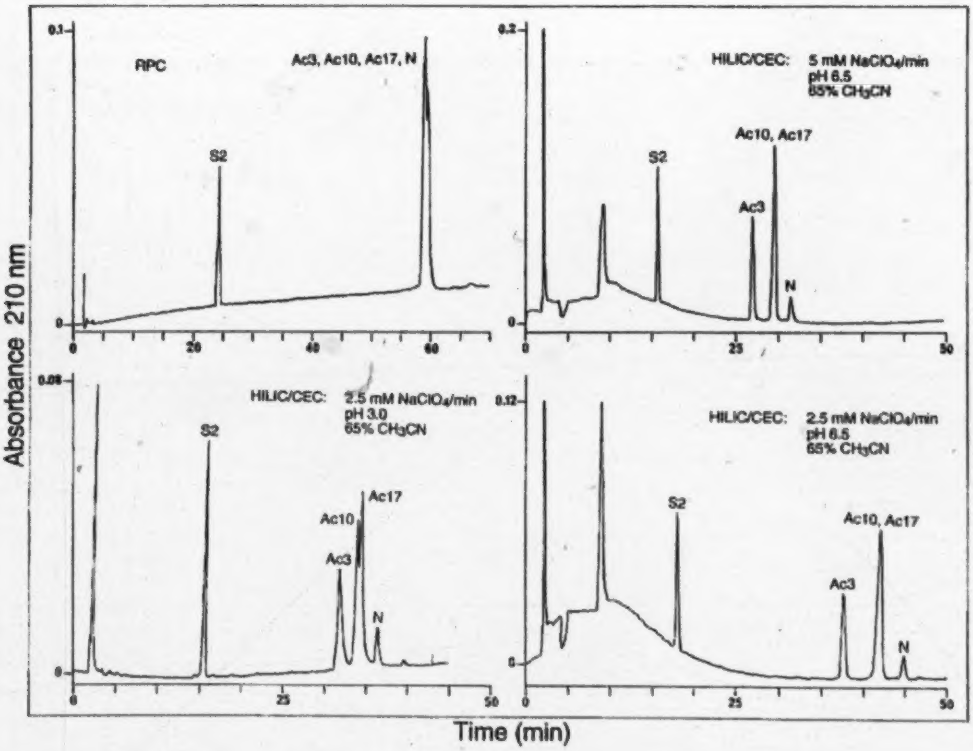

Figure 6-8. Separation of acetylated serine peptides by RPC and HILIC/CEC. Ac3, Ac10 and Ac17 refer to peptides with an acetylated serine at positions 3, 10 or 17, respectively (see Figure 6-5). N denotes the native form of the peptide which does not have acetylated serines. S2 is a non-helical synthetic peptide standard. The RPC column and conditions were the same as in Figure 6-1 (top left panel). HILIC/CEC was initially performed with a linear AB gradient (top right panel, 5 mM NaClO$_4$/min, following 5-min isocratic elution at 10% B), where eluent A is 10 mM aqueous TEAP, pH 6.5, containing 65% acetonitrile (v/v) and eluent B is eluent A containing 350 mM NaClO$_4$; the gradient was then reduced to 2.5 mM NaClO$_4$/min in an attempt to improve the separation (bottom right). The third HILIC/CEC run was carried out at pH 3.0 and a gradient rate of 2.5 mM NaClO$_4$/min (bottom left).

mM $NaClO_4$/min. From Figure 6-8 (lower right panel) this gradient reduction improved the separation of peptides Ac3 (4.5 min) and N (2.7 min) from Ac10 and Ac17, but these latter two peptides were still coeluted as a single peak. The next step in the optimization was to lower the pH to 3.0, which protonated the glutamic acid residues. As can be seen in the lower left panel, this caused a slight separation between peptides Ac10 and Ac17, a very interesting result given that the environment surrounding the serine residues at positions 10 and 17 is essentially identical.

With the encouraging partial separation of peptides Ac10 and Ac17 shown in Figure 6-8 (lower left), one avenue of potential optimization still available was manipulation of the acetonitrile concentration in the mobile phase. Thus, Figure 6-9 shows the effect of varying the concentration of acetonitrile in the mobile phase from 25% to 70% while keeping constant the other conditions used to produce the elution profile shown in Figure 6-8 (lower left). The optimum resolution of peptides Ac10 and Ac17 occurred in the presence of 40% acetonitrile (Figure 6-9, top right). Under these conditions, peptides Ac10 and Ac17 were resolved approximately two-thirds to baseline. In previous work, higher levels of acetonitrile (as high as 80 - 90%) were found to enhance hydrophilic interactions between the solute and the stationary phase, improving separation even more (Zhu *et al.* 1992a). However, in the present case, the acetylated serine peptides were not soluble in high levels of acetonitrile, leading to peak broadening and a decrease in resolution. Even with the restriction of 70% acetonitrile in the mobile phase in this case, HILIC/CEC has clearly proved to be highly sensitive to very subtle hydrophilicity changes.

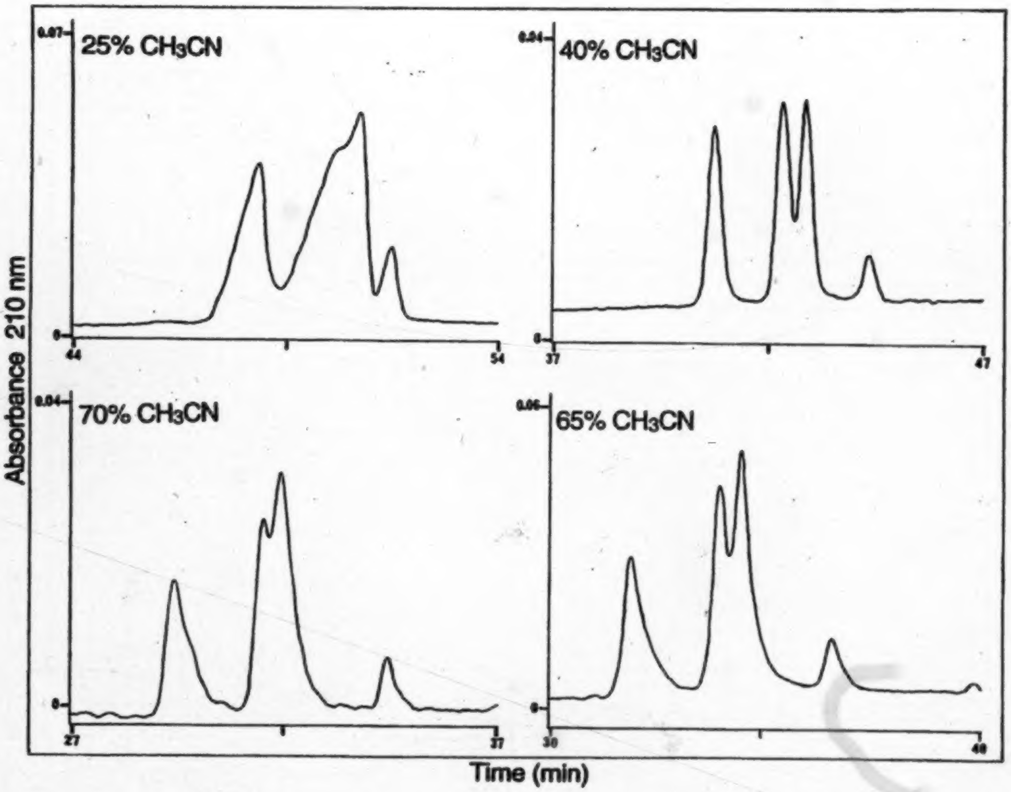

Figure 6-9. The effect of acetonitrile on the separation of the acetylated serine peptides. The relevant 10 min. period of each chromatogram is shown in expanded form to allow direct comparison. Conditions: linear AB gradient (2.5 mM $NaClO_4$/min, following 5-min isocratic elution with 10% B), where eluent A is 10 mM aqueous TEAP, pH 3.0, containing 25% - 70% acetonitrile (v/v), and eluent B is eluent A containing 350 mM $NaClO_4$.

D. Conclusions

The purification of peptide N was challenging because of the presence of impurities which had been O-acetylated at single serine sites on the hydrophilic face of an amphipathic helix, thus ruling out RPC as an effective purification mode. The peptide was successfully purified to homogeneity by a two-step protocol, consisting of HILIC/CEC followed by RPC. HILIC/CEC was able to separate peptides with identical composition and sequence, but side chain modifications in different positions. The synthesis of acetylated peptides Ac3, Ac10, and Ac17 demonstrated the sensitivity of this HPLC mode to subtle changes in hydrophilicity. In addition, a comparison of the elution profiles allowed impurity 3 to be identified as the peptide N analog acetylated at Ser3, and impurity 2 to be identified as peptide N acetylated at Ser10 or Ser17, or a mixture of both compounds. These results provide an explanation for the advantage of HILIC/CEC to RPC in the separation of amphipathic α-helical peptides with modifications on their hydrophilic face. Thus, mixed-mode HILIC/CEC is a valuable complement to RPC for the separation of peptides.

CHAPTER VII

Multiple Distinct Coiled-coils Are Involved in Dynamin Self-assembly

A version of this chapter has been published: Okamoto, P.M., Tripet, B., Litowski, J., Hodges, R.S., and Vallee, R.B. (1999) *J. Biol. Chem.* **274**(15), 10277-10286. Methods which are unique to this chapter are described in section C; the remaining methods are described in more detail in Chapter II.

This work was done in collaboration with Richard B. Vallee of Columbia University. I was responsible for the biophysical characterization of the synthetic peptides. Brian Tripet performed the Stablecoil analysis and peptide synthesis. Patricia Okamoto performed the expression and purification of the dynamin isoforms, the co-immunoprecipitation, yeast interaction trap, sucrose density gradient centrifugation, and endocytosis assays.

A. Summary

Dynamin, a 100-kDa GTPase, has been implicated to be involved in synaptic vesicle recycling, receptor-mediated endocytosis, and other membrane sorting processes. Dynamin self-assembles into helical collars around the necks of coated pits and other membrane invaginations and mediates membrane scission. *In vitro*, dynamin has been reported to exist as dimers, tetramers, ring-shaped oligomers, and helical polymers. In this study we sought to define self-assembly regions in dynamin. Deletion of two closely spaced sequences near the dynamin-1 C-terminus abolished self-association assayed by co-immunoprecipitation and the yeast interaction trap, and reduced the sedimentation coefficient from 7.5 to 4.5 S. Circular dichroism spectroscopy and equilibrium ultracentrifugation of synthetic peptides revealed coiled-coil formation within the C-terminal assembly domain and at a third, centrally located site. Two of the peptides formed tetramers, supporting a role for each in the monomer-tetramer transition and

providing novel insight into the organization of the tetramer. Partial deletions of the C-terminal assembly domain reversed the dominant inhibition of endocytosis by dynamin-1 GTPase mutants. Self-association was also observed between different dynamin isoforms. Taken altogether, our results reveal two distinct coiled-coil-containing assembly domains that can recognize other dynamin isoforms and mediate endocytic inhibition. In addition, our data strongly suggests a parallel model for dynamin subunit self-association.

B. Introduction

Dynamin is a high molecular mass GTPase (Obar *et al.* 1990, Shpetner & Vallee 1992) that has been implicated in various aspects of endocytosis, including synaptic vesicle recycling, the endocytosis of assorted receptors, internalization of caveolae, and more recently budding from the trans-Golgi network (reviewed in Schmid *et al.* 1998, Urrutia *et al.* 1997). Dynamin belongs to a growing family of functionally diverse, large GTPases (Urrutia *et al.* 1997). In mammals, multiple isoforms of dynamin itself have been identified (Cao *et al.* 1998, Urrutia *et al.* 1997), and functional dynamin homologs have been cloned from the lower eukaryotes Drosophila melanogaster (shibire Chen *et al.* 1991, van der Bliek & Meyerowitz 1991) and Caenorhabditis elegans (dyn-1 Takei *et al.* 1995).

Dynamin self-assembly is critical to its function. It has been shown to form helical collars around the necks of coated pits (Takei *et al.* 1995) and is postulated to be involved in the subsequent budding of coated vesicles and other early endocytic intermediates. Structures corresponding to the helical collars can be formed in vitro from purified protein (Hinshaw & Schmid 1995) as well as in combination with acidic substrata including microtubules (Shpetner & Vallee 1989), phospholipid tubules (Sweitzer & Hinshaw 1998), and native synaptosomal membranes (Takei *et al.* 1998). Polymerization is concentration-dependent (Tuma *et al.* 1993, Warnock *et al.* 1996) and inhibited in high ionic strength buffers (Hinshaw & Schmid 1995). Self-assembly does not require guanine nucleotides, although it is either stimulated or inhibited by them depending upon whether the protein is free or membrane-bound (Tuma & Collins 1995, Warnock *et al.* 1995). Once polymerized, dynamin can undergo a nucleotide-dependent conformational change that results in membrane fission in vitro (Sweitzer & Hinshaw 1998). In the depolymerized state, dynamin has been reported to exist as either a dimer (Tuma & Collins 1995) or a tetramer (Liu *et al.* 1996) based on cross-linking studies. Analytical ultracentrifugation has favored tetramer as the predominant species (Muhlberg *et al.* 1997).

The regions of dynamin that are important in self-association and in the interaction with lipids and other proteins have been a topic of considerable interest. Dynamin contains a highly conserved, N-terminal GTPase domain of ~300 aa1 and a centrally located pleckstrin homology (PH) domain that has been reported to bind to phosphatidyinositol 4,5-bisphosphate (Salim *et al.* 1996, Zheng *et al.* 1996) and G-protein βγ-subunits (Touhara *et al.* 1994). Downstream of the PH domain are two predicted regions of coiled-coil α-helix, and at the C terminus is a 100-aa basic, proline-rich region to which Src homology 3 domains (Gout *et al.* 1993, Ringstad *et al.* 1997, Roos & Kelly 1998), acidic phospholipids (Tuma *et al.* 1993), and microtubules

(Herskovits *et al.* 1993b) have been shown to bind. This domain has been implicated in targeting dynamin to coated pits through Src homology 3 domains (Shpetner *et al.* 1996).

Dynamin self-association stimulates its GTPase activity. Ligands that bind to the proline-rich domain stimulate both assembly and GTP hydrolysis, and removal of the domain inhibits both activities (Gout *et al.* 1993, Herskovits *et al.* 1993b, Tuma *et al.* 1993). More recently, proteolytic dynamin fragments missing the proline-rich domain were shown by electron microscopy to be capable of self-assembly when in the presence of GDP and metallofluorides at physiological salt conditions (Carr & Hinshaw 1997) or on lipid bilayer tubes (Sweitzer & Hinshaw 1998).

The role of the putative coiled-coil sequences in dynamin self-association is uncertain. Coiled-coil probability is only ~60% (see "Results"), and whether this region actually forms coiled-coil structure, amphipathic α-helix, or neither is uncertain. This region is conserved among the dynamin isoforms and dynamin-related proteins (Urrutia *et al.* 1997), and computer-based analysis (Newcoils Lupas *et al.* 1991) predicts comparable secondary structure in all of these proteins. The dynamin-related Mx proteins exhibit clear heptad repeats within this region consistent with a leucine zipper structure that, when fused to a reporter gene, was capable of self-association (Melen *et al.* 1992).

A potential role for the putative coiled-coil region of dynamin emerged from our previous analysis of the inhibitory endocytic phenotype in mammalian cells transiently transfected with a dominant negative, C-terminal deletion mutant (Herskovits *et al.* 1993a, Okamoto *et al.* 1997). Inhibition was unaffected by removal of the proline-rich domain but was reversed by further deletion into the putative coiled-coil region, suggesting that this part of the molecule might mediate the interaction of mutant dynamin with the endogenous wild-type protein (Okamoto *et al.* 1997). To gain further insight into the mechanism underlying the inhibitory phenotype and to understand the mechanism of dynamin self-association, we have used a series of deletion mutants to define sites of dynamin self-association and identify two distinct regions. Analysis of peptides reveals that at least three sequences in dynamin-1 are capable of self-association. These results suggest a critical role for the coiled-coil region in dynamin self-assembly.

C. Materials and Methods

cDNA Constructs

The dynamin-1ab isoform (Obar *et al.* 1990) was used for most experiments. C-terminal and internal deletion mutants were made via polymerase chain reaction and subcloned into the mammalian expression vector, pSVL (Amersham Pharmacia Biotech). Polymerase chain reaction was also used to fuse the HA (Field *et al.* 1988) or Myc epitope (Evan *et al.* 1985) to the N-terminus, and all constructs were sequenced to ascertain that the mutations and epitope tags were correct. The dynamin-2bb isoform (Okamoto *et al.* 1997) was also Myc-tagged at the N-terminal end using polymerase chain reaction.

Co-Immunoprecipitation Assay for Dynamin Self-association

For the co-immunoprecipitation assays, COS-7 cells were transiently transfected with both HA- and Myc-tagged dynamin-1 constructs using the LipofectAMINE reagent (Life Technologies, Inc.) as directed by the manufacturer. Cytosolic extracts of the co-expressed proteins were prepared by lysing the transfected cells in RIPA buffer (50 mM

Tris, pH 7.4, 150 mM NaCl, 1% Nonidet P-40, 1 mM phenylmethylsulfonyl fluoride, 1 μg/ml aprotinin, 1 μg/ml leupeptin) and clearing the lysates at 30,000 X *g* and 4°C for 20 min to remove any cellular debris. After preclearing the supernatants with protein A beads (Amersham Pharmacia Biotech) for several hours, fresh protein A beads were added along with either anti-HA monoclonal antibody (Babco, Berkeley, CA) or anti-Myc polyclonal antibody (a gift of Dr. Melissa Gee, University of Mass. Medical School, Worcester, MA). Co-immunoprecipitation assays were carried out overnight at 4°C with end-over-end rotation, after which the beads were washed several times in NET gel buffer (50 mM Tris, pH 7.4, 150 mM NaCl, 1 mM EDTA, 0.25% gelatin, 0.1% Nonidet P-40) and then resuspended in an equal volume of SDS sample buffer for SDS-polyacrylamide gel electrophoresis. Western analysis was done using either the HA monoclonal antibody (Babco) or the Myc monoclonal antibody (9E10, ATCC), and chemiluminescence was used to detect any protein interactions (Kirkgaard and Perry Laboratories).

Yeast Interaction Trap

The LexA-based interaction trap (Gyuris *et al.* 1993) was kindly provided by Dr. Erica Golemis (Fox Chase Cancer Center, Philadelphia, PA) and used to assay for dynamin-dynamin interactions in yeast. Wild-type dynamin-1 was subcloned into the JG202 bait expression vector, which contains a nuclear localization signal. Wild-type and deletion mutants of dynamin were constructed in the JG4-5 prey vector. We tested the suitability of the wild-type dynamin-1 in JG202 as bait and found that it did not activate transcription alone. The lithium acetate method was used to make yeast competent cells and for transformations (Ausubel *et al.* 1994). Dynamin-dynamin interactions were scored positive if transcription of the *lacZ* and *LEU2* reporter genes were activated.

Sucrose Density Gradient Centrifugation

Sucrose density gradients (5-20%) were prepared in 20 mM Tris, pH 7.4, 50 mM KCl buffer. Cytosolic extracts of COS cells transfected with Myc-tagged dynamin constructs were prepared as described above. For each gradient, 500 μg of the extract and 10 μg of each molecular mass marker (Sigma) were loaded. Centrifugation was at 26,500 rpm and 4°C for 17 h. Fractions were collected at 20-s intervals and analyzed by SDS-polyacrylamide gel electrophoresis. Detection of dynamin was by chemiluminescence using a Myc monoclonal antibody. The positions of the molecular mass markers in the gradients were detected by Coomassie stain. Densitometric measurements were made on a Bio-Rad model GS-700 Imaging Densitometer scanner interfaced to the Bio-Rad Multi-analyst computer program (version 1.1). Protein concentrations were determined by the Bradford assay (Bio-Rad), and the S values for the markers are as follows: bovine serum albumin, 4.5 S; alcohol dehydrogenase, 7.5 S; β-amylase, 9 S.

Endocytosis Assays

Transferrin uptake was measured in COS cells as described previously (Herskovits *et al.* 1993a) with the following modifications. After transient transfection of the cells with Myc-tagged dynamin constructs, the cells were grown in serum-free medium for 24 h. Transferrin endocytosis was then stimulated by adding 20 μg/ml of fluorescein isothiocyanate-labeled transferrin (Molecular Probes) for 10 min at 37°C, after which uptake was stopped by placing the cells on ice and washing several times with ice-cold phosphate-buffered saline. Cells were then fixed with 4% paraformaldehyde for 15 min at room temperature and subsequently extracted with either ice-cold methanol for 5 min or 0.5% Triton X-100 for 2 min. Cell staining was done as described previously (Herskovits *et al.* 1993a) and immunofluorescent imaging was with a Zeiss Axiophot microscope.

D. Results

Assays for Dynamin Self-association

As a first step in defining a self-association domain in dynamin-1, we tested for interactions between epitope-tagged dynamin-1 constructs co-expressed in COS cells. Full-length Myc- and HA-tagged wild-type dynamin-1 (C851; Figure 7-1, A and B; see also Figure 7-7) were observed to co-immunoprecipitate using antibody recognizing either epitope. Co-immunoprecipitation was still observed with C-terminal deletions that were lacking all or part of the proline-rich region (C750; Figure 7-1, A and B; see also Figure 7-7) as well as with mutants missing either the GTPase (N272; see Figure 7-7) or the PH domain (PH; Figure 7-1C; see also Figure 7-7). In contrast, co-immunoprecipitation was abolished by a C-terminal deletion which removed the second of the two potential coiled-coil forming segments (C695; Figure 7-1, A and B; see also Figure 7-7). Co-immunoprecipitation was also eliminated by internal deletions that removed the first of the two regions or both together (CC1 or CC12; Figure 7-1C; see also Figure 7-7). These data suggested that the sequence between aa 654 and aa 741 containing the two regions may represent an important self-assembly domain.

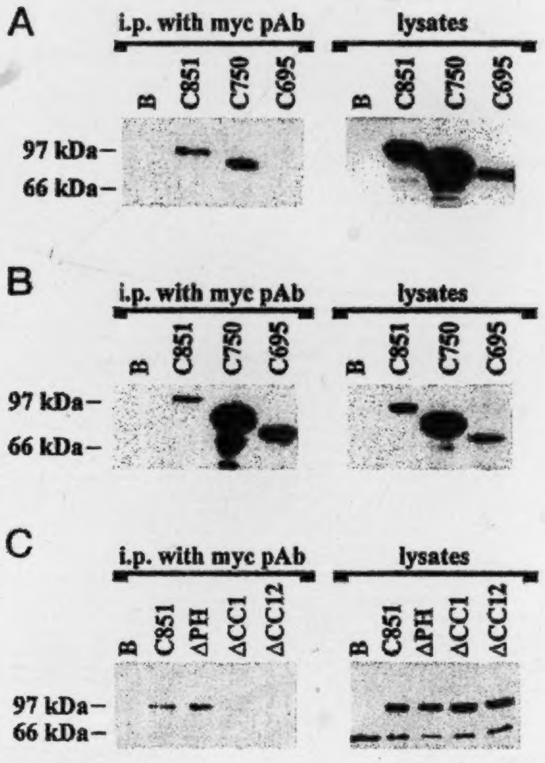
A
i.p. with myc pAb
lysates
B
C851
C750
C695
B
C851
C750
C695
97 kDa–
66 kDa–
B
i.p. with myc pAb
lysates
B
C851
C750
C695
B
C851
C750
C695
97 kDa–
66 kDa–
C
i.p. with myc pAb
lysates
B
C851
ΔPH
ΔCC1
ΔCC12
B
C851
ΔPH
ΔCC1
ΔCC12
97 kDa–
66 kDa–

Figure 7-1. Co-immunoprecipitation of HA- and Myc-tagged dynamin-1 constructs. Co-immunoprecipitations (i.p.) of HA- and Myc-tagged dynamin-1 constructs were performed using a Myc polyclonal antibody. Interactions were detected with either the Myc or HA monoclonal antibodies. The blots in panel A are probed with the HA mAb (lot L), those in panel B are probed with the Myc mAb, and those in panel C are probed with the HA mAb (lot N). The cross-reacting band observed in panel C was lot-specific. In panels A and B, co-immunoprecipitation was assayed between HA- and Myc-tagged C-terminal deletion mutants of similar lengths, whereas in panel C, Myc-tagged dynamin-1 internal deletion mutants were co-immunoprecipitated with full-length HA-tagged dynamin-1. The boundaries for the internal deletion mutants shown in panel C are as follows: ΔPH, aa 514-629; ΔCC1, aa 654-681; ΔCC12, aa 654-741. *C851*, full-length dynamin-1; B, beads alone, control.

As an alternative approach to defining interaction sites, we also used a yeast two-hybrid system. Interactions were assayed between a wild-type dynamin-1 bait and a panel of dynamin-1 deletion mutant prey constructs. In agreement with the co-immunoprecipitation results, dynamin-1 preys that were missing part of the proline-rich region still interacted with the wild-type dynamin-1 bait (C761; Figure 7-2; see also Figure 7-7), although deletion of the entire proline-rich region resulted in little, if any, interaction (C750; Figure 7-2; see also Figure 7-7). We also detected a reduction in interaction intensity with a C-terminal deletion mutant (C733; Figure 7-2; see also Figure 7-7) that had previously been shown to reverse the dominant negative endocytic effect of K44E (Herskovits *et al.* 1993a). As had been observed in the co-immunoprecipitation experiments, interactions persisted in prey devoid of either the GTP-binding domain (N272; Figure 7-2; see also Figure 7-7) or the PH domain (PH; Figure 7-2; see also Figure 7-7). C-terminal deletions missing some or all of the potential coiled-coil forming sequences resulted in no interaction with the full-length bait (C695, C648, and C514; Figure 7-2; see also Figure 7-7) as did partial or complete removal of the coiled-coil region between aa 654-741 (CC1, CC2, and CC12; Figure 7-2; see also Figure 7-7), consistent with our co-immunoprecipitation data.

These data were consistent with our hypothesis that dominant inhibitory dynamin polypeptides act through interaction with endogenous wild-type dynamin protein (Herskovits *et al.* 1993a). To test this possibility directly, we assayed for transferrin uptake in cells overexpressing dominant negative dynamin-1 K44E mutants that also had deletions in the self-assembly region. Figure 7-3 shows that removal of either of the two self-association sequences identified in our co-immunoprecipitation and yeast interaction

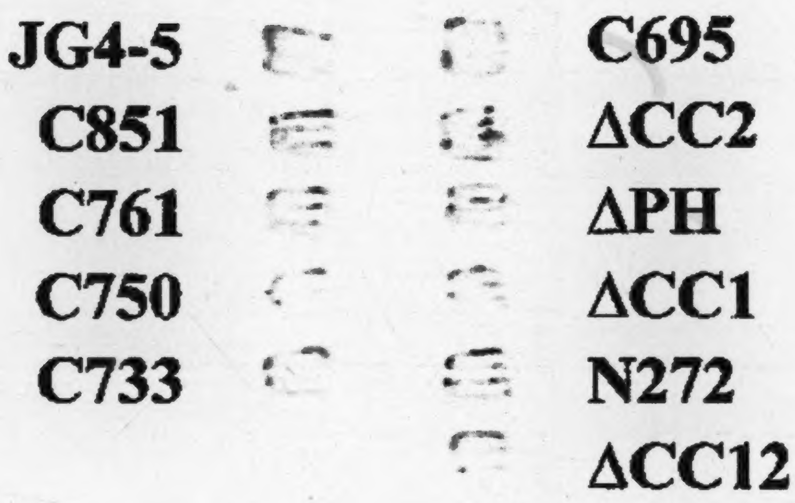

Figure 7-2. Assay for dynamin-dynamin interaction using the yeast interaction trap. Dynamin-dynamin interactions were assayed in the yeast strain EGY48 using a full-length dynamin-1 bait and dynamin-1 deletion mutant preys. Interactions were assayed on galactose plates lacking uracil, histidine, and tryptophan in the presence of 5-bromo-4-chloro-3-indolyl β-D-galactopyranoside. Blue colonies are positive; non-blue colonies are negative. The nomenclature of the various mutants are the same as in Figure 7-1. *JG4-5* refers to the prey vector alone.

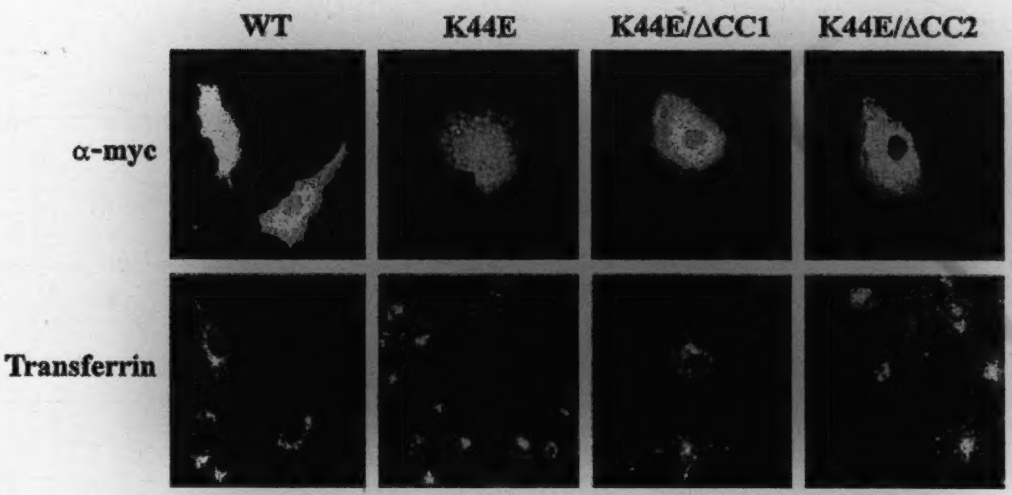

Figure 7-3. Reversal of endocytic inhibition by deletion of assembly sequences. Fluorescein isothiocyanate-transferrin internalization was measured in COS-7 cells transiently transfected with wild-type dynamin-1 (*WT*), a dominant inhibitory mutant form of dynamin-1 (*K44E*), or internal deletions of either of the latter construct (*K44E/ΔCC1* or *K44E/ΔCC2*). All constructs were Myc-tagged, and their expression was detected by the Myc monoclonal antibody 9E10. Transferrin internalization is inhibited in the cell overexpressing the K44E mutant construct but is restored in cells expressing the doubly mutant constructs.

trap assays resulted in reversal of the dominant negative endocytic phenotype, i.e. the resumption of transferrin uptake. Because dynamin-1-K44E exhibits its inhibitory effects in cells containing primarily the dynamin-2 and dynamin-3 isoforms (Herskovits *et al.* 1993a), we also tested for an interaction between isoforms. Interaction between dynamin-1 and dynamin-2 could be readily detected both by the yeast two-hybrid assay (Figure 7-4A) and by co-immunoprecipitation (Figure 7-4B).

To learn more about the identity of the dynamin self-association products, lysates of COS-7 cells expressing either epitope-tagged wild-type or mutant dynamin-1 were analyzed by sucrose density gradient centrifugation. We established that the COS-expressed Myc-tagged dynamin-1 isoform behaved similarly to rat brain dynamin-1 in the sucrose density gradients (data not shown). Both ran as a 7.5 S peak, indicating that they were not in a highly assembled state under these conditions. The S value was unaffected by the removal of either the proline-rich (Figure 7-5A; see also Figure 7-7) or PH domains (Figure 7-5B; see also Figure 7-7). However, deletions involving the self-assembly region identified by our co-immunoprecipitation and yeast interaction trap experiments resulted in a shift of the 7.5 S peak to 4.5 S (C695; Figure 7-5A; see also Figure 7-7; and CC12; Figure 7-5B; see also Figure 7-7), consistent with dissociation to a smaller species. No such shift was produced by deletion to aa 733 (C733; Figures 7-6 and 7-7), which reverses the dominant inhibitory endocytic effect (Okamoto *et al.* 1997), despite removal of several amino acids from the C-terminus of the self-assembly domain. However, partial dissociation was observed in a different gradient buffer (20 mM Hepes, pH 7, 50 mM KCl; Figures 7-6 and 7-7). These results indicated a decrease in the

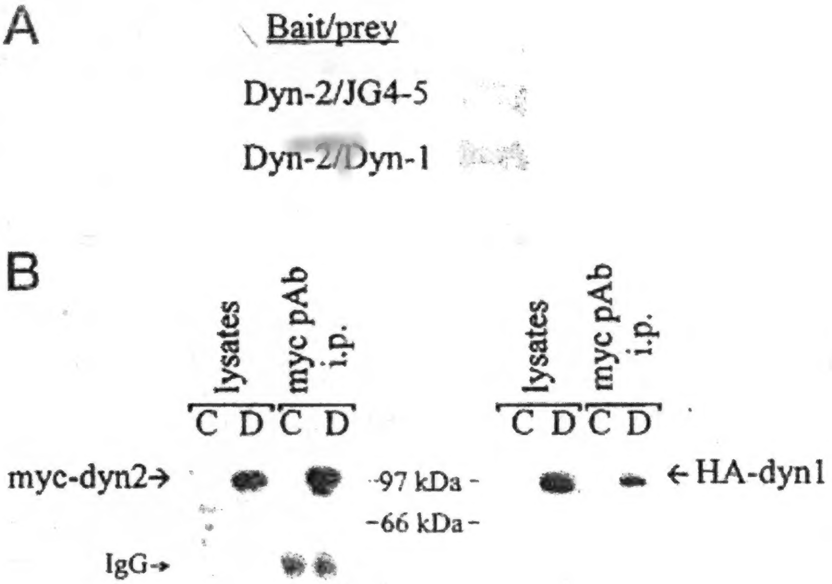
A
Bait/prey
Dyn-2/JG4-5
Dyn-2/Dyn-1
B
lysates
myc pAb i.p.
C D C D
lysates
myc pAb i.p.
C D C D
myc-dyn2→
97 kDa
66 kDa
← HA-dyn1
IgG→

Figure 7-4. Heterotypic interaction between the dynamin-1 and dynamin-2 isoforms. **A)** dynamin-2 (*Dyn-2*) bait was tested for an interaction with the dynamin-1 (*Dyn-1*) prey or with the JG4-5 vector as a control. Selection was on galactose lacking uracil, histidine, and tryptophan in the presence of 5-bromo-4-chloro-3-indolyl β-D-galactopyranoside medium. **B)** co-immunoprecipitation of dynamin isoforms. Myc-dynamin-2 and HA-dynamin-1 were co-expressed in COS-7 cells and immunoprecipitated using the Myc polyclonal antibody. **C)** beads alone, control. **D)** anti-Myc immunoprecipitants blotted with Myc (*left*) polyclonal or HA (*right*) monoclonal antibody. The arrow points to the dynamin isoform in each blot. IgG, cross-reacting antibody heavy chain.

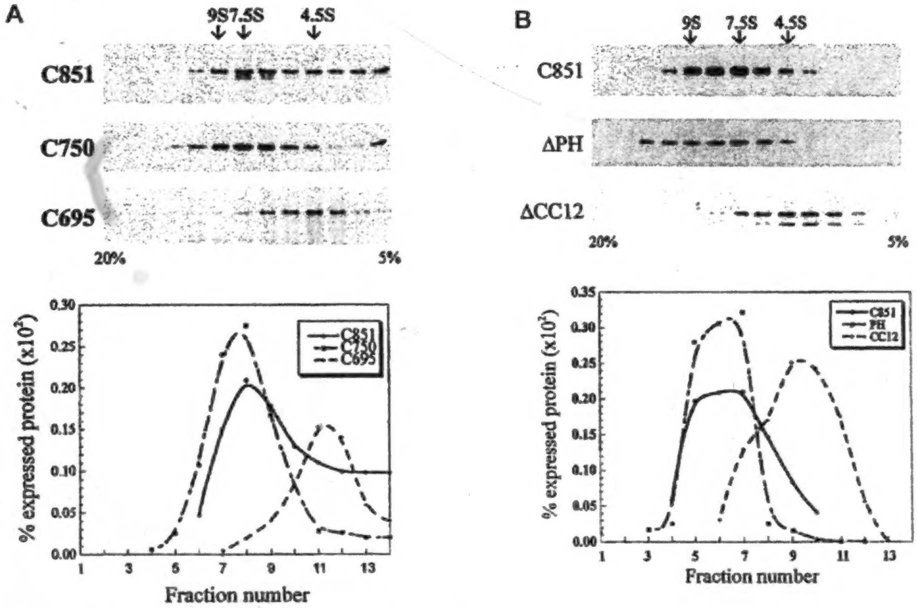

Figure 7-5. Sucrose density gradient centrifugation of various dynamin-1 C-terminal deletion mutants. COS-7-expressed Myc tagged dynamin-1 constructs were analyzed in 5-20% sucrose density gradients and immunoblotted using anti-Myc antibody. The blots were quantified by densitometry. The densitometric scans were normalized for expressed protein concentration for each construct. S values for markers used are shown at the top. **A)** data for full-length dynamin-1 (*C851*) and C-terminal deletions *C750* and *C695*. **B)** data for full-length dynamin-1 (*C851*) and the internal deletions ΔPH and ΔCC12.

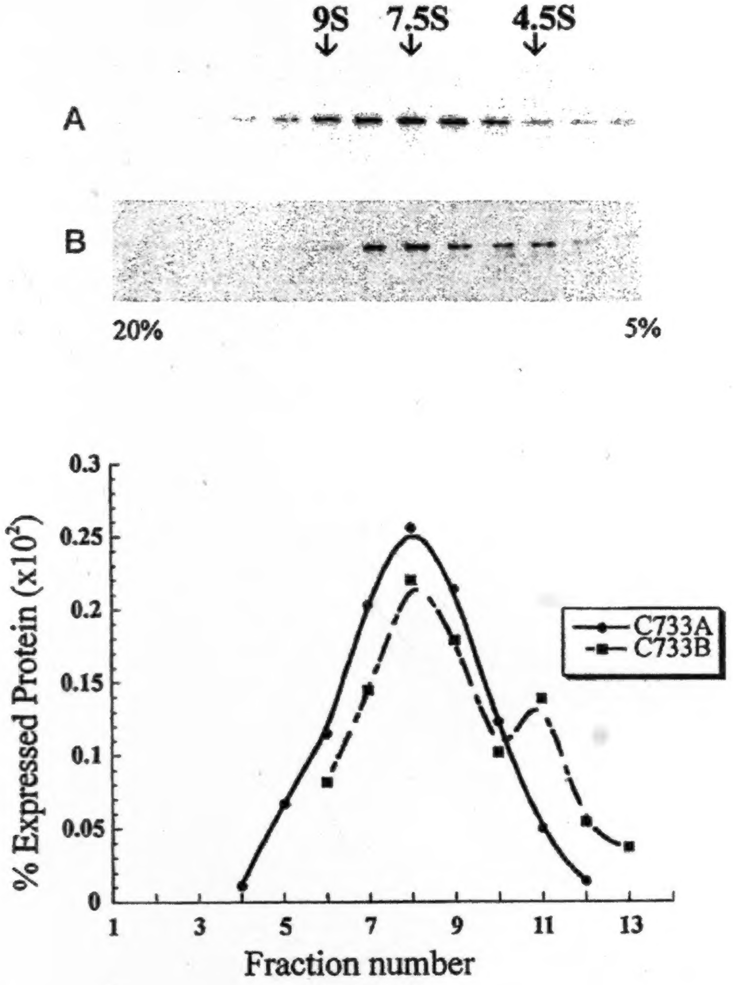

Figure 7-6. Buffer-dependent dissociation of C733. The C-terminal dynamin-1 truncation construct C733 was analyzed in 5-20% sucrose density gradients containing either the standard gradient buffer (20 mM Tris, pH 7.4, 50 mM KCl) **(A)** or 20 mM Hepes, pH 7, 50 mM KCl **(B)**. Other conditions are as described in the legend to Figure 7-5.

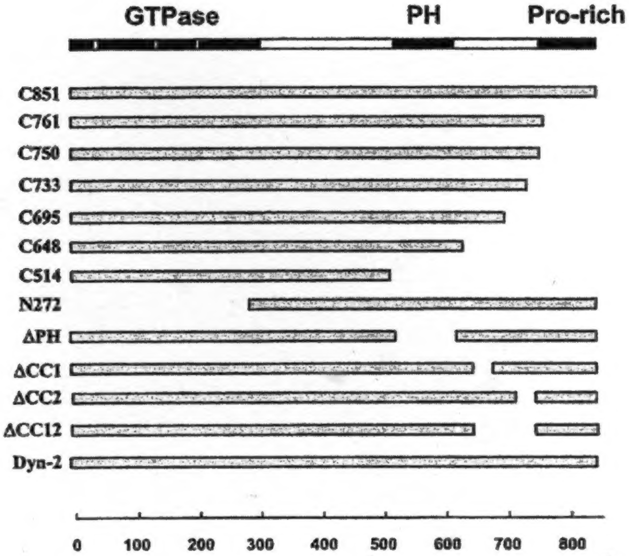
GTPase
PH
Pro-rich
C851
C761
C750
C733
C695
C648
C514
N272
ΔPH
ΔCC1
ΔCC2
ΔCC12
Dyn-2
0
100
200
300
400
500
600
700
800

	Co-IP	2-Hybrid	S-value
C851	++	++	7.5S
C761	++	++	
C750	++	+/-	7.5S
C733		+/-	7.5S, 4.5S
C695	-	-	4.5S
C648		-	
C514		-	
N272	++	+	
ΔPH	++	++	7.5S
ΔCC1	-	-	4.5S
ΔCC2		-	
ΔCC12	-	-	4.5S
Dyn-2	++	++	7.5S

Figure 7-7. Summary of the mapping results. Schematic representation summarizing the cDNA constructs used to map the C-terminal self-assembly region by co-immunoprecipitation (*Co-IP*), yeast two-hybrid (*2-Hybrid*), and sucrose density gradients (*S-value*). ++, very good interaction; +, good interaction; +/-, detectable interaction; -, no interaction; *Pro-rich*, proline-rich domain.

affinity between polypeptides, although the ability to self-associate was not abolished completely.

Peptide Analysis

The domain implicated in dynamin-1 self-assembly contains two short, closely spaced sequences (aa 654-681 and aa 712-740) predicted by the Newcoils program (Lupas *et al.* 1991) to have a propensity for coiled-coil formation based on analysis of a data base of known coiled-coil sequences (Figure 7-8A). However, the probability is only ~60%, with no more than four heptad repeats predicted for each region. Newcoils also predicts at even lower probability three short sequences downstream of the GTPase domain between aa 295-470 (Figure 7-8A). Paircoils, which is based on pairwise residue correlations (Berger *et al.* 1995) yielded a very different set of predictions, including a short sequence in near the center of the dynamin-1 polypeptide (Figure 7-8B). Because of the disparity in the two predictive approaches, we also examined dynamin-1 using a recently developed nonstatistically based algorithm termed Stablecoils, which is based on the direct analysis of coiled-coil formation by synthetic peptides of systematically varied composition (Tripet *et al.* 1997). The aa 651-675 region was judged to be the most hydrophobic with the highest propensity for amphipathic helix formation (Figure 7-8C). A lower, but significant, propensity for coiled-coil formation was observed for aa 715-738, and additional sequences were identified in the central portion of the polypeptide that differed from those identified by Newcoils and Paircoils (Figure 7-8).

To determine which of these short sequences in fact had properties consistent with coiled-coil formation, we analyzed synthetic peptides corresponding to five distinct regions by circular dichroism and equilibrium ultracentrifugation (Table 7-1). The CD

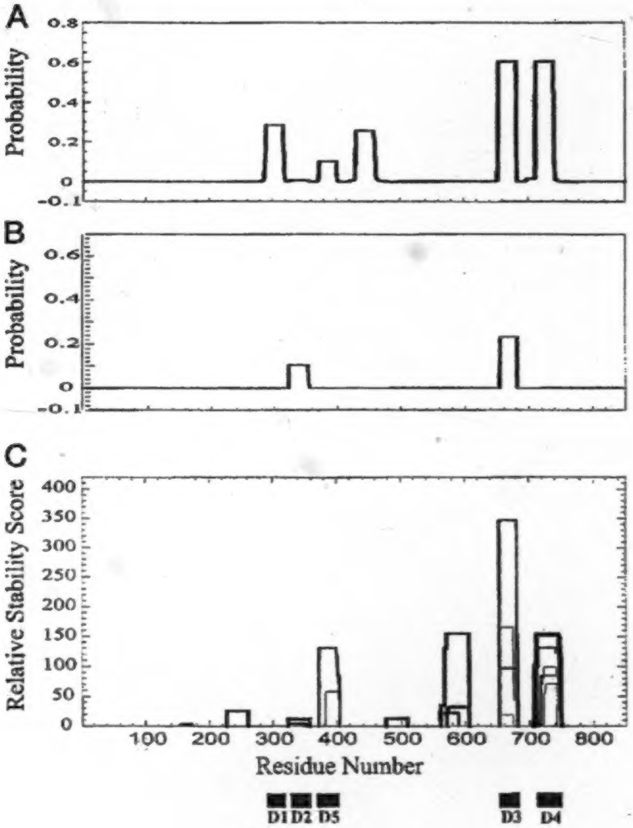

Figure 7-8. Secondary structure analysis. Newcoils (**A**), Paircoils (**B**), and Stablecoils (**C**) plots of dynamin-1 are shown, along with sequences selected for the design of synthetic peptides (*bottom*).

Table 7-1. Amino acid sequences of the synthetic peptides used in this study

Peptide[a]	Sequence[b]
	a d a d a d a d a
D1(295-318)	Ac-CGGGLRNKLQSQLLSIEKEVDEYKNFR-NH_2
D2(323-352)	Ac-CGGARKTKALLQMVQQFAVDFEKRIEGSGDQID-NH_2
D3(652-681)	Ac-CGGDPQLERQVETIRNLVDSYMAIVNKTVRDLM-NH_2
D4(712-740)	Ac-CGGNTLMEESAEQAQRRDEMLRMYHALKEALS-NH_2
D5(372-404)	Ac-CGGRFPFELVKMEFDEKELRREISYAIKNIHGIRTGLFT-NH_2

[a] Peptide sequence name followed by residues (indicated in parentheses) substituted from that of native rat dynamin-1.

[b] Amino acid sequence of the peptides. Residues proposed to form the 3-4 hydrophobic repeat (positions **a** and **d** of the heptad repeat "**abcdefg**" characteristic of coiled-coils) are underlined. "Ac" denotes N^{α}-acetyl, and "NH_2" denotes C^{α}-amide. A Cys-Gly-Gly linker has been added to the native sequences.

spectrum of the D1 peptide, which was derived near the GTPase domain of the dynamin-1 polypeptide, was predominantly random coil. We note, however, that in 50% TFE, a helix-inducing hydrophobic solvent, it could be forced into an α-helical conformation, indicating that this region of dynamin has the intrinsic ability to adopt a helical secondary structure (data not shown). Similarly, the centrally derived D5 peptide exhibited a mixture of random coil and β-sheet, but not α-helical, structure in benign solution (Figure 7-9A). In contrast, peptides D2, D3, and D4 exhibited α-helical CD spectra, with the characteristic minima at 208 and 222 nm (Figure 7-9B). An increase in α-helicity (10-20%) was observed for the D2 and D4 peptides at higher concentrations, whereas limited solubility of D3 precluded comparable analysis. CD spectra for a mixture of D2 and D4 were additive (data not shown). Curiously, D3/D4 or D2/D3 mixtures were less than additive (data not shown). This may be due to nonspecific interactions by D3, which also caused a similar, but smaller, decrease in the mean residue molar ellipticity at 222 nm when mixed with a known coiled-coil forming peptide from an unrelated protein, MMKif (Tripet *et al.* 1997 and data not shown). Peptides D2, D3, and D4 all exhibited low stability and were completely unfolded at low concentrations of guanidine HCl (0.75 M; Figure 7-10). Table 7-2 summarizes the CD data.

Equilibrium ultracentrifugation of peptides D2, D3, and D4 revealed that each is capable of oligomerization. The sedimentation data for D2 and D4 each fit to a homogenous species with mass average molecular masses of 14,051 and 15,210 Da, respectively, in both cases consistent with the formation of a tetramer (Figure 7-11, A and B). D3 was observed to have a mass average molecular mass of 23,873 Da, which

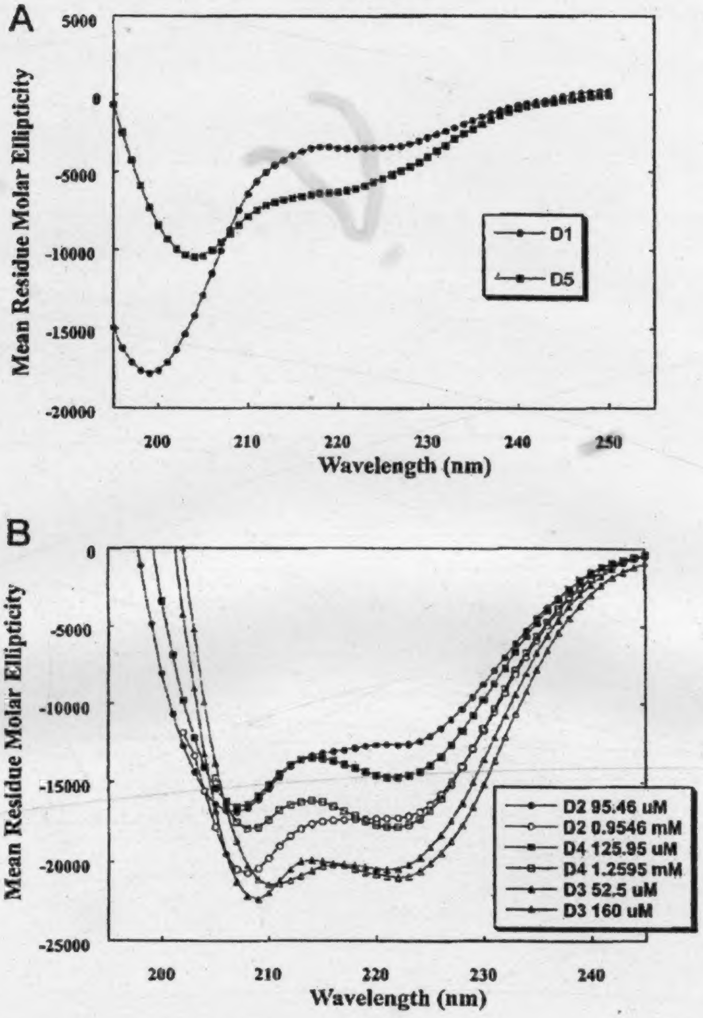

Figure 7-9. CD spectra of peptides D1-D5. Dynamin-1 peptides D1 and D5 (100 μM), which correspond to aa 295-318 and aa 372-404, respectively (**A**), and peptides D2, D3, and D4, which correspond to aa 323-352, aa 652-681, and aa 712-740, respectively (**B**), were analyzed at 20°C in benign buffer (0.1 M KCl, 0.05 M potassium phosphate, 2 mM dithiothreitol, pH 7). Petides D2, D3, and D4 showed characteristic α-helical spectra.

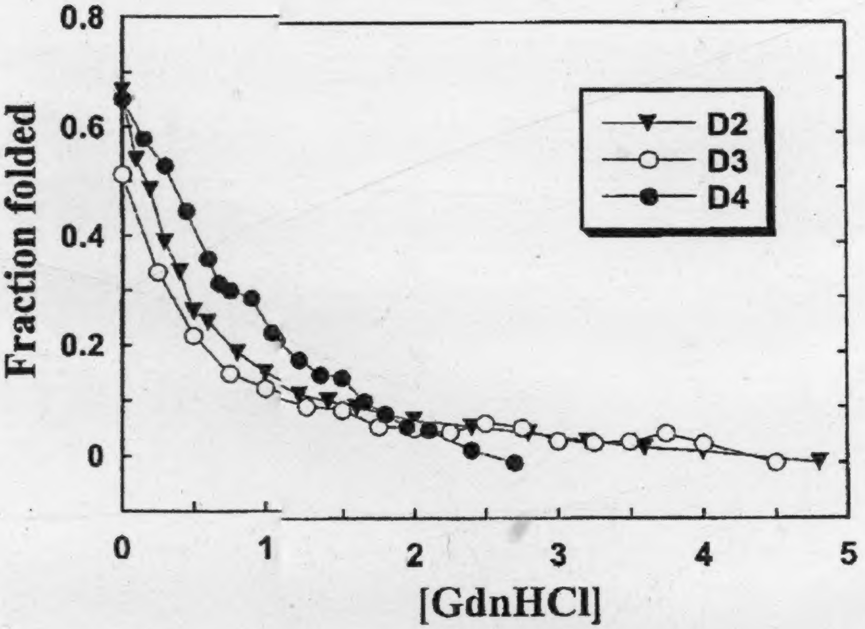

Figure 7-10. Denaturation of dynamin-1 peptides D2, D3, and D4. CD spectra of the three helical dynamin peptides D2, D3, and D4 in benign buffer at increasing molar concentrations of guanidine HCl. Peptide concentrations were 0.32, 0.07, and 0.47 mg/ml for D2, D3, and D4, respectively. The fraction folded of each peptide was calculated as $f = ([\theta]_{obs} - [\theta]_u)/([\theta]_f - [\theta]_u)$ where f is the fraction folded, $[\theta]_{obs}$ is molar ellipticity observed for a given [GdnHCl], $[\theta]_u$ is the molar ellipticity of the unfolded state, and $[\theta]_f$ is the molar ellipticity of the folded state.

Table 7-2. Ellipticities and stabilities of the synthetic peptides

Peptide	No. of residues/ peptide chain[a]	$[\theta]_{222}$[b]		$[\theta]_{222}$ at 1 mM	Helical content[c]	
		benign	50%TFE		%	residues
		degrees·cm^2·dmol^{-1}				
D2	30	-11,400	-19,400	-17,240	34(51)[d]	10(15)[d]
D3	30	-20,440	-29,250		60	18
D4	29	-15,130	-25,730	-17,810	45(53)	13(15)

[a] Not including the Cys-Gly-Gly linker.

[b] The mean residue molar ellipticities at 222 nm were measured at 20°C in benign buffer (0.1 M KCl, 0.05 M PO_4, pH 7, 2 mM DTT). For samples containing TFE, the above buffer was diluted 1:1 (v/v) with TFE. The peptide concentrations were 95.46, 52.5, and 125.95 μM for D2, D3, and D4, respectively.

[c] The percentage of helical content was calcalated from the ratio of the observed $[\theta]_{222}$ value divided by the predicted molar ellipticity x 100. The predicted molar ellipticity was calculated from the equation $[\theta]_{222} = 40 \times 10^3 \times (1-4.6/n)$ for the chain length dependence of an α-helix (Chang *et al.* 1978, Gans *et al.* 1991), where n is the number of residues in the peptide. The number of helical residues was calculated by multiplying the percentage of helical content x the total number of residues in the peptide.

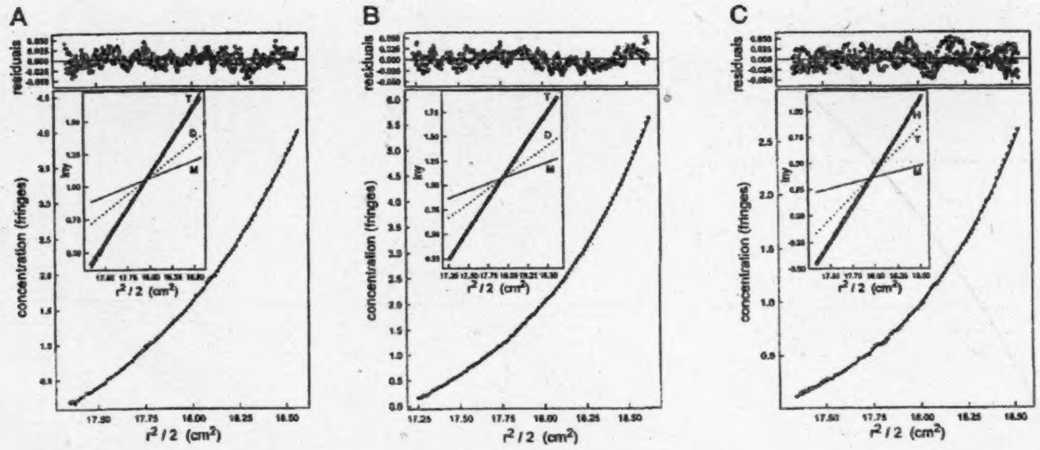

Figure 7-11. Equilibrium ultracentrifugation of helical peptides. **A)** peptide D2. **B)** peptide D4. **C)** peptide D3. Peptide concentration gradients are shown and fit to a tetramer (**A** and **B**), and hexamer for **C**. Residuals (*top*) show deviation of measured points from fit line. Insets, peptide concentration gradients compared with theoretical lines for monomer (M), dimer (D), tetramer (T), or hexamer (H). Sedimentation runs were at 25,000, 22,000, and 25,000 rpm, for D2, D3, and D4, respectively. *r2/2*, radial distance; *ln(y)*, natural log of fringe displacement (concentration).

approaches a hexameric species (Figure 7-11C). This suggests that D3 may not have a strictly defined oligomeric state but does have the ability to form helical bundles.

E. Discussion

Our results implicate two portions of dynamin in self-association, a complex region located between the PH and proline-rich domains and a region near the center of the polypeptide (Figure 7-12A). We will refer to these regions as the C-terminal and central self-assembly domain, respectively. Our peptide analysis further identified coiled-coil forming sequences within both regions (Figure 7-12A) and implicates coiled-coils as a primary mode of dynamin-dynamin interaction. Our results confirm our hypothesis that the C-terminal region mediates the interaction between dominant inhibitory dynamin mutants and endogenous wild-type protein. Furthermore, the identification of two distinct coiled-coil domains has important implications for dynamin structural organization, as discussed below.

Nature of Self-assembly Species

A significant issue in this study is the stage in self-assembly in which these regions participate. Dynamin has been reported to exist in the unassembled state primarily as a tetramer (Tuma & Collins 1995, Warnock *et al.* 1996), although whether this species represents a stable, minimal assembly unit is unclear. Dynamin and the Mx proteins also assemble to partial rings, complete rings, and helical stacks of rings. Our analysis has dealt primarily, if not exclusively, with dynamin in the disassembled state. Our immunoprecipitation studies were performed at a sufficiently high ionic strength range to prevent assembly (Warnock *et al.* 1996). The sucrose gradient analysis,

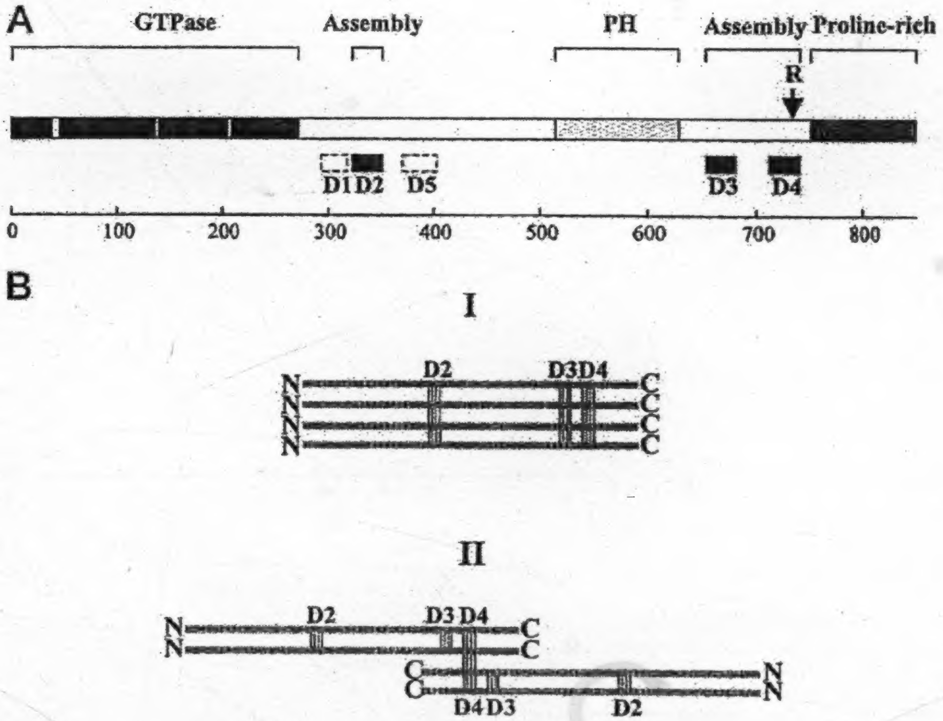
A
GTPase
Assembly
PH
Assembly
Proline-rich
R
D1
D2
D5
D3
D4
0
100
200
300
400
500
600
700
800
B
I
N
D2
D3
D4
C
II
D2
D3 D4
C
N
D4 D3
D2

Figure 7-12. Models for the structural organization of dynamin tetramers. **A)** summary of peptide analysis. Dark bars, location of peptides that were α-helical by CD analysis; dotted bars, location of peptides that were random coil or a mixture of random coil and β-sheet by CD; Assembly, self-assembly regions identified in this paper; R, shortest C-terminal deletion (aa 733) at which receptor-mediated endocytosis is observed in a dominant negative dynamin-1 mutant (Okamoto *et al.* 1997). **B)** dynamin-1 polypeptides are shown either in a parallel (model I) or anti-parallel (model II) orientation with coiled-coil sequences corresponding to peptides D2, D3, and D4 linking the individual polypeptides together.

although performed at lower ionic strength, revealed directly that the protein was in the disassembled state. The S value of 7.5 is consistent with a tetramer, albeit a highly asymmetric structure. This species is clearly oligomeric in view of the sharp decrease in S value caused by small changes in C-terminal sequence. The state of self-association of dynamin-1 expressed in yeast is uncertain. The N-terminal fusion sequences could inhibit assembly, although N-terminal GFP-dynamin appears to function normally in cells (Cao *et al.* 1998 and R. J. Vasquez and R. B. Vallee, unpublished observations). Because our mapping studies are so closely consistent with the results of our co-immunoprecipitation and centrifugation analysis, it is likely that the two-hybrid analysis primarily reflects monomer-dimer or monomer-tetramer formation, with one intriguing exception.

Previous studies of dynamin pointed to a role for the proline-rich domain in dynamin self-assembly (Hinshaw & Schmid 1995, Tuma & Collins 1995, Warnock *et al.* 1996). However, in these cases effects on polymer formation were assayed. Our data indicate that the proline-rich region is not required for self-association to the dimer or tetramer level; hence, it must be required for higher order assembly steps. We did observe diminution in the intensity of the yeast two-hybrid reaction using the C750 construct in the prey vector (Figure 7-2), although the extent of co-immunoprecipitation was not affected by a comparable deletion, nor was the mutant protein observed to dissociate to the 4.5 S species by sucrose density gradient centrifugation. How the yeast result is to be interpreted is unclear. It may indicate greater sensitivity in detecting changes in affinity between dynamin subunits, or it may indicate that some extent of co-polymerization of bait and prey dynamin does actually occur in this system. We do note that although we tested for interactions between identical truncation mutant constructs in our other assays, full-length bait was used in the two-hybrid analysis. Thus, it is also possible that interaction between wild-type and the C750 mutant dynamin could be sterically affected by the proline-rich region.

The GTPase and PH domains were not required for dynamin self-association in our assays. The former result contrasts with those for the antiviral Mx proteins. Among the dynamin-related family members, the structure of these proteins has been the most extensively characterized. Three self-assembly regions have been mapped within the Mx1 protein. The monomer-to-polymer transition was assayed by gel filtration chromatography of full-length and truncation mutant Mx constructs. This analysis identified one self-assembly site within the GTPase domain (Nakayama *et al.* 1993) and a second near the C-terminus (Melen *et al.* 1992). No role was detected for a putative leucine zipper domain further downstream at the extreme C-terminus. In contrast, the latter region was implicated in dimerization in a separate study in which it was fused to a reporter enzyme. The basis for the difference in these results is unclear. The latter results, however, seem to be more nearly consistent with our findings for dynamin. Although we find no obvious sequence homology between the leucine zipper region of Mx and the C-terminal assembly domain of dynamin, their secondary structures seem to be related. Thus, it is likely that C-terminal coiled-coils may play a common role throughout the greater dynamin protein family, a conclusion supported by secondary structure predictions for other family members (Yoon *et al.* 1998).

Role of Coiled-coils

Secondary structure predictions for dynamin-1 by the Newcoils, Stablecoils, or Paircoils algorithms suggested several possible coiled-coil regions in dynamin-1, although the predictions differed substantially. We tested the ability of five of these regions to form interacting α–helical structure using synthetic peptides. Intriguingly, the predictive success of each algorithm was variable. It is not yet clear whether this outcome reflects the choice of peptide boundaries or features of the predictive schemes. Three of the five peptides exhibited clear evidence for α-helix formation by CD spectroscopy: D3 and D4 within the C-terminal self-assembly domain, identified in our analysis of recombinant dynamin polypeptides, and D2, derived from the center of the polypeptide. D3 was predicted to have a 60% probability of coiled-coil formation by Newcoils, only 11% probability by Paircoils, and the strongest propensity for coiled-coil formation using Stablecoils. D4 also exhibited 60% probability using Newcoils and approximately half the propensity of D3 using Stablecoils. Results were most surprising for the other peptides. D2 showed insignificant probability using Newcoils, only slightly positive probability using Stablecoils, and 11% using Paircoils. We considered D1 worth examining because, despite moderate predictive scores from Newcoils and Stablecoils, the homologous region within dynamin-2 exhibited 95% probability using Newcoils. Nonetheless, the D1 peptide was observed as a random coil by CD. It is possible that the coiled-coil forming sequence within the complete dynamin-1 polypeptide is more extensive, encompassing the D1 region and other regions as well.

In the case of the C-terminal assembly domain our data support the existence of two short stretches of α-helix (D3 and D4) separated by a 31-aa intervening sequence of undetermined structure (pI = ~5.3). Whether this region also participates in coil formation is uncertain; however, the D3 coil cannot be much longer than predicted because proline residues flank the sequence on either side. Although the sequence of this C-terminal assembly domain is conserved among the dynamin isoforms (79%), only the D3 region is consistently predicted by the Newcoils program to form a potential coiled-coil, albeit with varying probability (42-60% between rat dynamin isoforms). It is of interest that the D4 region has very low coiled-coil probability in dynamin-2. Inspection of the latter sequence suggests that a single amino acid gap accounts for this difference. That dynamin-2 co-immunoprecipitated with dynamin-1 is significant; this result implies that isoforms are interchangeable in the cell. It helps to explain the dominant inhibition of endocytosis by heterologous isoforms. In addition, it raises questions about models that implicate dynamin isoforms in distinct cellular functions (Cao *et al.* 1998). Conceivably, targeting signals exist that override the tendency toward miscibility and segregate isoforms to different membranous compartments. However, dynamins appear to be predominantly cytoplasmic (Shpetner *et al.* 1996), where our results suggest they would be free to intermix. Finally, deletion of either of these regions in the dynamin-1-K44E mutant reversed the dominant negative endocytic effect and resulted in transferrin uptake, indicating that these regions are indeed functionally important.

CD spectra of mixtures revealed no obvious evidence for heterodimerization. However, despite their relatively short lengths, peptides D2, D3, and D4 all clearly self-associated. D2 and D4 were observed to be tetrameric, with no evidence for higher order aggregates. That self-association involved coiled-coil formation is supported by the increase in α-helical content with concentration for at least two of the three peptides. D3 associated to a somewhat nonhomogeneous mixture that was predominantly hexameric, with evidence of dissociation to smaller species in the lower concentration range. Because this peptide exhibited other evidence of nonspecific binding, caution must be exercised in interpreting its self-association behavior. It is possible that in the context of the entire protein, the D3 region is constrained to a four-stranded coiled-coil like the other regions. The self-association behaviors of D2 and D4 are particularly interesting in light of evidence that dynamin may exist in the depolymerized state as a tetramer. Our results not only add strong support to the latter claim but also suggest that the coiled-coil regions are sufficient for dynamin tetramerization.

Structural and Physiological Role of Assembly Domains

How the dynamin self-assembly regions are distributed within the folded tetramer is unknown. Two general models may be envisioned depending on whether the α-helices are arrayed in parallel or anti-parallel. In the first case, we imagine that each of the three coiled segments, corresponding to D2, D3, and D4, participates in the formation of a tetrameric backbone with uniformly oriented polypeptides. Such an arrangement is clearly feasible (Figure 7-12B, model I) and has a number of interesting structural consequences. For one, the tetramer would have structural polarity, a property required for the formation of a polymer with distinct membranous and cytoplasmic surfaces as may be expected for dynamin (Shpetner & Vallee 1989, Sweitzer & Hinshaw 1998). In addition, it may be argued based on symmetry considerations that the coiled-coil regions must be co-linear. Thus, we would predict that the dynamin tetramer is organized about a central coiled-coil shaft. It is also possible that the central and C-terminal self-assembly regions function at different levels of dynamin self-association, although the fact that both D2 and D4 form tetramers makes such models seem less likely. Our existing evidence indicates that the C-terminal region is important in the monomer-dimer or monomer-tetramer transition; conceivably, the central assembly domain might be involved in polymer formation. Although this is an attractive possibility, it would lead to network formation among dynamin polypeptides, inconsistent with the known features of the dynamin self-assembly pathway. Similar problems arise for models in which the peptides are proposed to interact in anti-parallel (Figure 7-12B, model II). In particular, it is difficult to see how interaction of both assembly domains could occur between polypeptides in an antiparallel manner. Thus, we strongly favor the parallel model.

It is of interest that the C-terminal self-assembly domain appears to lie within the boundaries of a previously identified 13-kDa proteolytic fragment of dynamin-1 implicated in GTPase regulation. This fragment, termed the GED (GTPase effector domain) was found to bind to the GTPase domain and stimulate its activity (Muhlberg *et al.* 1997). Whether the coiled-coil sequences we have identified within this fragment or additional sequences within this region are involved in GTPase effector activity is uncertain, and how self-association influences this interaction remain to be seen. However, it now seems clear that the coiled-coil segments of dynamin represent a new, functionally important element. Further analysis of these regions should be of considerable value in understanding how assembly of this remarkable protein is controlled.

CHAPTER VIII

Biophysical characterization of the dynein heavy chain stalk domain

This work was done in collaboration with Richard B. Vallee of Columbia University. His laboratory cloned, expressed and purified the recombinant dynein constructs, as described in section C, Methods and Materials. I was responsible for the sequence analysis and biophysical characterization.

A. Summary

The dynein heavy chain binds to microtubules through an elongated stalk, thought to be an antiparallel coiled-coil, that protrudes from the globular motor domain. We have performed a biophysical characterization of the dynein stalk domain in order to test this model. Circular dichroism spectroscopy showed that the stalk was highly α-helical and unfolded cooperatively, with a midpoint of 48°C. Both the coiled-coil domain and the microtubule-binding region were significantly destabilized when expressed individually, suggesting that the entire stalk domain is required to fold as a cooperative unit. Analytical ultracentrifugation experiments showed that the stalk domain was monomeric in solution and had an elongated shape. These results provide the first experimental confirmation that the dynein stalk is an intramolecular, antiparallel coiled-coil.

B. Introduction

The dynein heavy chain (HC) has an unusual structural organization, with the microtubule-binding region located at the tip of a stalk that protrudes from the globular motor domain, as described in Chapter I. This region is flanked by long regions of approximately 100 residues which are predicted to form coiled-coils. This led to a model proposing that the stalk is actually an intramolecular antiparallel coiled-coil with the microtubule-binding region located at its tip (Gee *et al.* 1997). This model has been well received, and is supported by the following evidence. First, similar coiled-coils are predicted to occur in all known dynein HC sequences, although the sequence conservation is low (Asai & Koonce 2001, Vallee & Gee 1998). Second, electron microscopy has shown dynein to make contact with microtubules via a slender stalk (Amos 1989, Goodenough & Heuser 1982, 1984). Finally, binding studies have shown that microtubule-binding is mediated by the region between the two coiled-coil sequences (Gee *et al.* 1997, Koonce 1997, Koonce & Tikhonenko 2000). However, no structural data has yet been obtained for the stalk domain.

We have carried out a biophysical analysis of the dynein stalk in order to prove the existence of the proposed antiparallel coiled-coil and to obtain structural information about it and the microtubule-binding region. Our approach was to analyze the sequence of the dynein stalk, design and express appropriate constructs, and perform biophysical characterizations.

C. Methods and Materials

Cloning, expression, and purification

Stalk DNA clones were obtained by PCR, using recombinant rat cytoplasmic dynein heavy chain (Gee *et al.* 1997) as a template. The forward primers introduced a BamH1 site and the reverse primers an EcoRI site. The amplified products were digested with BamH1 and EcoRI and subcloned into the bacterial expression vector pGEX-2T (Amersham Biosciences) carrying an N-terminal GST tag. The engineered pGEX-2T constructs were transformed into BL21 (DE3) bacterial cells for expression of the GST stalk fusion proteins. Expression was induced by adding IPTG to an overnight cell culture. The cells were lysed and the lysate was passed over a glutathione affinity column (Amersham Biosciences), washed with PBS containing 4 mM ATP, and eluted with 10 mM glutathione in a 50 mM Tris, 100 mM NaCl, pH 8 buffer. Thrombin was then used to cleave the GST domain from the stalk fusion proteins, which were then further purified with a HiTrap MonoQ column.

D. Results

Sequence Analysis

The sequence of the dynein stalk region was analyzed for secondary structure with the program PepTool (Wishart *et al.* 2000). This program creates a consensus secondary structure prediction through the use of several algorithms, including Chou and Fasman, Garnier, homology based, hydrophobic moment, and comparisons with known structural motifs. The stalk sequence was predicted to be highly α-helical (89.6%), with a small fraction predicted to be random coil (10.4%). No regions were predicted to contain β-sheet structure. The regions predicted to be random coils were typically 2-7 residues in length, contained proline residues, and were found within the knob region. This suggests that these regions are small loops or turns separating sequential α-helices.

Three different coiled-coil prediction programs were used to analyze the stalk sequence: COILS, PAIRCOIL, and STABLECOIL. The STABLECOIL program (Tripet & Hodges 2001) scores protein sequences with values for hydrophobic core stability (positions **a** and **d** (Tripet *et al.* 2000, Wagschal *et al.* 1999b) and α-helical propensity (positions **b**, **c**, **e**, **f** and **g** (Zhou *et al.* 1994c)). A unique aspect of this program is that it predicts variations in coiled-coil stability along the sequence length. Coiled-coils are predicted to exist from L3175-Q3245, named Coil 1, and from L3410-T3490, named Coil 2 (Figure 8-1A). The sequence is shown in Figure 8-2, with the **a** and **d** positions of the heptad repeat highlighted in red. The C-terminal border of Coil 1 is somewhat ambiguous; the score drops at Q3245, due to the presence of polar residues in the hydrophobic core, but a heptad repeat can still be observed to continue to V3283. COILS is based on the frequency with which each amino acid occurs at each position of the heptad repeat in a database of coiled-coil sequences (Lupas *et al.* 1991). Coil 1 is predicted to extend from R3189-S3255 and Coil 2 to extend from A3396-T3490 (Figure 8-1B). The predicted heptad repeats are the same as those yielded by STABLECOIL, although the borders of the coiled-coils are different. The PAIRCOIL program calculates pair wise correlations between residues at i, i+1, i+2, and i+4 heptad repeat positions, reducing the number of false positives observed with COILS (Berger *et al.* 1995). This program predicts Coil 1 to extend from F3185-E3278 and Coil 2 to extend from L3410-F3500 (Figure 8-1C). The heptad repeat predicted for Coil 2 agrees with those predicted by COILS and STABLECOIL, but a different heptad repeat is predicted for Coil 1. In summary, there is good agreement between these three programs in the location of coiled-coil sequences in the dynein stalk region, although the specific borders vary. Interestingly, both COILS and STABLECOIL predict that Coil 2 is longer than Coil 1. In reality, both strands of a coiled-coil must be the same length, but this illustrates some of the ambiguity that exists in sequence analysis.

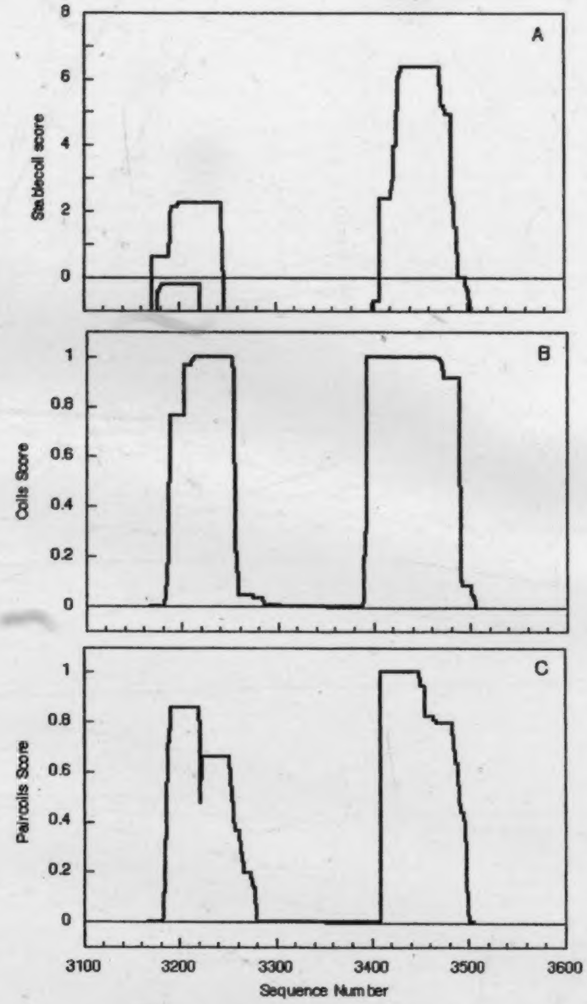

Figure 8-1. The analysis of the dynein stalk sequence by the coiled-coil prediction programs STABLECOIL (**A**), COILS (**B**), and PAIRCOIL (**C**).

A 3203

```
LRKIKET VDQVEEL RRALRIK SQELEVK NAAANDK
LKKMVKD QQEAEKK KVMSQEI QEQLHKQ QEVIADK
QMSVKED LDKVE PAVIEAQNAVKSIKKQHLVEVRSMA
NPPAAVKLALESICLLLGESTTDWKQIRSIIMRENFIP
TIVNFSAEEISDAIREKMKKNYMSNPSYNYEIVNRASLA
CGPMVKWAIAQLNYADMLKRVEP LRNE LQKLEDD
AKDNQQK ANEVEQM IRDLEAS IARYKEE YAVLISE
AQAIKAD LAAVEAK VNRSTAL LKSLSAE RERWEKT
```

3490

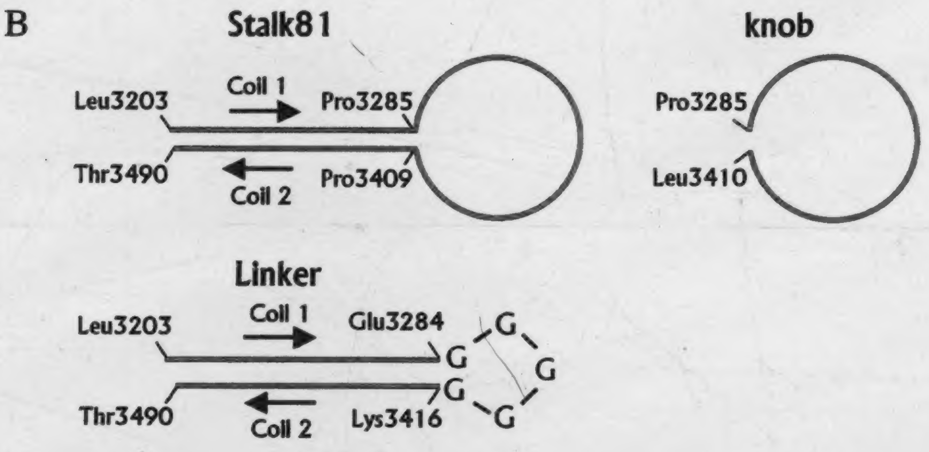
B
Stalk81
Leu3203
Coil 1
Pro3285
Thr3490
Coil 2
Pro3409
knob
Pro3285
Leu3410
Linker
Leu3203
Coil 1
Glu3284
G
G
G
G
G
Thr3490
Coil 2
Lys3416

Figure 8-2. The sequence of the dynein stalk and knob domains from Leu3203 to Thr3490. **A)** The putative heptad repeat is illustrated by marking the **a** and **d** position residues in red and the knob region is underlined. The first coiled-coil region (Leu3203-Glu3284) is called Coil 1 and the second (Lys3416-Thr3490) is called Coil 2. **B)** The dynein constructs used in this study. Stalk81 extends from Leu3203 to Thr3490. Knob extends from Pro3285 to Leu3410. Linker contains the two regions predicted to be coiled-coils (Leu3203-Glu3284 and Lys3416-Thr3490), but the knob region has been replaced by five glycine residues.

One distinct weakness of all of these sequence analysis programs is their inability to take hetero-association and antiparallel alignment into account. One approach to accounting for hetero-association is to predict the probability and/or stability of the individual sequences and then average the scores for the heterodimer. The problem with this approach is that heterodimers typically have a greater stability than either homodimer, which provides the thermodynamic driving force for association. This is frequently caused by charge complementarity (e.g. c-Myc/Max (Lavigne *et al.* 1998)) or by complementary hydrophobic surfaces in the core (e.g. a Trp/Ala layer, (Kiyokawa *et al.* 2001)). We don't know enough about these compensatory interactions to accurately predict them.

Antiparallel alignments cause other complications in sequence analysis. In parallel coiled-coils, the hydrophobic core is composed of two types of layers, as illustrated in Figure 8-3. The **a** position residues pack against each other in a parallel fashion (**a**-**a′** layer) and the **d** position residues pack against each other in a perpendicular fashion (**d**-**d′** layer) (Harbury *et al.* 1993, Monera *et al.* 1993). In contrast, the hydrophobic core of antiparallel coiled-coils have a single type of mixed **a**-**d′** layer, with packing geometries in between the two. This difference in packing interactions is reflected in the frequency with which each amino acid is found at the different heptad positions. Walshaw and Woolfson (2001b) found that two-stranded antiparallel coiled-coils had a greater variety of residues at each heptad position than was seen in two-stranded parallel coiled-coils. For example, Ile and Val are preferentially found at position **a** vs. position **d** by a ratio of 14.2 in parallel coiled-coils, but only by a ratio of 1.8 in antiparallel coiled-coils. Because of these issues, none of these programs can

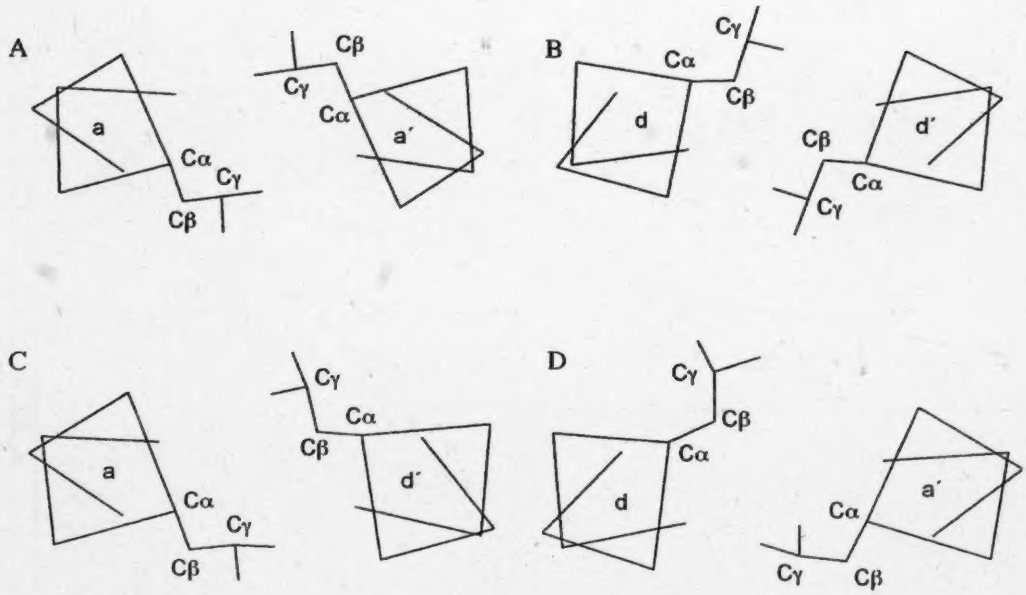
A
a
Cα
Cγ
Cβ
Cβ
Cγ
Cα
a′
B
Cγ
Cα
Cβ
d
Cβ
d′
Cα
Cγ
C
a
Cα
Cγ
Cβ
Cγ
Cα
Cβ
d′
D
Cγ
Cβ
Cα
d
a′
Cα
Cγ
Cβ

Figure 8-3. Computer modeling of the parallel and antiparallel coiled-coil structures to show the orientations of leucine side chains at positions **a** and **d**. In a parallel coiled-coil, the **a-a′** layer has parallel packing **(A)**, while the **d-d′** layer has perpendicular packing **(B)**. In an antiparallel coiled-coil, the **a-d′ (C)** and **d-a′ (D)** layers have mixed packing. Only side chain carbons of leucine and seven main chain α-carbons around this leucine are displayed. The figure is adapted from Monera *et al.* (1993).

predict that a particular sequence will form an antiparallel coiled-coil. We have used them to find a 3, 4 hydrophobic repeat, but, at present, the orientation of the strands must be determined experimentally.

An additional complication in the analysis of hetero-stranded coiled-coils is to predict their alignment, i.e. which residues interact in the hydrophobic core. We used the following set of criteria to further analyze the sequence of the dynein stalk. First, proline does not occur in coiled-coils, but can mark the end of an α-helix. Second, any cluster of three or more hydrophobic residues in predicted **a** or **d** positions is probably in the coiled-coil domain. Third, the interaction between hydrophobic residues in an **a-d′** layer is very stabilizing. Finally, i to i′+5 electrostatic interactions should be considered. Our starting point was to assume that P3285 and P3409 mark the beginning of the knob domain. The first **a-d′** layer (at the knob end) would then be between L3280(**a**) and L3410 (**d'**). This is referred to as the Pro/Pro alignment and forms the longest potential coiled-coil. Additional alignments were created by displacing the two strands, Coil 1 and Coil 2, by seven residues in either direction (Table 8-1). If Coils 1 and 2 are displaced by greater amounts, too many of the "good" hydrophobes are excluded from the coiled-coil. Our three candidate alignments were then examined in more detail. Interactions in the hydrophobic core were categorized as "hydrophobic" if they consisted of two residues with large hydrophobic side chains, as "mixed" if they consisted of one residue with a large hydrophobic side chain and one residue with a polar or charged side chain (this includes alanine), and as "polar" if they consisted of two residues with polar or charged side chains (Table 8-1). The Pro/Pro alignment has 8 hydrophobic interactions, 14 mixed interactions and 5 polar interactions. The +7 alignment appears nearly as favourable,

Table 8-1. Sequence analysis of the dynein stalk coiled-coil

Parameter	+ 7[a]	Pro/Pro [a]	-7[a]
Knob alignment[b]	S3508/L3410	L3280/L3410	Q3272/L3410
ATPase alignment[c]	R3189/V3287	R3189/I3501	R3189/F3194
Hydrophobic layer[d]	8	8	6
Mixed core pairs[e]	10	14	15
Polar core pairs[f]	5	5	4
i to i′+5 electrostatic attractions	5	9	5
i to i′+5 electrostatic repulsions	6	1	3

[a] Proposed alignments for the antiparallel coiled-coil of the dynein stalk. Described in more detail under *Sequence Analysis*.

[b] Leu3410 (Coil 2) is chosen as a reference point to describe the alignment at the end of the coiled-coil nearest the knob region. The other residue, found in Coil 1, is opposite to Leu3410 across the hydrophobic core.

[c] Arg3189 (Coil 1) is chosen as a reference point to describe the alignment at the end of the coiled-coil nearest the globular ATPase domain. The other residue, found in Coil 2, is opposite to Arg3189 across the hydrophobic core.

[d] An **a-d′** or **d-a′** layer in the hydrophobic core that is occupied by two large hydrophobic residues (Ile, Leu, Met, Phe, and Val).

[e] An **a-d′** or **d-a′** layer in the hydrophobic core that is occupied by one large hydrophobic residues (see note d) and one polar or charged residue (including Ala).

[f] An **a-d′** or **d-a′** layer in the hydrophobic core that is occupied by two polar or charged residues (including Ala).

with 8 hydrophobic, 10 mixed, and 5 polar interactions. The -7 alignment is less favourable, with 6 hydrophobic, 15 mixed, and 4 polar interactions. We then examined the number of potential i to i´+5 electrostatic interactions, which have been shown to be important in controlling the specificity of the interaction partner and specific alignments in both native (Lavigne *et al.* 1995, 1998, Moll *et al.* 2000, Vinson *et al.* 1993) and de novo designed coiled-coils (Kohn *et al.* 1995a, 1995b, 1998b, Krylov *et al.* 1998, Zhou *et al.* 1994b). Here, the Pro/Pro alignment was clearly the most favourable, with 9 attractions and 1 repulsion. In comparison, the +7 alignment had 5 attractions and 6 repulsions, and the -7 alignment had 5 attractions and 3 repulsions.

These analyses suggest that the Pro/Pro alignment is the most likely to exist. It is illustrated in Figure 8-4, with the hydrophobic core interactions marked by horizontal lines and the i to i´+5 electrostatic interactions marked by arrows. However, this analysis also illustrates the difficulties involved in the prediction of structural motifs. A definitive answer to the location and alignment of a coiled-coil can only be provided by an experimental approach.

Construct Design

We wanted to investigate the structural and biophysical properties of both regions of the dynein stalk (the coiled-coil and the knob). To do this, three constructs were designed (Figure 8-2B). The first construct, Stalk81 (residues Leu3203-Thr3409), represents the entire stalk domain containing both the knob region and 80 residues of the flanking coiled-coil regions (assuming that we have correctly identified the borders of the knob region). In designing the second construct, named Linker, we attempted to isolate the coiled-coil by replacing the knob with a flexible, five glycine spacer. Linker extends

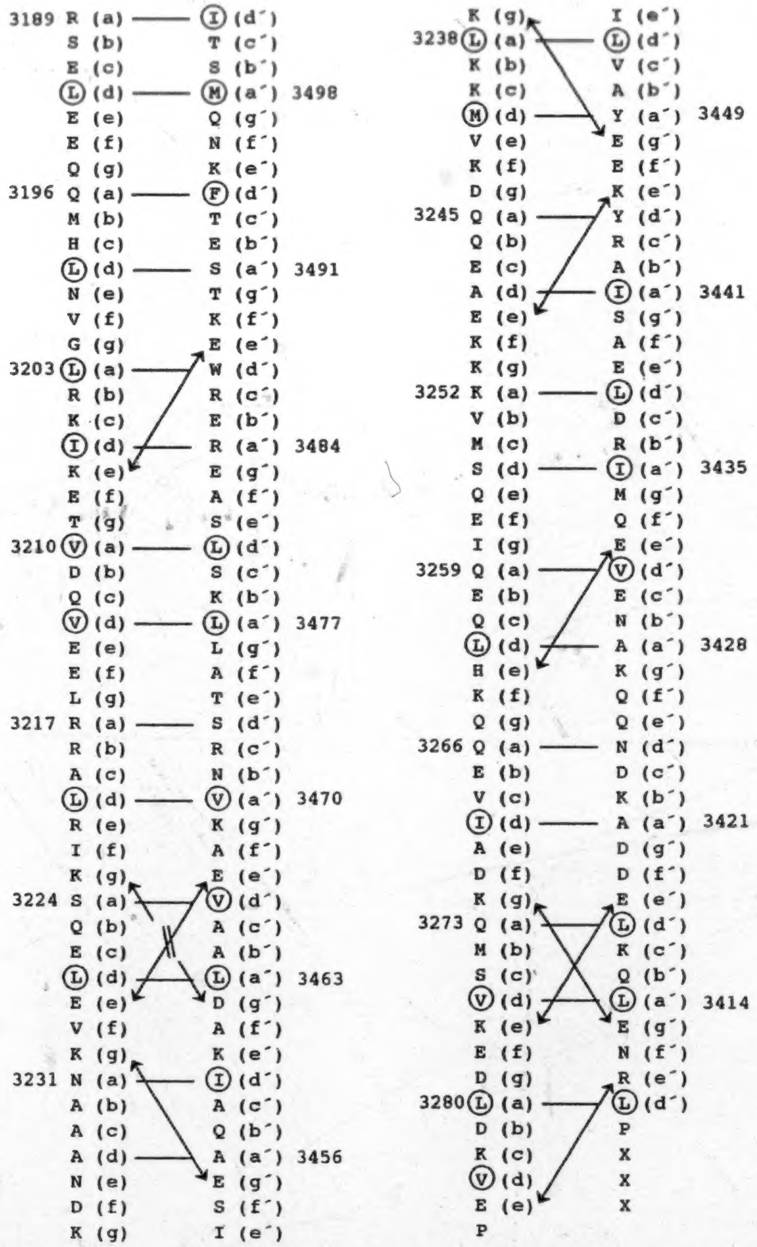
3189 R (a) — I (d')
S (b) T (c')
E (c) S (b')
L (d) — M (a') 3498
E (e) Q (g')
E (f) N (f')
Q (g) K (e')
3196 Q (a) — F (d')
M (b) T (c')
H (c) E (b')
L (d) — S (a') 3491
N (e) T (g')
V (f) K (f')
G (g) E (e')
3203 L (a) — W (d')
R (b) R (c')
K (c) E (b')
I (d) — R (a') 3484
K (e) E (g')
E (f) A (f')
T (g) S (e')
3210 V (a) — L (d')
D (b) S (c')
Q (c) K (b')
V (d) — L (a') 3477
E (e) L (g')
E (f) A (f')
L (g) T (e')
3217 R (a) — S (d')
R (b) R (c')
A (c) N (b')
L (d) — V (a') 3470
R (e) K (g')
I (f) A (f')
K (g) E (e')
3224 S (a) — V (d')
Q (b) A (c')
E (c) A (b')
L (d) — L (a') 3463
E (e) D (g')
V (f) A (f')
K (g) K (e')
3231 N (a) — I (d')
A (b) A (c')
A (c) Q (b')
A (d) — A (a') 3456
N (e) E (g')
D (f) S (f')
K (g) I (e')
K (g) I (e')
3238 L (a) — L (d')
K (b) V (c')
K (c) A (b')
M (d) — Y (a') 3449
V (e) E (g')
K (f) E (f')
D (g) K (e')
3245 Q (a) — Y (d')
Q (b) R (c')
E (c) A (b')
A (d) — I (a') 3441
E (e) S (g')
K (f) A (f')
K (g) E (e')
3252 K (a) — L (d')
V (b) D (c')
M (c) R (b')
S (d) — I (a') 3435
Q (e) M (g')
E (f) Q (f')
I (g) E (e')
3259 Q (a) — V (d')
E (b) E (c')
Q (c) N (b')
L (d) — A (a') 3428
H (e) K (g')
K (f) Q (f')
Q (g) Q (e')
3266 Q (a) — N (d')
E (b) D (c')
V (c) K (b')
I (d) — A (a') 3421
A (e) D (g')
D (f) D (f')
K (g) E (e')
3273 Q (a) — L (d')
M (b) K (c')
S (c) Q (b')
V (d) — L (a') 3414
K (e) E (g')
E (f) N (f')
D (g) R (e')
3280 L (a) — L (d')
D (b) P
K (c) X
V (d) X
E (e) X
P

Figure 8-4. The "Pro/Pro" antiparallel alignment of the dynein stalk coiled-coil. Large hydrophobes (F, I, L, M, and V) at **a** and **d** positions are circled. Interactions in the hydrophobic core (**a-d′** and **d-a′**) are denoted by horizontal lines. Potential i to i′+5 electrostatic attractions are marked with arrows. The predicted i to i′+5 electrostatic repulsion is marked by an arrow with crossed lines.

from residues Leu3203 to Glu3284, then there are five glycines, and it then continues from residues Lys3416 to Thr3490. Finally, the third construct, named Knob, consists of the knob region alone (Pro3285-Leu3410).

Stalk81 and Linker could be produced in high concentrations and at high purity. The knob construct, on the other hand has bee difficult to produce. It has a much lower solubility, due to its tendency to aggregate and precipitate. Proteolysis has also been a recurring problem in producing the knob construct. We have been able to obtain enough of the knob construct for preliminary studies, but a more thorough investigation is still needed when we are able to produce more sample.

CD Spectroscopy

The solution conformations of the dynein stalk constructs were investigated by CD spectroscopy, which is sensitive to secondary structure content. CD spectra were obtained for each construct in both benign buffer and in the presence of 50% TFE, a helix inducing solvent (Shiraki *et al.* 1995, Sonnichsen *et al.* 1992). All three constructs have CD spectra typical of α-helices (Figure 8-5), with the characteristic strong negative bands at 208 and 222 nm (Woody 1995). Stalk81 is highly α-helical, as indicated by a molar ellipticity of -29,730 $deg \cdot cm^2 \cdot dmol^{-1}$ at 222 nm (Table 8-2). The ratio of the molar ellipticity values at 222 and 208 nm is 1.04, typical of helices interacting in a coiled-coil structure (Lau *et al.* 1984, Zhou *et al.* 1992a). In the presence of 50% TFE, a small amount of additional helical structure was induced, indicated by the small increase in the ellipticity at 222 nm. This indicates that this domain is stably folded and highly α-helical, entirely consistent with the antiparallel coiled-coil model. This also indicates that the knob domain must contain a substantial amount of α-helical structure. TFE induces

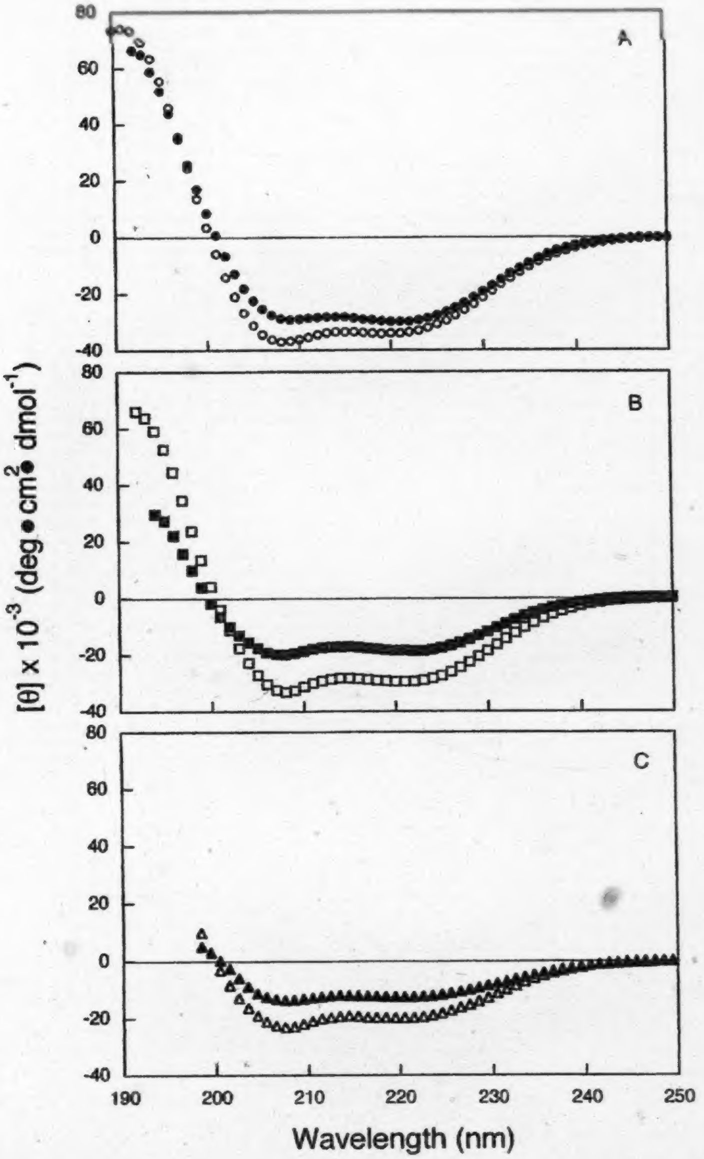

Figure 8-5. CD spectra of the dynein constructs were measured in benign buffer (50 mM PO_4, 150 mM KCl, pH 7.0). The Stalk81 and Knob samples also contained 2 mM DTT. **A)** Stalk81 in benign buffer (●) and in 50% TFE (○) at 8.9 μM. **B)** Linker in benign buffer (■) and in 50% TFE (□) at 35.7 μM. **C)** Knob in benign buffer (▲) and in 50% TFE (Δ) at 12.4 μM.

Table 8-2. CD Analysis of Dynein Constructs

	$[\theta]_{222}$[a]		$[\theta]_{222}/[\theta]_{208}$		T_m (°C)
	benign	50% TFE	benign	50% TFE	
Stalk81	-29,730	-33,560	1.04	0.91	48
Linker	-18,600	-29,450	0.93	0.88	23, 59[b]
Knob	-12,510	-19,740	0.91	0.85	>40[c]

[a] The mean residue molar ellipticities ($deg \cdot cm^2 \cdot dmol^{-1}$) were measured in benign buffer (50 mM PO_4, 150 mM KCl, pH 7). For the Stalk81 and Knob samples, the buffer included 2 mM DTT. For samples containing TFE, the above buffer was diluted 1:1 (v/v) with TFE.

[b] The Linker denaturation profile has two transitions (Figure 8-6).

[c] The Knob construct precipitated at high temperatures, preventing an accurate determination of T_m.

α-helical structure, but disrupts tertiary interactions between helices, reflected in the reduced ratio of the ellipticity values at 222 and 208 nm (0.91, typical for single α-helices (Lau *et al.* 1984, Zhou *et al.* 1992a)).

The Linker construct has a CD spectrum typical of an α-helix, with a $[\theta]_{222}$ value of -18,600 deg·cm^{2}·dmol^{-1} (Figure 8-5B and Table 8-2). This is entirely consistent with its predicted coiled-coil structure. The presence of 50% TFE induced a significant amount of additional α-helical structure, illustrated by the increase in molar ellipticity at 222 nm to -29,450 deg·cm^{2}·dmol^{-1}. This indicates that the Linker construct is not fully folded in benign buffer, in contrast to the stably folded Stalk81 construct. The Knob construct also has a CD spectrum typical of an α-helix, with a $[\theta]_{222}$ value of -12,510 deg·cm^{2}·dmol^{-1} (Figure 8-5C and Table 8-2). This agrees with the high α-helical content predicted by secondary structure analysis. It also exhibits a large increase in α-helical structure in the presence of 50% TFE, with a $[\theta]_{222}$ value of -19,740 deg·cm^{2}·dmol^{-1}. This shows that significant portions of the Knob construct are also unfolded in benign buffer. It appears that removal of either the knob or the coiled-coil had a destabilizing effect on the remaining structure.

Conformational Stability

Temperature denaturations were performed on the dynein constructs and monitored by CD spectroscopy at 222 nm (Figure 8-6 and Table 8-2). Stalk81 has a cooperative denaturation profile, with a T_m of 48°C. This is typical of stably folded proteins, and supports the idea that the dynein stalk is a cooperatively folded domain. In contrast, the Linker construct has an unusual biphasic denaturation profile, with transition

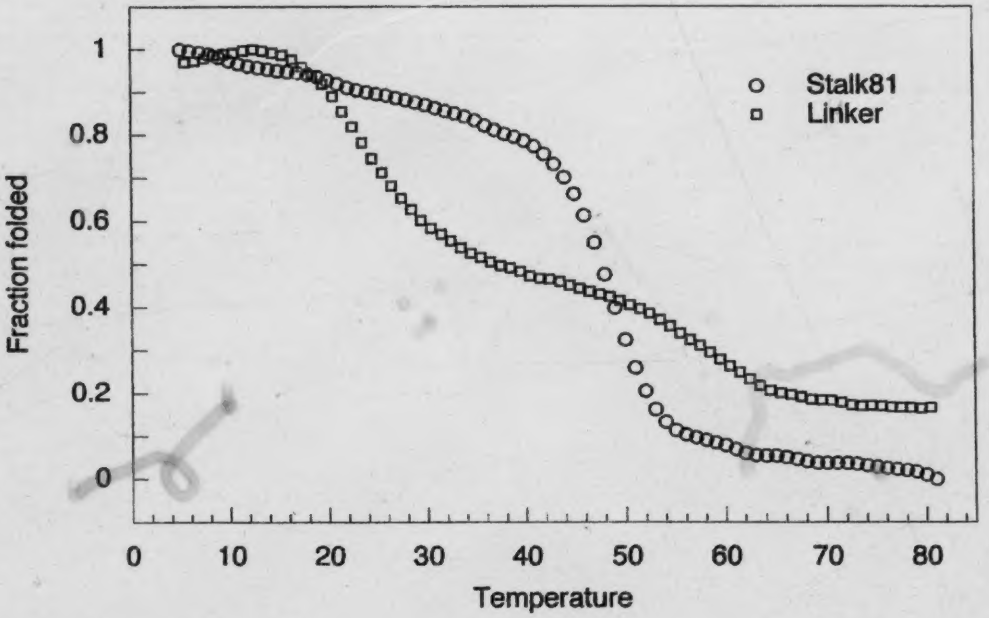

Figure 8-6. Temperature denaturation profiles of Stalk81 (○, 1.1 μM) and Linker (□, 35.7 μM) were measured in benign buffer (50 mM PO_4, 150 mM KCl, pH 7.0) and monitored at 222 nm. The Stalk81 sample also contained 2 mM DTT.

midpoints at 23 and 59°C. Removal of the knob has significantly altered the denaturation profile, suggesting that this region is critical in maintaining the stalk structure. The knob precipitated at high temperatures, preventing an accurate determination of the T_m. This behaviour is also suggestive of a disrupted structure. This confirms that both the coiled-coil and the knob are required for the stalk to be a stable, cooperatively folded domain. Similar behaviour is seen in kinesin, where the coiled-coil obtains an additional 1.5 kcal/mol of stabilization from N-capping and hydrophobic staple interactions with residues in the neighbouring neck linker region (Kozielski *et al.* 1997, Tripet & Hodges 2002).

Analytical Ultracentrifugation

Sedimentation equilibrium experiments were performed on the Stalk81 and Linker constructs in benign buffer. Stalk81 was best fit to a single species model with no indication of self-association (Figure 8-7B). The observed weight-averaged molecular weight was 31,000 Da, slightly below the calculated value of 34,387 Da. The high quality of this fit is shown by the random nature of the residuals (Figure 8-7A). This is entirely consistent with the model proposing the formation of an intramolecular, antiparallel coiled-coil. The Linker construct was best fit to a monomer-dimer association model, with a K_d of approximately 100 μM (Figure 8-7C, D). As self-association is not observed for the intact domain, this is further evidence that the structure and folding of the Linker construct has been disturbed by the removal of the knob region.

In order to obtain information about the shape of Stalk81, a sedimentation velocity experiment was performed. The sedimentation coefficient was determined to be 2.2 S by both second moment and time derivative analysis, using the program Ultrascan.

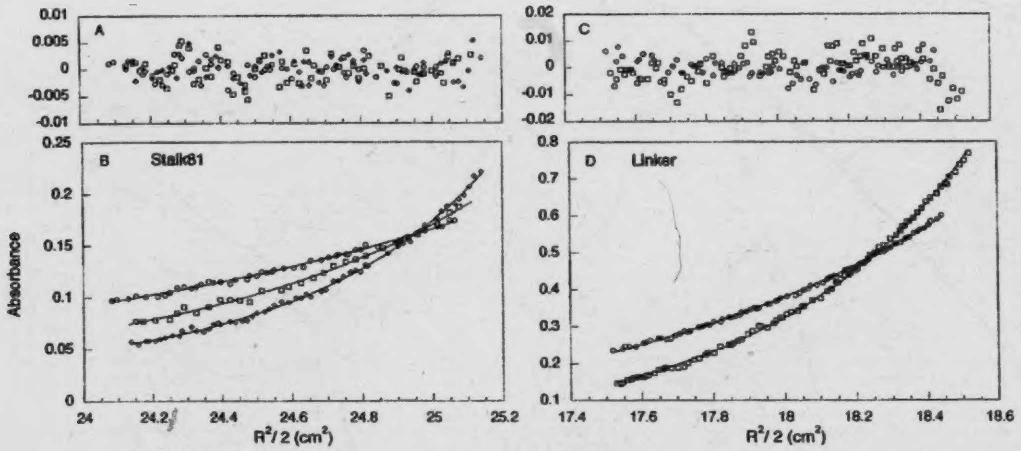

Figure 8-7. Sedimentation equilibrium analysis of Stalk81 (**A**, **C**) and Linker (**B**, **D**). Stalk81 samples were run at 14,000, 18,000, and 22,000 rpm in 20 mM HEPES, 150 mM KCl, 2 mM TCEP, pH 7.0. The data was best fit to a single species model, as shown in **C**, with the residuals shown in **A**. Linker samples were run at 18,000 and 24,000 rpm in 50 mM PO_4, 150 mM KCl, pH 7.0. The data was best fit to a monomer-dimer association model, as shown in **D**, with the residuals shown in **B**.

This value is converted to a standardized sedimentation coefficient of 2.4 S, which assumes conditions of 20°C and aqueous solution. The effect of molecular shape was evaluated as follows, and the calculated parameters are listed in Table 8-3. First, the protein was assumed to be a sphere, and the radius was calculated by the empirical equation (Waxman *et al.* 1993):

$$R_p = (6.723 \times 10^{-9})\, M_r^{1/3}$$

where R_p is the radius of the protein and M_r is the calculated molecular weight. This value is then used to calculate the volume of the protein, V_p ($V_p = 4/3\ \pi r^3$). The hydration, δ, is an estimate of the amount of water bound to the protein and was calculated based on the protein's amino acid composition. The hydration value was then used to calculate the volume of the protein, modeled as a hydrated sphere (Cantor & Schimmel 1980, Waxman *et al.* 1993):

$$V = V_p\,[(\text{v-bar} + \delta)/\ \text{v-bar}]$$

where v-bar is the partial specific volume and is calculated by amino acid composition (Laue *et al.* 1992). V is then used to calculate the radius of the protein as a hydrated sphere, R_{sph}. The next step is to use Stokes' Law to calculate the frictional coefficient of the protein (f_{sph}), again modeled as a rigid sphere:

$$f_{sph} = 6\pi\eta R_{sph}$$

where η is the solvent viscosity. In the case of Stalk81, f_{sph} is predicted to be 4.87×10^{-8} g/s. However, most proteins are not rigid spheres. Any deviation from a spherical shape (that is, asymmetry) will increase the degree of friction, slowing the movement of the

Table 8-3. Stalk81 Hydrodynamic Parameters

Parameter	Value	Description
M_r	34 387 Da	Calculated molecular weight
R_p	2.19×10^{-7} cm	Radius of the anhydrous protein (spherical model)
V_p	4.40×10^{-20} ml	Volume of the anhydrous protein (spherical model)
v-bar[a]	0.7425	Partial specific volume
δ[a]	0.4512 g H_2O/g protein	Hydration value
V	7.07×10^{-20} ml	Protein volume as a hydrated sphere
R_{sph}	2.57×10^{-7} cm	Protein radius as a hydrated sphere
f_{sph}	4.87×10^{-8} g/s	Frictional coefficient as a hydrated sphere
s_{obs}	2.2 S	Sedimentation coefficient
$s^{o}_{20,w}$	2.4 S	Standardized sedimentation coefficient
f_{obs}	6.45×10^{-8} g/s	Frictional coefficient
f_{obs}/f_{sph}	1.32	Frictional ratio

[a] Calculated with the program SEDNTERP (Hayes *et al.* 1998, Laue *et al.* 1992).

molecule through solution. Molecular flexibility, on the other hand, will reduce the frictional coefficient, allowing the molecule to move through the solution more quickly. We can use the experimentally observed sedimentation coefficient (2.2 S, Table 8-3) to calculate the observed frictional coefficient (f_{obs}):

$$s = \frac{M_r\,(1 - \text{v-bar} * \rho)}{N_a * f_{obs}}$$

where s is the sedimentation coefficient, ρ is the solvent density, and N_a is Avogadro's number. Stalk81 was found to have an observed frictional coefficient of 6.45×10^{-8} g/s and a frictional ratio (f_{obs} / f_{sph}) of 1.32. This is a clear indication of Stalk81's molecular asymmetry.

Further information can be obtained by modeling the protein as an ellipsoid. A prolate ellipsoid is a reasonable model for an extended coiled-coil, so we proceeded with the analysis. This yielded a model of Stalk81 as a prolate ellipsoid in which the a and b radii have a ratio of 6.4 (Figure 8-8). If we assume that all 81 residues of the proposed coiled-coil do adopt a coiled-coil structure, the length of the molecule will be ~ 120 Å (based on a rise of 1.5 Å/residue in an α-helix). X-ray crystal structures have shown that the radius of a typical two-stranded coiled-coil is approximately 10 nm. The axial ratio of our model coiled-coil will then be 60/10 = 6, a reasonable agreement with that of the ellipsoid modeled to our data. Unfortunately, this type of analysis is inherently ambiguous, because numerous different ellipsoids can be fit to most sedimentation velocity data. We can, however, say that the data is consistent with what would be expected for an elongated molecule, such as an antiparallel, intramolecular coiled-coil.

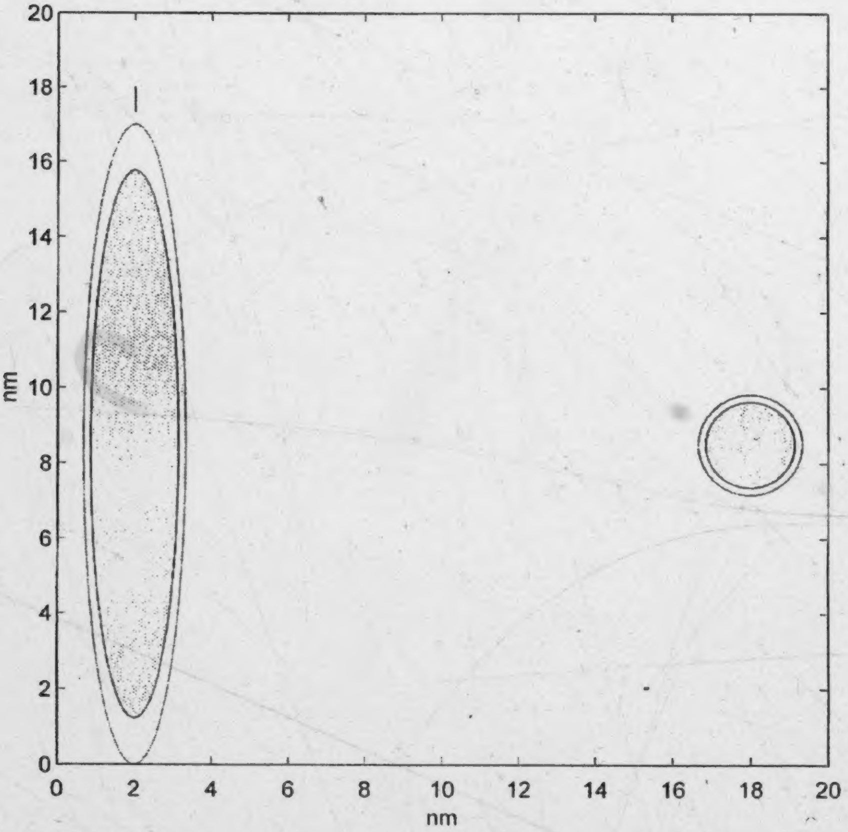

Figure 8-8. Stalk81 sedimentation velocity data was modeled as a prolate ellipsoid, using the program SEDNTERP. The resulting ellipsoid had a ratio of 6.4 for the radii in the a and b directions. The figure at the left shows the ellipsoid from a side view and the figure at the right shows it from an end-on view.

E. Discussion and Future Directions

With the use of CD spectroscopy and analytical ultracentrifugation, we have shown that the dynein stalk is highly α-helical, stably and cooperatively folded, monomeric in solution, and has an elongated shape. Together, these results provide the first biophysical evidence that the dynein stalk forms an antiparallel, intramolecular coiled-coil. We have also shown that both the coiled-coil and the knob regions are required for the stalk domain to fold stably and cooperatively; when expressed individually, each subdomain exhibits destabilized behaviour. This suggests that there are stabilizing interactions between the two domains, possibly analogous to the N-cap and hydrophobic staple observed in kinesin (Tripet & Hodges 2002).

There is still some work needed to take this project to a point suitable for publication. There have been difficulties in producing the knob construct, for it tends to aggregate and to precipitate. Proteolytic cleavage has been used to remove the leading sequence left by the expression vector, but the cleavage tends to be nonspecific and significant amounts of the protein becomes degraded. We have obtained cells transfected with these constructs from Dr. Vallee's lab, and are in the process of expressing them here, eliminating the need to freeze samples for shipping. We also plan to develop an RP-HPLC protocol to simplify purification and to prevent excessive proteolysis by separating our product from the protease. Once we have reasonable amounts of the knob construct, its biophysical characterization will be completed.

It is also important to obtain the high-resolution, three-dimensional structure of the stalk domain, and projects with this goal have been started. Stalk81 has been crystallized by Dr. Vallee's lab and they are in the process of solving the structure. David Zoetewey, a new graduate student in our lab, intends to express the dynein stalk constructs as the ^{13}C, ^{15}N labeled products for NMR studies.

References

Acharya, A., Runinov, S. B., Gal, J., Moll, J. R. and Vinson, C. (2002) A heterodimerizing leucine zipper coiled coil system for examining the specificity of **a** position interactions: amino acids I, V, L, N, A, and K. *Biochem.* **41**: 14122-14131.

Aguilar, M. and Hearn, M. T. W. (1996) High-resolution reversed-phase high-performance liquid chromatography of peptides and proteins. *Methods Enzymol.* **270**: 3-26.

Akey, D. L., Malashkevich, V. N. and Kim, P. S. (2001) Buried polar residues in coiled-coil interfaces. *Biochem.* **40**: 6352-6360.

Alonso, D. O. V. and Dill, K. A. (1991) Solvent denaturation and stabilization of globular proteins. *Biochem.* **30**: 5974-5985.

Alpert, A. J. (1990) Hydrophilic-interaction chromatography for the separation of peptides, nucleic acids and other polar compounds. *J. Chromatogr.* **499**: 177-196.

Amos, L. A. (1989) Brain dynein crossbridges microtubules into bundles. *J. Cell Sci.* **93**: 19-28.

Arndt, K. M., Muller, K. M. and Pluckthun, A. (2001) Helix-stabilized Fv (hsFv) antibody fragments: substituting the constant domains of a Fab fragment for a heterodimeric coiled-coil domain. *J. Mol. Biol.* **312**: 221-228.

Arndt, K. M., Pelletier, J. N., Muller, K. M., Alber, T., Michnick, S. W. and Pluckthun, A. (2000) A heterodimeric coiled-coil peptide pair selected *in vivo* from a designed library-*versus*-library ensemble. *J. Mol. Biol.* **295**: 627-639.

Arndt, K. M., Pelletier, J. N., Muller, K. M., Pluckthun, A. and Alber, T. (2002) Comparison of in vivo selection and rational design of heterodimeric coiled coils. *Structure* **10**: 1235-1248.

Arrizon-Lopez, V., Biehler, R., Cummings, J. and Harbaugh, J. (1991) Beckman System 6300 high-performance amino acid analyzer. *High-Performance Liquid Chromatography of Peptides and Proteins: Separation, Analysis, and Conformation*. (Eds. Mant, C. T. and Hodges, R. S.) Boca Raton, CRC Press, pp. 859-863.

Asai, D. J. and Koonce, M. P. (2001) The dynein heavy chain: structure, mechanics and evolution. *Trends Cell Biol.* **11**: 196-202.

Ausubel, F. M., Brent, R., Kingston, R. E., Moore, D. D., Seidman, J. G., Smith, J. A. and Struhl, E., Eds. (1994) *Current Protocols in Molecular Biology*, Vol. 2, New York, John Wiley & Sons, Inc., pp. 13.7.1-13.7.10.

Baker, D. (2000) A surprising simplicity to protein folding. *Nature* **405**: 39-42.

Baldwin, R. L. and Rose, G. D. (1999a) Is protein folding hierarchic? I. Local structure and peptide folding. *TIBS* **24**: 26-33.

Baldwin, R. L. and Rose, G. D. (1999b) Is protein folding hierarchic? II. Folding intermediates and transition states. *TIBS* **24**: 77-83.

Baskakov, I. V. and Bolen, D. W. (1999) The paradox between *m* values and ΔCp's for denaturation of ribonuclease T1 with disulfide bonds intact and broken. *Protein Sci.* **8**: 1314-1319.

Baxevanis, A. D. and Vinson, C. R. (1993) Interactions of coiled coils in transcription factors: where is the specificity? *Curr. Opin. Genet. Dev.* **3**: 278-285.

Beck, K., Gambee, J. E., Kamawal, A. and Bachinger, H. P. (1997) A single amino acid can switch the oligomerization state of the α-helical coiled-coil domain of cartilage matrix protein. *EMBO J.* **16**: 3767-3777.

Behncken, S. N., Billestrup, N., Brown, R., Amstrup, J., Conway-Campbell, B. and Waters, M. J. (2000) Growth hormone (GH)-independent dimerization of GH receptor by a leucine zipper results in constitutive activation. *J. Biol. Chem.* **275**: 17000-17007.

Berger, B., Wilson, D. B., Wolf, E., Tonchev, T., Milla, M. and Kim, P. S. (1995) Predicting coiled coils by use of pairwise residue correlations. *Proc. Natl. Acad. Sci.* **92**: 8259-8263.

Betz, S. F., Liebman, P. A. and DeGrado, W. F. (1997) *De novo* design of native proteins: characterization of proteins intended to fold into antiparallel, Rop-like, four-helix bundles. *Biochem.* **36**: 2450-2458.

Bilgicer, B., Fichera, A. and Kumar, K. (2001) A coiled coil with a fluorous core. *J. Am. Chem. Soc.* **123**: 4393-4399.

Bilsel, O. and Matthews, C. R. (2000) Barriers in protein folding reactions. *Adv. Protein Chem.* **53**: 153-207.

Bochtler, M., Hartmann, C., Song, H. K., Bourenkov, G. P., Bartunik, H. D. and Huber, R. (2000) The structures of HslU and the ATP-dependent protease HlsU-HslV. *Nature* **403**: 800-805.

Bodanszky, M. (1988) *Peptide Chemistry*. Berlin, Springer-Verlag.

Bodanszky, M. (1993) *Peptide Chemistry*. Berlin, Springer-Verlag.

Bolen, D. W. and Yang, M. (2000) Effects of guanidine hydrochloride on the proton inventory of proteins: implications on interpretations of protein stability. *Biochem.* **39**: 15208-15216.

Boyes, B. E. and Walker, D. G. (1995) Selectivity optimization of reversed-phase high-performance liquid chromatographic peptide and protein separations by varying bonded-phase functionality. *J. Chromatogr.* **691**: 337-347.

Bradley, J. V. (1968) *Distribution-Free Statistical Tests*. N. J., Prentice-Hall, Inc.

Brahms, S. and Brahms, J. (1980) Determination of protein secondary structure in solution by vacuum ultraviolet circular dichroism. *J. Mol. Biol.* **138**:149-178.

Brandon, C. and Tooze, J. (1991) *Introduction to Protein Structure*. New York, Garland Publishing, Inc.

Brown, J. H., Cohen, C. and Parry, D. A. (1996) Heptad breaks in α-helical coiled coils: Stutters and stammers. *Proteins* **26**: 134-145.

Burke, T. W. L., Black, J. A., Mant, C. T. and Hodges, R. S. (1991) Preparative reversed-phase shallow gradient approach to the purification of closely related peptide analogs on analytical instrumentation. *High-Performance Liquid Chromatography of Peptides and Proteins.* (Eds. Mant, C. T. and Hodges, R. S.) Boca Raton, CRC Press, pp. 783-791.

Burkhard, P., Ivaninski, S. and Lustig, A. (2002) Improving coiled-coil stability by optimizing ionic interactions. *J. Mol. Biol.* **318**: 901-910.

Burkhard, P., Kammerer, R. A., Steinmetz, M. O., Bourenkov, G. P. and Aebi, U. (2000a) The coiled-coil trigger site of the rod domain of cortexillin I unveils a distinct network of interhelical and intrahelical salt bridges. *Structure* **8**: 223-230.

Burkhard, P., Meier, M. and Lustig, A. (2000b) Design of a minimal protein oligomerization domain by a structural approach. *Protein Sci.* **9**: 2294-2301.

Burkhard, P., Stetefeld, J. and Strelkov, S. V. (2001) Coiled coils: a highly versatile protein folding motif. *Trends Cell Biol.* **11**: 82-88.

Campbell, K. M. and Lumb, K. J. (2002) Complementation of buried lysine and surface polar residues in a designed heterodimeric coiled coil. *Biochem.* **41**: 7169-7175.

Cantor, C. R. and Schimmel, P. R. (1980) *Biophysical Chemistry*. San Francisco, W. H. Freeman and Company.

Cao, H., Garcia, F. and McNiven, M. A. (1998) Differential distribution of dynamin isoforms in mammalian cells. *Mol. Biol. Cell* **9**: 2595-2609.

Carr, J. F. and Hinshaw, J. E. (1997) Dynamin assembles into spirals under physiological salt conditions upon the addition of GDP and gamma-phosphate analogues. *J. Biol. Chem.* **272**: 28030-28035.

Catimel, B., Faux, M. C., Nerrie, M., Rothacker, J., Otvos Jr., L., Wade, J. D., Nice E. C. and Burgess, A. W. (2001) The use of coiled-coil interactions for the analysis and micropreparative isolation of adenomatous polyposis coli protein (APC) complexes. *J. Pept. Res.* **58**: 493-503.

Cedervall, T., Johansson M. U. and Akerstrom, B. (1997) Coiled-coil structure of group A Streptococcal M proteins. Different temperature stability of class A and C proteins by hydrophobic-nonhydrophobic amino acid substitutions at heptad positions **a** and **d**. *Biochem.* **36**: 4987-4994.

Chakrabartty, A., Kortemme, T. and Baldwin, R. L. (1994) Helix propensities of the amino acids measured in alanine-based peptides without helix-stabilizing side-chain interactions. *Protein Sci.* **3**: 843-852.

Chakrabartty, A. and Baldwin, R. L. (1995) Stability of α-helices. *Adv. Protein Chem.* **46**: 141-176.

Chang, C. T., Wu, C.-S. and Yang, J. T. (1978) Circular dichroic analysis of protein conformation: inclusion of the β-turns. *Anal. Biochem.* **91**: 13-31.

Chao, H., Bautista, D. L., Litowski, J., Irvin R. T. and Hodges, R. S. (1998) Use of a heterodimeric coiled-coil system for biosensor application and affinity purification. *J. Chromatogr.* **715**: 307-329.

Chao, H., Houston Jr., M. E., Grothe, S., Kay, C. M., O'Connor-McCourt, M., Irvin, R. T. and Hodges, R. S. (1996) Kinetic study on the formation of a de novo designed heterodimeric coiled-coil: use of surface plasmon resonance to monitor the association and dissociation of polypeptide chains. *Biochem.* **35**: 12175-12185.

Chen, M. S., Obar, R. A., Schroeder, C. C., Austin, T. W., Poodry, C. A., Wadsworth, S. C. and Vallee, R. B. (1991) Multiple forms of dynamin are encoded by shibire, a Drosophila gene involved in endocytosis. *Nature* **351**: 583-586.

Chen, Y. H., Yang, J. T. and Chau, K. H. (1974) Determination of the helix and β form of proteins in aqueous solution by circular dichroism. *Biochem.* **13**: 3350-3359.

Chou, P. Y. and Fasman, G. D. (1978) Empirical predictions of protein conformation. *Ann. Rev. Biochem.* **47**: 251-276.

Cocca, B. A., Seal, S. N. and Radic, M. Z. (1999) Tandem affinity tags for the purification of bivalent anti-DNA single-chain Fv expressed in *Escherichia coli*. *Protein Exp. Purif.* **17**: 290-298.

Cohen, C. (1998) Why fibrous proteins are romantic. *J. Struct. Biol.* **122**: 3-16.

Cohen, C. and Parry, D. A. (1990) α-Helical coiled coils and bundles: how to design an α-helical protein. *Proteins* **7**: 1-15.

Cohen, S. A. and Gilby, A. (2002) Detection and analysis of proteins by high-performance liquid chromatography with photodiode array detection. *HPLC of Biological Macromolecules*. (Eds. Gooding, K. M. and Regnier, F. E.) New York, Marcel Dekker, Inc., pp. 739-771.

Cole, J. L. and Hansen, J. C. (1999) Analytical ultracentrifugation as a contemporary biomolecular research tool. *Journal of Biomolecular Techniques* **10**: 163-176.

Cornette, J. L., Cease, K. B., Margalit, H., Spouge, J. L., Berzofsky, J. A. and DeLisi, C. (1987) Hydrophobicity scales and computational techniques for detecting amphipathic structures in proteins. *J. Mol. Biol.* **195**: 659-685.

Creamer, T. P. and Rose, G. D. (1992) Side-chain entropy opposes α-helix formation but rationalizes experimentally determined helix-forming propensities. *Proc. Natl. Acad. Sci.* **89**: 5937-5941.

Crick, F. H. C. (1953) The packing of α-helices: simple coiled-coils. *Acta Crystallogr.* **6**: 689-698.

Cunico, R. L., Gooding, K. M. and Wehr, T. (1998) *Basic HPLC and CE of Biomolecules*. Richmond, CA, USA, Bay Bioanalytical Laboratory.

d'Agostino, P. A., Hancock, J. R., Provost, L. R., Semchuk, P. D. and Hodges, R. S. (1998) Liquid chromatographic-high-resolution mass spectrometric and tandem mass spectrometric identification of synthetic peptides using electrospray ionization. *J. Chromatogr.* **800**: 89-100.

d'Avignon, D. A., Bretthorst, G. L., Holtzer, M. E. and Holtzer, A. (1998) Site-specific thermodynamics and kinetics of a coiled-coil transition by spin inversion transfer transfer NMR. *Biophys. J.* **74**: 3190-3197.

d'Avignon, D. A., Bretthorst, G. L., Holtzer, M. E. and Holtzer, A. (1999) Thermodynamics and kinetics of a folded-folded' transition at valine-9 of a GCN4-like leucine zipper. *Biophys. J.* **76**: 2752-2759.

Danino, D. and Hinshaw, J. E. (2001) Dynamin family of mechanoenzymes. *Curr. Opin. Cell Biol.* **13**: 454-460.

De Crescenzo, G., Grothe, S., Lortie, R., Debanne, M. T. and O'Connor-McCourt, M. (2000) Real-time kinetic studies on the interaction of transforming growth factor alpha with the epidermal growth factor receptor extracellular domain reveal a conformational change model. *Biochem.* **39**: 9466-9476.

De Francesco, R., Pastore, A., Vecchio, G. and Cortese, R. (1991) Circular dichroism study on the conformational stability of the dimerization domain of transcription factor LFB1. *Biochem.* **30**: 143-147.

Delahay, R. M. and Frankel, G. (2002) Coiled-coil proteins associated with type III secretion systems: A versatile domain revisited. *Mol. Microbiol.* **45**: 905-916.

Dill, K. A. (1990) Dominant forces in protein folding. *Biochem.* **29**: 7133-7155.

Dill, K. A. and Chan, H. S. (1997) From Levinthal to pathways to funnels. *Nature Struct. Biol.* **4**: 10-19.

Dinner, A. R., Sali, A., Smith, L. J., Dobson, C. M. and Karplus, M. (2000) Understanding protein folding via free-energy theory and experiment. *TIBS* **25**: 331-339.

Dragan, A. I. and Privalov, P. L. (2002) Unfolding of a leucine zipper is not a simple two-state transition. *J. Mol. Biol.* **321**: 891-908.

Drees, B. L., Grotkopp, E. K. and Nelson, H. C. M. (1997) The GCN4 leucine zipper can functionally substitute for the heat shock transcription factor's trimerization domain. *J. Mol. Biol.* **273**: 61-74.

Durr, E. and Bosshard, H. R. (2000) Folding of a three-stranded coiled-coil. *Protein Sci.* **9**: 1410-1415.

Durr, E., Jelesarov, I. and Bosshard, H. R. (1999) Extremely fast folding of a very stable leucine zipper with a strengthened hydrophobic core and lacking electrostatic interactions between helices. *Biochem.* **38**: 870-880.

Eisenberg, D. and McLachlan, A. D. (1986) Solvation energy in protein folding and binding. *Nature* **319**: 199-203.

Erickson, B. W. and Merrifield, R. B. (1976) Solid-Phase Peptide Synthesis. *The Proteins*. Neurath, H.,Hill, R. L. andBoeder, C.-L. New York, Academic Press. Vol. **II**, pp. 255-527.

Evan, G. I., Lewis, G. K., Ramsay, G. and Bishop, J. M. (1985) Isolation of monoclonal antibodies specific for human c-myc proto- oncogene product. *Mol. Cell. Biol.* **5**: 3610-3616.

Fairman, R., Chao, H. G., Mueller, L., Lavoie, T. B., Shen, L., Novotny, J. and Matsueda, G. R. (1995) Characterization of a new four-chain coiled-coil: influence of chain length on stability. *Protein Sci.* **4**: 1457-1469.

Fairman, R., Chao, H. G., Lavoie, T. B., Villafranca, J. J., Matsueda, G. R. and Novotny, J. (1996) Design of heterotetrameric coiled coils: evidence for increased stabilization by Glu(-)-Lys(+) ion pair interactions. *Biochem.* **35**: 2824-2829.

Fasman, G. D., Ed. (1996) *Circular Dichroism and the Conformational Analysis of Biomolecules*. New York, Plenum Press.

Fassler, J., Landsman, D., Acharya, A., Moll, J. R., Bonovich, M. and Vinson, C. (2002) B-ZIP proteins encoded by the *Drosophila* genome: Evaluation of potential dimerization partners. *Genome Res.* **12**: 1190-1200.

Fauchere, J. and Pliska, V. (1983) Hydrophobic parameters of amino acid side chains from the partitioning of N-acetyl-amino-acid amides. *Eur. J. Med. Chem.* **18**: 369-375.

Fersht, A. R. and Serrano, L. (1993) Principles of protein stability derived from protein engineering experiments. *Curr. Opin. Struct. Biol.* **3**: 75-83.

Field, J., Nikawa, J., Broek, D., MacDonald, B., Rodgers, L., Wilson, I. A., Lerner, R. A. and Wigler, M. (1988) Purification of a RAS-responsive adenylyl cyclase complex from Saccharomyces cerevisiae by use of an epitope addition method. *Mol. Cell. Biol.* **8**: 2159-2165.

Fields, G. B., Ed. (1997) *Solid-Phase Peptide Synthesis. Methods Enzymol.* New York, Academic Press.

Fiori, W. R., Miick, S. M. and Millhauser, G. L. (1993) Increasing sequence length favors α-helix over 3_{10}-helix in alanine-based peptides: evidence for a length-dependent structural transition. *Biochem.* **32**: 11957-11962.

Fisher, R. J. and Fivash, M. (1994) Surface plasmon resonance based methods for measuring the kinetics and binding affinities of biomolecular interactions. *Curr. Opin. Biotechnol.* **5**: 389-395.

Fivash, M., Towler, E. M. and Fisher, R. J. (1998) BIAcore for macromolecular interaction. *Curr. Opin. Biotechnol.* **9**: 97-101.

Frank, S., Lustig, A., Schulthess, T., Engel, J. and Kammerer, R. A. (2000) A Distinct Seven-residue Trigger Sequence Is Indispensable for Proper Coiled-coil Formation of the Human Macrophage Scavenger Receptor Oligomerization Domain. *J. Biol. Chem.* **275**: 11672-11677.

Fu, H., Reis, N., Lee, Y., Glickman, M. H. and Vierstra, R. D. (2001) Subunit interaction maps for the regulatory particle of the 26S proteasome and the COP9 signalosome. *EMBO J.* **20**: 7096-7107.

Gans, P. J., Lyu, P. C., Manning, M. C., Woody, R. W. and Kallenbach, N. R. (1991) The helix-coil transition in heterogeneous peptides with specific side-chain interactions: theory and comparison with CD spectral data. *Biopolym.* **31**: 1605-1614.

Gee, M. A., Heuser, J. E. and Vallee, R. B. (1997) An extended microtubule-binding structure within the dynein motor domain. *Nature* **390**: 636-639.

Gee, M. A. and Vallee, R. B. (1998) The role of the dynein stalk in cytoplasmic and flagellar motility. *Eur. Biophys. J.* **27**: 466-473.

Gibbons, I. R. and Rowe, A. J. (1965) Dynein: A protein with adenosine triphosphatase activity from cilia. *Science* **149**: 424-426.

Gonzalez Jr., L., Plecs, J. J. and Alber, T. (1996) An engineered allosteric switch in leucine-zipper oligomerization. *Nature Struct. Biol.* **3**: 510-515.

Goodenough, U. and Heuser, J. E. (1982) Substructure of the outer dynein arm. *J. Cell Biol.* **95**: 798-815.

Goodenough, U. and Heuser, J. (1984) Structural comparison of purified dynein proteins with *in situ* dynein arms. *J. Mol. Biol.* **180**: 1083-1118.

Gooding, K. M. and Regnier, F. E., Eds. (1990) *HPLC of Biological Macromolecules.* Chromatographic Science Series. New York, Marcel Dekker, Inc.

Gooding, K. M. and Regnier, F. E., Eds. (2002) *HPLC of Biological Macromolecules.* Chromatographic Science Series. New York, Marcel Dekker, Inc.

Goodman, E. M. and Kim, P. S. (1991) Periodicity of amide proton exchange rates in a coiled-coil leucine zipper peptide. *Biochem.* **30**: 11615-11620.

Gout, I., Dhand, R., Hiles, I. D., Fry, M. J., Panayotou, G., Das, P., Truong, O., Totty, N. F., Hsuan, J. and Booker, G. W. (1993) The GTPase dynamin binds to and is activated by a subset of SH3 domains. *Cell* **75**: 25-36.

Graddis, T. J., Myszka, D. G. and Chaiken, I. M. (1993) Controlled formation of model homo- and heterodimer coiled-coil polypeptides. *Biochem.* **32**: 12664-12671.

Grant, G. A., Ed. (1992). *Synthetic Peptides: A User's Guide*. New York, W. H. Freeman and Company.

Greenfield, N. J. (1996) Methods to estimate the conformation of proteins and polypeptides from circular dichroism data. *Anal. Biochem.* **235**: 1-10.

Greenfield, N. J. and Hitchcock-DeGregori, S. E. (1995) The stability of tropomyosin, a two-stranded coiled-coil protein, is primarily a function of the hydrophobicity of residues at the helix-helix interface. *Biochem.* **34**: 16797-16805.

Guo, D., Mant, C. T. and Hodges, R. S. (1987) Effects of ion-pairing reagents on the prediction of peptide retention in reversed-phase high-performance liquid chromatography. *J. Chromatogr.* **386**: 205-222.

Gutin, A. M., Abkevich, V. I. and Shakhnovich, E. I. (1996) Chain length scaling of protein folding time. *Phys. Rev. Lett.* **77**: 5433-5436.

Gutte, B., Ed. (1995). *Peptides: Synthesis, Structures, and Applications*. San Diego, Academic Press.

Gyuris, J., Golemis, E., Chertkov, H. and Brent, R. (1993) Cdi1, a human G1 and S phase protein phosphatase that associates with Cdk2. *Cell* **75**: 791-803.

Habura, A., Tikhonenko, I., Chisholm, R. L. and Koonce, M. P. (1999) Interaction mapping of a dynein heavy chain: Identification of dimerization and intermediate-chain binding domains. *J. Biol. Chem.* **274**: 15447-15453.

Hagihara, Y., Aimoto, S., Fink, A. L. and Goto, Y. (1993) Guanidine hydrochloride-induced folding of proteins. *J. Mol. Biol.* **231**: 180-184.

Hagihara, Y., Tan, Y. and Goto, Y. (1994) Comparison of the conformational stability of the molten globule and native states of horse cytochrome c. *J. Mol. Biol.* **237**: 336-348.

Harbury, P. B., Zhang, T., Kim, P. S. and Alber, T. (1993). A switch between two-, three, and four-stranded coiled coils in GCN4 leucine zipper mutants. *Science* **262**: 1401-1407.

Hayes, D. B., Laue, T. and Philo, J. (1998). Sedimentation Interpretation Program, Copyright (c) 1995-1998.

Hearn, M. T. W., Ed. (1991). *HPLC of Proteins, Peptides, and Polynucleotides*. New York, VCH.

Herskovits, J. S., Burgess, C. C., Obar, R. A. and Vallee, R. B. (1993a) Effects of mutant rat dynamin on endocytosis. *J. Cell Biol.* **122**: 565-578.

Herskovits, J. S., Shpetner, H. S., Burgess, C. C. and Vallee, R. B. (1993b) Microtubules and Src homology 3 domains stimulate the dynamin GTPase via its C-terminal domain. *Proc. Natl. Acad. Sci.* **90**: 11468-11472.

Hicks, M. R., Holberton, D. V., Kowalczyk, C. and Woolfson, D. N. (1997) Coiled-coil assembly by peptides with non-heptad sequence motifs. *Folding and Design* **2**: 149-158.

Hinshaw, J. E. and Schmid, S. L. (1995) Dynamin self-assembles into rings suggesting a mechanism for coated vesicle budding. *Nature* **374**: 190-192.

Hirokawa, N. (1998) Kinesin and dynein superfamily proteins and the mechanism of organelle transport. *Science* **279**: 519-526.

Hirose, K. and Amos, L. A. (1999) Three-dimensional structure of motor molecules. *Cell. Mol. Life Sci.* **56**: 184-199.

Hodges, R. S. (1996) De novo design of α-helical proteins: basic research to medical applications. *Biochem. Cell Biol.* **74**: 133-154.

Hodges, R. S., Semchuk, P. D., Taneja, A. K., Kay, C. M., Parker, J. M. R. and Mant, C. T. (1988) Protein design using model synthetic peptides. *Pept. Res.* **1**: 19-30.

Hodges, R. S., Sodek, J., Smillie, L. B. and Jurasek, L. (1972) Tropomyosin: amino acid sequence and coiled-coil structure. *Cold Spring Harbor Symp. Quant. Biol.* **37**: 299-310.

Hodges, R. S., Zhou, N. E., Kay, C. M. and Semchuk, P. D. (1990) Synthetic model proteins: contribution of hydrophobic residues and disulfide bonds to protein stability. *Pept. Res.* **3**: 123-137.

Holtzer, A. and Holtzer, M. E. (1990) α-Helix to random-coil transitions of two-chain coiled coils: the use of physical models in treating thermal denaturation equilibria of isolated subsequences of αα-tropomyosin. *Biopolym.* **30**: 1231-1241.

Holtzer, M. E., Bretthorst, G. L., d'Avignon, D. A., Angeletti, R. H., Mints, L. and Holtzer, A. (2001a) Temperature dependence of the folding and unfolding kinetics of the GCN4 leucine zipper via $^{13}\mathrm{C}^{\alpha}$-NMR. *Biophys. J.* **80**: 939-951.

Holtzer, M. E., Crimmins, D. L. and Holtzer, A. (1994) Structural stability of short subsequences of the tropomyosin chain. *Biopolym.* **35**: 125-136.

Holtzer, M. E. and Holtzer, A. (1991) Uncooperative block in the tropomyosin coiled coil. *J. Am. Chem. Soc.* **113**: 7444-7445.

Holtzer, M. E., Lovett, E. G., d'Avignon, D. A. and Holtzer, A. (1997) Thermal unfolding in a GCN4-like leucine zipper: $^{13}\mathrm{C}^{\alpha}$ NMR chemical shifts and local unfolding curves. *Biophys. J.* **73**: 1031-1041.

Holtzer, M. E., Mints, L., Angeletti, R. H., d'Avignon, D. A. and Holtzer, A. (2001b) CD and $^{13}\mathrm{C}^{\alpha}$-NMR studies of folding equilibria in a two-stranded coiled coil formed by residues 190-254 of α-tropomyosin. *Biopolym.* **59**: 257-265.

Honig, B. (1999) Protein folding: from the Levinthal paradox to structure prediction. *J. Mol. Biol.* **293**: 283-293.

Honig, B. and Yang, A.-S. (1995) Free energy balance in protein folding. *Adv. Protein Chem.* **46**: 27-58.

Hoshino, M., Yumoto, N., Yoshikawa, S. and Goto, Y. (1997) Design and characterization of the anion-sensitive coiled-coil peptide. *Protein Sci.* **6**: 1396-1404.

Hoyne, P. A., Cosgrove, L. J., McKern, N. M., Bentley, J. D., Ivancic, N., Elleman, T. C. and Ward, C. W. (2000) High affinity insulin binding by soluble insulin receptor extracellular domain fused to a leucine zipper. *FEBS Lett.* **479**: 15-18.

Hu, J. C., O'Shea, E. K., Kim, P. S. and Sauer, R. T. (1990) Sequence requirements for coiled-coils: analysis with lambda repressor- GCN4 leucine zipper fusions. *Science* **250**: 1400-1403.

Ibarra-Molero, B., Makhatadze, G. I. and Matthews, C. R. (2001) Mapping the energy surface for the folding reaction of the coiled-coil peptide GCN4-p1. *Biochem.* **40**: 719-731.

Jelesarov, I. and Bosshard, H. R. (1996) Thermodynamic characterization of the coupled folding and association of heterodimeric coiled coils (leucine zippers). *J. Mol. Biol.* **263**: 344-358.

Jelesarov, I., Durr, E., Thomas, R. M. and Bosshard, H. R. (1998) Salt effects on hydrophobic interaction and charge screening in the folding of a negatively charged peptide to a coiled coil (leucine zipper). *Biochem.* **37**: 7539-7550.

Johnson, K. A. (1983) The pathway of ATP hydrolysis by dynein: kinetics of a presteady state phosphate burst. *J. Biol. Chem.* **258**: 13825-13832.

Johnson, M. L., Correia, J. J., Yphantis, D. A. and Halvorson, H. R. (1981) Analysis of data from the analytical ultracentrifuge by nonlinear least-squares techniques. *Biophys. J.* **36**: 575-588.

Johnson Jr., W. C. (1990) Protein secondary structure and circular dichroism: a practical guide. *Proteins* **7**: 205-214.

Kamal, A. and Goldstein, L. S. B. (2000) Connecting vesicle transport to the cytoskeleton. *Curr. Opin. Cell Biol.* **12**: 503-508.

Kammerer, R. A., Jaravine, V. A., Frank, S., Schulthess, T., Landwehr, R., Lustig, A., Garcia-Echeverria, C., Alexandrescu, A. T., Engel, J. and Steinmetz, M. O. (2001) An intrahelical salt bridge within the trigger site stabilizes the GCN4 leucine zipper. *J. Biol. Chem.* **276**: 13685-13688.

Kammerer, R. A., Schulthess, T., Landwehr, R., Lustig, A., Engel, J., Aebi, U. and Steinmetz, M. O. (1998) An autonomous folding unit mediates the assembly of two-stranded coiled coils. *Proc. Natl. Acad. Sci.* **95**: 13419-13424.

Karcher, R. L., Deacon, S. W. and Gelfand, V. I. (2002) Motor-cargo interactions: the key to transport specificity. *Trends Cell Biol.* **12**: 21-27.

Karki, S. and Holzbaur, E. L. F. (1995) Affinity chromatography demonstrates a direct binding between cytoplasmic dynein and the dynactin complex. *J. Biol. Chem.* **270**: 28806-28811.

Karki, S. and Holzbaur, E. L. F. (1999) Cytoplasmic dynein and dynactin in cell division and intracellular transport. *Curr. Opin. Cell Biol.* **11**: 45-53.

Karlsson, R., Michaelsson, A. and Mattsson, L. (1991) Kinetic analysis of monoclonal antibody-antigen interactions with a new biosensor based analytical system. *J. Immunol. Methods* **145**: 229-240.

Karlsson, R. and Falt, A. (1997) Experimental design for kinetic analysis of protein-protein interactions with surface plasmon resonance biosensors. *J. Immunol. Methods* **200**: 121-133.

Karplus, P. A. (1997) Hydrophobicity regained. *Protein Sci.* **6**: 1302-1307.

Kellis Jr., J. T., Nyberg, K. and Fersht, A. R. (1989) Energetics of complementary side-chain packing in a protein hydrophobic core. *Biochem.* **28**: 4914-4922.

Kellis Jr., J. T., Nyberg, K., Sali, D. and Fersht, A. R. (1988) Contribution of hydrophobic interactions to protein stability. *Nature* **333**: 784-786.

Kelly, S. M. and Price, N. C. (1997) The application of circular dichroism to studies of protein folding and unfolding. *Biochim. Biophys. Acta* **1338**: 161-185.

Kim, K. K., Yokota, H. and Kim, S.-H. (1999) Four-helical-bundle structure of the cytoplasmic domain of a serine chemotaxis receptor. *Nature* **400**: 787-792.

King, S. J. and Schroer, T. A. (2000) Dynactin increases the processivity of the cytoplasmic dynein motor. *Nature Cell Biol.* **2**: 20-24.

King, S. M. (2000a) AAA domains and organization of the dynein motor unit. *J. Cell Sci.* **113**: 2521-2526.

King, S. M. (2000b) The dynein microtubule motor. *Biochim. Biophys. Acta* **1496**: 60-75.

Kini, A. R. and Collins, C. A. (2001) Modulation of cytoplasmic dynein ATPase activity by the accessory subunits. *Cell Motil. Cytoskel.* **48**: 52-60.

Kirkland, J. J., Dilks Jr., C. H. and Henderson, J. E. (1993) Technologies for an improved C18 stationary phase in reversed-phase HPLC separations. *LC-GC* **11**: 290-297.

Kiyokawa, T., Kanaori, K., Tajima, K. and Tanaka, T. (2001) Engineering of the hydrophobic core of an α-helical coiled coil. *Biopolym.* **55**: 407-414.

Knappenberger, J. A., Smith, J. E., Thorpe, S. H., Zitzewitz, J. A. and Matthews, C. R. (2002) A buried polar residue in the hydrophobic interface of the coiled-coil peptide, GCN4-p1, plays a thermodynamic, not a kinetic role in folding. *J. Mol. Biol.* **321**: 1-6.

Kohn, W. D. and Hodges, R. S. (1998) De novo design of α-helical coiled coils and bundles: models for the development of protein-design principles. *TIBTECH* **16**: 379-389.

Kohn, W. D., Kay, C. M. and Hodges, R. S. (1995a) Protein destabilization by electrostatic repulsions in the two-stranded α-helical coiled-coil/leucine zipper. *Protein Sci.* **4**: 237-250.

Kohn, W. D., Kay, C. M. and Hodges, R. S. (1998a) Effects of lanthanide binding on the stability of *de novo* designed α-helical coiled-coils. *J. Pept. Res.* **51**: 9-18.

Kohn, W. D., Kay, C. M. and Hodges, R. S. (1998b) Orientation, position, additivity, and oligomerization-state effects of interhelical ion pairs in α-helical coiled-coils. *J. Mol. Biol.* **283**: 993-1012.

Kohn, W. D., Mant, C. T. and Hodges, R. S. (1997) α-Helical protein assembly motifs. *J. Biol. Chem.* **272**: 2583-2586.

Kohn, W. D., Monera, O. D., Kay, C. M. and Hodges, R. S. (1995b) The effects of interhelical electrostatic repulsions between glutamic acid residues in controlling the dimerization and stability of two-stranded α-helical coiled-coils. *J. Biol. Chem.* **270**: 25495-25506.

Koonce, M. P. (1997) Identification of a microtubule-binding domain in a cytoplasmic dynein heavy chain. *J. Biol. Chem.* **272**: 19714-19718.

Koonce, M. P. and Tikhonenko, I. (2000) Functional elements within the dynein microtubule-binding domain. *Mol. Biol. Cell* **11**: 523-529.

Kortt, A. A., Oddie, G. W., Iliades, P., Gruen, L. C. and Hudson, P. G. (1997) Nonspecific amine immobilization of ligand can be a potential source of error in BIAcore binding experiments and may reduce binding affinities. *Anal. Biochem.* **253**: 103-111.

Kostelny, S. A., Cole, M. S. and Tso, J. Y. (1992) Formation of a bispecific antibody by the use of leucine zippers. *J. Immunol.* **148**: 1547-1553.

Kozielski, F., Sack, S., Marx, A., Thormahlen, M., Schonbrunn, E., Biou, V., Thompson, A., Mandelkow, E. M. and Mandelkow, E. (1997) The crystal structure of dimeric kinesin and implications for microtubule-dependent motility. *Cell* **91**: 985-994.

Krittanai, C. and Johnson Jr., W. C. (2000) The relative order of helical propensity of amino acids changes with solvent environment. *Proteins* **39**: 132-141.

Krylov, D., Barchi, J. and Vinson, C. (1998) Inter-helical interactions in the leucine zipper coiled coil dimer: pH and salt dependence of coupling energy between charged amino acids. *J. Mol. Biol.* **279**: 959-972.

Krylov, D., Mikhailenko, I. and Vinson, C. (1994) A thermodynamic scale for leucine zipper stability and dimerization specificity: **e** and **g** interhelical interactions. *EMBO J.* **13**: 2849-2861.

Kumar, K. and Nussinov, R. (2002) Close-range electrostatic interactions in proteins. *ChemBioChem* **3**: 604-617.

Kwok, S. C., Mant, C. T. and Hodges, R. S. (1998) Effects of α-helical and β-sheet propensities of amino acids on protein stability *Peptides 1998*. (Eds. S. Bajusz and F. Hudecz) Budapest, Akademiai Kiado pp. 34-35.

Landschulz, W. H., Johnson, P. F. and McKnight, S. L. (1988) The leucine zipper: a hypothetical structure common to a new class of DNA binding proteins. *Science* **240**: 1759-1764.

Lau, S. Y. M., Taneja, A. K. and Hodges, R. S. (1984) Synthesis of a model protein of defined secondary and quaternary structure: effect of chain length on the stabilization and formation of two-stranded α-helical coiled-coils. *J. Biol. Chem.* **259**: 13253-13261.

Laue, T. M., Shah, B. D., Ridgeway, T. M. and Pelletier, S. L. (1992) Computer-aided interpretation of analytical sedimentation data for proteins. *Analytical ultracentrifugation in biochemistry and polymer science*. (Eds. Harding, S. E., Rowe, A. J. and Horton, J. C.), The Royal Society of Chemistry pp. 90-125.

Lavigne, P., Crump, M. P., Gagne, S. M., Hodges, R. S., Kay, C. M. and Sykes, B. D. (1998) Insights into the mechanism of heterodimerization from the 1H-NMR solution structure of the c-Myc-Max heterodimeric leucine zipper. *J. Mol. Biol.* **281**: 165-181.

Lavigne, P., Kondejewski, L. H., Houston Jr., M. E., Sonnichsen, F. D., Lix, B., Sykes, B. D., Hodges, R. S. and Kay, C. M. (1995) Preferential heterodimeric parallel coiled-coil formation by synthetic Max and c-Myc leucine zippers: a description of putative electrostatic interactions responsible for the specificity of heterodimerization. *J. Mol. Biol.* **254**: 505-520.

Lavigne, P., Sonnichsen, F. D., Kay, C. M. and Hodges, R. S. (1996) Interhelical salt bridges, coiled-coil stability, and specificity of dimerization. *Science* **271**: 1136-1138.

Lazar, G. A. and Handel, T. M. (1998) Hydrophobic core packing and protein design. *Curr. Op. Chem. Biol.* **2**: 675-679.

Lee, D. L., Lavigne, P. and Hodges, R. S. (2001) Are trigger sequences essential in the folding of two-stranded α-helical coiled-coils? *J. Mol. Biol.* **306**: 539-553.

Levinthal, C. (1968) Are there pathways for protein folding? *J. Chim. Phys.* **65**: 44-45.

Lindner, H., Sarg, B., Meraner, C. and Helliger, W. (1996) Separation of acetylated core histones by hydrophilic-interaction liquid chromatography. *J. Chromatogr.* **743**: 137-144.

Lindner, H., Sarg, B. and Helliger, W. (1997) Application of hydrophilic-interaction liquid chromatography to the separation of phosphorylated H1 histones. *J. Chromatogr.* **782**: 55-62.

Litowski, J. R. and Hodges, R. S. (2001) Designing heterodimeric two-stranded α-helical coiled-coils: The effect of chain length on protein folding, stability and specificity. *J. Pept. Res.* **58**: 477-492.

Liparoto, S. F. and Ciardelli, T. L. (1999) Biosensor analysis of the interleukin-2 receptor complex. *J. Mol. Recognit.* **12**: 316-321.

Liu, J. and Rost, B. (2001) Comparing function and structure between entire proteomes. *Protein Sci.* **10**: 1970-1979.

Liu, J. P., Zhang, Q. X., Baldwin, G. and Robinson, P. J. (1996) Calcium binds dynamin I and inhibits its GTPase activity. *J. Neurochem.* **66**: 2074-2081.

Liu, R., Baase, W. A. and Matthews, B. W. (2000) The introduction of strain and its effects on the structure and stability of T4 lysozyme. *J. Mol. Biol.* **295**: 127-145.

Lovett, E. G., d'Avignon, D. A., Holtzer, M. E., Braswell, E., Zhu, D. and Holtzer, A. (1996) Observation via one-dimensional $^{13}C^{\alpha}$ NMR of local conformational substates in thermal unfolding equilibria of a synthetic analog of the GCN4 leucine zipper. *Proc. Natl. Acad. Sci.* **93**: 1781-1785.

Lowey, S. (1965) Comparative study of the α-helical muscle proteins. Tyrosyl titration and effect of pH on conformation. *J. Biol. Chem.* **240**: 2421-2427.

Lu, S. M. and Hodges, R. S. (2002) A de novo designed template for generating conformation-specific antibodies that recognize α-helices in proteins. *J. Biol. Chem.* **277**: 23515-23524.

Lumb, K. J. and Kim, P. S. (1995a) A buried polar interaction imparts structural uniqueness in a designed heterodimeric coiled coil. *Biochem.* **34**: 8642-8648.

Lumb, K. J. and Kim, P. S. (1995b) Measurement of interhelical electrostatic interactions in the GCN4 leucine zipper. *Science* **268**: 436-439.

Luo, P. and Baldwin, R. L. (1999) Interaction between water and polar groups of the helix backbone: an important determinant of helix propensities. *Proc. Natl. Acad. Sci.* **96**: 4930-4935.

Lupas, A. (1996) Coiled coils: new structures and new functions. *TIBS* **21**: 375-382.

Lupas, A., Van Dyke, M. and Stock, J. (1991) Predicting coiled coils from protein sequences. *Science* **252**: 1162-1164.

Lyu, P. C., Liff, M. I., Marky, L. A. and Kallenbach, N. R. (1990) Side chain contributions to the stability of α-helical structure in peptides. *Science* **250**: 669-673.

Mann, M., Hendrickson, R. C. and Pandey, A. (2001) Analysis of proteins and proteomes by mass spectrometry. *Ann. Rev. Biochem.* **70**: 437-473.

Mant, C. T. and Hodges, R. S. (1985) Separation of peptides by strong cation-exchange high-performance liquid chromatography. *J. Chromatogr.* **327**: 147-155.

Mant, C. T. and Hodges, R. S., Eds. (1991a) *High-Performance Liquid Chromatography of Peptides and Proteins: Separation, Analysis, and Conformation.* Boca Raton, FL., CRC Press.

Mant, C. T. and Hodges, R. S. (1991b) The use of peptide standards for monitoring ideal and non-ideal behavior in cation-exchange chromatography. *High-Performance Liquid Chromatography of Peptides and Proteins: Separation, Analysis, and Conformation.* (Eds. Mant, C. T. and Hodges, R. S. Boca Raton, FL.), CRC Press, pp. 171-185.

Mant, C. T., Kondejewski, L. H., Cachia, P. J., Monera, O. D. and Hodges, R. S. (1997) Practical aspects of analysis of synthetic peptides by high-performance liquid chromatography. *Methods Enzymol.* **289**: 426-469.

Mant, C. T., Kondejewski, L. H. and Hodges, R. S. (1998a) Hydrophilic interaction/cation-exchange chromatography for separation of cyclic peptides. *J. Chromatogr.* **816**: 79-88.

Mant, C. T., Litowski, J. R. and Hodges, R. S. (1998b) Hydrophilic interaction/cation-exchange chromatography for separation of amphipathic α-helical peptides. *J. Chromatogr.* **816**: 65-78.

Mant, C. T. and Hodges, R. S. (2002). Analytical HPLC of peptides. *HPLC of Biological Macromolecules.* (Eds. Gooding, K. M. and Regnier, F. E.) New York, Marcel Dekker, Inc., pp. 433-511.

Marquardt, D. W. (1963) *J. Soc. Indust. Appl. Math.* **11**: 431-441.

Marti, D. N., Jelesarov, I. and Bosshard, H. R. (2000) Interhelical Ion Pairing in Coiled Coils: Solution Structure of a Heterodimeric Leucine Zipper and Determination of pKa Values of Glu Side Chains. *Biochem.* **39**: 12804-12818.

Matthews, B. W. (1995) Studies on protein stability with T4 lysozyme. *Adv. Protein Chem.* **46**: 249-278.

Mayr, L. M. and Schmid, F. X. (1993) Stabilization of a protein by guanidinium chloride. *Biochem.* **32**: 7994-7998.

McClain, D. L., Binfet, J. P. and Oakley, M. G. (2001) Evaluation of the energetic contribution of interhelical coulombic interactions for coiled-coil helix orientation specificity. *J. Mol. Biol.* **313**: 371-383.

McClain, D. L., Gurnon, D. G. and Oakley, M. G. (2002) Importance of potential interhelical salt-bridges involving interior residues for coiled-coil stability and quaternary structure. *J. Mol. Biol.* **324**: 257-270.

McRorie, D. K. and Voelker, P. J. (1993). *Self-Associating Systems in the Analytical Ultracentrifuge*. Palo Alto, CA, Beckman, Inc.

Meier, M., Lustig, A., Aebi, U. and Burkhard, P. (2002) Removing an interhelical salt bridge abolishes coiled-coil formation in a de novo designed peptide. *J. Struct. Biol.* **137**: 65-72.

Melen, K., Ronni, T., Broni, B., Krug, R. M., von Bonsdorff, C. H. and Julkunen, I. (1992) Interferon-induced Mx proteins form oligomers and contain a putative leucine zipper. *J. Biol. Chem.* **267**: 25898-25907.

Merrifield, R. B. (1963) Solid phase peptide synthesis. I. The synthesis of a tetrapeptide. *J. Am. Chem. Soc.* **85**: 2149-2154.

Merrifield, R. B. (1995). Solid-Phase Peptide Synthesis. *Peptides: Synthesis, Structures, and Applications.* Gutte, B. San Diego, Academic Press, Inc., pp.93-169.

Mikami, A., Paschal, B. M., Mazumdar, M. and Vallee, R. B. (1993) Molecular cloning of the retrograde transport motor cytoplasmic dynein (MAP 1C). *Neuron* **10**: 787-796.

Milisav, I. (1998) Dynein and dynein-related genes. *Cell Motil. Cytoskel.* **39**: 261-272.

Mo, J., Holtze, M. E. and Holtzer, A. (1991) Kinetics of self-assembly of *αα*-tropomyosin coiled coils from unfolded chains. *Proc. Natl. Acad. Sci.* **88**: 916-920.

Mocz, G. and Gibbons, I. R. (1996) Phase partition analysis of nucleotide binding to axonemal dynein. *Biochem.* **35**: 9204-9211.

Mocz, G. and Gibbons, I. R. (2001) Model for the motor component of dynein heavy chain based on homology to the AAA family of oligomeric ATPases. *Structure* **9**: 93-103.

Mohanty, D., Kolinski, A. and Skolnick, J. (1999) De novo simulations of the folding thermodynamics of the GCN4 leucine zipper. *Biophys. J.* **77**: 54-69.

Moitra, J., Szilak, L., Krylov, D. and Vinson, C. (1997) Leucine is the most stabilizing aliphatic amino acid in the **d** position of a dimeric leucine zipper coiled-coil. *Biochem.* **36**: 12567-12573.

Moll, J. R., Olive, M. and Vinson, C. (2000) Attractive interhelical electrostatic interactions in the proline- and acidic-rich (PAR) leucine zipper subfamily preclude heterodimerization with other basic leucine zipper subfamilies. *J. Biol. Chem.* **275**: 34826-34832.

Moll, J. R., Runinov, S. B., Pastan, I. and Vinson, C. (2001) Designed heterodimerizing leucine zippers with a range of pIs and stabilities up to 10^{-15} M. *Protein Sci.* **10**: 649-655.

Monera, O. D., Kay, C. M. and Hodges, R. S. (1994) Electrostatic interactions control the parallel and antiparallel orientation of α-helical chains in two-stranded α-helical coiled-coils. *Biochem.* **33**: 3862-3871.

Monera, O. D., Kay, C. M. and Hodges, R. S. (1994) Protein denaturation with guanidine hydrochloride or urea provides a different estimate of stability depending on the contributions of electrostatic interactions. *Protein Sci.* **3**: 1984-1991.

Monera, O. D., Sereda, T. J., Zhou, N. E., Kay, C. M. and Hodges, R. S. (1995) Relationship of sidechain hydrophobicity and α-helical propensity on the stability of the single-stranded amphipathic α-helix. *J. Pept. Sci.* **1**: 319-329.

Monera, O. D., Sonnichsen, F. D., Hicks, L., Kay, C. M. and Hodges, R. S. (1996a) The relative positions of alanine residues in the hydrophobic core control the formation of two-stranded or four-stranded α-helical coiled-coils. *Protein Eng.* **9**: 353-363.

Monera, O. D., Zhou, N. E., Kay, C. M. and Hodges, R. S. (1993) Comparison of antiparallel and parallel two-stranded α-helical coiled-coils. *J. Biol. Chem.* **268**: 19218-19227.

Monera, O. D., Zhou, N. E., Lavigne, P., Kay, C. M. and Hodges, R. S. (1996b) Formation of parallel and antiparallel coiled-coils controlled by the relative positions of alanine residues in the hydrophobic core. *J. Biol. Chem.* **271**: 3995-4001.

Moran, L. B., Schneider, J. P., Kentsis, A., Reddy, G. A. and Sosnick, T. R. (1999) Transition state heterogeneity in GCN4 coiled coil folding studied by using multisite mutations and crosslinking. *Proc. Natl. Acad. Sci.* **96**: 10699-10704.

Morrice, N. A. and Carrey, E. A. (1997) Peptide mapping. *Protein Structure: A Practical Approach.* (Ed. Creighton, T. E). New York, Oxford University Press, pp. 117-149.

Morton, T. A., Myszka, D. G. and Chaiken, I. M. (1995) Interpreting complex binding kinetics from optical biosensors: a comparison of analysis by linearization, the integrated rate equation, and numerical integration. *Anal. Biochem.* **227**: 176-185.

Muhlberg, A. B., Warnock, D. E. and Schmid, S. L. (1997) Domain structure and intramolecular regulation of dynamin GTPase. *EMBO J.* **16**: 6676-6683.

Muller, K. M., Arndt, K. M. and Alber, T. (2000) Protein fusions to coiled-coil domains. *Methods Enzymol.* **328**: 261-282.

Myers, J. K., Pace, C. N. and Scholtz, J. M. (1995) Denaturant *m* values and heat capacity changes: relation to changes in accessible surface areas of protein unfolding. *Protein Sci.* **4**: 2138-2148.

Myers, J. K., Pace, C. N. and Scholtz, J. M. (1997) Helix propensities are identical in proteins and peptides. *Biochem.* **36**: 10923-10929.

Myers, J. K., Smith, J. S., Pace, C. N. and Scholtz, J. M. (1996) The α-helix of ribonuclease T1 as an independent stability unit: direct comparison of peptide and protein stability. *J. Mol. Biol.* **263**: 390-395.

Myszka, D. G. and Chaiken, I. M. (1994) Design and characterization of an intramolecular antiparallel coiled-coil peptide. *Biochem.* **33**: 2363-2372.

Myszka, D. G., Arulanantham, P. R., Sana, T., Wu, Z., Morton, T. A. and Ciardelli, T. L. (1996) Kinetic analysis of ligand binding to interleukin-2 receptor complexes created on an optical biosensor surface. *Protein Sci.* **5**: 2468-2478.

Myszka, D. G. (1997) Kinetic analysis of macromolecular interactions using surface plasmon resonance biosensors. *Curr. Opin. Biotechnol.* **8**: 50-57.

Myszka, D. G., Morton, T. A., Doyle, M. L. and Chaiken, I. M. (1997) Kinetic analysis of a protein antigen-antibody interaction limited by mass transport on an optical biosensor. *Biophys. Chem.* **64**: 127-137.

Nakayama, M., Yazaki, K., Kusano, A., Nagata, K., Hanai, N. and Ishihama, A. (1993) Structure of mouse Mx1 protein. Molecular assembly and GTP-dependent conformational change. *J. Biol. Chem.* **268**: 15033-15038.

Nautiyal, S. and Alber, T. (1999) Crystal structure of a designed, thermostable, heterotrimeric coiled coil. *Protein Sci.* **8**: 84-90.

Nautiyal, S., Woolfson, D. N., King, D. S. and Alber, T. (1995) A designed heterotrimeric coiled-coil. *Biochem.* **34**: 11645-51.

Neuwald, A. F., Aravind, L., Spouge, J. L. and Koonin, E. V. (1999) AAA+: A class of chaperone-like ATPases associated with the assembly, operation, and disassembly of protein complexes. *Genome Res.* **9**: 27-43.

Noelkin, M. and Holtzer, A. (1964) The denaturation of paramyosin and tropomyosin by guanidine hydrochloride. *Biochemistry of Muscle Contraction.* (Ed. Gergely, J.). Boston, Little, Brown, and Co., pp. 374-378.

O'Brien, R., Sturtevant, J. M., Wrabl, J., Holtzer, M. E. and Holtzer, A. (1996) A scanning calorimetric study of unfolding equilibria in homodimeric chicken gizzard tropomyosins. *Biophys. J.* **70**: 2403-2407.

O'Connor-McCourt, M., De Crescenzo, G., Lortie, R., Lenferink, A. E. G. and Grothe, S. (1998) *Quantitative Analysis of Biospecific Interactions.* (Eds. Lundqvist, A. and Greijer, E. Chur), Switzerland, Harwood Academic Publisher, GMBH, pp. 175-190.

O'Neil, K. T. and DeGrado, W. F. (1990) A thermodynamic scale for the helix-forming tendencies of the commonly occurring amino acids. *Science* **250**: 646-651.

O'Shannessy, D. J. and Winzor, D. J. (1996) Interpretation of deviations from pseudo-first-order kinetic behavior in the characterization of ligand binding by biosensor technology. *Anal. Biochem.* **236**: 275-283.

O'Shea, E. K., Klemm, J. D., Kim, P. S. and Alber, T. (1991) X-ray structure of the GCN4 leucine zipper, a two-stranded, parallel coiled-coil. *Science* **254**: 539-544.

O'Shea, E. K., Lumb, K. J. and Kim, P. S. (1993) Peptide 'Velcro': design of a heterodimeric coiled-coil. *Curr. Biol.* **3**: 658-667.

O'Shea, E. K., Rutkowski, R. and Kim, P. S. (1989a) Evidence that the leucine zipper is a coiled-coil. *Science* **243**: 538-542.

O'Shea, E. K., Rutkowski, R. and Kim, P. S. (1992) Mechanism of specificity in the Fos-Jun oncoprotein heterodimer. *Cell* **68**: 699-708.

O'Shea, E. K., Rutkowski, R., Stafford III, W. F. and Kim, P. S. (1989b) Preferential heterodimer formation by isolated leucine zippers from Fos and Jun. *Science* **245**: 646-648.

Oakley, M. G. and Kim, P. S. (1998) A buried polar interaction can direct the relative orientation of helices in a coiled-coil. *Biochem.* **37**: 12603-12610.

Oas, T. G. and Endow, S. A. (1994) Springs and hinges: dynamic coiled coils and discontinuities. *TIBS* **19**: 51-54.

Obar, R. A., Collins, C. A., Hammarback, J. A., Shpetner, H. S. and Vallee, R. B. (1990) Molecular cloning of the microtubule-associated mechanochemical enzyme dynamin reveals homology with a new family of GTP-binding proteins. *Nature* **347**: 256-261.

Ogihara, N. L., Weiss, M. S., DeGrado, W. F. and Eisenberg, D. (1997) The crystal structure of the designed trimeric coiled coil coil-V*a*L*d*: Implications for engineering crystals and supramolecular assemblies. *Protein Sci.* **6**: 80-88.

Okamoto, P. M., Herskovits, J. S. and Vallee, R. B. (1997) Role of the basic, proline-rich region of dynamin in Src homology 3 domain binding and endocytosis. *J. Biol. Chem.* **272**: 11629-11635.

Omoto, C. K. and Johnson, K. A. (1986) Activation of the dynein adenosinetriphosphatase by microtubules. *Biochem.* **25**: 419-427.

Ozols, J. (1990) Amino acid analysis. *Methods Enzymol.* **182**: 587-601.

Pace, C. N. (1986) Determination and analysis of urea and guanidine hydrochloride denaturation curves. *Methods Enzymol.* **131**: 266-280.

Pace, C. N. and Shaw, K. L. (2000) Linear extrapolation method of analyzing solvent denaturation curves. *Proteins* **4**: 1-7.

Pace, C. N., Shirley, B. A., McNutt, M. and Gajiwala, K. (1996) Forces contributing to the conformational stability of proteins. *FASEB J.* **10**: 75-83.

Padmanabhan, S., York, E. J., Stewart, J. M. and Baldwin, R. L. (1996) Helix propensities of basic amino acids increase with the length of the side-chain. *J. Mol. Biol.* **257**: 726-734.

Paschal, B. M., King, S. M., Moss, A. G., Collins, C. A., Vallee, R. B. and Witman, G. B. (1987a) Isolated flagellar outer arm dynein translocates brain microtubules *in vitro*. *Nature* **330**: 672-674.

Paschal, B. M., Shpetner, H. S. and Vallee, R. B. (1987b) MAP 1C is a microtubule-activated ATPase which translocates microtubules in vitro and has dynein-like properties. *J. Cell Biol.* **105**: 1273-1282.

Paschal, B. M. and Vallee, R. B. (1987) Retrograde transport by the microtubule-associated protein MAP 1C. *Nature* **330**: 181-183.

Paulucci, A. A., Hicks, L., Machado, A., Miranda, M. T. M., Kay, C. M. and Farah, C. S. (2002) Specific sequences determine the stability and cooperativity of folding of the C-terminal half of tropomyosin. *J. Biol. Chem.* **277**: 39574-39584.

Pelletier, J. N., Arndt, K. M., Pluckthun, A. and Michnick, S. W. (1999) An in vivo library-versus-library selection of optimized protein-protein interactions. *Nature Biotechnol.* **17**: 683-690.

Peng, Z.-Y. and Wu, L. C. (2000) Autonomous protein folding units. *Adv. Protein Chem.* **53**: 1-47.

Phelan, P., Gorfe, A. A., Jelesarov, I., Marti, D. N., Warwicker, J. and Bosshard, H. R. (2002) Salt bridges destabilize a leucine zipper designed for maximized ion pairing between helices. *Biochem.* **41**: 2998-3008.

Phillips Jr., G. N. (1992) What is the pitch of the α-helical coiled-coil? *Proteins* **14**: 425-429.

Ploubidou, A. and Way, M. (2001) Viral transport and the cytoskeleton. *Curr. Opin. Cell Biol.* **13**: 97-105.

Press, W. H., Flannery, B. P., Teukolsky, S. A. and Vetterling, W. T. (1986) *Numerical recipes, the art of scientific computing*. Cambridge, Cambridge University Press.

Qian, H. (1994) A thermodynamic model for the helix-coil transition coupled to dimerization of short coiled-coil peptides. *Biophys. J.* **67**: 349-355.

Rabanal, F., DeGrado, W. F. and Dutton, P. L. (1996) Use of 2,2'-dithiobis(5-nitropyridine) for the heterodimerization of cysteine containing peptides. Introduction of the 5-nitro-2-pyridinesulfenyl group. *Tetrahedron Lett.* **37**: 1347-1350.

Radford, S. E. (2000) Protein folding: progress made and promises ahead. *TIBS* **25**: 611-618.

Regan, L., Rockwell, A., Wasserman, Z. and DeGrado, W. F. (1994) Disulfide crosslinks to probe the structure and flexibility of a designed four-helix bundle protein. *Protein Sci.* **3**: 2419-2427.

Rich, R. L. and Myszka, D. G. (2000) Advances in surface plasmon resonance biosensor analysis. *Curr Opin Biotechnol* **11**: 54-61.

Richards, F. M. (1977) Areas, volumes, packing, and protein structure. *Ann. Rev. Biophys. Bioeng.* **6**: 151-176.

Richards, F. M. and Lim, W. A. (1994) An analysis of packing in the protein folding problem. *Quart. Rev. Biophys.* **26**: 423-498.

Rieker, J. D. and Hu, J. C. (2000) Molecular applications of fusions to leucine zippers. *Methods Enzymol.* **328**: 282-296.

Ringstad, N., Nemoto, Y. and De Camilli, P. (1997) The SH3p4/Sh3p8/SH3p13 protein family: binding partners for synaptojanin and dynamin via a Grb2-like Src homology 3 domain. *Proc. Natl. Acad. Sci.* **94**: 8569-8574.

Rohl, C. A., Scholtz, J. M., York, E. J., Stewart, J. M. and Baldwin, R. L. (1992) Kinetics of amide proton exchange in helical peptides of varying chain lengths. Interpretation by the Lifson-Roig equation. *Biochem.* **31**: 1263-1269.

Roos, J. and Kelly, R. B. (1998) Dap160, a neural-specific Eps15 homology and multiple SH3 domain- containing protein that interacts with Drosophila dynamin. *J. Biol. Chem.* **273**: 19108-19119.

Root, M. J., Kay, M. S. and Kim, P. S. (2001) Protein Design of an HIV-1 Entry Inhibitor. *Science* **291**: 884-888.

Sakakibara, H., Kojima, H., Sakai, Y., Katayama, E. and Oiwa, K. (1999) Inner-arm dynein c of *Chlamydomonas* flagella is a single-headed processive motor. *Nature* **400**: 586-590.

Sale, W. S. and Fox, L. A. (1988) Isolated β-heavy chain subunit of dynein translocates microtubules in vitro. *J. Cell Biol.* **107**: 1793-1797.

Salim, K., Bottomley, M. J., Querfurth, E., Zvelebil, M. J., Gout, I., Scaife, R., Margolis, R. L., Gigg, R., Smith, C. I., Driscoll, P. C., Waterfield, M. D. and Panayotou, G. (1996) Distinct specificity in the recognition of phosphoinositides by the pleckstrin homology domains of dynamin and Bruton's tyrosine kinase. *EMBO J.* **15**: 6241-6250.

Samso, M., Radermacher, M., Frank, J. and Koonce, M. P. (1998) Structural characterization of a dynein motor domain. *J. Mol. Biol.* **276**: 927-937.

Schellman, J. A. (1978) Solvent denaturation. *Biopolym.* **17**: 1305-1322.

Schmid, S. L., McNiven, M. A. and De Camilli, P. (1998) Dynamin and its partners: a progress report. *Curr. Opin. Cell Biol.* **10**: 504-512.

Schnarr, N. A. and Kennan, A. J. (2001) Coiled-coil formation governed by unnatural hydrophobic core side chains. *J. Am. Chem. Soc.* **123**: 11081-11082.

Schnarr, N. A. and Kennan, A. J. (2002) Peptide Tic-Tac-Toe: Heterotrimeric coiled-coil specificity from steric matching of multiple hydrophobic side chains. *J. Am. Chem. Soc.* **124**: 9779-9783.

Schneider, J. P., Lear, J. D. and DeGrado, W. F. (1997) A designed buried salt bridge in a heterodimeric coiled coil. *J. Am. Chem. Soc.* **119**: 5742-5743.

Scholtz, J. M., Marqusee, S., Baldwin, R. L., York, E. J., Stewart, J. M., Santoro, M. and Bolen, D. W. (1991) Calorimetric determination of the enthalpy change for the α-helix to coil transition of an alanine peptide in water. *Proc. Natl. Acad. Sci.* **88**: 2854-2858.

Scholtz, J. M., Qian, H., York, E. J., Stewart, J. M. and Baldwin, R. L. (1991) Parameters of helix-coil transition theory for alanine-based peptides of varying chain lengths in water. *Biopolym.* **31**: 1463-1470.

Schuster, T. M. and Toedt, J. M. (1996) New revolutions in the evolution of analytical ultracentrifugation. *Curr. Opin. Struct. Biol.* **6**: 650-658.

Scott, C. A., Garcia, K. C., Carbone, F. R., Wilson, I. A. and Teyton, L. (1996) Role of chain pairing for the production of functional soluble IA major histocompatibility complex class II molecules. *J. Exp. Med.* **183**: 2087-2095.

Seo, J. and Cohen, C. (1993) Pitch diversity in α-helical coiled coils. *Proteins* **15**: 223-234.

Sereda, T. J., Mant, C. T. and Hodges, R. S. (1997) Use of sodium perchlorate at low pH for peptide separations by reversed-phase liquid chromatography. Influence of perchlorate ion on apparent hydrophilicity of positively charged amino acid side-chains. *J. Chromatogr.* **776**: 153-165.

Sereda, T. J., Mant, C. T., Sonnichsen, F. D. and Hodges, R. S. (1994) Reversed-phase chromatography of synthetic amphipathic α-helices as a model for ligand/receptor interactions. Effect of changing hydrophobic environment on the relative hydrophilicity/hydrophobicity of amino acid side-chains. *J. Chromatogr.* **676**: 139-153.

Serrano, L. (2000) The relationship between sequence and structure in elementary folding units. *Adv. Protein Chem.* **53**: 49-85.

Serrano, L., Horovitz, A., Avron, B., Bycroft, M. and Fersht, A. R. (1990) Estimating the contribution of engineered surface electrostatic interactions to protein stability by using double-mutant cycles. *Biochem.* **29**: 9343-52.

Sever, S. (2002) Dynamin and endocytosis. *Curr. Opin. Cell Biol.* **14**: 463-467.

Shiraki, K., Nishikawa, K. and Goto, Y. (1995) Trifluoroethanol-induced stabilization of the α-helical structure of β-lactoglobulin: implication for non-hierarchical protein folding. *J. Mol. Biol.* **245**: 180-194.

Shpetner, H. S., Paschal, B. M. and Vallee, R. B. (1988) Characterization of the microtubule-activated ATPase of brain cytoplasmic dynein (MAP1C). *J. Cell Biol.* **107**: 1001-1009.

Shpetner, H. S. and Vallee, R. B. (1989) Identification of dynamin, a novel mechanochemical enzyme that mediates interactions between microtubules. *Cell* **59**: 421-432.

Shpetner, H. S. and Vallee, R. B. (1992) Dynamin is a GTPase stimulated to high levels of activity by microtubules. *Nature* **355**: 733-735.

Shpetner, H. S., Herskovits, J. S. and Vallee, R. B. (1996) A binding site for SH3 domains targets dynamin to coated pits. *J. Biol. Chem.* **271**: 13-16.

Shortle, D. (1989) Probing the determinants of protein folding and stability with amino acid substitutions. *J. Biol. Chem.* **264**: 5315-5318.

Shortle, D., Stites, W. E. and Meeker, A. K. (1990) Contributions of the large hydrophobic amino acids to the stability of staphylococcal nuclease. *Biochem.* **29**.

Sibanda, B. L., Critchlow, S. E., Begun, J., Pei, X. Y., Jackson, S. P., Blundell, T. L. and Pellegrini, L. (2001) Crystal structure of an Xrcc4-DNA ligase IV complex. *Nature Struct. Biol.* **8**: 1015-1019.

Siegert, R., Leroux, M. R., Scheufler, C., Hartl, F. U. and Moarefi, I. (2000) Structure of the molecular chaperone prefoldin: unique interaction of multiple coiled coil tentacles with unfolded proteins. *Cell* **103**: 621-632.

Skehel, J. J. and Wiley, D. C. (1998) Coiled coils in both intracellular vesicle and viral membrane fusion. *Cell* **95**: 871-874.

Smillie, L. B. and Nattriss, M. (1991) Amino acid analysese of proteins and peptides: An overview. *High-Performance Liquid Chromatography of Peptides and Proteins:*

Separation, Analysis, and Conformation. (Eds. Mant, C. T. and Hodges, R. S.) Boca Raton, CRC Press, pp. 847-858.

Sodek, J., Hodges, R. S., Smillie, L. B. and Jurasek, L. (1972) Amino-acid sequence of rabbit skeletal tropomyosin and its coiled-coil structure. *Proc. Natl. Acad. Sci.* **69**: 3800-3804.

Sonnichsen, F. D., Van Eyk, J. E., Hodges, R. S. and Sykes, B. D. (1992) Effect of trifluoroethanol on protein secondary structure: an NMR and CD study using a synthetic actin peptide. *Biochem.* **31**: 8790-8798.

Sosnick, T. R., Jackson, S., Wilk, R. R., Englander, S. W. and DeGrado, W. F. (1996) The role of helix formation in the folding of a fully α-helical coiled coil. *Proteins* **24**: 427-432.

Spek, E. J., Bui, A. H., Lu, M. and Kallenbach, N. R. (1998) Surface salt bridges stabilize the GCN4 leucine zipper. *Protein Sci.* **7**: 2431-2437.

Steinmetz, M. O., Stock, A., Schulthess, T., Landwehr, R., Lustig, A., Faix, J., Gerisch, G., Aebi, U. and Kammerer, R. A. (1998) A distinct 14 residue site triggers coiled-coil formation in cortexillin I. *EMBO J.* **17**: 1883-1891.

Strelkov, S. V. and Burkhard, P. (2002) Analysis of α-helical coiled coils with the program TWISTER reveals a structural mechanism for stutter compensation. *J. Struct. Biol.* **137**: 54-64.

Su, J. Y., Hodges, R. S. and Kay, C. M. (1994) Effect of chain length on the formation and stability of synthetic α-helical coiled coils. *Biochem.* **33**: 15501-15510.

Susalka, S. J., Hancock, W. O. and Pfister, K. K. (2000) Distinct cytoplasmic dynein complexes are transported by different mechanisms in axons. *Biochim. Biophys. Acta* **146**: 76-88.

Sweitzer, S. M. and Hinshaw, J. E. (1998) Dynamin undergoes a GTP-dependent conformational change causing vesiculation. *Cell* **93**: 1021-1029.

Szokan, G., Torok, A. and Penke, B. (1987) High-performance liquid chromatographic detection of side reactions in peptide synthesis. *J. Chromatogr.* **387**: 267-280.

Takei, K., McPherson, P. S., Schmid, S. L. and De Camilli, P. (1995) Tubular membrane invaginations coated by dynamin rings are induced by GTP-gamma S in nerve terminals. *Nature* **374**: 186-190.

Takei, K., Haucke, V., Slepnev, V., Farsad, K., Salazar, M., Chen, H. and De Camilli, P. (1998) Generation of coated intermediates of clathrin-mediated endocytosis on protein-free liposomes. *Cell* **94**: 131-141.

Tang, Y., Ghirlanda, G., Vaidehi, N., Kua, J., Mainz, D. T., Goddard III, W. A., DeGrado, W. F. and Tirrell, D. A. (2001) Stabilization of coiled-coil peptide domains by introduction of trifluoroleucine. *Biochem.* **40**: 2790-2796.

Touhara, K., Inglese, J., Pitcher, J. A., Shaw, G. and Lefkowitz, R. J. (1994) Binding of G protein beta gamma-subunits to pleckstrin homology domains. *J. Biol. Chem.* **269**: 10217-10220.

Tripet, B., De Crescenzo, G., Grothe, S., O'Connor-McCourt, M. and Hodges, R. S. (2002) Kinetic analysis of the interactions between Troponin C and the C-terminal Troponin I regulatory region and validation of a new peptide delivery/capture system used for surface plasmon resonance. *J. Mol. Biol.* **323**: 345-362.

Tripet, B. and Hodges, R. S. (2001) STABLECOIL: an algorithm designed to predict the location and relative stability of coiled-coils in native protein sequences. *Peptides: The Wave of the Future, Proceedings of the 17th American Peptide Symposium.* (Eds. Lebl, M. and Houghten, R. A.) San Diego, American Peptide Society, pp. 365-366.

Tripet, B. and Hodges, R. S. (2002) Helix capping interactions stabilize the N-terminus of the kinesin neck coiled-coil. *J. Struct. Biol.* **137**: 220-235.

Tripet, B., Vale, R. D. and Hodges, R. S. (1997) Demonstration of coiled-coil interactions within the kinesin neck region using synthetic peptides. Implications for motor activity. *J. Biol. Chem.* **272**: 8946-8956.

Tripet, B., Wagschal, K., Lavigne, P., Mant, C. T. and Hodges, R. S. (2000) Effects of side-chain characteristics on stability and oligomerization state of a *de novo*-designed model coiled-coil: 20 amino acid substitutions in position "**d**". *J. Mol. Biol.* **300**: 377-402.

Tripet, B., Yu, L., Bautista, D. L., Wong, W. Y., Irvin, R. T. and Hodges, R. S. (1996) Engineering a *de novo*-designed coiled-coil heterodimerization domain for the rapid detection, purification and characterization of recombinantly expressed peptides and proteins. *Protein Eng.* **9**: 1029-1042.

Trybus, K. M., Freyzon, Y., Faust, L. Z. and Sweeney, H. L. (1997) Spare the rod, spoil the regulation: necessity for a myosin rod. *Proc. Natl. Acad. Sci.* **94**: 48-52.

Tuma, P. L., Stachniak, M. C. and Collins, C. A. (1993) Activation of dynamin GTPase by acidic phospholipids and endogenous rat brain vesicles. *J. Biol. Chem.* **268**: 17240-17246.

Tuma, P. L. and Collins, C. A. (1995) Dynamin forms polymeric complexes in the presence of lipid vesicles. Characterization of chemically cross-linked dynamin molecules. *J. Biol. Chem.* **270**: 26707-26714.

Tynan, S. H., Gee, M. A. and Vallee, R. B. (2000) Distinct but overlapping sites within the cytoplasmic dynein heavy chain for dimerization and for intermediate chain and light intermediate chain binding. *J. Biol. Chem.* **275**: 32769-32774.

Unger, K. K. (2002). Silica as a support in HPLC of Biomacromolecules. *HPLC of Biological Macromolecules*. (Eds. Gooding, K. M. and Regnier, F. E.) New York, Marcel Dekker, Inc., pp. 1-16.

Urrutia, R., Henley, J. R., Cook, T. and McNiven, M. A. (1997) The dynamins: redundant or distinct functions for an expanding family of related GTPases? *Proc. Natl. Acad. Sci.* **94**: 377-384.

Vale, R. D. (2000) AAA proteins: lords of the ring. *J. Cell Biol.* **150**: F13-F19.

Vale, R. D. and Milligan, R. A. (2000) The way things move: looking under the hood of molecular motor proteins. *Science* **288**: 88-95.

Vale, R. D., Soll, D. R. and Gibbons, I. R. (1989) One-dimensional diffusion of microtubules bound to dynein. *Cell* **59**: 915-925.

Vale, R. D. and Toyoshima, Y. Y. (1988) Rotation and translocation of microtubules in vitro induced by dyneins from *Tetrahymena* cilia. *Cell* **52**: 459-469.

Vallee, R. B. and Gee, M. A. (1998) Make room for dynein. *Trends Cell Biol.* **8**: 490-494.

van der Bliek, A. M. and Meyerowitz, E. M. (1991) Dynamin-like protein encoded by the Drosophila shibire gene associated with vesicular traffic. *Nature* **351**: 411-414.

van Holde, K. E. (1975). Sedimentation analysis of proteins. *The Proteins*. (Eds. Neurath, H. and Hill, R. L.) New York, Academic Press, Inc. Vol. **1**, pp. 225-291.

Vieth, M., Kolinski, A., Brooks III, C. L. and Skolnick, J. (1994) Prediction of the folding pathways and structure of the GCN4 leucine zipper. *J. Mol. Biol.* **237**: 361-367.

Vinson, C., Myakishev, M., Acharya, A., Mir, A. A., Moll, J. R. and Bonovich, M. (2002) Classification of human B-ZIP proteins based on dimerization properties. *Mol. Cell. Biol.* **22**: 6321-6335.

Vinson, C. R., Hai, T. and Boyd, S. M. (1993) Dimerization specificity of the leucine zipper-containing bZIP motif on DNA binding: prediction and rational design. *Gene & Dev.* **7**: 1047-1058.

Vu, C., Robblee, J., Werner, K. M. and Fairman, R. (2001) Effects of charged amino acids at **b** and **c** heptad positions on specificity and stability of four-chain coiled coils. *Protein Sci.* **10**: 631-637.

Wagschal, K., Tripet, B. and Hodges, R. S. (1999a) *De novo* design of a model peptide sequence to examine the effects of single amino acid substitutions in the hydrophobic core on both stability and oligomerization state of coiled-coils. *J. Mol. Biol.* **285**: 785-803.

Wagschal, K., Tripet, B., Lavigne, P., Mant, C. T. and Hodges, R. S. (1999b) The role of position "**a**" in determining the stability and oligomerization state of α-helical coiled-coils: 20 amino acid stability coefficients in the hydrophobic core of proteins. *Protein Sci.* **8**: 2312-2329.

Walshaw, J. and Woolfson, D. N. (2001a) Open-and-shut cases in coiled-coil assembly: α-Sheets and α-cylinders. *Protein Sci.* **10**: 668-673.

Walshaw, J. and Woolfson, D. N. (2001b) SOCKET: a program for identifying and analysing coiled-coil motifs within protein structures. *J. Mol. Biol.* **307**: 1427-1450.

Wang, Z., Khan, S. and Sheetz, M. P. (1995) Single cytoplasmic dynein molecule movements: characterization and comparison with kinesin. *Biophys. J.* **69**: 2011-2023.

Warnock, D. E., Terlecky, L. J. and Schmid, S. L. (1995) Dynamin GTPase is stimulated by crosslinking through the C-terminal proline-rich domain. *EMBO J.* **14**: 1322-1328.

Warnock, D. E., Hinshaw, J. E. and Schmid, S. L. (1996) Dynamin self-assembly stimulates its GTPase activity. *J. Biol. Chem.* **271**: 22310-22314.

Wendt, H., Baici, A. and Bosshard, H. R. (1994) Mechanism of assembly of a leucine zipper domain. *J. Am. Chem. Soc.* **116**: 6973-6974.

Wendt, H., Berger, C., Baici, A., Thomas, R. M. and Bosshard, H. R. (1995) Kinetics of folding of leucine zipper domains. *Biochem.* **34**: 4097-4107.

Wendt, H., Leder, L., Harma, H., Jelesarov, I., Baici, A. and Bosshard, H. R. (1997) Very rapid, ionic strength-dependent association and folding of a heterodimeric leucine zipper. *Biochem.* **36**: 204-213.

Woody, R. W. (1995) Circular dichroism. *Methods Enzymol.* **246**: 34-71.

Woolfson, D. N. and Alber, T. (1995) Predicting oligomerization states of coiled-coils. *Protein Sci.* **4**(8): 1596-1607.

Wu, Z., Goldstein, B., Laue, T. M., Liparoto, S. F., Nemeth, M. J. and Ciardelli, T. L. (1999) Solution assembly of the pseudo-high affinity and intermediate affinity interleukin-2 receptor complexes. *Protein Sci.* **8**: 482-489.

Wu, Z., Johnson, K. W., Goldstein, B., Choi, Y., Eaton, S. F., Laue, T. M. and Ciardelli, T. L. (1995) Solution assembly of a soluble, heterodimeric, high affinity interleukin-2 receptor complex. *J. Biol. Chem.* **270**: 16039-16044.

Xu, J., Baase, W. A., Baldwin, E. and Matthews, B. W. (1998) The response of T4 lysozyme to large-to-small substitutions within the core and its relation to the hydrophobic effect. *Protein Sci.* **7**: 158-177.

Yang, J., Spek, E. J., Gong, Y., Zhou, H. and Kallenbach, N. R. (1997) The role of context on α-helix stabilization: host-guest analysis in a mixed background peptide model. *Protein Sci.* **6**: 1264-1272.

Yoon, Y., Pitts, K. R., Dahan, S. and McNiven, M. A. (1998) A novel dynamin-like protein associates with cytoplasmic vesicles and tubules of the endoplasmic reticulum in mammalian cells. *J. Cell Biol.* **140**: 779-793.

Young, W. S. and Brooks III, C. L. (1996) A microscopic view of helix propagation: N and C-terminal helix growth in alanine helices. *J. Mol. Biol.* **259**: 560-572.

Yu, Y., Monera, O. D., Hodges, R. S. and Privalov, P. L. (1996) Ion pairs significantly stabilize coiled-coils in the absence of electrolyte. *J. Mol. Biol.* **255**: 367-372.

Zheng, J., Cahill, S. M., Lemmon, M. A., Fushman, D., Schlessinger, J. and Cowburn, D. (1996) Identification of the binding site for acidic phospholipids on the pH domain of dynamin: implications for stimulation of GTPase activity. *J. Mol. Biol.* **255**: 14-21.

Zhou, N. E., Kay, C. M. and Hodges, R. S. (1992a) Synthetic model proteins: positional effects of interchain hydrophobic interactions on stability of two-stranded α-helical coiled-coils. *J. Biol. Chem.* **267**: 2664-2670.

Zhou, N. E., Kay, C. M. and Hodges, R. S. (1992b) Synthetic model peptides: the relative contribution of leucine residues at the nonequivalent positions of the 3-4 hydrophobic repeat to the stability of the two-stranded α-helical coiled-coil. *Biochem.* **31**: 5739-5746.

Zhou, N. E., Kay, C. M. and Hodges, R. S. (1994a) The net energetic contribution of interhelical electrostatic attractions to coiled-coil stability. *Protein Eng.* **7**: 1365-1372.

Zhou, N. E., Kay, C. M. and Hodges, R. S. (1994b) The role of interhelical ionic interactions in controlling protein folding and stability. *J. Mol. Biol.* **237**: 500-512.

Zhou, N. E., Mant, C. T. and Hodges, R. S. (1990) Effect of preferred binding domains on peptide retention behaviou in reversed-phase chromatography: amphipathic α-helices. *Pept. Res.* **3**: 8-20.

Zhou, N. E., Monera, O. D., Kay, C. M. and Hodges, R. S. (1994c) α-Helical propensities of amino acids in the hydrophobic face of an amphipathic α-helix. *Prot. Pept. Lett.* **1**: 114-119.

Zhou, N. E., Zhu, B.-Y., Kay, C. M. and Hodges, R. S. (1992c) The two-stranded α-helical coiled-coil is an ideal model for studying protein stability and subunit interactions. *Biopolym.* **32**: 419-426.

Zhou, N. E., Zhu, B.-Y., Kay, C. M. and Hodges, R. S. (1993) Importance of intra-chain ionic interactions in stabilizing α-helices in proteins. *The Chinese Peptide Symposium,* Escom Science Publishers, pp. 217-220.

Zhu, B.-Y., Mant, C. T. and Hodges, R. S. (1991) Hydrophilic-interaction chromatography of peptides on hydrophilic and strong cation-exchange columns. *J. Chromatogr.* **548**: 13-24.

Zhu, B.-Y., Mant, C. T. and Hodges, R. S. (1992) Mixed-mode hydrophilic and ionic interaction chromatography rivals reversed-phase liquid chromatography for the separation of peptides. *J. Chromatogr.* **594**: 75-86.

Zhu, B.-Y., Zhou, N. E., Kay, C. M. and Hodges, R. S. (1993) Packing and hydrophobicity effects on protein folding and stability: Effects of β-branched amino acids, valine and isoleucine, on the folding and stability of two-stranded α-helical coiled coils/leucine zippers. *Protein Sci.* **2**: 383-394.

Zhu, B.-Y., Zhou, N. E., Semchuk, P. D., Kay, C. M. and Hodges, R. S. (1992) Design, synthesis and structural characterization of model heterodimeric coiled-coil proteins. *Int. J. Pept. Protein Res.* **40**: 171-179.

Zhu, H., Celinski, S. A., Scholtz, J. M. and Hu, J. C. (2001) An engineered leucine zipper **a** position mutant with an unusual three-state unfolding pathway. *Protein Sci.* **10**: 24-33.

Zitzewitz, J. A., Bilsel, O., Luo, J., Jones, B. E. and Matthews, C. R. (1995) Probing the folding mechanism of a leucine zipper peptide by stopped-flow circular dichroism spectroscopy. *Biochem.* **34**: 12812-12819.

Zitzewitz, J. A., Ibarra-Molero, B., Fishel, D. R., Terry, K. L. and Matthews, C. R. (2000) Preformed secondary structure drives the association reaction of GCN4-p1, a model coiled-coil system. *J. Mol. Biol.* **296**: 1105-1116.

Zou, Q., Habermann-Rottinghaus, S. M. and Murphy, K. P. (1998) Urea effects on protein stability: hydrogen bonding and the hydrophobic effect. *Proteins* **31**: 107-115.

APPENDIX I

Use of a heterodimeric coiled-coil system for biosensor application and affinity purification

A version of this paper has been published: Chao, H., Bautista, D.L., Litowski, J., Irvin, R.T., and Hodges, R.S. (1998) *J. Chromatogr.* 715: 307-329.

A. Summary

The two-stranded α-helical coiled-coil is now recognized as one of nature's favorite ways of creating a dimerization motif. Based on the knowledge of protein folding studies and de novo design model systems, a novel heterodimeric coiled-coil protein was synthesized. The heterodimeric E/K coiled-coil was constructed with two distinct peptides (E and K) that will spontaneously associate into a full helical coiled-coil structure in solution. Equilibrium CD, NMR and real time biosensor kinetics experiments showed that the E/K coiled-coil is both structurally (ΔG_{unfold}=11.3 kcal/mol) and kinetically ($K_d \approx 1$ nM) stable in solution at neutral pH. The engineered coiled-coil had been applied as a dimerization and capture domain for biosensor based applications and used in an expression/detection/affinity chromatography system. Specific test examples demonstrated the usefulness of the E/K heterodimeric system in these applications. The universality of coiled-coil as a dimerization motif in nature and our ability to design and synthesize these proteins suggest a wide variety of applications.

B. Introduction

The two-stranded α-helical coiled-coil is a universal dimerization domain used by nature in a diverse group of proteins (Adamson *et al.* 1993, Cohen & Parry 1994, Lupas *et al.* 1991, Zhu *et al.* 1992). The existence of such a domain was first predicted by Crick in 1953 based on the X-ray diffraction pattern of α-keratin (Crick 1953). He suggested that a coiled-coil is a structural domain where two right-handed amphipathic α-helices wrap around each other to adopt a left-handed supercoil. In order for an α-helix to participate in such a motif, several structural and sequence-related parameters are required. Some of these parameters include amphipathicity and placement of appropriate amino acids, mostly non-polar, into a 'knobs-into-holes' type packing at the interfacial area between the amphipathic a-helices (Crick 1953).

The amino acid sequence of the first coiled-coil was identified initially in 1972 (Hodges *et al.* 1972, Sodek *et al.* 1972). This protein, tropomyosin, was the smallest and simplest protein postulated to contain a coiled-coil structure at that time. Analysis of the primary sequence of tropomyosin revealed a seven-amino acid repeating motif (**a–b–c–d–e–f–g**) where the **a** and **d** positions were occupied by hydrophobic residues. This 3–4 or 4–3 hydrophobic repeat (NXXNXXXNXXN . . .) was shown to be continuous throughout the entire 284- residue polypeptide chain of tropomyosin (Biro 1975). A small de novo designed peptide model based on this repeat was first synthesized in 1981 (Hodges *et al.* 1981) and employed to demonstrate experimentally the requirements of a 3–4 hydrophobic repeat in the formation and stability of a coiled-coil dimer.

Since 1972, coiled-coil sequences have been found in a number of fibrous proteins (Titus 1993) and intermediate filaments (Stewart 1993), and it is now recognized that the coiled-coil is a common structural domain found in a large range of proteins that play pivotal roles. In 1988, Landscultz *et al.* compared the primary sequence of a number of DNA binding proteins and recognized a homologous region containing a repeating pattern of leucine residues at every seventh position (Landschulz *et al.* 1988). They proposed that this domain formed an amphipathic α-helix aligning the leucine residues along one face such that the leucine side chains in adjacent helices interdigitated like teeth in a zipper thus allowing the proteins to dimerize. It was pointed out later that the leucine zipper sequence contained the 3–4 hydrophobic repeat characteristic of coiled-coils (O'Shea *et al.* 1989). Subsequently, NMR (Oas *et al.* 1990) and eventually X-ray crystallographic studies confirmed the molecular interactions initially proposed for coiled-coils (Ellenberger *et al.* 1992, Glover & Harrison 1995, Konig & Richmond 1993, O'Shea *et al.* 1991). These structures confirmed some of the fundamental structural characteristics predicted by Crick some 40 years earlier.

The discovery of coiled-coil motifs in DNA binding proteins tremendously expanded the field of research for this protein structural element. At the same time, the simplicity and elegance of this motif make it an ideal platform for studying protein folding. More recently, it has become a template for rational protein design. We, along with other groups, have also attempted to engineer new coiled-coils for specific biomedical applications (Butcher *et al.* 1997, Carter *et al.* 1995, Crameri & Suter 1993, de Kruif & Logtenberg 1996, Hodges 1996, Kalandadze *et al.* 1996, Liu *et al.* 1997, Miceli *et al.* 1996, Patel *et al.* 1996, Scott *et al.* 1996, Slate *et al.* 1995, Terskikh *et al.* 1997, Tso *et al.* 1995). In this review, we will describe a de novo designed coiled-coil that is currently being used for biosensor and affinity chromatography purposes. The advantages and limitations of this heterodimeric system are highlighted. This article is divided into several sections. Section 2 details the structural characteristics of a coiled-coil based on the current state of knowledge. Section 3 contains the description of the designed coiled-coil and its applications to biosensors and affinity chromatographic systems. Section 4 contains a brief description of other common affinity chromatographic systems for comparison. Finally, in section 5, the advantages of the coiled-coil system are described and summarized. The subject of coiled-coils has been reviewed extensively by our laboratory (Adamson *et al.* 1993, Hodges 1992, 1996, Mant *et al.* 1993) and others (Cohen & Parry 1994, Lupas *et al.* 1991, Woolfson & Alber 1995).

C. The structural characteristics of coiled-coils

Hydrophobicity and side chain packing in the hydrophobic core

It is obvious from the conserved nature of the 3–4 hydrophobic repeat in native coiled-coils that hydrophobicity is a critical issue in the formation and stability of coiled-coils. The hydrophobic residues at position **a** and **d** of the repeating heptad align their side chains on the same face of the amphipathic helix forming a hydrophobic interface through which two adjacent helices can interact (Hodges 1992, Mant *et al.* 1993, O'Shea *et al.* 1991). The inter-chain hydrophobic interactions provide the primary driving force for tertiary folding and account for the stability of coiled-coils.

The primary sequence of tropomyosin provided an early indication of the importance of leucine residues in stabilizing the coiled-coil structure (Hodges *et al.* 1972, Sodek *et al.* 1972). In the 284-residue polypeptide chains of tropomyosin homodimers there are 71 residue pairs involved in hydrophobic interactions, 25 of which are L–L interactions, 23 of them are V, M, I, and Y interactions, and the rest are A–A interactions

(Hodges *et al.* 1981). It was later shown that synthetic coiled-coil model systems consisting of only four or five repeating heptads (28–35 residues) with L at all **a** and **d** positions formed very stable coiled-coils that were considerably more stable than native tropomyosin (Lau *et al.* 1984). More recently, Hodges and co-workers have examined the effect of polypeptide chain length on the stability and formation of coiled-coils when the hydrophobic core was maximally stabilized with I at position **a** and L at position **d** (Su *et al.* 1994, Zhu *et al.* 1993). Peptides as short as three heptads (21 residues) employing L at positions **a** and **d** were shown to form stable two-stranded α-helical coiled-coils. It was also suggested that other hydrophobes may be destabilizing relative to the bulky aliphatic side chains of I and L. In addition, the occurrence of charged or polar residues in positions **a** and **d** of the hydrophobic core may be further destabilizing relative to one comprised entirely of leucines (Lau *et al.* 1984, Moitra *et al.* 1997). Indeed, the consistent presence of leucines in the **d** positions in the short coiled-coil motifs of transcription factors has corroborated its significant role in the hydrophobic core. This requirement for hydrophobicity is demonstrated in the dimerization tendencies of the c-Myc and Max leucine zippers (Lavigne *et al.* 1995). The **d** positions of the c-Myc leucine zipper are predominantly occupied by leucines, whereas three of the four **a** positions are occupied by charged residues. As a result, one would expect homodimerization of the c-Myc leucine zipper to bring six charged side chains into the coiled-coil interface, and therefore predict the interaction to be unfavorable. Synthetic peptides corresponding to the homodimer of the c-Myc leucine zipper were found to be non-interacting α-helices in benign medium (Lavigne *et al.* 1995, Muhle-Goll *et al.* 1994). In contrast, synthetic peptides of the Max protein exhibited considerable formation of homodimeric coiled-coils under the same conditions (Lavigne *et al.* 1995). An explanation for these observations can be drawn from the Max leucine zipper sequence. Apart from two pairs of N residues at two **a** positions and a pair of H residues at a **d** position, the remainder of the **a** and **d** positions are occupied by hydrophobic residues, thereby allowing for more stabilizing tertiary interactions than are possible with the c-Myc homodimer (Lavigne *et al.* 1995). The presence of polar and charged residues acts to destabilize homodimeric coiled-coil formation and thus promotes the formation of the heterodimeric form. This strategy is particularly effective in short coiled-coils (1998, Lavigne *et al.* 1995).

The sequence of tropomyosin demonstrates that both the **a** and **d** positions of the heptad repeat could be occupied by β-branched side chains (Sodek *et al.* 1972). On the other hand, coiled-coil (leucine zipper) sequences of DNA binding proteins show a conserved requirement for leucine residues in the **d** position and a distinct tendency for β-branched side chains at position **a** (Hu *et al.* 1990). These observations proved to be puzzling. However, in 1991, the first high-resolution X-ray structure of a coiled-coil protein, the GCN4 leucine zipper, brought much insight into the apparent preference for a particular type of hydrophobes at position **a** and **d** (O'Shea *et al.* 1991). The three-dimensional structure clearly indicated that the **a** and **d** positions of the heptad were structurally distinct, with the side chains at these positions having different orientations relative to the dimer axis in parallel and antiparallel coiled-coils (Monera *et al.* 1993). The hydrophobic side chains at position **a** point away from the hydrophobic interface, while those at position **d** point into the dimer interface. The apparent preference of β-branched residues at position **a** may contribute to the stabilization of the hydrophobic core by allowing for closer contacts with adjacent residues than would be possible with a linear aliphatic side chain (O'Shea *et al.* 1991). Zhu et al. (1993) showed that β-branched amino acids, I and V, are preferred at position **a** compared to position **d** in order to maximize coiled-coil stability.

The X-ray three-dimensional structure of GCN4 (O'Shea *et al.* 1991) also confirmed the knobs-into-holes model first proposed by Crick almost 40 years earlier (Crick 1953). The hydrophobic interface in parallel two-stranded coiled-coils is formed by two distinct layers which alternate to produce a closely packed hydrophobic core. One layer consists of the side chain of residue **a** which packs between residues **a** and **g** of the corresponding heptad on the opposite helix, and similarly, the alternate layer is composed of the **d** side chain packing between side chains of positions **d** and **e**. In this respect, the leucine side chains at position **d** do not interdigitate, as the leucine zipper proposed (Stewart 1993), but instead pack side to side, as do the side chains at position **a**. Furthermore, the close packing of alternate layers allows the side chain of the **a** residue (knob) to pack into a hole formed by side chains of **a**, **g** and **d** of the preceding and succeeding layer of the opposite helix. Side chains of position **d** pack into the holes formed by consecutive **d** and **e** residues and two **a** residues of the opposing helix. As a result of this close packing, the residues at positions **a** and **d** of the GNC4 leucine zipper sequence were almost totally buried within the dimer interface, with a portion of the buried surface area also coming from the **e** and **g** side chains.

The concept of close packing brings into focus the effects of alanine, relatively large hydrophobes, F, Y, and W, and polar and charged residues in the destabilization of the hydrophobic core (Moitra *et al.* 1997). Homodimers containing either small or large hydrophobes (in relation to L, V, and I) could produce packing defects at the interface, potentially destabilizing the coiled-coil structure. Thus, there may be a requirement for heterodimerization with complementary surfaces to achieve close packing and maintain stability. Similarly, polar side chains cannot pack into a solvent inaccessible hydrophobic environment without causing dramatic energetic consequences unless there is a complementary surface/environment to compensate for the disruption.

These results, taken together, establish hydrophobicity and close core packing to be the major driving forces in coiled-coil formation. Local destabilization of the hydrophobic core, created by variations of side chain hydrophobicity and packing effects at the **a** and **d** positions of the heptad, may suggest a mechanism for subtle control of coiled-coil stability that is important in carrying out diverse functions.

Electrostatic interactions in coiled-coils

Positions **e** and **g** of the heptad repeat flank the hydrophobic interface of the coiled-coil and may contribute to the hydrophobicity of the core by folding over the interface to interact with the hydrophobes through their side chain methylene groups, thereby shielding the core from water (Talbot & Hodges 1982). Sequence analysis of coiled-coil domains displayed a preponderance of oppositely charged residues at these positions, which has led to a suggestion that interhelical ionic interactions (*i* to *i*'+5 interhelical interactions) could exist to stabilize the coiled-coil (Biro 1975, McLachlan & Stewart 1975, Talbot & Hodges 1982). Confirmation of the presence of interhelical salt bridges was subsequently found in the three dimensional structures of the DNA-binding proteins GCN4 (O'Shea *et al.* 1991) and Fos/Jun (Glover & Harrison 1995); and their contributions to stability have been demonstrated (Kohn *et al.* 1995a, 1995b, 1997a, Yu *et al.* 1996a, 1996b, Zhou *et al.* 1994).

It must be noted, however, that the contributions of electrostatic interactions in a protein are variable and dependent on the local micro-environment (Fairman *et al.* 1996, Krylov *et al.* 1994, Lavigne *et al.* 1996, Lumb & Kim 1995). Electrostatic interactions between largely solvent-exposed areas on surfaces are usually weak and contribute little to stability (Pace *et al.* 1990, Serrano *et al.* 1990). Conversely, buried ion pairs can be stabilizing (Anderson *et al.* 1990). Charged interactions may contribute to coiled-coil stability if the micro-environment surrounding the charged interaction is not entirely aqueous, such as that near the hydrophobic interface (Talbot & Hodges 1982). In this light, the effect of ion pairs on stability is interdependent with the hydrophobicity of the hydrophobic core. The partially non-aqueous micro-environment of the core may allow for the formation of the interchain salt bridge and, in return, formation of the salt bridge may reduce the solvent accessibility of the core. Both effects increase the stability of the coiled-coil structure. Many studies have tried to quantitate the stability contributed by ion pairs to two-stranded α-helical coiled-coils (Kohn *et al.* 1995a, 1995b, 1997a, Krylov *et al.* 1994, Lavigne *et al.* 1996, Lumb & Kim 1995, Zhou *et al.* 1994). However, a more interesting question may lie in the destabilizing effects that ion pairs can create. This concept is best illustrated by mutagenic studies on the Fos and Jun leucine zippers in which residues of the **e** and **g** positions were grafted onto the leucine zipper of GCN4 (John *et al.* 1994). The **e** and **g** positions of the Fos leucine zipper contain mainly negatively charged residues, whereas the Jun leucine zipper harbors positive charges. Mutant GCN4-Fos and GCN4-Jun leucine zippers preferentially formed heterodimers (Fos/Jun) over either homodimer (Fos/Fos or Jun/Jun). The relative instability of the

GCN4-Fos homodimer suggested that the repulsion created by four E side chains may have provided the primary driving force for the heterodimerization of the peptides.

In addition to interhelical ionic interactions (*i* to *i*'+5) in coiled-coils, X-ray crystal structures have also shown the presence of intrahelical electrostatic interactions (*i* to *i*+3 and *i* to *i*+4) which may compete for ion pairs between the **e** and **g** positions (Glover & Harrison 1995). Solvent-exposed interactions often do not contribute significantly to overall heterodimer stability (Lyu *et al.* 1992). However, it was found that intrastrand ionic interactions which alter the stability of individual helices may also directly influence coiled-coil stability (Zhou *et al.* 1993).

Oligomerizaton and chain orientation

Coiled-coil structures in nature can exist as dimeric, trimeric, tetrameric and larger oligomeric assemblies of α-helices with either parallel and/or antiparallel orientations of the peptide chains (Fairman *et al.* 1996, Monera *et al.* 1993, 1994a, 1996). Recent evidence for a pentameric coiled-coil has also been obtained (Efimov *et al.* 1996). Despite this diversity, all coiled-coil proteins share a common sequence pattern, implying that structural features superimposed on the heptad repeats specify different oligomerization states and alternate topologies (Cohen & Parry 1994, Lupas *et al.* 1991).

Many studies have been carried out in an attempt to characterize the structural requirements that determine the preferred states of oligomerization (Cohen & Parry 1990, Woolfson & Alber 1995). Harbury et al. (1993) investigated the role of residues **a** and **d** of the heptad repeat on oligomerization states. Variations in the hydrophobic side chains at these positions generated two-, three- and four-stranded helices of the GCN4 leucine zipper. They concluded that coiled-coil oligomerization can be based in part on the distribution of β-branched residues at the **a** and **d** positions due to the constraints imposed by distinct local geometries at these positions. In addition, Monera *et al.* (1996) showed by Ala substitution in the hydrophobic core of a model coiled-coil that close packing of hydrophobes to avoid cavity formation also can direct the oligomerization state. The effect of interhelical electrostatic interactions on specifying the heterodimer formation of Fos and Jun has long been recognized (O'Shea *et al.* 1992). These interhelical electrostatic interactions can have a direct role in the formation of parallel and antiparallel coiled-coils (Monera *et al.* 1993, 1994a). Nautiyal et al. (1995) succeeded in designing a heterotrimeric coiled-coil based on the requirements of interchain electrostatic interactions. However, the parameters for oligomeric and orientation topology are not clear cut. A coiled-coil designed to form a dimer was shown to be assembled as a trimer with the helices running up–up–down (Lovejoy *et al.* 1993). Similarly, a 19-residue peptide designed to self associate into a four-helix bundle formed both hexamers and tetramers (Hill *et al.* 1990). Despite the inability to define the structural features specifying oligomerization and chain topology, a recurring conclusion is that hydrophobic side chain packing and electrostatic interactions work in synergy as a finely tuned control for defining the oligomerization states of coiled-coil assemblies.

Coiled-coil (leucine zipper) dimerization of transcription factors brings together two functional domains (Hurst 1995). Correct alignment (parallel and in register) of their DNA-binding regions is imperative for function (Ellenberger *et al.* 1992, Marmorstein *et al.* 1992), whereupon another critical parameter in coiled-coil assembly is the determination of chain orientation and alignment. As previously described, positions **a** and **d** are structurally distinct and packing at the hydrophobic core of two parallel helices is composed of alternating **a–a'** and **d–d'** layers (O'Shea *et al.* 1991). In contrast, for a coiled-coil to pack in the antiparallel orientation (Cusack *et al.* 1990), hydrophobic side chains of position **a** in one helix must pack against those in the **d** position of the adjacent helix, and vice versa, resulting in mixed pair **a–d'** and **d–a'** packing. These packing differences result in altered coiled-coil stability. In fact, synthetic models have demonstrated the increased stability of antiparallel coiled-coils over parallel coiled-coils which have the same hydrophobic interface (Monera *et al.* 1993, 1994a). However, based on the abundance of parallel coiled-coils in natural proteins, other factors such as electrostatic interactions may direct the orientation of helices (Monera *et al.* 1993).

The leucine zipper motifs of many b-zip proteins contain a conserved N residue at position **a**16. Based on the X-ray structure of GCN4 (PDB accession number 2ZTA), O'Shea *et al.* (1991) proposed a role for the conserved residue in positioning the two helices in a parallel and unstaggered orientation. The N sidechains form a hydrogen bond which partially compensates for the destabilizing effect of burying polar groups in the hydrophobic core. Packing of the polar N residue against nonpolar side chains in the hydrophobic interface may destabilize antiparallel or staggered arrangements and therefore specify for complementary polar groups. A similar strategy appears to be employed for the preferential heterodimerization of the Max and c-Myc leucine zippers (Lavigne *et al.* 1995, 1998), as will be discussed in the next section.

Specificity for homo- or heterodimerization

The coiled-coil formation of leucine zipper proteins is critical in mediating interactions of different dimerization partners, thereby not only defining the DNA specificity of the transcription factor but also the combination of regulatory molecules assembled on the gene regulatory element (Hurst 1995). Having addressed the structural requirements involved in controlling coiled-coil formation and stabilization, we need to examine what governs the selectivity for specific homo or heterodimerization. Whereas hydrophobicity and side chain packing were the major contributors to coiled-coil formation and stability, it has become apparent that electrostatic interactions play the dominant role in determining specificity of helix association. Ionic attractions are not essential for coiled-coil formation but electrostatic interactions can control heterodimerization versus homodimerization and may also control parallel or antiparallel alignment in coiled-coils (Baxevanis & Vinson 1993, Graddis *et al.* 1993, Kohn *et al.* 1995b, Lavigne *et al.* 1995, Monera *et al.* 1993, Nautiyal *et al.* 1995, Schuermann *et al.* 1991, Zhou *et al.* 1992). A model example of electrostatically controlled specificity is apparent in the Fos/Jun leucine zippers discussed previously.

Recently, evidence has been obtained to support the role of charged residues within the actual core of the hydrophobic interface in specifying for heterodimerization (Lavigne *et al.* 1995). The c-Myc family of the b-HLH-zip transcription factors represent a group of regulatory proteins implicated in controlling genes whose functions are important in the machinery of cell growth and proliferation (Amati & Land 1994). The primary sequences of the coiled-coil (leucine zipper) region in these proteins display a number of charged residues in the **a** position of the heptad repeat. Of particular interest is a conserved acidic side chain at an equivalent **a** position in one heptad of c-Myc, N-Myc, L-Myc, Mxi1 and Mad, which appears to align with a conserved H residue in the corresponding heptad of the Max leucine zipper (Lavigne *et al.* 1995). Lavigne et al. have investigated the role of these ionizable residues in the specific recognition of heterodimerization in this sub-family of b-HLH-zip DNA-binding proteins (Lavigne *et* *al.* 1995, 1998). Their results support the presence of specific electrostatic interactions in the hydrophobic core of the heterodimeric c-Myc and Max coiled-coil. In the folded heterodimeric protein, the ionizable groups are fully engaged in hydrogen bonding and salt bridges. This arrangement negated the destabilizing effect of bringing a charged group from a polar solvent environment into a non-polar protein core. It also has a positive energetic contribution since the salt bridges are shielded from the solvent. In addition, these ionic interactions within the protein core serve to specify correct dimerization partners. Selective heterodimerization, mediated by a specified coiled-coil macromolecular interaction, can define the ultimate function for a given protein completely, and thus play a significant role in cellular regulation.

D. A de novo designed heterodimeric coiled-coil

Design features

A helical wheel representation of the designed heterodimeric coiled-coil is presented in Figure 1. This protein was designed for biosensor-based and affinity chromatographic applications after considering parameters that are important for coiled-coil formation, protein stability and chemical peptide synthesis. Some of these design features include: (1) selecting amino acids that are non-disruptive to helical structure; (2) placement of complementary non-polar residues that can form a stable hydrophobic core (positions **a** and **d**); (3) choosing appropriately charged amino acids for the **e** and **g** positions that will promote heterodimeric rather than homodimeric coiled-coil formation; (4) inclusion of charged amino acids at the **f** positions for solubility; (5) balancing the net charge on the individual α-helices by having opposite charged residues at positions **f**

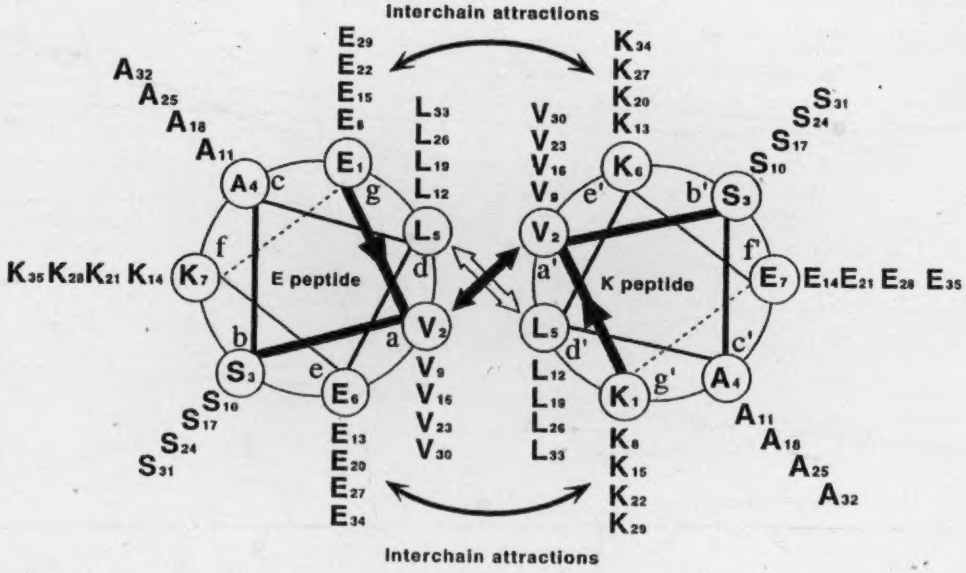
Interchain attractions
E29 E22 E15 E8
L33 L26 L19 L12
V30 V23 V16 V9
K34 K27 K20 K13
A32 A25 A18 A11
S31 S24 S17 S10
A4 c E1 g
L5 d
K35 K28 K21 K14 K7 f
E peptide
V2 a
b S3 e E6
S10 S17 S24 S31
E13 E20 E27 E34
V9 V16 V23 V30
K6 e' b' S3
V2 a'
K peptide
f' E7 E14 E21 E28 E35
L5 d'
c' A4
K1 g'
L12 L19 L26 L33
K8 K15 K22 K29
A11 A18 A25 A32
Interchain attractions

Figure 1. Helical wheel representation of the heterodimeric parallel E/K coiled-coil. The polypeptide chain propagates into the page from the N- to the C-terminus. The K peptide is made up of five heptad (**g'-a'-b'-c'-d'-e'-f'**) repeats of the sequence K-V-S-A-L-K-E and the E peptide consists of the same number of heptad repeats with the sequence E-V-S-A-L-E-K (**g-a-b-c-d-e-f**). The hydrophobic residues at positions **a**, **a'**, **d** and **d'** interact and are mainly responsible for the formation and stability of the coiled-coil. Potential electrostatic attractions at positions **g-e'** or **g'-e** provide additional stability to the system by encouraging E and K salt bridge formation. Formation of these interchain salt bridges can also shield the non-polar core from solvent, further stabilizing the E/K coiled-coil. In addition to a role in protein stability, the E/K interaction also specifies heterodimerization rather than homodimerization in pH neutral buffer.

compared to positions **e** and **g**; (6) selecting an optimal protein sequence length for the designed applications which can still be made efficiently by synthetic means; (7) maintaining a balance of the stability of the hydrophobic core which drives homodimer formation with electrostatic repulsions which prevent homodimer formation in order to favor the heterodimeric form. Several designs were considered before selecting the E/K coiled-coil as our prototype.

The E/K coiled-coil is made of two distinct peptides, each with a unique repeating heptad sequence. The heptad sequence for the E peptide is E–V–S–A–L–E–K (position *g–a–b–c–d–e–f*) and the sequence for the K peptide is K–V–S–A–L–E–K. Each heptad is repeated five times in the respective peptide. When the two peptides associate, a dimeric protein of 70 amino acids in size with a molecular mass of 7682 is formed. The E and K peptides are amidated and acetylated at the C and N termini, respectively, to increase helix-forming propensity and to reduce the likelihood of proteolysis. Furthermore, this limits the available charged groups to those of the amino acid side chains only.

The hydrophobic core of the E/K coiled-coil is made of V and L residues at the respective **a** and **d** positions. These amino acids are commonly found in natural and synthetic coiled-coil sequences, and coiled-coils with this hydrophobic core tend to favor a dimeric conformation (Cohen & Parry 1990, Graddis *et al.* 1993, Kohn *et al.* 1995a, Zhu *et al.* 1993). Although a V and L hydrophobic core would be less stable than an all-leucine one or an I and L core, it is important to note that a weaker core will reduce the likelihood of forming unwanted higher order aggregates in solution (Harbury *et al.* 1993, Lovejoy *et al.* 1993, Zhu *et al.* 1993) and prevent homodimerization in the presence of electrostatic repulsions. In line with choosing commonly observed non-polar residues for the hydrophobic interface, the same strategy was used in selecting residues for the **e** and **g** inter-helical salt bridge positions. In this case, glutamate and lysine are logical candidates since they are frequently observed to occupy these positions in natural coiled-coils (Cohen & Parry 1990, Zhou *et al.* 1994). Studies also showed that they can form energetically favorable **e–g'** interhelical salt bridges in coiled-coils (Kohn *et al.* 1995a, Zhou *et al.* 1994). Furthermore, the methylene group of the K side chain can contribute to the overall stability of the protein by interacting with the partially exposed hydrophobic interface during salt bridge formation (O'Shea *et al.* 1991). In addition, at neutral pH, the ionized side chains of E and K will discourage formation of homodimeric E/E or K/K coiled-coils as a result of like-charge repulsion, thus promoting the formation of heterodimeric E/K coiled-coil (Kohn *et al.* 1995a, 1995b, 1997b, Yu *et al.* 1996a, 1996b).

Physical characterization of the E/K heterodimeric coiled-coil

The E and K peptides preferred to form a heterodimeric coiled-coil under benign conditions and at moderate protein concentrations, as designed (Chao *et al.* 1996). Neither peptide adopted significant structure on its own, suggesting that the designed E/K salt bridges are important for protein folding. As shown in Figure 2, the CD spectrum of a solution of E or K peptide is largely random in character. In contrast, a solution containing both peptides displays a CD profile that is characteristic of a helical structure, with spectral minima near 208 and 222 nm. The ratio of $[\Theta]_{222}$ vs. $[\Theta]_{208}$ of the heterodimer is 1.07, which is consistent with previous empirical observations that a coiled-coil structure will have a ratio greater than unity (Graddis *et al.* 1993, Lau *et al.* 1984).

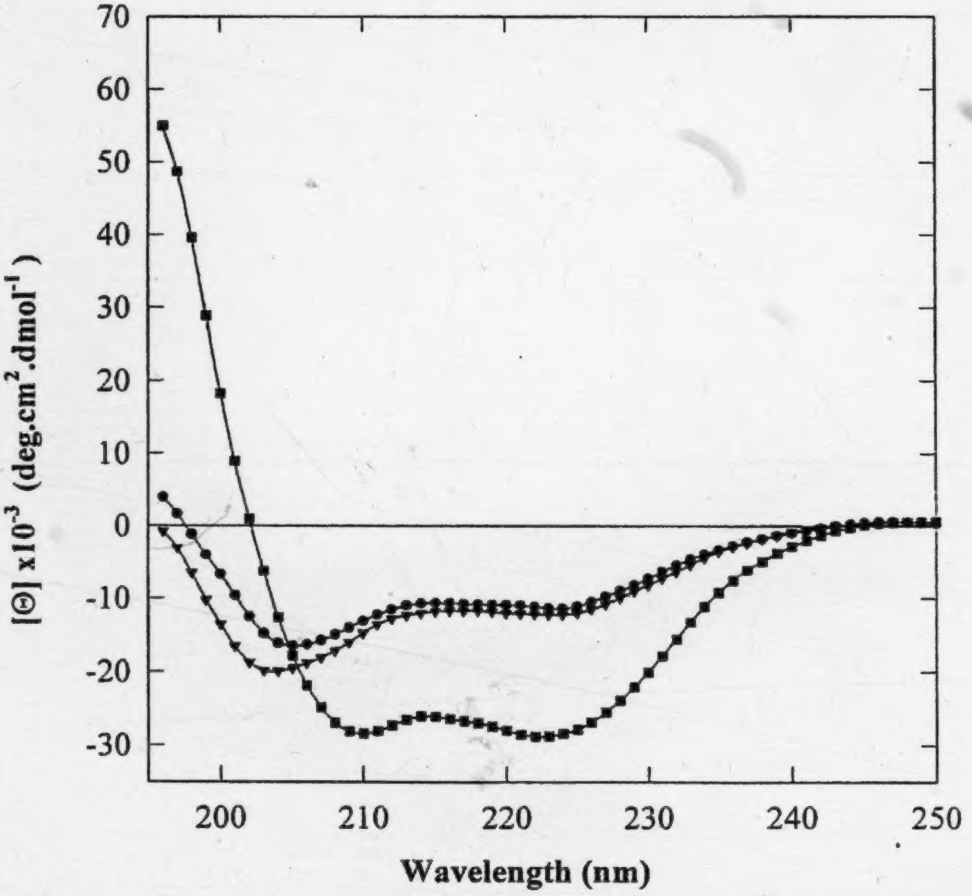

Figure 2. CD spectra of the E peptide (▼), K peptide (●) and the E/K coiled-coil (■) recorded at 20°C. Protein concentrations were 20 μM for each sample. Sample buffer was 50 mM phosphate, 100 mM KCl, pH 7.0. Each sample was scanned four times from 250 to 195 nm at a rate of 5 nm/min. Data were sampled at 0.1 nm intervals and averaged (figure adapted from Chao *et al.* (1996)).

In order to corroborate the data from CD experiments, the K peptide was also selectively labeled with [^{13}C]α-L at position 19 (central heptad of the hydrophobic core) and analyzed by NMR experiments. In the absence of the E peptide, the chemical shift value of the leucine α-proton was 4.31 ppm and the α-carbon was 52.81 ppm from a 2D ^{1}H–^{13}C heteronuclear multiple quantum filtered correlation (HMQC) experiment (Cavanagh *et al.* 1996). Both of these values are consistent with the leucine residue being in a random or rapidly interconverting conformation (Wishart *et al.* 1991). Titration of the E peptide into this solution changes the respective shift values to 4.17 ppm (^{1}H) and 53.41 ppm (^{13}C). When compared with the idealized averaged values of 3.98 and 55.6 ppm for the ^{1}H and ^{13}C atoms for a leucine residue in a fully helical environment (Wishart *et al.* 1991), the NMR data are consistent with the CD observations that the K peptide will adopt a helical conformation when the E peptide is present.

The stability of the E/K coiled-coil was also studied by both chemical and temperature denaturation experiments as monitored by CD spectroscopy (Chao *et al.* 1996). The E/K coiled-coil was resistant to heat denaturation up to 85°C or urea denaturation. More than 50% of the observed helicity was retained at 8 M urea (Figure 3). A combination of heat (85°C) and 5 M urea also was unable to denature the E/K coiled-coil (Figure 3). Guanidine HCl (GdnHCl) was the only agent tested which could denature the E/K coiled-coil completely (Figure 3). A GdnHCl denaturation midpoint of 3.9 M was observed and a ΔG_{GdnHCl} of unfolding of 11.3 kcal/mol was estimated based on data fitting to a dimer <--> monomer model (E/K=E+K). The differential ability of urea and GdnHCl to denature the E/K coiled-coil is consistent with the energetic

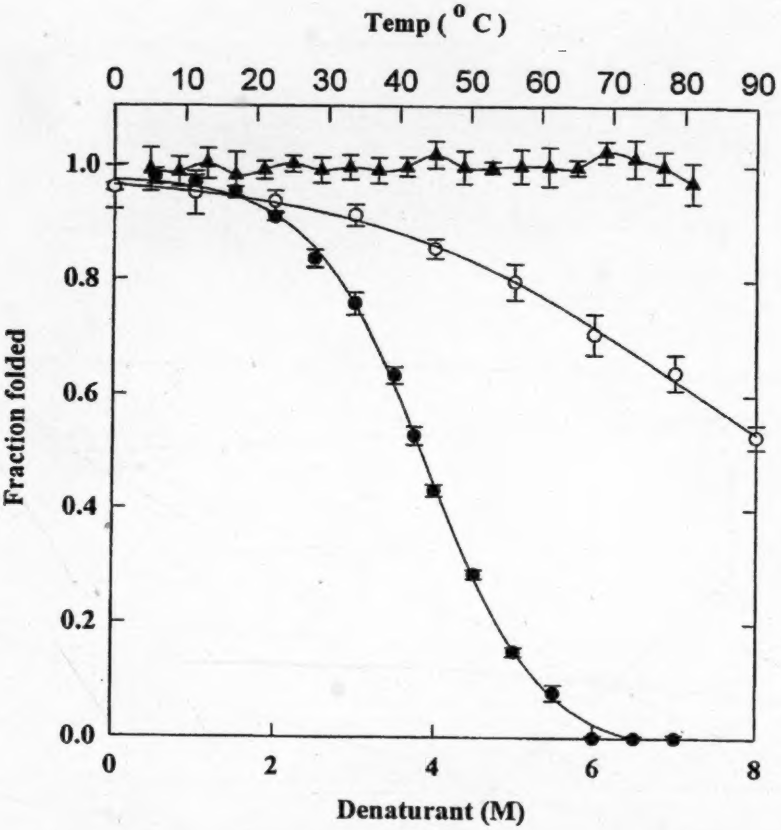

Figure 3. Urea (○), GdnHCl (●) and heat denaturation (▲) profiles of the E/K coiled-coil (Chao *et al.* 1996). The protein concentration was 20 μM for each experiment. The buffer used for the chemical denaturation experiments was 50 mM phosphate, 100 mM KCl, pH 7.0. In the case of heat denaturation, the buffer also contained 5 M urea. The progress of the experiment was monitored at 222 nm by CD spectroscopy. Each data point is the average of eight samplings.

importance of glutamate and lysine salt bridges and that GdnHCl is more efficient in denaturing highly charged proteins (Monera *et al.* 1994b).

The ability of the E/K coiled-coil to remain stable in a biological medium was also tested. E and K peptides and E/K coiled-coil were incubated in human serum over an extended period of time at 37°C. The integrity of the individual peptides and the coiled-coil was assessed by reversed-phase HPLC and mass spectrometry, and compared to controls incubated in a phosphate buffer. As shown in Figure 4, the coiled-coil and the individual peptides are stable in this medium for 50 h with no significant degradation when compared to controls. Thus the highly charged random coil peptides or the folded coiled-coil are very resistant to proteolysis.

E/K coiled-coil formation and dissociation kinetics

The good stability of the E/K coiled-coil points to a small equilibrium dissociation constant in solution. Sedimentation equilibrium data suggested that the E/K coiled-coil remained predominantly a dimer at concentrations as low as 0.4 mg/ml. Based on the well-known relationship of free energy of unfolding and equilibrium dissociation constant ($\Delta G = -RT \ln K$), the K_d was estimated to be 3.53×10^{-9} M (Table 1). This value is consistent with a value of 2.45×10^{-9} M obtained from a protein dilution experiment (Chao *et al.* 1996).

The association and dissociation behavior of the E/K coiled-coil was further studied on a Pharmacia BIAcore^{TM} biosensor in order to obtain the individual association and dissociation rate constants (Chao *et al.* 1996). The BIAcore^{TM} biosensor monitors the changes in the solution refractive index near a gold metal surface as a result of

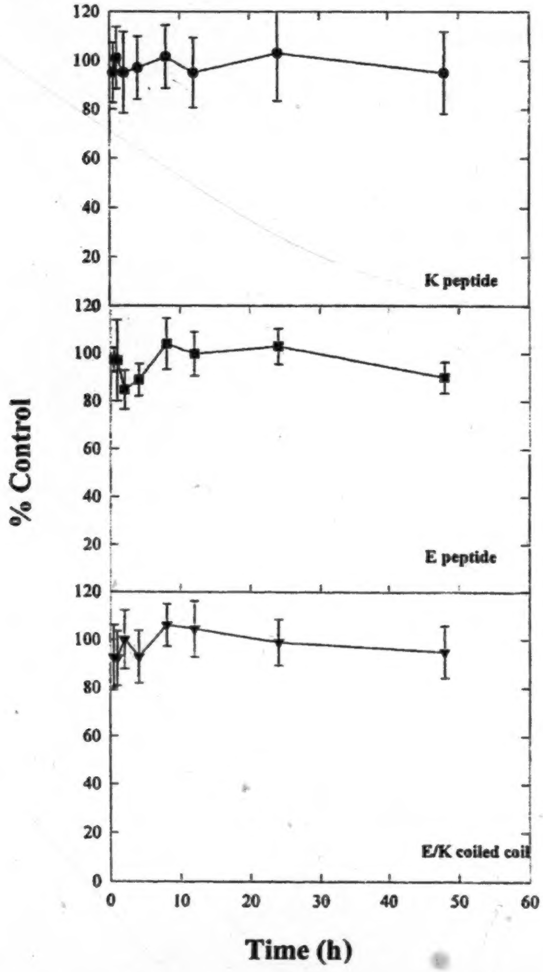

Figure 4. Stability of the E/K coiled-coil (▼), E peptide (■) and K peptide (●) in human serum. Protein was dissolved in human serum, to a concentration of 1 mg/ml or 0.26 mM and the samples were incubated for a total of 50 h at 37°C. Aliquots were removed at various time intervals and extracted with dichloromethane. The sample was further clarified by the addition of acetonitrile to a concentration of 50% (v/v) and centrifuged (13 000 g, 10 min) to remove precipitates. The peptides E, K and E.K coiled-coil, which remained in the supernatant, were stored at -20°C. The integrity of the E.K coiled-coil and peptides were analyzed by reversed phase HPLC and later by mass spectrometry. Data were compared to controls that were run in parallel. For the controls, proteins were incubated in 50 mM phosphate, 100 mM KCl at pH 7.0. Each data point is the average of three samplings. The standard deviation is also displayed.

Table 1. Summary of equilibrium dissociation and rate constants by CD-based and biosensor-based methods (adapted from Chao et al. (1996))

	K_d (x 10^{-9} M)	
GdnHCl denaturation[a]	Dilution study[b]	Biosensor[c]
3.53 ± 0.48	2.45 ± 0.71	0.50 ± 0.13

[a] Dissociation constant estimated from the GdnHCl denaturation data. The K_d was calculated by the relationship $\Delta G = -RT \ln K$, where ΔG is the free energy of unfolding, R is the gas constant, T is the temperature (K), and K is the equilibrium dissociation constant.

[b] Estimated equilibrium dissociation constant from protein dilution experiments as monitored by CD spectroscopy.

[c] Calculated dissociation constant from the BIAcore™ biosensor study. The individual on and off rate constants were derived by fitting a monomer to dimer model to the sensor data. The presented K_d is the ratio of the k_{off} vs. k_{on} observed.

molecular interaction near that surface in real time. Therefore, it allows the experimenter to quantitate the binding event over a finite period. In the E/K coiled-coil experiments, the K peptide was modified with an N-terminal 'C-G-G-G' linker. The terminal thiol group provides an anchoring site for the K peptide to a derivatized biosensor surface in order to capture the E peptide during a binding experiment. In a typical kinetic experiment, a solution of the E peptide was injected over a K peptide-coated surface at a fixed flow-rate over a defined period of time. This measures the binding of the E peptide to the immobilized K peptide. The slow release of the K peptide from the sensor surface is observed by injecting buffer over a defined period. These types of experiments were repeated with several different concentrations of the E peptide and with sensor surfaces that had been functionalized with different amounts of the K peptide in order to get a proper sampling of the data. The reversed experiment, that is an E peptide-modified sensor surface and a K peptide-containing mobile phase, was also done to rule out artifacts caused by immobilization. In some experiments, the mobile phase peptide, E or K, was conjugated with a biotin/avidin complex in order to enhance the response signal.

Representative plots of the biosensor experiment are shown in Figure 5. Both the injection or association phase (0–300 s) and the buffer or dissociation phase (300–600 s) are presented. During the injection phase, the signal (response unit) rises quickly which is indicative of a fast interaction. A slow signal decay over the buffer phase suggests a slowly dissociating system. Analysis of the individual runs provided a set of k_{on} and k_{off} rate constants that were in good agreement with each other. The averaged k_{on} was $4.3 \pm 0.83 \times 10^{5}$ $M^{-1}s^{-1}$ and the averaged k_{off} was $2.21 \pm 0.2 \times 10^{-4}$ s^{-1}. This corresponded to

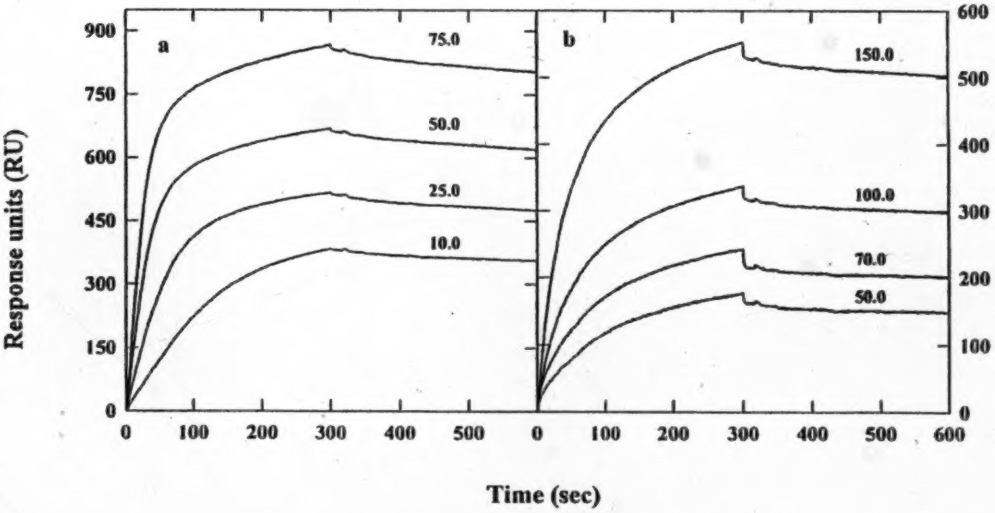

Figure 5. Overlaid sensorgrams showing the binding of the streptavidin/biotinylated K peptide to an E peptide-coated sensor surface (panel a) and the binding of streptavidin/biotinylated E peptide to a K peptide-coated sensor surface (panel b) (Chao *et al.* 1996). Each kinetic cycle involved a 300-s peptide injection phase (0-300 s), a 300-s dissociation phase (300-600 s) and a 60-s regeneration phase (not shown). An injection of 5 μl of 10 mM NaOH followed by buffer was used to dissociate the E/K coiled-coil and to regenerate the sensor surface. The concentrations of the biotinylated K peptide used on the E-coated sensor surface were 10, 25, 50, and 75 nM. For the K surface, the concentrations of the biotinylated E peptide used were 50, 75, 100, and 150 nM. Experiments were performed at 20°C, and sensor signals were recorded in real time with a sampling interval of 0.5 s. The data are presented after subtracting the baseline and repositioning the time of injection to the origin. Each panel represents the result from one set of experiments performed on the same sensor surface. All experiments were performed on a Pharmacia BIAcore^{TM} instrument. The CM5 sensor chip was used and peptide was immobilized on the surface via a terminal cysteine according to the manufacturer's thiol immobilization procedure (diagram modified from Chao *et al.* (1996)).

a calculated equilibrium dissociation constant ($K_d = k_{off}/k_{on}$) of 0.5×10^{-9} M. Current analyses of these data by global analyses (simultaneous fitting of all data) and with more complex kinetic models suggest that the K_d value is probably slightly larger and therefore closer to those estimated by CD-based equilibrium methods (M. O'Connor-McCourt, personal communication).

The use of E/K coiled-coil for biosensor applications.

The inherent stability of the E/K coiled-coil, the fast association kinetics and the relatively slow dissociation kinetics of the polypeptide chains make this protein ideal for biosensor applications that require a stable dimerization and capture domain. In this scenario (Figure 6), one strand of the heterodimeric coiled-coil (e.g., K peptide) is first covalently attached to the biosensor surface. This surface is then charged with the E peptide that has been modified with a ligand for which its interaction with its receptor is to be studied. A significant advantage of the use of coiled-coils is that a single chemistry is used for attachment of one of the coiled-coil peptides to the surface of the biosensor. The particular chemistry for attachment of the other coiled-coil peptide to a variety of different molecules can be developed in solution rather than with the biosensor surface, which lacks the chemical flexibility.

In order for this application to be successful, the conjugated coiled-coil peptide in the mobile phase must be accessible to the anchored peptide. A test was performed on the Pharmacia BIAcore™ biosensor to address this issue. In this experiment, the E peptide was first immobilized on the sensor surface via a C-terminal C residue. The surface was then challenged with a solution containing a monoclonal antibody that was covalently linked to K peptides (K-mAb). The peptide to antibody conjugation ratio was

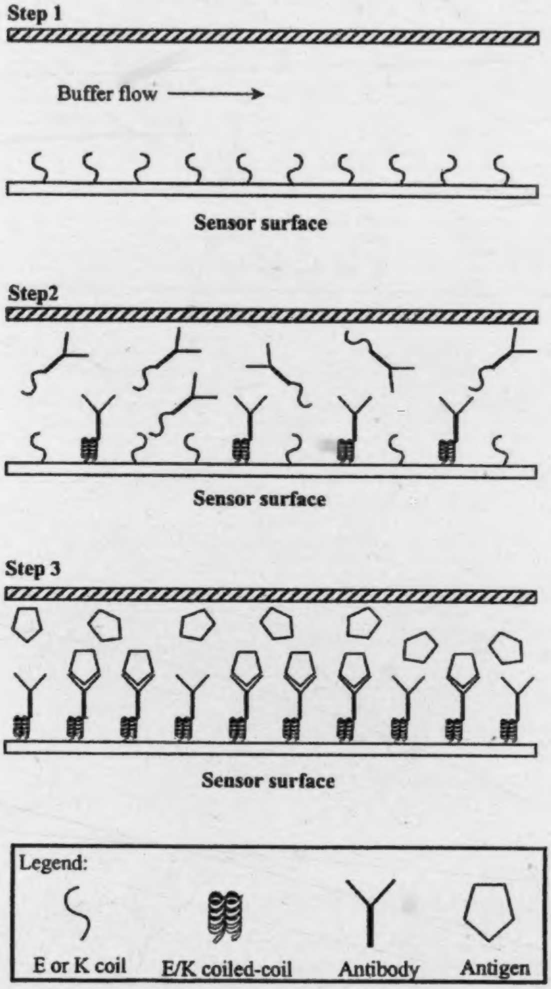
Step 1
Buffer flow
Sensor surface
Step2
Sensor surface
Step 3
Sensor surface
Legend:
E or K coil
E/K coiled-coil
Antibody
Antigen

Figure 6. Utility of the E/K heterodimerization domain for biosensor experiments. The E/K coiled-coil is used as a capture and dimerization domain. In this application, one of the two peptides (step 1) is first immobilized on the sensor surface. The second peptide is conjugated to an antibody, for instance, and injected over the sensor surface (step 2). Formation of the heterodimeric coiled-coil generates an antibody surface for biosensing (step 3). In theory, the sensor surface can be used repeatedly as long as it is charged with a sufficient amount of the coiled-coil peptide conjugate. A test of this application is currently being done on the Pharmacia BIAcore™ Biosensor.

estimated to be 3:1. Figure 7 displays a representative diagram of one such experiment. The results of five K-mAb injections with different protein concentrations are shown. Qualitatively, the association phase (0–300 s) and the dissociation phase (300–600 s) kinetics are very similar to those observed previously for the E and K peptides alone. A fast on (association) and a slow off (dissociation) kinetics regime consistent with the behavior of the E/K coiled-coil was observed.

The interaction of the anchored E peptide and the K-mAb was specific. Injecting a free K peptide solution prior to the delivery of an K-mAb solution over the E-coated sensor surface prevented the binding of K-mAb conjugate. A similar result was observed when free E peptide (equimolar concentration) was added to the K-mAb solution prior to injection. Antibody that had not been conjugated with the K peptide did not interact with the E peptide sensor surface. Addition of up to 10 mg/ml bovine serum albumin (BSA) in the K-mAb solution had no effect on the anchored E peptide and K-mAb interaction. These data suggest that despite the presence of a conjugated molecule (i.e., mAb) that is over 35 times larger in its mass, or placement in a complex medium (i.e. BSA), the ability of the E and K peptides to associate is not significantly impaired.

It should be noted that current analysis of the aforementioned data does reveal a more complex E/K kinetic picture. A simple one-on-one model can no longer satisfy the observed data. In fact, the result is more consistent with models that describe multiple-site interactions. This perhaps should not be surprising since the injected mAb is conjugated with more than one copy of the K peptide. It should be mentioned that even though the underlying E/K formation kinetics has become more complex, it does not significantly affect one's ability to use the E/K coiled-coil for biosensor-based studies since the coiled-coil dissociation phase is sufficiently slow and occurs at a constant rate. Therefore, it is possible to correct for the background signal of the E/K coiled-coil

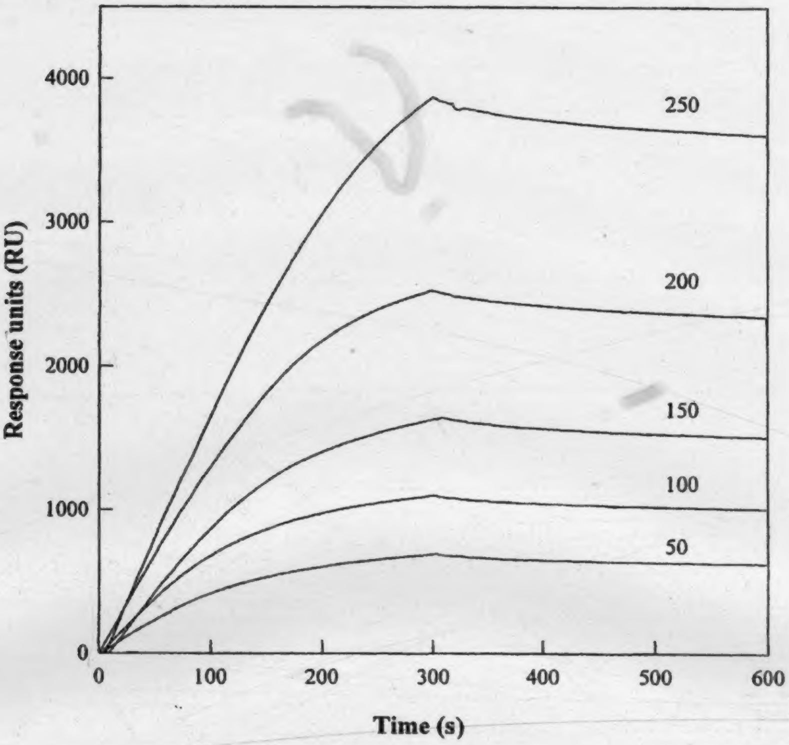

Figure 7. Biacore™ biosensor experiments demonstrating the utility of the E/K coiled-coil as a capture and dimerization domain on a biosensor surface. A CM5 chip was coated with E peptide via a terminal cysteine according to the manufacturer's instructions. The coated chip is then charged with a K peptide monoclonal antibody conjugate (K-mAb). Representative sensorgrams showing the charging of an E-coated surface with five different concentrations (50, 100, 150, 200, and 250 nM) of K-mAb are shown in an overlay format. Each run consisted of an injection or charging phase (0-300 s) and a buffer phase (300-600 s). It is during the buffer phase where the desired interaction (e.g., antibody and antigen) would be run. The buffer phase can be extended significantly to accommodate most kinetic experiments. For this set of experiments, the surface was regenerated with a pulse (5 μl) of 10 mM NaOH to remove the K-mAb. Surface regeneration can be performed eight to 10 times without significantly affecting the ability of the E-coated sensor surface to be recharged.

mathematically.

A heterodimeric coiled-coil affinity matrix protein tag system

The versatility of the E/K heterodimeric coiled-coil as a dimerization and capture domain led us to explore the possibility of using this protein as an affinity purification tag (Figure 8) (Tripet *et al.* 1996). In this application, a recombinant bacterial expression vector pRLDE was engineered to contain a copy of the E peptide at the C-terminus of the newly expressed peptides or proteins (Tripet *et al.* 1996). The plasmid contained an IPTG inducible promoter for selective recombinant protein expression, a multiple cloning site for gene insertion, an ampicillin resistance gene for clone selection and a signal sequence to direct the newly made protein to the periplasmic space to simplify purification. The complementary HPLC affinity matrix was prepared by the conjugation of the K peptide to an insoluble silica (Figure 9). The entire system would allow the researcher to express an E peptide fusion protein and to purify the protein from crude cell lysate in one step by an on-line HPLC K peptide affinity column. Detection of the fusion products can be carried out at any stage in the process by detecting the fusion tag using a free labeled coiled-coil strand in an immunoblot-type or even biosensor-based experiment. The E peptide can be removed easily by a conventional cyanogen bromide cleavage if necessary.

A test of this concept has been demonstrated and reported (Tripet *et al.* 1996). In this specific example, a gene encoding the 17-amino acid pilus epithelial cell-binding domain of the *Pseudomonas aeruginosa* strain K pilin (PAK-pilin) with a methionine flanking the C- and N-termini was inserted upstream of the E peptide-coding region of pRLDE. Positive clones were selected and cultured as single colony isolates.

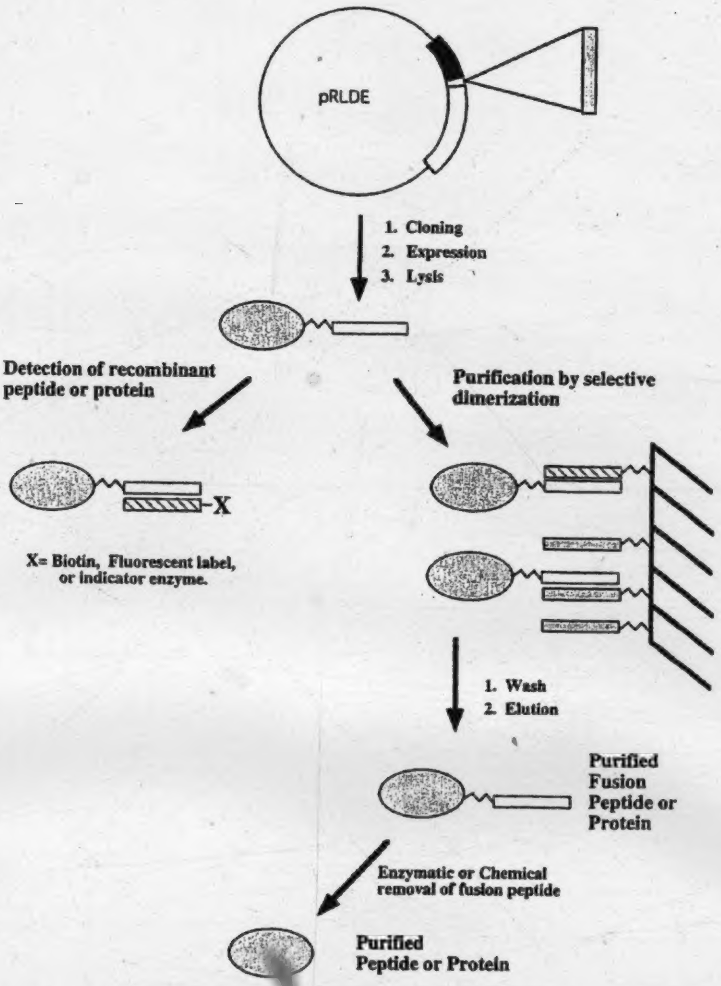
pRLDE
1. Cloning
2. Expression
3. Lysis
Detection of recombinant peptide or protein
Purification by selective dimerization
X
X= Biotin, Fluorescent label, or indicator enzyme.
1. Wash
2. Elution
Purified Fusion Peptide or Protein
Enzymatic or Chemical removal of fusion peptide
Purified Peptide or Protein

Figure 8. The use of the E/K coiled-coil in an expression and purification system for recombinant proteins (Tripet *et al.* 1996). The system consists of an expression vector pRLDE and a K-peptide affinity column. The expression vector pRLDE codes for one copy of the E peptide with a signal peptide that directs the fusion product to the periplasmic space of the bacteria. The fusion protein can be released from the bacteria by osmotic shock and the lysate can be loaded onto the K-affinity column directly after clarification by centrifugation or filtration. The loaded column is then washed with appropriate buffer and the desired product can be eluted. If necessary, chemical or enzymatic cleavage can be carried out to remove the tag (diagram modified from Tripet *et al.* (1996)).

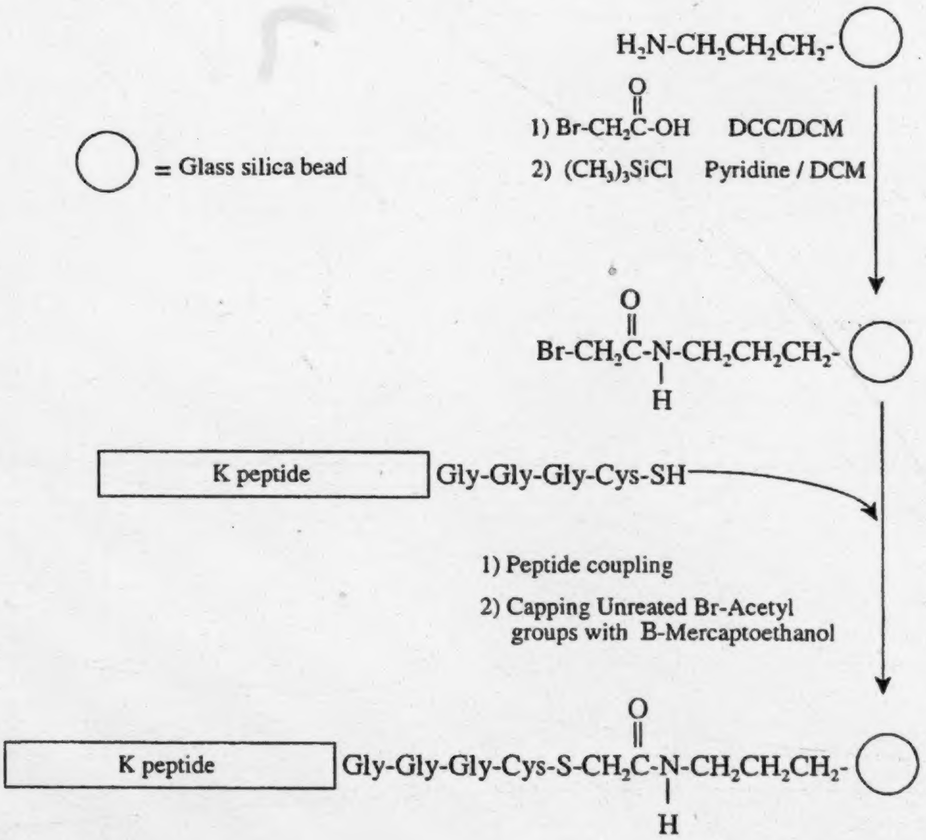
H2N-CH2CH2CH2-
= Glass silica bead
1) Br-CH2C(O)-OH DCC/DCM
2) (CH3)3SiCl Pyridine / DCM
Br-CH2C(O)-N(H)-CH2CH2CH2-
K peptide
Gly-Gly-Gly-Cys-SH
1) Peptide coupling
2) Capping Unreated Br-Acetyl groups with B-Mercaptoethanol
K peptide
Gly-Gly-Gly-Cys-S-CH2C(O)-N(H)-CH2CH2CH2-

Figure 9. Schematic representation of the steps involved in the formation of the K peptide affinity matrix. The glass beads are acetylated with bromoacetic acid and the free silanol groups are capped with trimethylchlorosilane. E peptide modified with a C-terminal cysteine is then added to the matrix slurry to be coupled to the resin. Residual bromoacetyl groups are quenched with the addition of β-mercaptoethanol. The affinity matrix is washed and equilibrated in standard phosphate buffer. DCC and DCM denote dicyclohexylcarbodiimide and dichloromethane, respectively (diagram adapted from Tripet *et al.* (1996)).

Recombinant protein synthesis was induced by the addition of IPTG to cells grown to an A_{550} of 0.5–0.6 in LB medium with carbenicillin as the selecting antibiotic for 3 h at 25°C. Cells were then harvested by centrifugation and the fusion protein was released from the periplasmic space by osmotic shocks. The supernatant which contained the E fusion protein was clarified by passage through a 0.22-µm filter and stored in the cold until ready for the K affinity column (Tripet *et al.* 1996).

Several affinity matrix supports were considered initially for the K affinity column. The selection was narrowed down to an aminopropyl control pore glass resin (CPG, 125 µm particle size, 500 Å pore size; Sigma Chemical Company, St. Louis, MO, USA). This glass bead was chosen because of the desire to generate a matrix that is compatible with an HPLC system. For the preparation of the K affinity matrix, CPG was washed in dimethylformide and dichloromethane. The glass beads were then neutralized in a solution of 5% diisopropylethylamine–dichloromethane (Figure 9). The aminopropyl functional group on the glass bead was bromoacetylated by adding to the glass beads a solution of bromoacetic acid dissolved in dicyclohexylcarbodimide/ dichloromethane and dimethylformamide. The functionalized glass beads were washed with organic solvents and coupling was verified by a qualitative ninhydrin test. Free silanol groups on the resin beads were capped by chlorotrimethylsilane in pyridine and dichloromethane. Capped resin was rinsed thoroughly to conjugate the K peptide.

The conjugation of the K peptide to the functionalized glass beads was done at pH 8.0 and at room temperature. A solution containing 100 mg (24 mmol) of the K peptide was added to 1 g of the activated glass and stirred for 30 min. The K peptide was synthetically made and was modified with a C-terminal G–G–G–norleucine–cysteine linker. After the reaction was completed, β-mercaptoethanol was added to quench the remaining bromoacetyl groups. The K affinity resin was washed in water, ethanol, and acetone, and then air dried. A substitution ratio of 12.5 μmol of peptide to 1 g of resin was obtained.

The dried resin (1 g) was packed in a stainless steel HPLC column (200 x 4.6 mm I.D.) and washed at a flow-rate of 0.5 ml/min with water, 5.0 M GdnHCl in 50 mM KH_2PO_4, pH 7.0, 50% aqueous acetonitrile containing 0.1% TFA and then with water again. The column was stored in 50% aqueous acetonitrile until used.

During the purification run, the filtered bacterial lysate containing the PAK-pilin E fusion protein was applied to the K column at a flow-rate of 0.2–0.5 ml/min with 10 mM KH_2PO_4, pH 6.0, as the running buffer. The loaded column was first washed with 0.5 M KCl in the running buffer and the fusion protein was eluted with 50% aqueous acetonitrile and 0.1% TFA. Representative chromatograms from the reversed-phase HPLC analysis of the crude bacterial lysate, the 0.5 M KCl wash, and the eluted product are shown in Figure 10a–c, respectively. Mass spectrometry analysis of the final eluate revealed a homogeneous product that is indistinguishable from the expected PAK-pilin E fusion protein (data not shown) (Tripet *et al.* 1996).

The unique design of the E/K coiled-coil permitted the use of high-ionic strength wash buffer during the purification process. In the presence of 0.5 M KCl, which would remove most of contaminants from the affinity matrix, the E fusion protein remained bound on the column. This is because the presence of salt strengthened the hydrophobic interaction of the E and K peptides despite the competition with interchain *e* and *g* salt bridges. Similarly, moderate amounts of organic solvent can also be used to wash the bound column with little effect on the E/K dimerization state. In this case, the presence of the *e* and *g* interchain salt bridges compensated for the weakened hydrophobic core in

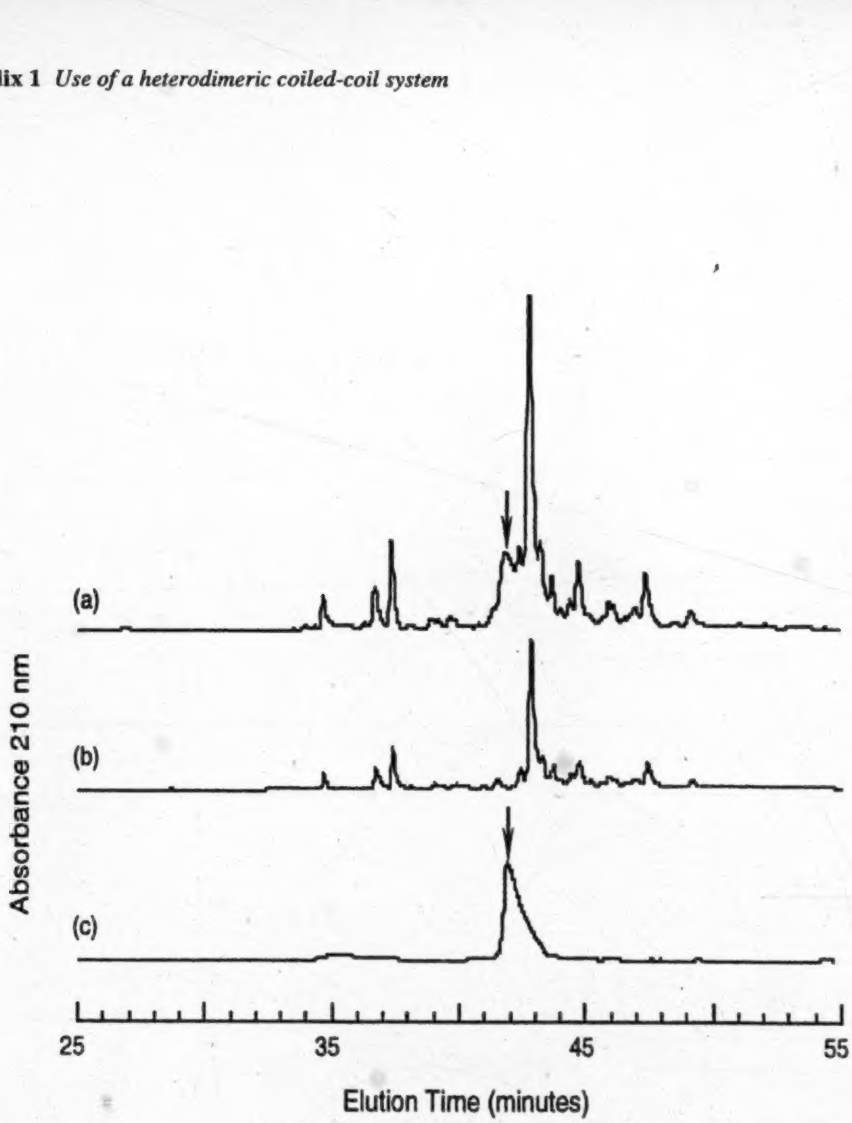

Figure 10. Reversed-phase HPLC analysis of the eluates from each step of the affinity purification of the recombinantly expressed PAK-pilin-E coil using the K coil affinity column: (a) crude periplasmic extract; (b) 0.5 M KCl wash; (c) product eluted with 50% acetonitrile and 0.1% TFA. All runs were performed on an HP 1090 HPLC with a Zorbax RP-C8 column (250 x 4.6 mm I.D., 6.5 μm particle size, 300 Å pore size). A linear AB gradient (1% B/min), where solvent A is 0.05% TFA in water and solvent B is 0.05% TFA in acetonitrile with a flow-rate of 1 ml/min was applied. The runs were monitored at 210 nm.

the presence of organic solvent. For this reason the elution procedure required both a lowering of the pH and the use of an organic buffer. The former condition is needed to remove the stabilizing effect of the ionic interactions while the latter condition disrupts the hydrophobic core and the bound material is eluted.

The recombinant expression and on-line affinity chromatography system has now been expanded to provide more flexibility. Recently, we have successfully generated a K fusion expression vector and a complementary E affinity column. Experiments are in progress to generate expression vectors where the K or E coding region is placed upstream of the multiple cloning site. Enzymatic cleavage site(s) other than the existing methionine chemical cleavage are being tested in the linker region to provide more efficient fusion tag removal. We are also experimenting with new affinity resins to order to increase the versatility of the purification system. Some of these modifications include the use of uniformly sized non-porous glass beads which might be suitable for batch-type purification. Liquid chromatography-compatible resins that are suitable for in situ chemical peptide synthesis are also being tested in an attempt to streamline the production of the affinity chromatography system.

E. Other affinity chromatographic systems

The E/K coiled-coil affinity chromatography module is a flexible and versatile purification unit. When coupled with the recombinant expression module, the entire system significantly economizes and streamlines an often labor-intensive multi-step process. The coiled-coil system, in our opinion, offers a good alternative to existing affinity purification systems. The following section describes briefly several affinity systems that are used today. Their advantages and limits are also highlighted.

Immunoaffinity chromatography

The recognition of antibodies by their antigens is highly specific and usually of high affinity. This has been the basis of many biodetection techniques, including ELISAs and immunoaffinity chromatography. The antibody can be immobilized on the matrix to purify the antigen or vice versa. In 1951, Campbell *et al.* (1951) were the first to do this when they immobilized bovine serum albumin on aminobenzylcellulose in order to purify antibodies that were raised against the protein. Polyclonal antibodies can be used as immunoaffinity ligands, but the development of monoclonal antibodies has made this technique much more popular. Monoclonal antibodies are generally preferred because they can be obtained reproducibly and a particular strain can be selected for the appropriate affinity.

The kinetics of the antibody–antigen interaction determine how well affinity chromatography will work. The antibody must have high affinity for its ligand, indicated by a small equilibrium dissociation constant (K_d). The dissociation rate constant (k_{off}) must be finite, or the Ab–Ag complex will be too difficult to dissociate (Jones *et al.* 1995). Ideally, the K_d should be between 10^{-4} and 10^{-8} M for affinity chromatography. If the K_d is greater than 10^{-4} M, the affinity is too weak, leading to loss of product. If it is less than 10^{-8} M, the complex will be very difficult to dissociate, making elution difficult (Phillips 1989).

The antibody–antigen complex is stabilized by the same forces which stabilize protein structure: electrostatic interactions, hydrogen bonding and hydrophobic interactions. This makes dissociation very difficult, and the elution conditions will frequently denature the target protein. The two most common elution methods are a change in pH and the introduction of chaotropic salts. Many stabilizing forces, such as electrostatic interactions, are disrupted at low pH by the protonation of acidic groups and at high pH by the deprotonation of basic groups. Typical elution buffers include 0.1 M glycine (pH 3) (Yang *et al.* 1997), 0.1 M acetic acid (pH 3.0) (Jones *et al.* 1995), and 0.1 M triethylamine HCl (pH 11) (Frankel *et al.* 1996). In contrast, chaotropic salts disrupt the structure of water which decreases hydrophobic interactions and so weakens the antibody–antigen complex. Examples include CCl_3COO^-, CF_3COO^-, ClO_4^-, I^-, and Cl^- at concentrations between 1.5 and 8 M. The most common elution buffer is 3 M NaSCN (Phillips 1989). Chaotropic salt elution tends to be less denaturing than pH elution.

Despite the popularity of immunoaffinity chromatography, it has significant disadvantages. Ironically, the greatest strength of immunological techniques, the high specificity of antibody/antigen recognition, is also its greatest disadvantage. No general purification strategy exists because a new antibody must be raised against each protein, which can be time consuming and expensive, and the elution conditions must be optimized. This process is particularly difficult and time consuming if the protein of interest has never been purified before. The denaturing elution conditions are also a problem, because it is usually desirable to have a protein in its native conformation, especially if its activity is to be studied and in some cases where in vitro refolding is not possible. Antibodies may be structurally altered or functionally inactivated while being coupled to the matrix. There are problems with antibodies leaching from the matrix. Additionally, immobilization of either the antibody or the antigen can interfere with their interaction due to steric hindrance (Gretch *et al.* 1987). Many variations of immunoaffinity chromatography have been developed in an effort to overcome these problems.

A more general technique takes advantage of the ability of Protein A and Protein G to bind to the constant heavy chain of the Fc region of immunoglobins. Protein A, from *Staphylococcus aureus*, binds a variety of immunoglobins (for example, IgG, IgM, IgA, and IgE) while Protein G, from Group G Streptococci, is specific for IgG immunoglobins (Sambrook & Russell 2001). Both proteins are stable, specific and can be obtained at relatively low cost. Either Protein A or G can be coupled to the chromatography matrix for monoclonal antibody purification. Alternately, Protein A can be used to anchor the antibody to the resin in the correct orientation for the subsequent purification of the antigen (Jones *et al.* 1995). Recently, Yang *et al.* (1997) have used the Fc domain of human immunoglobin as a C-terminal affinity tag in the purification of recombinant acetylcholine receptor-inducing activity protein. The fusion protein was immobilized on a Protein G–agarose column, the impurities were washed away, and the protein was eluted with 0.1 *M* glycine.

Berry and Davies (1992) developed a single-step purification of turkey lysozyme using the Fv fragment of a monoclonal antibody raised against the enzyme. The resulting lysozyme was highly pure and recovered in high yields. There are several advantages to the use of the Fv fragments. Unlike complete antibodies, Fv fragments can be recombinantly expressed in bacteria, which is cheaper and more dependable than producing monoclonal antibodies. They are small enough to be immobilized within the pores of the silica matrix, and have more binding sites per mg of protein – thereby increasing the efficiency of the purification. This technique could be useful if a monoclonal antibody with a known Fv sequence were available for the protein to be purified. The interaction between the protein and the Fv fragment is still very strong, and hence elution may still be a problem.

Immunoaffinity tags have been developed as a generalized approach to the purification of recombinant proteins. The target protein to be purified is expressed as a fusion protein with a short antibody epitope at either the N- or C-terminus. The epitope must be a linear peptide, not a conformational epitope (Jones *et al.* 1995). This technique was used by Templeton (1992) in the purification of retinoblastoma susceptibility gene product. They used the hemagglutinin antigen epitope of the influenza virus as a C-terminal affinity tag. The recombinant protein was purified with an anti-hemagglutinin antibody coupled to Protein A Sepharose. After washing, the protein was eluted by a competing peptide ligand (YPYDVPDYA). A protease cleavage site can be engineered between the protein and the peptide tag to remove the peptide.

Affinity tags

Affinity tags were designed to make affinity chromatography simpler and standardized. A peptide with a known affinity for a particular ligand is genetically engineered onto the N- or C-terminus of the target protein. A standardized purification scheme can then be used, with minimal adaptation, for any recombinant protein. This greatly increases the speed with which an expression system can be evaluated and optimized. The time required for purification is also reduced, especially since it can often be accomplished in a single step. Many affinity-tags are commercially available, along with the necessary reagents. This means that the same affinity resin and column can be used in the purification of many proteins, a significant advantage over individually tailored monoclonal antibodies. The same tag can then be used to anchor the protein directly to a microtiter well for assays. Finally, proteins which are truncated due to an error in synthesis can be extremely difficult to remove. When affinity tags are used, the truncated protein will not carry the tag and will not bind to the affinity matrix (Phillips 1989).

There are limitations to the use of affinity tags that one must be aware of. Occasionally, the unnatural amino acids at one terminus of the protein may interfere with the expression or folding of the protein. It is also possible for the activity of the protein to be affected by the presence of a tag. These problems can frequently be alleviated by switching the tag from one terminus to the other. If physical characterization or structural determination is to be done with the recombinant protein, the native amino acid sequence is preferred. In this case it would be best to include a protease cleavage site between the tag and the protein sequence (Jones *et al.* 1995). Despite these potential problems, affinity tags have become extremely popular in the last several years.

Biotin /streptavidin affinity system

One of the best known examples of molecular recognition is that of streptavidin for biotin. Biotin, or vitamin H, is a small cofactor required by enzymes involved in CO_2 transfer. Streptavidin, a protein isolated from *Streptomyces avidinii*, binds biotin with a high affinity. Each protein molecule has four binding sites for biotin and is highly specific for it. Because many biodetection assays make use of the interaction between biotin and streptavidin, various types of biotinylation reagents and derivatized streptavidin are commercially available (Diamandis & Christopoulos 1991).

The affinity of streptavidin for biotin is one of the highest known, with a K_d equal to 10^{-15} M. This is 10^3–10^6 times greater than the affinity of antibodies for their antigens. The resulting complex is very stable and is unaffected by pH, chaotropic salts, and washing steps. Dissociation requires harsh, denaturing conditions, such as heating in 2% SDS or treatment with 70% formic acid (Thiele & Fahrenholz 1994). This has seriously limited the usefulness of this system in affinity chromatography.

Cleavable biotin analogs have been introduced to allow the elution of proteins with their native structure. Thiele and Fahrenholz (1994) attached a photocleavable biotin analog to the cholecystokinin (CCK) peptide. This peptide was incubated with an anti-CCK antibody and then with streptavidin agarose. After a wash step, the mixture was irradiated (λ>320 nm) to cleave the antibody–CCK complex from the resin. They succeeded in purifying the antibody 360-fold, but the peptide was still bound to the resin.

The Strep-tag was developed by Schmidt and Skerra (1993) as an alternate streptavidin ligand. Through the use of a peptide library, they isolated a nine residue peptide (AWRHPQFGG) that bound to streptavidin. It was used as a C-terminal affinity tag for the recombinant expression of an antibody Fv fragment. In a single-step purification process, the protein was immobilized on streptavidin agarose and eluted with 1 mM iminobiotin, a competing ligand. The mild elution conditions allowed the Fv fragment to be purified as a heterodimer. The equilibrium dissociation constant between streptavidin and the Strep-tag was found to be 3.7×10^{-5} M by isothermal titration calorimetry (Schmidt *et al.* 1996). The Strep-tag is a small hydrophillic peptide which is resistant to proteolysis in vivo. It did not interfere with the expression and secretion of the Fv fragment. It also binds competitively with biotin.

Histidine-Tag purification system

The Histidine-Tag is one of the most common affinity-tags in use. This is a form of immobilized-metal affinity chromatography (IMAC). An oligohistidine peptide is engineered into a recombinant protein as an affinity tag. The histidine residues bind to Ni^{2+}, which has been immobilized onto a column by covalently bound chelating agents. This system has become extremely popular due to its flexible conditions and mild elution.

The His-Tag and Ni^{2+} columns are commercially available.

This technique is based on the principle that transition metal ions will coordinate to electron donating groups on the protein surface (Ostrove & Weiss 1990, Sawadogo & Van Dyke 1995). This binding is dominated by the imidazole group of histidine residues, but cysteine and tryptophan can also play a role under some conditions. Different metal ions have been used, and they are listed in the order of their affinity for imidazole: $Cu^{2+}>Ni^{2+}>Zn^{2+}\approx Co^{2+}$. An average single histidine residue has a $Kd = 2.2 \times 10^{-4}$ M for Cu^{2+}, while that for Ni^{2+} is 15 times weaker (Arnold 1991).

The chelating agents are small molecules covalently linked to the matrix. The two most common ones are iminodiacetic acid (IDA) and nitrilotriacetic acid (NTA). Since IDA is a tridentate chelator, three of the six Ni^{2+} coordination sites bind to IDA and three are available to bind to the protein. This means that the protein is bound relatively strongly, and 250 mM–1 M imidazole, a competing ligand, is required for elution. Ni^{2+} is bound more strongly to NTA, a tetradentate ligand, and hence there is less problem with the metal 'bleeding' from an NTA column. As only two metal coordination sites remain, proteins are bound less strongly and can be eluted with 100–200 mM imidazole (Sawadogo & Van Dyke 1995).

Proteins are coordinated through the ε- or δ- nitrogen of surface-accessible histidine residues. Few proteins have more than a couple of surface histidines, as the residue is only found at about 2% of the positions in proteins, only half of which will be surface accessible (Arnold 1991). This makes the engineered His-Tag, which is usually six to eight histidine residues in length, a very specific binding domain. Ni^{2+}–NTA has only two free coordination sites and so can only bind to two histidine residues. Optimal binding occurs when the two histidines are found on subsequent turns of an α-helix. This can be achieved by engineering a –His–X_3–His tag, but this will only bind to Ni^{2+} when correctly folded and presented. Better results can often be obtained by a tag of five or six histidine residues in a row. Only two will bind, but there is a better chance of there being two in the correct orientation. The pK of surface histidines is from 6 to 7. As it is the unprotonated form which binds to Ni^{2+}, the best metal binding occurs at pH 6–8.

There are three common ways to elute His-tagged proteins from a Ni^{2+} column. The first is by a pH gradient. A drop to pH 4–5 is generally sufficient to protonate the histidine residues and elute the protein. This is dependent on the number of surface-accessible histidines, and hence proteins with higher number of histidines require a lower pH for elution. The second method is to introduce a competing ligand, usually imidazole. Imidazole elution is generally milder, especially for proteins which are not stable at low pH. The third technique is to flush the column with a chelating agent such as EDTA. Unlike with the first two methods, EDTA elution will provide no resolution between species with different affinities to the resin – everything will elute at once. This would be a disadvantage if there were a Ni^{2+} binding impurity that might have been separated by pH or imidazole elution. In addition, the chelating agent will strip the column of Ni^{2+} ions (Arnold 1991, Ostrove & Weiss 1990, Sawadogo & Van Dyke 1995).

There are only a few constraints on the conditions for His–Ni^{2+} purification. First, the pH should be in the range of 6–8. Since this pH range encompasses the physiological pH, this is rarely a problem. Second, a high salt buffer, typically 0.5–1.0 M

NaCl, is required to reduce nonspecific binding through an ion exchange effect. Finally, chelating agents must be avoided for they will strip the Ni^{2+} from the column. The most common include EDTA, EGTA, β-mercaptoethanol, dithiothreitol, and citrate. Other than this, Ni^{2+} chromatography is compatible with a wide range of conditions, including many salts, detergents, and denaturants (Sawadogo & Van Dyke 1995).

There are some advantages to carrying out His–Ni^{2+} purification under denaturing conditions. If the target protein has a low solubility or tends to associate with other proteins, extraction and purification in the presence of 6 M guanidine HCl will disrupt those interaction without interfering with the Ni^{2+} chromatography. However, there may be more impurities due to the unfolding of proteins with internal histidines which can then bind to Ni^{2+}.

The His–Ni^{2+} system can also be used to purify noncovalently bound protein complexes. If a single member of the complex has a His-Tag, the entire complex can be immobilized on the matrix. This can be done with protein complexes formed either in vivo or in vitro. Obviously denaturing conditions should be avoided and imidazole elution would be preferred to a pH gradient (Sawadogo & Van Dyke 1995).

There are several advantages to using the His-Tag for the purification of recombinant proteins. It is a small tag which rarely alters the properties and functions of the target protein. Therefore, proteolytic cleavage to remove the tag is seldom necessary. The small chelating agents are stable over a wide range of temperature and solvent conditions. The resin is capable of high metal loading, allowing high protein capacities (2–10 mg protein per ml resin) (Hoffmann & Roeder 1991). The elution process is simple and allows the native structure to be maintained. Should the resin be stripped of Ni^{2+}, it can be regenerated by simply pumping a $NiSO_4$ solution through the column. Finally, the entire system is quite inexpensive (Arnold 1991, Hoffmann & Roeder 1991, Sawadogo & Van Dyke 1995). Despite the general usefulness of the His-Tag, there are some instances where the histidine residues interfere with the expression or folding of the protein. In addition, some proteins, such as Fv fragments, tend to dissociate in the high salt conditions which are necessary (Schmidt & Skerra 1993).

F. The advantages of the E/K coiled-coil system

The heterodimeric E/K coiled-coil system is a comprehensive and versatile research tool. It integrates the laborious processes of recombinant protein expression, product detection, biosensor functional assays and protein purification into a common platform. The E/K coiled-coil serves as a capture and dimerization domain for the biosensor; a detection and an affinity tag for protein expression and purification. The E/K system allows the researcher to produce, detect, purify and analyze the protein product in an integrative manner. The efficiency and convenience of this system are the main reasons for its usefulness as a research tool.

The versatility of the E/K coiled-coil system stems from the ability of a coiled-coil to be used as a dimerization domain and our ability to design these proteins with specific dimerization characteristics. In theory, any native heterodimeric coiled-coil such as Fos/Jun or Myc/Max can be used in this system. However, the use of these native proteins has several disadvantages. Firstly, natural coiled-coils such as those found in transcription factors usually have a modest dimerization affinity (10^5–10^8 M). Although this may be an important characteristic of the transcription factor from a regulatory perspective, the weak affinity reduces the usefulness of these coiled-coils as capture domains. The weak affinity can place a limit on the sensitivity of the biosensor-based assays as it reduces the number of captured acceptors presented on the surface to be studied. This may also mean a lower overall yield from the purification process because it probably constrains the type and number of washes one can do during the affinity purification process. Secondly, many of the native proteins that form coiled-coils can dimerize with multiple partners. A good example is the c-Myc/Max family as described previously. From an application perspective, the apparent lack of specificity will be a disadvantage since the presence of complementary protein dimer-forming partners in the biological medium other than the anticipated one can compromise the expression system, the biosensor based assay and even the affinity purification process. Thirdly, naturally occurring proteins are usually degraded rapidly in serum or cell extracts. This will no doubt reduce the overall efficiency of the system and increase the cost associated per analysis.

A good way to overcome these disadvantages is the use of de novo designed coiled-coils. This is a practical alternative because of the large pool of knowledge that is currently available in the field to design a coiled-coil. Theoretically, the current stage of knowledge will permit the design of a coiled-coil with specific dimerization affinity, unique specificity, good stability and appropriate size. We along with other groups have demonstrated that such efforts are feasible. The E/K coiled-coil is a specific example of such an effort.

The E/K coiled-coil is designed to be very stable in solution. Its resistance to urea and heat denaturation demonstrated this characteristic. Yet the E/K coiled-coil can be dissociated under specific conditions which ensure its usefulness in affinity chromatography. The ability of the E and K peptides to dimerize, even when one is fused with a large protein (e.g. antibody), showed that it is a useful purification tag. The unique amino acid sequence of the E and K peptides enables them to dimerize specifically and minimizes the probability of interference from naturally occurring coiled-coils. The fast formation and slow dissociation kinetics of the dimeric coiled-coil also permit the construction of a stable capture domain to be used in the biosensor-based applications. Lastly, its apparent stability in serum suggests that the system should be useful in a variety of applications.

The E/K coiled-coil is only one of the many possible designs that can be used with the system described. Given the inherent flexibility of chemical peptide syntheses, and the number of structural variations that are possible as learned from nature and ongoing research, the heterodimeric coiled-coil system can truly be tailor-made to the exact needs of the researcher.

G. References

Adamson, J. G., Zhou, N. E. and Hodges, R. S. (1993) Structure, function and application of the coiled-coil protein folding motif. *Curr. Opin. Biotechnol.* **4**: 428-437.

Amati, B. and Land, H. (1994) Myc-Max-Mad: a transcription factor network controlling cell cycle progression, differentiation and death. *Curr. Opin. Genet. Dev.* **4**: 102-108.

Anderson, D. E., Becktel, W. J. and Dahlquist, F. W. (1990) pH-induced denaturation of proteins: a single salt bridge contributes 3- 5 kcal/mol to the free energy of folding of T4 lysozyme. *Biochem.* **29**: 2403-2408.

Arnold, F. H. (1991) Metal-affinity separations: a new dimension in protein processing. *Bio/Technology* **9**: 151-156.

Baxevanis, A. D. and Vinson, C. R. (1993) Interactions of coiled coils in transcription factors: where is the specificity? *Curr. Opin. Genet. Dev.* **3**: 278-285.

Berry, M. J. and Davies, J. (1992) Use of antibody fragments in immunoaffinity chromatography. Comparison of FV fragments, VH fragments and paralog peptides. *J. Chromatogr.* **597**: 239-245.

Biro, E. N. A. e., Ed. (1975) *Proceedings of the IX Federation of European Biochemical Societies Meeting, Protein of Contractile Systems.* Amsterdam, North Holland Publishing Co.

Butcher, D. J., Kowalska, M. A., Li, S., Luo, Z., Shan, S., Lu, Z., Niewiarowski, S. and Huang, Z. (1997) A natural motif approach to protein design: a synthetic leucine zipper peptide mimics the biological function of the platelet factor 4 protein. *FEBS Lett.* **409**: 183-187.

Campell, D. H., Luescher, E. and Lerman, L. S. (1951) Immunologic adsorbents. I. Isolation of antibody by means of a cellulose-protein antigen. *Proc. Natl. Acad. Sci.* **37**: 575-578.

Carter, P., Ridgway, J. and Zhu, Z. (1995) Toward the production of bispecific antibody fragments for clinical applications. *J. Hematother.* **4**: 463-470.

Cavanagh, J., Fairbrother, W. J., Palmer III, A. G. and Skeleton, N. J., Eds. (1996) *Protein NMR Spectroscopy: Principles and Practice.* San Diego, CA, Academic Press.

Chao, H., Houston Jr., M. E., Grothe, S., Kay, C. M., O'Connor-McCourt, M., Irvin, R. T. and Hodges, R. S. (1996) Kinetic study on the formation of a de novo designed heterodimeric coiled-coil: use of surface plasmon resonance to monitor the association and dissociation of polypeptide chains. *Biochem.* **35**: 12175-12185.

Cohen, C. and Parry, D. A. (1990) α-Helical coiled coils and bundles: how to design an α-helical protein. *Proteins* **7**: 1-15.

Cohen, C. and Parry, D. A. (1994) α-Helical coiled coils: more facts and better predictions. *Science* **263**: 488-489.

Crameri, R. and Suter, M. (1993) Display of biologically active proteins on the surface of filamentous phages: a cDNA cloning system for selection of functional gene products linked to the genetic information responsible for their production. *Gene* **137**: 69-75.

Crick, F. H. C. (1953) The packing of α-helices: simple coiled-coils. *Acta Crystallogr.* **6**: 689-698.

Cusack, S., Berthet-Colominas, C., Hartlein, M., Nassar, N. and Leberman, R. (1990) A second class of synthetase structure revealed by X-ray analysis of Escherichia coli seryl-tRNA synthetase at 2.5 A. *Nature* **347**: 249-255.

de Kruif, J. and Logtenberg, T. (1996) Leucine zipper dimerized bivalent and bispecific scFv antibodies from a semi-synthetic antibody phage display library. *J. Biol. Chem.* **271**: 7630-7634.

Diamandis, E. P. and Christopoulos, T. K. (1991) The biotin-(strept)avidin system: principles and applications in biotechnology. *Clin. Chem.* **37**: 625-636.

Efimov, V. P., Engel, J. and Malashkevich, V. N. (1996) Crystallization and preliminary crystallographic study of the pentamerizing domain from cartilage oligomeric matrix protein: a five- stranded α-helical bundle. *Proteins* **24**: 259-262.

Ellenberger, T. E., Brandl, C. J., Struhl, K. and Harrison, S. C. (1992) The GCN4 basic region leucine zipper binds DNA as a dimer of uninterrupted α-helices: crystal structure of the protein-DNA complex. *Cell* **71**: 1223-1237.

Fairman, R., Chao, H. G., Lavoie, T. B., Villafranca, J. J., Matsueda, G. R. and Novotny, J. (1996) Design of heterotetrameric coiled coils: evidence for increased stabilization by Glu(-)-Lys(+) ion pair interactions. *Biochem.* **35**: 2824-2829.

Frankel, A. E., Burbage, C., Fu, T., Tagge, E., Chandler, J. and Willingham, M. (1996) Characterization of a ricin fusion toxin targeted to the interleukin-2 receptor. *Protein Eng.* **9**: 913-919.

Glover, J. N. and Harrison, S. C. (1995) Crystal structure of the heterodimeric bZIP transcription factor c-Fos- c-Jun bound to DNA. *Nature* **373**: 257-261.

Graddis, T. J., Myszka, D. G. and Chaiken, I. M. (1993) Controlled formation of model homo- and heterodimer coiled-coil polypeptides. *Biochem.* **32**: 12664-12671.

Gretch, D. R., Suter, M. and Stinski, M. F. (1987) The use of biotinylated monoclonal antibodies and streptavidin affinity chromatography to isolate herpesvirus hydrophobic proteins or glycoproteins. *Anal. Biochem.* **163**: 270-277.

Harbury, P. B., Zhang, T., Kim, P. S. and Alber, T. (1993) A switch between two-, three-, and four-stranded coiled coils in GCN4 leucine zipper mutants. *Science* **262**: 1401-1407.

Hill, C. P., Anderson, D. H., Wesson, L., DeGrado, W. F. and Eisenberg, D. (1990) Crystal structure of alpha 1: implications for protein design. *Science* **249**: 543-546.

Hodges, R. S. (1992) Unzipping the secrets of coiled-coil. *Curr. Biol.* **2**: 122-124.

Hodges, R. S. (1996) De novo design of α-helical proteins: basic research to medical applications. *Biochem. Cell Biol.* **74**: 133-154.

Hodges, R. S., Saund, A. K., Chong, P. C., St-Pierre, S. A. and Reid, R. E. (1981) Synthetic model for two-stranded α-helical coiled-coils. Design, synthesis, and characterization of an 86-residue analog of tropomyosin. *J. Biol. Chem.* **256**: 1214-1224.

Hodges, R. S., Sodek, J., Smillie, L. B. and Jurasek, L. (1972) Tropomyosin: amino acid sequence and coiled-coil structure. *Cold Spring Harbor Symp. Quant. Biol.* **37**: 299-310.

Hoffmann, A. and Roeder, R. G. (1991) Purification of his-tagged proteins in non-denaturing conditions suggests a convenient method for protein interaction studies. *Nucleic Acids Res.* **19**: 6337-6338.

Hu, J. C., O'Shea, E. K., Kim, P. S. and Sauer, R. T. (1990) Sequence requirements for coiled-coils: analysis with lambda repressor- GCN4 leucine zipper fusions. *Science* **250**: 1400-1403.

Hurst, H. C. (1995) Transcription factors 1: bZIP proteins. *Protein Profile* **2**: 101-168.

John, M., Briand, J. P., Granger-Schnarr, M. and Schnarr, M. (1994) Two pairs of oppositely charged amino acids from Jun and Fos confer heterodimerization to GCN4 leucine zipper. *J. Biol. Chem.* **269**: 16247-16253.

Jones, C., Patel, A., Griffin, S., Martin, J., Young, P., O'Donnell, K., Silverman, C., Porter, T. and Chaiken, I. (1995) Current trends in molecular recognition and bioseparation. *J. Chromatogr.* **707**: 3-22.

Kalandadze, A., Galleno, M., Foncerrada, L., Strominger, J. L. and Wucherpfennig, K. W. (1996) Expression of recombinant HLA-DR2 molecules. Replacement of the hydrophobic transmembrane region by a leucine zipper dimerization motif allows the assembly and secretion of soluble DR alpha beta heterodimers. *J. Biol. Chem.* **271**: 20156-20162.

Kohn, W. D., Kay, C. M. and Hodges, R. S. (1995a) Protein destabilization by electrostatic repulsions in the two-stranded α-helical coiled-coil/leucine zipper. *Protein Sci.* **4**: 237-250.

Kohn, W. D., Kay, C. M. and Hodges, R. S. (1997a) Salt effects on protein stability: two-stranded alpha-helical coiled-coils containing inter- or intrahelical ion pairs. *J. Mol. Biol.* **267**: 1039-1052.

Kohn, W. D., Mant, C. T. and Hodges, R. S. (1997b) α-Helical protein assembly motifs. *J. Biol. Chem.* **272**: 2583-2586.

Kohn, W. D., Monera, O. D., Kay, C. M. and Hodges, R. S. (1995b) The effects of interhelical electrostatic repulsions between glutamic acid residues in controlling the dimerization and stability of two-stranded α-helical coiled-coils. *J. Biol. Chem.* **270**: 25495-25506.

Konig, P. and Richmond, T. J. (1993) The X-ray structure of the GCN4-bZIP bound to ATF/CREB site DNA shows the complex depends on DNA flexibility. *J. Mol. Biol.* **233**: 139-154.

Krylov, D., Mikhailenko, I. and Vinson, C. (1994) A thermodynamic scale for leucine zipper stability and dimerization specificity: e and g interhelical interactions. *EMBO J.* **13**: 2849-2861.

Landschulz, W. H., Johnson, P. F. and McKnight, S. L. (1988) The leucine zipper: a hypothetical structure common to a new class of DNA binding proteins. *Science* **240**: 1759-1764.

Lau, S. Y. M., Taneja, A. K. and Hodges, R. S. (1984) Synthesis of a model protein of defined secondary and quaternary structure: effect of chain length on the stabilization and formation of two-stranded α-helical coiled-coils. *J. Biol. Chem.* **259**: 13253-13261.

Lavigne, P., Crump, M. P., Gagne, S. M., Hodges, R. S., Kay, C. M. and Sykes, B. D. (1998) Insights into the mechanism of heterodimerization from the 1H-NMR solution structure of the c-Myc-Max heterodimeric leucine zipper. *J. Mol. Biol.* **281**: 165-181.

Lavigne, P., Kondejewski, L. H., Houston Jr., M. E., Sonnichsen, F. D., Lix, B., Sykes, B. D., Hodges, R. S. and Kay, C. M. (1995) Preferential heterodimeric parallel coiled-coil formation by synthetic Max and c-Myc leucine zippers: a description of putative electrostatic interactions responsible for the specificity of heterodimerization. *J. Mol. Biol.* **254**: 505-520.

Lavigne, P., Sonnichsen, F. D., Kay, C. M. and Hodges, R. S. (1996) Interhelical salt bridges, coiled-coil stability, and specificity of dimerization. *Science* **271**: 1136-1138.

Liu, N., Caderas, G., Gutte, B. and Thomas, R. M. (1997) An artificial HIV enhancer-binding peptide is dimerized by the addition of a leucine zipper. *Eur. Biophys. J.* **25**: 399-403.

Lovejoy, B., Choe, S., Cascio, D., McRorie, D. K., DeGrado, W. F. and Eisenberg, D. (1993) Crystal structure of a synthetic triple-stranded alpha-helical bundle. *Science* **259**: 1288-1293.

Lumb, K. J. and Kim, P. S. (1995) Measurement of interhelical electrostatic interactions in the GCN4 leucine zipper. *Science* **268**: 436-439.

Lupas, A., Van Dyke, M. and Stock, J. (1991) Predicting coiled coils from protein sequences. *Science* **252**: 1162-1164.

Lyu, P. C., Gans, P. J. and Kallenbach, N. R. (1992) Energetic contribution of solvent-exposed ion pairs to alpha-helix structure. *J. Mol. Biol.* **223**: 343-350.

Mant, C. T., Zhou, N. E. and Hodges, R. S. (1993) The role of amphipathic helices in stabilizing peptide and protein structure. *The Amphipathic Helix*. R. M. Epand, CRC Press Inc. pp. 39-64.

Marmorstein, R., Carey, M., Ptashne, M. and Harrison, S. C. (1992) DNA recognition by GAL4: structure of a protein-DNA complex. *Nature* **356**: 408-414.

McLachlan, A. D. and Stewart, M. (1975) Tropomyosin coiled-coil interactions: evidence for an unstaggered structure. *J. Mol. Biol.* **98**: 293-304.

Miceli, R., Myszka, D., Mao, J., Sathe, G. and Chaiken, I. (1996) The coiled coil stem loop miniprotein as a presentation scaffold. *Drug Des. Discov.* **13**: 95-105.

Moitra, J., Szilak, L., Krylov, D. and Vinson, C. (1997) Leucine is the most stabilizing aliphatic amino acid in the **d** position of a dimeric leucine zipper coiled-coil. *Biochem.* **36**: 12567-12573.

Monera, O. D., Kay, C. M. and Hodges, R. S. (1994a) Electrostatic interactions control the parallel and antiparallel orientation of α-helical chains in two-stranded α-helical coiled-coils. *Biochem.* **33**: 3862-3871.

Monera, O. D., Kay, C. M. and Hodges, R. S. (1994b) Protein denaturation with guanidine hydrochloride or urea provides a different estimate of stability depending on the contributions of electrostatic interactions. *Protein Sci.* **3**: 1984-1991.

Monera, O. D., Sonnichsen, F. D., Hicks, L., Kay, C. M. and Hodges, R. S. (1996) The relative positions of alanine residues in the hydrophobic core control the formation of two-stranded or four-stranded α-helical coiled-coils. *Protein Eng.* **9**: 353-363.

Monera, O. D., Zhou, N. E., Kay, C. M. and Hodges, R. S. (1993) Comparison of antiparallel and parallel two-stranded α-helical coiled-coils. *J. Biol. Chem.* **268**: 19218-19227.

Muhle-Goll, C., Gibson, T., Schuck, P., Schubert, D., Nalis, D., Nilges, M. and Pastore, A. (1994) The dimerization stability of the HLH-LZ transcription protein family is modulated by the leucine zippers: a CD and NMR study of TFEB and c-Myc. *Biochem.* **33**: 11296-11306.

Nautiyal, S., Woolfson, D. N., King, D. S. and Alber, T. (1995) A designed heterotrimeric coiled-coil. *Biochem.* **34**: 11645-51.

O'Shea, E. K., Klemm, J. D., Kim, P. S. and Alber, T. (1991) X-ray structure of the GCN4 leucine zipper, a two-stranded, parallel coiled-coil. *Science* **254**: 539-544.

O'Shea, E. K., Rutkowski, R. and Kim, P. S. (1989) Evidence that the leucine zipper is a coiled-coil. *Science* **243**: 538-542.

O'Shea, E. K., Rutkowski, R. and Kim, P. S. (1992) Mechanism of specificity in the Fos-Jun oncoprotein heterodimer. *Cell* **68**: 699-708.

Oas, T. G., McIntosh, L. P., O'Shea, E. K., Dahlquist, F. W. and Kim, P. S. (1990) Secondary structure of a leucine zipper determined by nuclear magnetic resonance spectroscopy. *Biochem.* **29**: 2891-2894.

Ostrove, S. and Weiss, S. (1990) Affinity chromatography: specialized techniques. *Methods Enzymol.* **182**: 371-379.

Pace, C. N., Laurents, D. V. and Thomson, J. A. (1990) pH dependence of the urea and guanidine hydrochloride denaturation of ribonuclease A and ribonuclease T1. *Biochem.* **29**: 2564-2572.

Patel, N., Herrman, J. M., Timans, J. C. and Kastelein, R. A. (1996) Functional replacement of cytokine receptor extracellular domains by leucine zippers. *J. Biol. Chem.* **271**: 30386-30391.

Phillips, T. M. (1989) High-performance immunoaffinity chromatography. *Adv. Chromatogr.* **29**: 133-173.

Sambrook, J. and Russell, D. W. (2001) *Molecular Cloning: A Laboratory Manual.* 3rd Ed., Cold Spring Harbor Laboratory Press, Cold Spring Harbor, NY, pp. A9.46-A9.48.

Sawadogo, M. and Van Dyke, M. W. (1995) Indirect use of immobilized metal affinity chromatography for isolation and characterization of protein partners. *Genet Eng* **17**: 53-65.

Schmidt, T. G., Koepke, J., Frank, R. and Skerra, A. (1996) Molecular interaction between the Strep-tag affinity peptide and its cognate target, streptavidin. *J. Mol. Biol.* **255**: 753-766.

Schmidt, T. G. and Skerra, A. (1993) The random peptide library-assisted engineering of a C-terminal affinity peptide, useful for the detection and purification of a functional Ig Fv fragment. *Protein Eng.* **6**: 109-122.

Schuermann, M., Hunter, J. B., Hennig, G. and Muller, R. (1991) Non-leucine residues in the leucine repeats of Fos and Jun contribute to the stability and determine the specificity of dimerization. *Nucleic Acids Res.* **19**: 739-746.

Scott, C. A., Garcia, K. C., Carbone, F. R., Wilson, I. A. and Teyton, L. (1996) Role of chain pairing for the production of functional soluble IA major histocompatibility complex class II molecules. *J. Exp. Med.* **183**: 2087-2095.

Serrano, L., Horovitz, A., Avron, B., Bycroft, M. and Fersht, A. R. (1990) Estimating the contribution of engineered surface electrostatic interactions to protein stability by using double-mutant cycles. *Biochem.* **29**: 9343-52.

Slate, C. A., Weninger, S. C., Church, F. C. and Erickson, B. W. (1995) Engineering of five 88-residue receptor-adhesive modular proteins containing a parallel α-helical coiled-coil and two RGD ligand sites. *Int. J. Pept. Protein Res.* **45**: 290-298.

Sodek, J., Hodges, R. S., Smillie, L. B. and Jurasek, L. (1972) Amino-acid sequence of rabbit skeletal tropomyosin and its coiled-coil structure. *Proc. Natl. Acad. Sci.* **69**: 3800-3804.

Stewart, M. (1993) Intermediate filament structure and assembly. *Curr. Opin. Cell Biol.* **5**: 3-11.

Su, J. Y., Hodges, R. S. and Kay, C. M. (1994) Effect of chain length on the formation and stability of synthetic α-helical coiled coils. *Biochem.* **33**: 15501-15510.

Talbot, J. A. and Hodges, R. S. (1982) Tropomyosin: a model protein for studying coiled-coil and α-helix stabilization. *Acc. Chem. Res.* **15**: 224-230.

Templeton, D. J. (1992) Nuclear binding of purified retinoblastoma gene product is determined by cell cycle-regulated phosphorylation. *Mol. Cell. Biol.* **12**: 435-443.

Terskikh, A. V., Le Doussal, J. M., Crameri, R., Fisch, I., Mach, J. P. and Kajava, A. V. (1997) "Peptabody": a new type of high avidity binding protein. *Proc. Natl. Acad. Sci.* **94**: 1663-1668.

Thiele, C. and Fahrenholz, F. (1994) Photocleavable biotinylated ligands for affinity chromatography. *Anal. Biochem.* **218**: 330-337.

Titus, M. A. (1993) Myosins. *Curr. Opin. Cell Biol.* **5**: 77-81.

Tripet, B., Yu, L., Bautista, D. L., Wong, W. Y., Irvin, R. T. and Hodges, R. S. (1996) Engineering a *de novo*-designed coiled-coil heterodimerization domain for the rapid detection, purification and characterization of recombinantly expressed peptides and proteins. *Protein Eng.* **9**: 1029-1042.

Tso, J. Y., Wang, S. L., Levin, W. and Hakimi, J. (1995) Preparation of a bispecific F(ab')2 targeted to the human IL-2 receptor. *J. Hematother.* **4**: 389-394.

Wishart, D. S., Sykes, B. D. and Richards, F. M. (1991) Relationship between nuclear magnetic resonance chemical shift and protein secondary structure. *J. Mol. Biol.* **222**: 311-333.

Woolfson, D. N. and Alber, T. (1995) Predicting oligomerization states of coiled-coils. *Protein Sci.* **4**: 1596-1607.

Yang, J. F., Ng, Y. P., Pun, S., Ip, N. Y. and Tsim, K. W. (1997) The EGF-like domain of chick acetylcholine receptor-inducing activity (ARIA) contains its full biological activity. *FEBS Lett.* **403**: 163-167.

Yu, Y., Monera, O. D., Hodges, R. S. and Privalov, P. L. (1996a) Investigation of electrostatic interactions in two-stranded coiled- coils through residue shuffling. *Biophys. Chem.* **59**: 299-314.

Yu, Y., Monera, O. D., Hodges, R. S. and Privalov, P. L. (1996b) Ion pairs significantly stabilize coiled-coils in the absence of electrolyte. *J. Mol. Biol.* **255**: 367-372.

Zhou, N. E., Kay, C. M. and Hodges, R. S. (1994) The net energetic contribution of interhelical electrostatic attractions to coiled-coil stability. *Protein Eng.* **7**: 1365-1372.

Zhou, N. E., Zhu, B.-Y., Kay, C. M. and Hodges, R. S. (1992) The two-stranded α-helical coiled-coil is an ideal model for studying protein stability and subunit interactions. *Biopolym.* **32**: 419-426.

Zhou, N. E., Zhu, B.-Y., Kay, C. M. and Hodges, R. S. (1993). *Importance of intra-chain ionic interactions in stabilizing α-helices in proteins.* The Chinese Peptide Symposium, Escom Science Publishers.

Zhu, B.-Y., Zhou, N. E., Kay, C. M. and Hodges, R. S. (1993) Packing and hydrophobicity effects on protein folding and stability: Effects of β-branched amino acids, valine and isoleucine, on the folding and stability of two-stranded α-helical coiled coils/leucine zippers. *Protein Sci.* **2**: 383-394.

Zhu, B.-Y., Zhou, N. E., Semchuk, P. D., Kay, C. M. and Hodges, R. S. (1992) Design, synthesis and structural characterization of model heterodimeric coiled-coil proteins. *Int. J. Pept. Protein Res.* **40**: 171-179.